Cranfield University

P.A.Thompson

Nonlinear Optical Materials

SCHOOL OF INDUSTRIAL AND MANUFACTURING SCIENCE

CENTRE FOR MOLECULAR ELECTRONICS

PhD

CRANFIELD UNIVERSITY

SCHOOL OF INDUSTRIAL AND MANUFACTURING SCIENCE

CENTRE FOR MOLECULAR ELECTRONICS

PhD

Academic Year 1993-94

PETER ANTHONY THOMPSON

Nonlinear Optical Materials

Supervisor: G.J.Ashwell

June 1994

That was the river....

this is the sea.

ABSTRACT

Twenty different materials have been successfully deposited as Langmuir-Blodgett monolayer films. All exhibit second harmonic generation (SHG) when irradiated with laser light at 1064 nm.

E-1-docosyl-4-{2-(4-dimethylaminophenyl)ethenyl}quinolinium bromide ($C_{22}H_{45}QHBr$) and E-1-docosyl-4-{2-(4-dimethylaminonaphthyl)ethenyl}quinolinium bromide ($C_{22}H_{45}QNBr$) have been deposited separately as multilayer films. They form Y-type structures when deposition is alternated with the material N-docosyl-4-methylquinolinium bromide. The nonlinear responses are quadratic up to 20 and 10 bilayers respectively and the response from the thick films is only 2 orders less than that produced by a Y-cut quartz plate. Similar results were obtained with $C_{22}H_{45}QHBr$ when interleaved with 4,4'-dioctadecyl-3,5,3',5'-tetramethyldipyrrylmethenehydrobromide. Ellipsometry studies of the 10 bilayer film of $C_{22}H_{45}QNBr$ indicate that the structure is interdigitated. This explains the stability of the film which gave the same SH response up to 6 months after deposition. A 10 bilayer films has also been fabricated using E-1-docosyl-4-{2-(4-{2-(4-dimethylaminophenyl)ethenyl}benzyl)ethenyl}pyridinium bromide ($C_{22}H_{45}PBHBr$) alternated with E-1-docosyl-4-{2-(4-methylphenyl)ethenyl}pyridinium bromide ($C_{22}H_{45}PT$).

E-1-octadecyl-4-{2-(4-methyloxyphenyl)ethenyl}pyridinium iodide and E-1-methyl-4-{2-(4-octadecyloxyphenyl)ethenyl}pyridinium iodide have been fabricated into monolayer films that are transparent at 1064 and 532 nm, therefore resonant enhancement does not contribute to their nonlinear response which is attributed solely to charge transfer in the molecule.

Mixed solutions of E-1-octadecyl-4-{2-(4-methyloxyphenyl)ethenyl}pyridinium iodide and sodium octadecylsulphate ($C_{18}H_{37}OSO_3^-Na^+$) have been deposited as very stable monolayers. The nonlinear response from the mixed film offers a significant improvement upon the performance of the film containing pure hemicyanine.

Novel zwitterionic materials have been fabricated as LB monolayers that also exhibit SHG.

CONTENTS

1.0 INTRODUCTION 1

1.1 Molecular Electronics. 1

1.2 Nonlinear Optical Materials. 4

1.3 Derivation of Optical Nonlinearity. 6

1.4 Langmuir-Blodgett Films. 10

1.4.1 A Brief History. 10

1.4.2 The Langmuir-Blodgett Film. 12

1.5 Potential Applications of Langmuir-Blodgett Films. 20

1.5.1 Devices Utilizing Electrical or Electronic Properties. 20

1.5.2 Gas Sensors. 22

1.5.3 Biological Sensors. 23

1.5.4 Optics. 24

1.5.5 Other Potential Applications. 27

1.6 Second Harmonic Generation from Langmuir-Blodgett Films. 28

1.6.1 Early Reports of Monolayer SHG. 28

1.6.2 Molecular Structure and SH Response. 29

1.6.3 Multilayer Films. 37

1.6.4 Aggregates. 44

1.6.5 Quadratic SHG Enhancement from Y-type Films. 50

1.6.6 Quadratic SHG Enhancement from Z-type Films. 54

1.6.7 Polymers. 56

1.6.8 DCANP. 64

1.6.9 Summary of Findings. 68

2.0 EXPERIMENTAL 69

2.1 Synthesis 69

2.1.1 Quinolinium Hemicyanines. 69

2.1.2 Pyridinium Hemicyanines. 70

2.1.3 E-1-alkyl-4-{2-(4-dimethylaminobenzylphenyl) ethenyl}quinolinium or pyridinium bromide. 72

2.1.4 E-1-alkyl-4-{2-(4-dimethylaminophenyl) butadienyl}pyridinium bromide. 73

2.1.5 E-1-docosyl-4-{2-(4-dimethylaminophenyl) ethenyl-4-naphthyl}pyridinium bromide. 74

2.1.6 E-1-alkyl-4-{2-(4-alkoxystyryl)ethenyl} pyridinium iodide. 75

2.1.7 4-octadecyloxybenzaldehyde. 76

2.1.8 E-1-methyl-4-{2-(4-octadecyloxystyryl)ethenyl} pyridinium iodide. 77

2.1.9 Mechanism of Hemicyanine Synthesis. 78

2.1.10 Zwitterion Adducts. 79

2.2 Langmuir-Blodgett Films 80

2.2.1 The Nima Technology Langmuir-Blodgett Trough. 80

2.2.2 LB Trough Cleanliness. 81

2.2.3 The Subphase. 84

2.2.4 Solvents. 84

2.2.5 Substrates. 85

2.2.6 Treatment and Storage of LB Films. 85

2.3 Measurement of Second Harmonic Generation. 85

3.0 RESULTS AND DISCUSSION 88

3.1 Standard Quinolinium and Pyridinium Hemicyanines 88

3.1.1 Absorbance Spectra of Solutions. 88

3.1.2 Molar Absorption Coefficient. 90

3.1.3 Isotherms. 91

3.1.4 Stability of Langmuir Films. 97

3.1.5 Monolayer Deposition. 98

3.1.6 Absorbance Spectra of LB Films. 99

3.1.7 Second Harmonic Generation from Monolayers. 102

3.1.8 Multilayer LB Films. 103

3.2 Novel Hemicyanines 113

3.2.1 Absorbance Spectra of Solutions. 113

3.2.2 Isotherms. 115

3.2.3 LB Films of $C_{22}H_{45}QNBr$. 118

3.2.4 LB Films of $C_{18}H_{37}PNBr$ and $C_{22}H_{45}PNBr$. 122

3.2.5 LB films of $C_{22}H_{45}PEHBr$. 124

3.2.6 LB films of $C_{22}H_{45}PBHBr$. 126

3.3 Transparent Materials for Nonlinear Optics 128

3.3.1 Absorbance Spectra of Solutions. 128

3.3.2 Isotherms. 130

3.3.3 Stability of Langmuir Films 132

3.3.4 Monolayer Deposition. 132

3.3.5 Absorbance Spectra of LB Films. 133

3.3.6 Second Harmonic Generation from Monolayers. 133

3.3.7 Multilayer LB Films. 134

3.3.8 LB Monolayers of Mixtures. 136

3.3.9 LB Multilayers of Mixtures. 142

3.4 Zwitterionic Adducts 143

3.4.1 Absorbance Spectra of Solutions. 144

3.4.2 Molar Absorption Coefficient. 146

3.4.3 Isotherms. 146

3.4.4 Deposition of Monolayers. 148

3.4.5 Absorbance Spectra of LB Films. 149

3.4.6 SHG from Monolayers. 150

3.4.7 Multilayer LB Films. 151

4.0 CONCLUSION 152

5.0 REFERENCES 159

6.0 APPENDIX 170

6.1 Abbreviations of Systematic Nomenclature. 170

1.0 Introduction

A brief description of molecular electronics is presented, containing a detailed look at one aspect of this field, nonlinear optical materials. The nonlinear effect of particular interest in this study is second harmonic generation (SHG), and the accepted mathematical and theoretical definitions are offered. The method chosen to prepare materials for SHG study was Langmuir-Blodgett (LB) films, and a short history of LB films is given. The theory of deposition and a summary of the possible applications of such films is also presented. Finally, an exhaustive review of SHG from LB films can be found in section 1.6, the conclusions from which formed the motivation for this thesis.

1.1 Molecular Electronics

Molecular electronics endeavours to recreate one of the functions that occurs in a biological organism. In such organisms, organic molecules perform electronic operations useful to the integrity of an hierarchical system. There are two accepted definitions of molecular electronics, and these are discussed below.

It can be defined as *organic molecular materials performing an active function in the processing of information and its transmission and storage*[1]. These processes are presently achieved with solid state electronics, using very large scale integration (VLSI). These are usually wafers of crystalline silicon, producing circuits containing components as little as 10 μm long. Solid state electronics first became popular in the 1960's when it was associated with transistors made of doped semiconductors. These components were about a millimetre long, and before that, lengths of about 10 cm were used with the advent of vacuum electronics[2].

The ultimate limits of silicon circuits are already known. The circuits are made at the surface of a single crystal, giving them a two-dimensional character. Since the material is three-dimensional, superimposing further circuit layers would require

alternate layers of insulating and semiconducting materials. This is not expected to be available on already circuited chips. A 3D circuit architecture however, is the prerequisite for parallel processing, in which very large amounts of data are processed simultaneously.

The highly prospective field of molecular electronics offers the most prominent qualities required for mass data processing: speed (approximately 10^{-12} s); 3D architectures are possible; the size of the elementary cell is molecular size; the molecular assemblies can be varied, and the advantages of molecular self organisation can be used instead of the micro-lithographic limits of silicon wafers[3].

Functional materials have, of course, already being used to advantage in several electronic applications. The best known is that of liquid crystals and their use in displays and digital thermometers[4]. Other examples are piezoelectric polymers as very sensitive hydrophones[5], photo-conducting polymers for copying[6], photochromic molecules for reversible high density optical storage and signal processing[7], and bio or chemical sensors for converting specific solute or gas interactions into electrical signals for use in industrial or medical diagnostics[8].

One body of opinion estimates that the growth of molecular electronics is expected to merge into supermolecular electronics[9]. The reason offered is that the requirements of reliability and testing of complex structures suggest a system approach instead of the traditional one which uses the properties of individual circuit elements. Therefore sequential designs, because of their vulnerability, will be abandoned in favour of supermolecular arrays acting as concurrent processor networks, this evolution is traced in figure 1.

The second definition of molecular electronics is that of *switching on a molecular scale*[10]. This is aimed more at the long term problem of fabricating molecular electronic devices. A method of achieving this is by the use of molecular optics, i.e. utilizing the optical qualities of materials for information processing and storage. An optical transistor, for example, would perform the same operations as its electronic

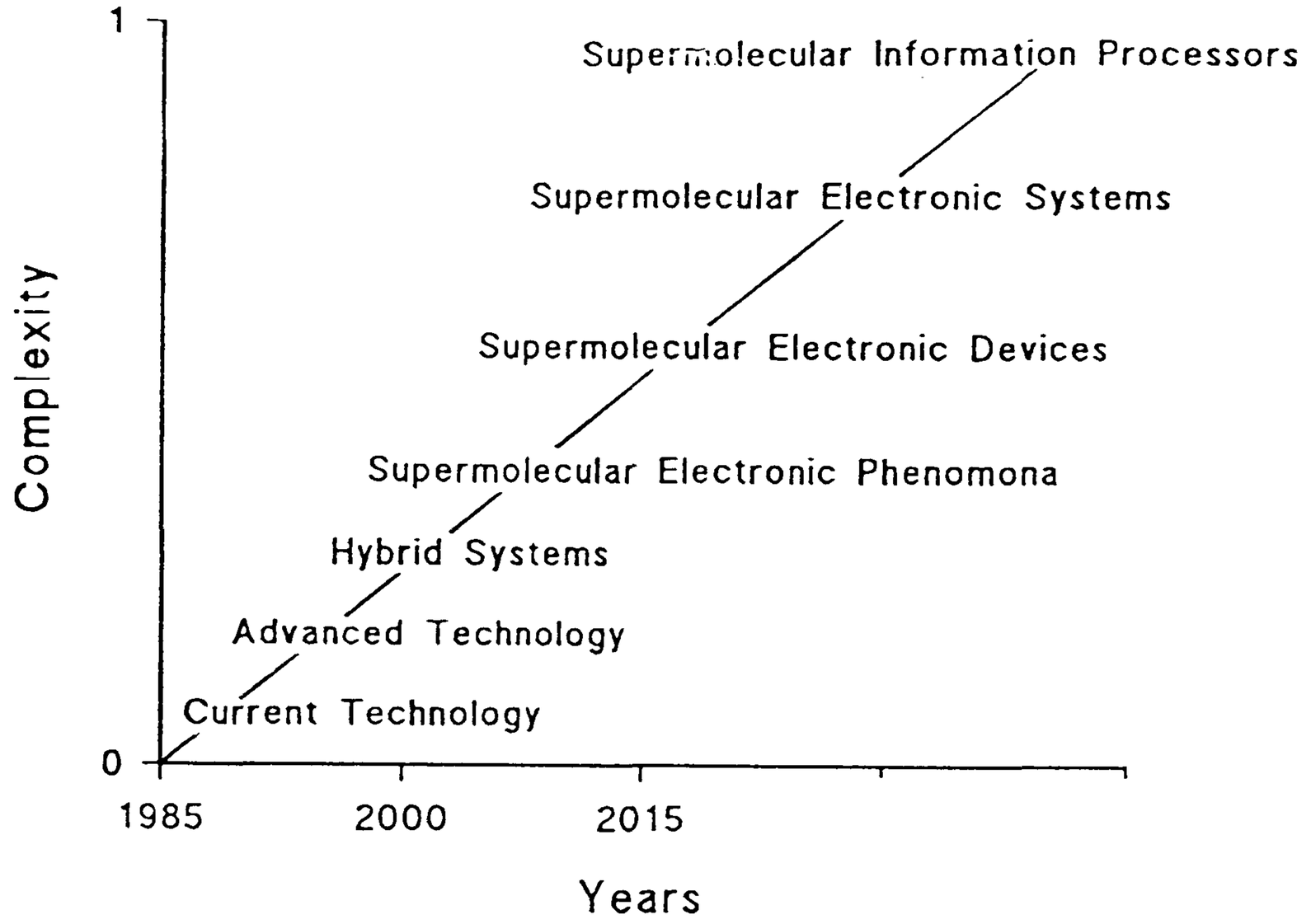

Figure 1. The proposed future of molecular electronics[1].

analogue, but it would modulate light rather than control an electrical signal. In doing so it could operate at a much higher speed (10^{-12} s compared to 10^{-9} s). It would not incur increased power consumption unlike electronic devices, and as mentioned previously, there is the possibility of parallel processing.

Molecular materials used for optical switching are surprisingly more resistant to laser damage than ionic crystalline materials. Many are more transparent at relevant frequencies than inorganic materials, and the wavelength-dependent transparency can be controlled by synthetic design to match specific laser frequencies.

Switching can be achieved by utilizing the photochromic behaviour of molecules[11]. Organic photochromic materials such as spiropyrans[12], azobenzenes[13] and zwitterions[14] exhibit distinct optical states that change colour when irradiated at a suitable wavelength. By absorbing light in a different spectral range, for example at wavelengths which overlap the absorption band of the switched material, the colour

change can be reversed; therefore, information can be recorded (pre-switched form) and read (switched form).

Research has been in progress on optical memories since the end of the 1960's. However it was not until 1982 that the breakthrough finally came with the audio compact disc[15], although clearly this is not a photochromic device. This was closely linked with the availability of new semiconductor lasers as light sources. If the laser frequency were doubled in this system then the optical data storage would be quadrupled, as the minimum area of the beam is dependent upon $1/\lambda^2$. A method of achieving this is to use materials that have a nonlinear response to light, i.e. nonlinear optical materials[16,17].

1.2 Nonlinear Optical Materials.

The electric field from the usually intense electromagnetic radiation of a laser can produce many responses in optically nonlinear materials: for example, second harmonic generation (SHG)[18]; the pockels effect[19]; parametric mixing[20] and third harmonic generation (THG)[21].

Materials that exhibit any of these effects do so because the oscillating electric and magnetic field associated with light disturbs the electronic system within the material[22]. This induces an oscillating dipole moment, or polarisation, which in turn radiates a second oscillating electric field. The interference of the two fields produces the optical properties. If the fields are equal then the response is linear; however, the secondary field can be made up of a series of frequencies different from the incident but analogous, i.e. harmonics. This arises in real materials when a strong field, for example from a laser, induces oscillations of the charges that are no longer proportional to the applied field, i.e. anharmonic. A mathematical derivation of this phenomena is presented in section 1.3. Thus nonlinear effects can be used to control, convert and even amplify

signals. In work with pulsed lasers they have proved to be a very versatile way of controlling the wavelength, envelope and duration of the pulse.

The ability to control pulses of light is also desirable in telecommunications, where the growing cost-effectiveness of optical fibres may lead to the increased transmission of data in the form of modulated infra-red beams. The peak power levels in this case are much lower than from a pulsed laser, so that nonlinear response is proportionally quite small, but here the manifest benefits of being able to switch the fibre optic signal directly without conversion to electrical form has led to the development of new and much more responsive materials.

The first nonlinear process discovered, the pockels effect, is the change in refractive index of a material when a voltage is applied across it[19]. This provides a way of converting the modulations in an electrical signal into an optical wave. It can also be used to form fast switching shutters, called Q switches, within the cavities of high powered lasers. These produce short pulses and modulate the amplitude of light so that it can carry information in the same way the radio wave does. In addition the effect can be used as a "waveguide" for switching optical signals between alternative routes in optical fibres[23].

At present almost all nonlinear optical and electro-optical devices are fabricated from inorganic materials such as $LiNbO_3$, $LiIO_3$ and the group III - V compounds[24]. Organic materials have a number of advantages over these. Firstly, at optical frequencies the nonlinear optical effect is electronic in origin and the increased electron delocalization occurring in conjugated organic molecules leads to much greater intrinsic nonlinearities than in the inorganic case. For example. the second order susceptibility of 2-methyl-4-nitroaniline (MNA) is about six times that of $LiNbO_3$. Secondly, organic materials have a higher optical damage threshold[25] and a quasi-instantaneous response which qualifies them for ultra fast optical signal processing. Finally there is a virtually unlimited potential of chemical synthesis allowing for the fine tuning of physical properties.

1.3 Derivation of Optical Nonlinearity.

In a *linear optical* material, the polarisation (P) induced in a unit volume by an optical electric field (E) is directly proportional to this field[26]:

$$P = \varepsilon_o \chi E \qquad (1)$$

where ε_o is the permittivity of free space, and χ is the constant of proportionality denoted as the "susceptibility of the material". Note that:

$$n^2 = 1 + \chi \qquad (2)$$

where n is the refractive index of the material.

In a *nonlinear optical* material, this strict proportionality no longer holds. The polarisation is expanded in powers of the electric field:

$$P = \varepsilon_o(\chi^{(1)}E^1 + \chi^{(2)}E^2 + \chi^{(3)}E^3 + ...) \qquad (3)$$

The higher order terms, E^2 and E^3 become important only at high electric field strengths, such as from a pulsed laser. They are the origins of the nonlinear optical effects. The fields, E and P, are vectors and the χ coefficients are tensors. The third order nonlinear susceptibility, $\chi^{(3)}$, can be finite in all materials. In order to obtain a non-zero second order susceptibility, $\chi^{(2)}$, there must be a noncentrosymmetric arrangement of atoms or molecules within the material.

The optical electric field, E, is described by the equation:

$$E = E_o \sin(\omega t) \qquad (4)$$

where E_o is the amplitude of the electric field and ω is the frequency of the light at time, t. Combination of equations (3) and (4), and excluding terms above the second order, gives:

$$(P/\varepsilon_o) = \chi^{(1)}E_o^{1}\sin(\omega t) + \chi^{(2)}E_o^{2}\sin^2(\omega t) \quad (5)$$

but as $\sin^2\theta = 1/2[1 - \cos(2\theta)]$ substitution into equation (5) gives:

$$(P/\varepsilon_o) = 1/2\chi^{(2)}E_o^{2} + \chi^{(1)}E_o^{1}\sin(\omega t) - 1/2\chi^{(2)}E_o^{2}\cos(2\omega t) \quad (6)$$

The third term shows a component of the polarisation varies at double the input frequency and the light irradiated as a result of this component is known as the second harmonic. Second harmonic generation (SHG) occurs when two photons, of energy $\hbar\omega$, combine. They form a new photon, of energy $2\hbar\omega$. SHG is commonly denoted by the term, $\chi^{(2)}(-2\omega;\omega,\omega)$, where $\chi^{(2)}$ denotes the order of susceptibility from which the nonlinear phenomena arises. The terms in brackets denote the output frequency and two input frequencies respectively.

For a single nonlinear optical molecule, (3) becomes:

$$p = \varepsilon_o(\alpha E + \beta E^2 + \gamma E^3 .....) \quad (7)$$

where α, β, γ etc are the nonlinear susceptibilities of the molecules.

To fully understand the mechanism of nonlinearity, particularly second order nonlinearity, from organic materials, the structure of a known nonlinear compound, p-nitroaniline (pNA, figure 2), is considered[27]. The carbon and nitrogen atoms in pNA have one p_z or π orbital. These are orientated normal to the plane of the molecule and bonded comparatively weakly to similar orbitals on neighbouring atoms. The interconnected set of p_z orbitals forms a mobile source of electron distribution. Each

aromatic carbon contributes one electron, the amino contributes two, and the nitro nitrogen has a net deficit of one. This satisfies the in-plane bonding requirements.

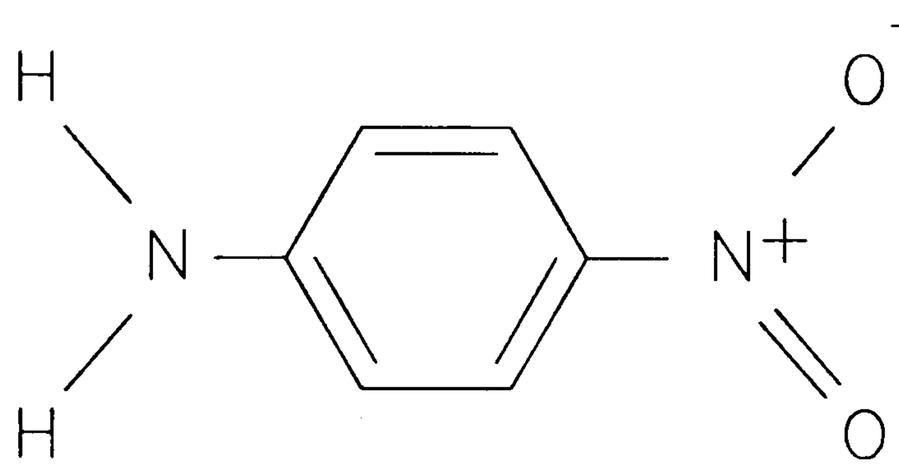

Figure 2. Molecular structure of p-Nitroaniline[27]

If the π-electrons were to spread themselves out evenly over the p_z orbital network there would be a net transfer of electronic charge. This would go from the amino group across the ring to the nitro group. This tendency is opposed by two factors; the net positive charge left on the amino nitrogen when an electron is moved from it, and the net negative charge present on the nitro group when an electron moves to it. There is therefore a partial rearrangement of charge which produces a change in the dipole moment. This is directed in the positive sense, from the nitro to the amino group.

Upon excitation, the molecule is elevated to a momentary excited state. In this state the kinetic energy of the π-electrons is greater and the influence of the core potential is less. Therefore more uniformity of the distribution occurs. The result is that the excited state dipole moment is larger, but in the same direction.

The contribution to ß from charge transfer ($ß_{CT}$, the dominant term) and the component due to the induced symmetry in the charge distribution ($ß_{ADD}$), have been separated, such that:

$$ß = ß_{ADD} + ß_{CT} \quad (8)$$

It has been shown that:

$$\beta_{CT} = \omega\mathcal{F}.\Delta\mu/(\omega - 2\hbar\omega)^2(\omega - \hbar\omega)^2 \qquad (9)$$

where $\hbar\omega$ is the energy gap, $\mathcal{F}$ is the oscillator strength of the charge transfer transition in the molecule and $\Delta\mu$ is the change in the dipole moment involved in the transition[27].

$\mathcal{F}$ is also high because the orbitals of the π-electron system are coupled across the whole molecule so that the transition is symmetrical. The ground state dipole moments of a variety of organic materials have been studied for many years and extensive compilations of data exist[25]. Excited state dipole moments are less well understood because the experimental measurements are more difficult. The situation is unfortunate since it is the absolute difference $|\Delta\mu|$ between the excited and ground state dipoles that is of the most relevance to ß. Nonetheless, the perusal of tables of μ_g of organic compounds can provide useful information in order to identify chemical functionality with the appropriate properties.

In organic molecular solids each molecule largely retains its electronic integrity. If each is suitably aligned it will contribute its second order nonlinear polarizability, ß, to the overall macroscopic quantity $\chi^{(2)}$. The intensity of the second harmonic is related to the macroscopic second-order nonlinear susceptibility as follows[28]:

$$I_{2\omega} = (I_\omega\chi^{(2)}l)^2/2(\varepsilon_o c^3 n_{2\omega} n_\omega^2).\ \mathrm{sinc}^2(\pi l/2l_c) \qquad (10)$$

where $I_{2\omega}$ is the intensity of the second harmonic radiation; I_ω is the intensity of the wave propagating through the nonlinear material; l is the path length; c is the velocity of light and l_c is the coherence length. Note that when $l/l_c << 1$, $\mathrm{sinc}^2(\pi l/2l_c) \approx 1$[29]. When the film thickness is less than the coherence length, the conversion efficiency $(I_{2\omega}/I_\omega)$ is seen to be proportional to the product $(\chi^{(2)})^2l^2$. Therefore for a given material the intensity of the second harmonic should increase quadratically with thickness.

The molecules, therefore, must be aligned noncentrosymmetrically to prevent their susceptibilities, ß, from cancelling each other out. Unfortunately the large dipole moments present in most nonlinear materials causes the molecules to align centrosymmetrically in the crystal. This problem has been overcome by using a number of techniques such as poled polymers and liquid crystals. This work will concentrate on a further method, *Langmuir-Blodgett* (LB) film deposition. The LB technique offers a unique method of fabricating molecular arrays, specifically designed to enhance reproducible nonlinear properties.

1.4 Langmuir-Blodgett Films

The consequence of a gas or liquid being in contact with a solid or liquid is the basis for colloid and interface science. The layer of molecules at the interface are often regularly orientated and, if so, possess distinct properties that differ from those of the molecules in the two phases. It is this concept on which Langmuir films and Langmuir-Blodgett film deposition is founded. This has great importance in biology and in many industrial and domestic operations.

1.4.1 A Brief History.

The history of the observations and utilization of this concept is an irregular one; the babylonians noted the effect of oil on water and Aristotle observed similar phenomena[30]. The first person to address the subject of monolayer films at an interface and place it on a scientific basis was Benjamin Franklin, in the eighteenth century[31]. Franklin's account to the Royal Society in 1774 contained the observation of the calming effect of a drop of oil on the water in a Clapham pond. This "pouring oil on troubled waters" effect was employed by relatively few people until 1890 when Lord Rayleigh suggested correctly that oil films on water ultimately extend until they are one molecule thick[32].

The first model of what is now termed a Langmuir trough was designed and used by Agnes Pockels. Her simple apparatus was used to deduce the molecular size of a monolayer of olive oil. In a letter to Lord Rayleigh in 1891[33] she described the methods which have remained to this day the essentials of monolayer research.

This work was largely ignored until 1917 when Irving Langmuir documented his own and Rayleigh's and Pockels' work in the "Proceedings of the Royal Society"[34]. He confirmed that a film on water was orientated, one molecule thick, with the polar functional group immersed and the long nonpolar chain directed almost vertically to the surface.

The first formal report describing the preparation of Langmuir-Blodgett (LB) films did not appear until 1935 in a report by Katherine Blodgett to the American Chemical Society[35]. She had been acknowledged for her experimental work as early as 1919 by Langmuir, but the war delayed their now historical observations. It seems astonishing that the explosion of interest in LB films has only occurred in the last 20 years, despite Blodgett's report appearing nearly 60 years ago.

Around 1970, Langmuir-Blodgett studies were used only as a tool of surface science for the study of surface interactions and wetting. It was then that Kuhn[36,37] added a new approach by applying these layers as spacers to study energy transfer. Here a sensitizer molecule was separated from an acceptor molecule by a variable number of inactive layers. The changes in absorption spectra allowed a determination of the dependence on separation of the transfer of excitation from the sensitizer to the acceptor.

Kuhn's work inspired investigations by others and during the 1970's electrical data was reported for LB films, offering scope for applications in electronics. Various reports from British and French groups suggested applications for LB films which stimulated the considerable research that has developed since. In 1978 a field effect transistor (FET) LB layer on InP was reported, on which no satisfactory insulating layer had previously been formed[38].

One of the first classes to be studied as LB film-forming materials were the alkanoic acids and their salts. Most of the "rules" governing surface behaviour have been

suggested using these materials. Such an LB film has been suggested for use as a microlithographical resist[39], since exposure of the monomer film to suitable UV or electron beam radiation results in polymerisation of the alkene function. In addition the prerequisites for applicable materials, i.e. solubility in organic solvents, surface stability and so on, are met.

Unfortunately, systematic studies of LB films in an attempt to yield structure-property correlations have been sparse, compared to random studies using available materials. To date, there are no important industrial applications of Langmuir-Blodgett films in use. It is significant, however, that the level of financial investment, even in the general field of organic molecular solids, is still a small fraction of the sum being devoted to inorganic semiconducting materials.

1.4.2 The Langmuir-Blodgett Film.

Surface-active molecules can form *Langmuir films* on an aqueous surface. This film can often be transferred to a solid substrate, forming a *Langmuir-Blodgett film*. The hydrophobic part of the molecule is insoluble in water whereas the hydrophilic part is strongly attracted to water; therefore, the molecules sit at the air/water interface.

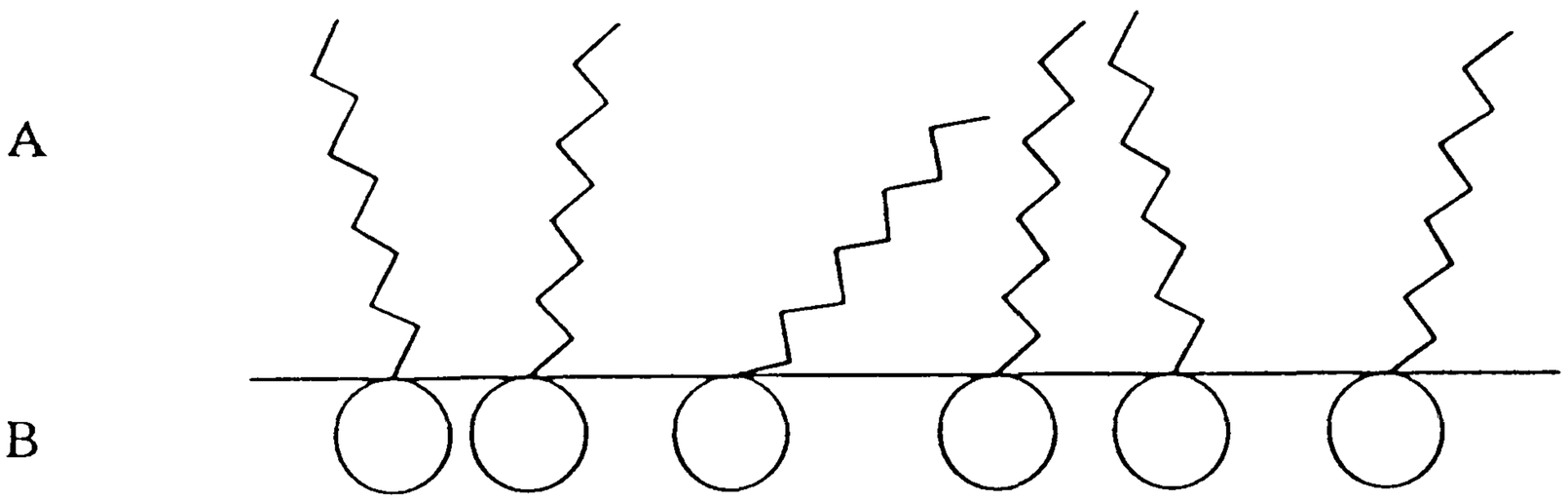

Figure 3. Position of molecules at air/water interface for a Langmuir film, (A) hydrophobic part, (B) hydrophilic part.

Langmuir films are commonly formed by dissolving a surface-active material in a suitable solvent and by spreading the solution onto the surface of the pure water subphase. The solvent should be pure, and capable of dissolving sufficient material. It is preferable that the solvent is volatile and ideally it should be immiscible with water. Commonly used solvents are chloroform, dichloromethane and n-hexane.

After evaporation the attraction between the water molecules and the hydrophilic groups will have the effect of pulling the monomolecular layer into the bulk of the aqueous phase. This gives rise to *surface tension*. This is defined as "the work required to expand the surface isothermally by unit area" and has units of mN m^{-1}. Since surface-active molecules expand the surface they lower the surface tension. If the area that the molecules occupy at the surface is reduced then the surface tension will be further reduced. This reduction is denoted as *surface pressure* (π).

The surface pressure versus area (π-A) *isotherm* can provide valuable information concerning the surface properties of the material. An example of a π-A isotherm is shown in Figure 4 for the Langmuir film forming material, stearic acid, and the important regions are shown in figure 5.

When there is no external pressure applied to the subphase, the molecules act as a *two-dimensional gas*. The initial compression will cause a slight increase in surface pressure as the molecules are pushed together. Upon further compression there is a transition to a *two-dimensional liquid phase* where small changes in area per molecule cause significant increases in surface pressure. Finally the slope increases to near vertical. This represents a transition to an ordered *two-dimensional solid phase* characterized by a steep, approximately linear relationship between surface pressure and molecular area. Strictly speaking this isotherm should be described as a *liquid condensed* film[40]. This is because materials can also exhibit isotherms with a different shape. In these there are no clear phase transitions and the "area per molecule" remains at values much higher than those required for close packing. This type of film is known as *liquid expanded*.

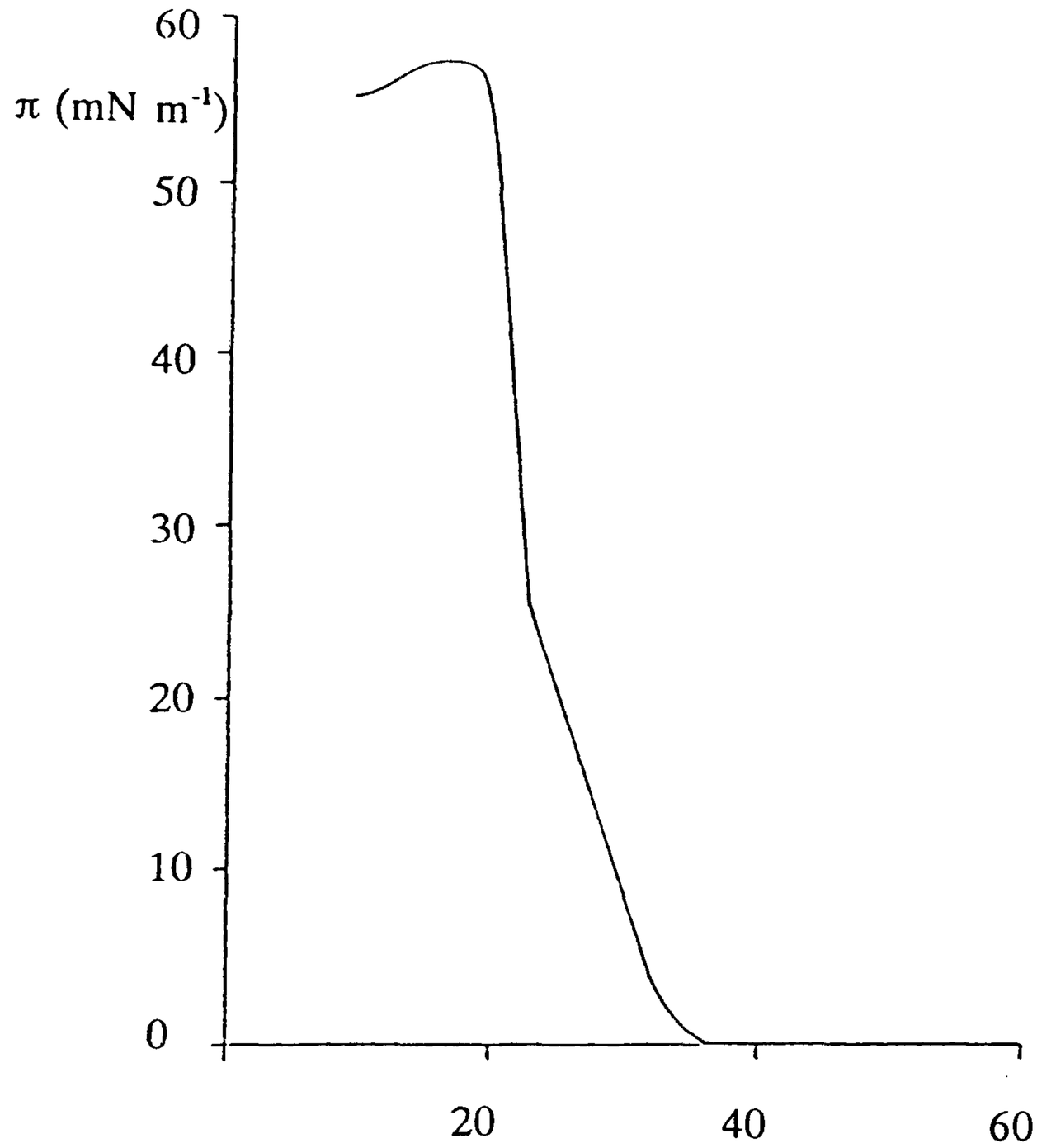

Figure 4. Pressure-area isotherm of stearic acid[40].

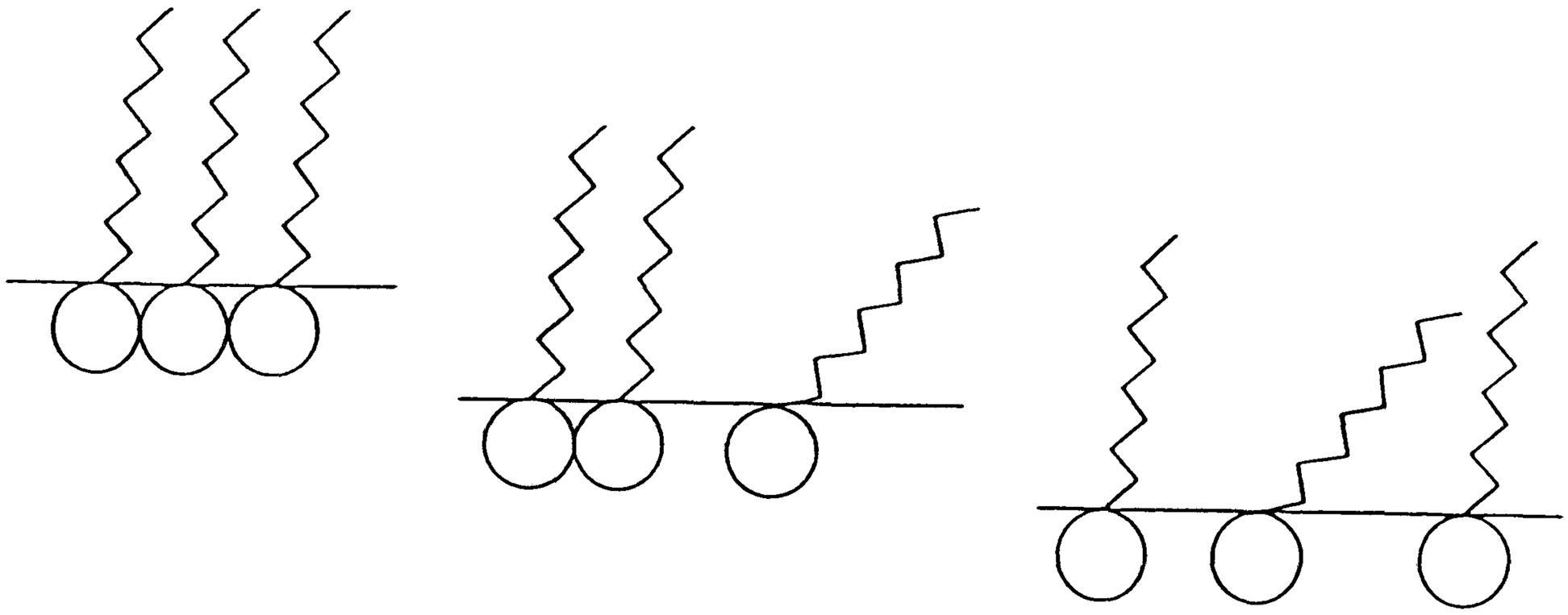

Figure 5. Three phases observed when compressing a Langmuir film[41]; (A) 2D solid, (B) 2D liquid, (C) 2D gaseous.

Extrapolation of the isotherm indicates the area per molecule that the material would occupy as an non-compressed, close-packed layer. For stearic acid this corresponds to approximately 22 $Å^2$ $molecule^{-1}$. This is similar to the cross-section of stearic acid molecules in a single crystal[42], thus supporting the two-dimensional solid theory.

Eventually the forces exerted upon the monomolecular layer become too strong for confinement in two dimensions and *collapse* occurs. The collapse pressure can be defined as the maximum to which a monolayer can be compressed without the detectable expulsion of molecules from the Langmuir film. The onset of collapse is dependent upon factors such as the rate of compression and history of the film. Collapse is believed to usually result in molecular layers riding on top of each other and forming multilayers.

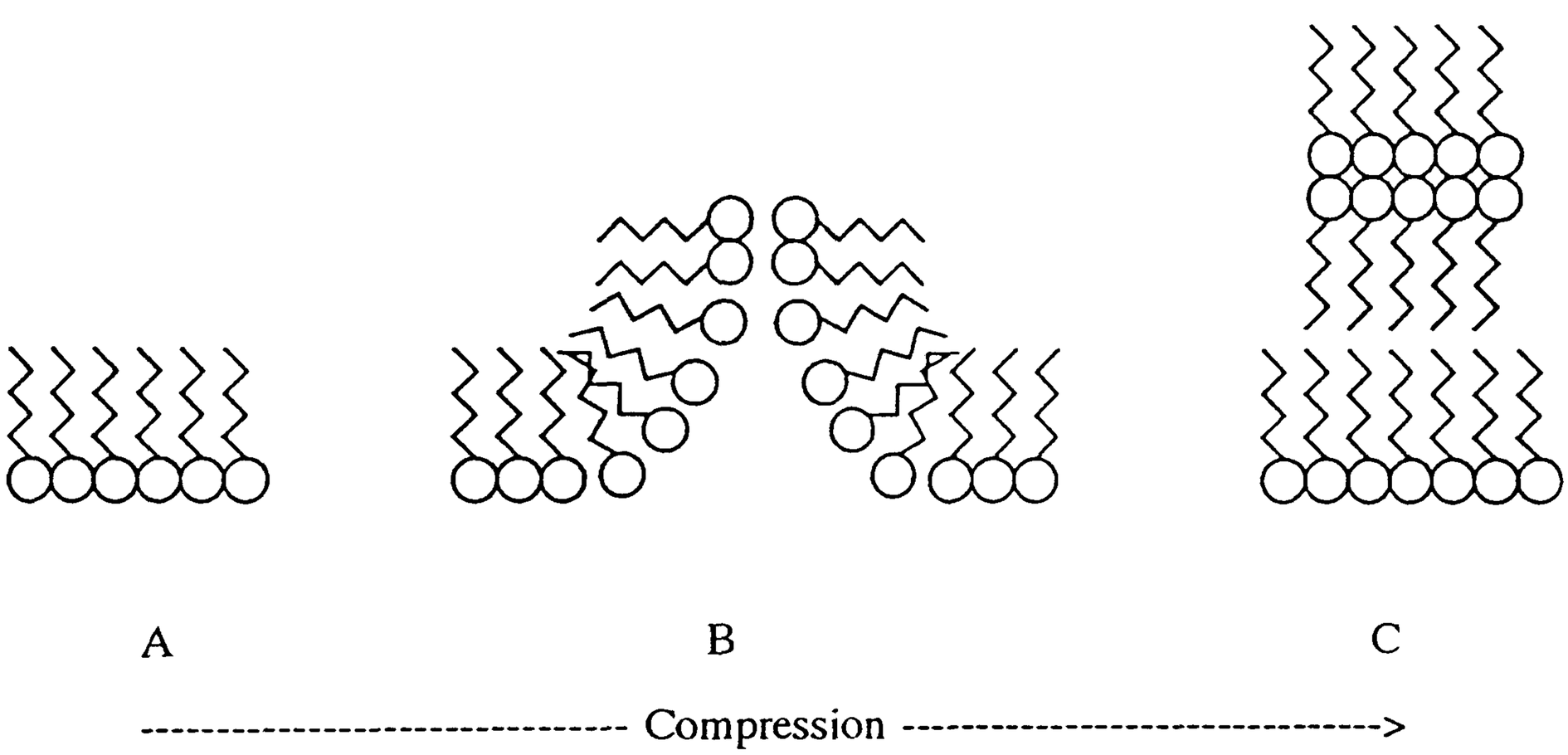

Figure 6. Monolayer collapse[41]: (A) 2D solid; (B) onset of collapse; (C) multilayer formation.

Characteristics including collapse pressure, range of two-dimensional solid phase and stability of monolayer at constant pressure, have to be determined so that conditions for transfer to a substrate can be optimised.

Langmuir-Blodgett film transfer is achieved by passing a suitable substrate through a compressed Langmuir film. The material is transferred to the substrate as a monolayer because of the attractive forces between the substrate and material. Treatment of the substrate so that it is either hydrophobic or hydrophilic dictates the method of deposition.

Transfer onto a hydrophilic substrate can occur when the substrate is passed vertically up through the air/water interface. The direction of the meniscus allows direct contact between the hydrophilic end group and the hydrophilic substrate.

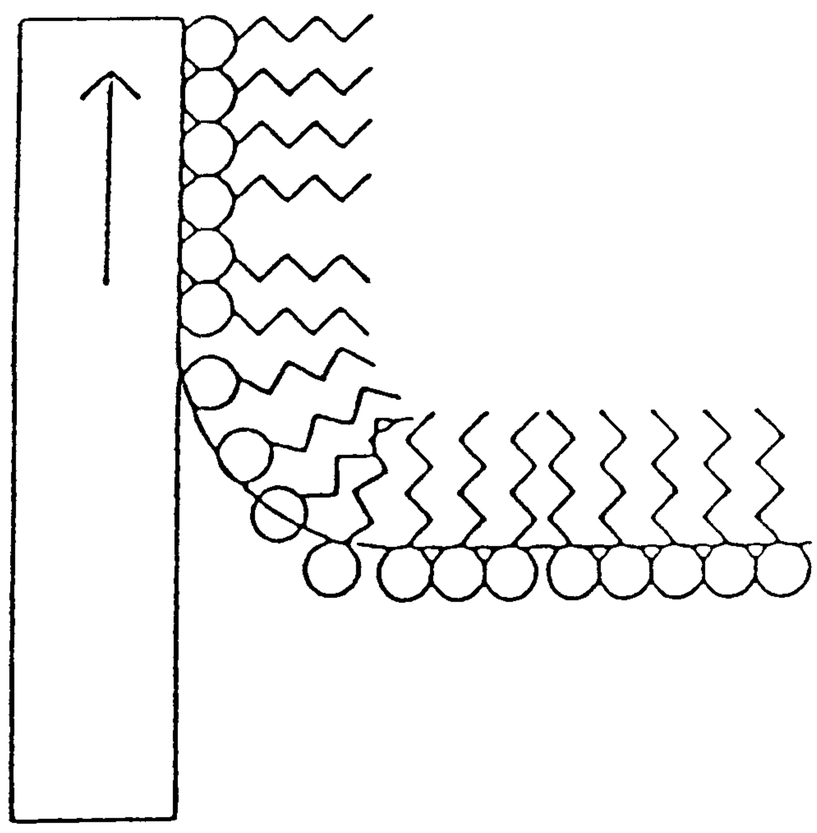

Figure 7. Transfer of a monolayer onto a hydrophilic substrate[41].

Transfer onto a hydrophobic substrate occurs in the opposite sense (see figure 8). The substrate will cause the meniscus to dip below the level of the water surface and wet the substrate at a wetting angle of 180°. This allows direct contact between hydrophobic tail and hydrophobic substrate.

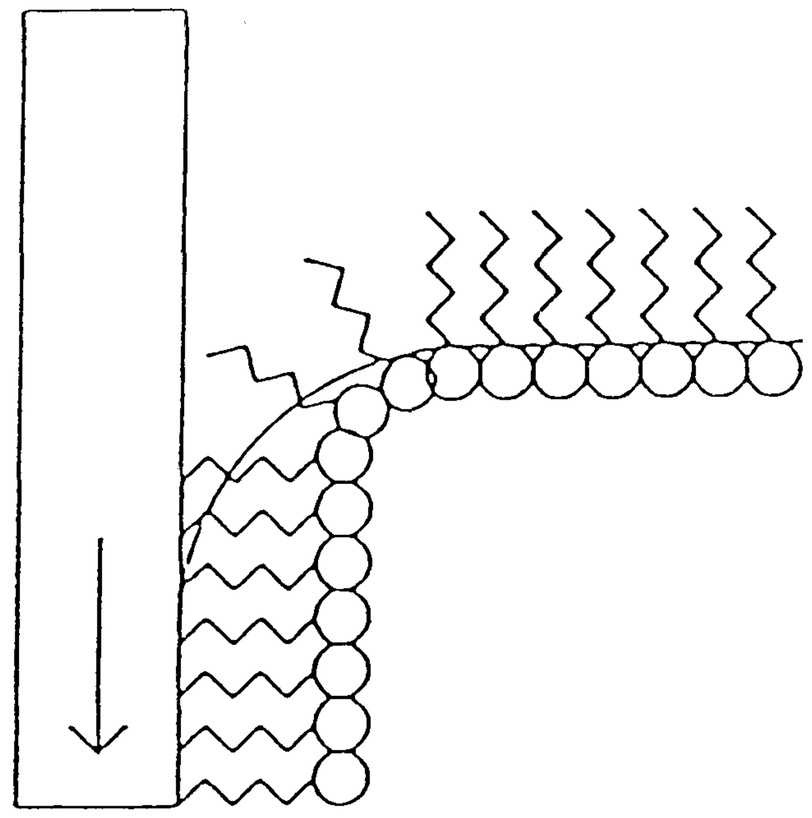

Figure 8. Transfer of a monolayer onto a hydrophobic substrate[41].

These methods are used in the majority of LB deposition procedures. A novel alternative method is the "Langmuir and Schaeffer method"[43], in which the hydrophobic substrate is placed flat on top of the Langmuir film. In this way the hydrophobic tails have direct contact with the substrate.

Multilayer deposition follows the general rules of upstroke and downstroke deposition. *X-type* multilayers are assembled on hydrophobic substrates by repeated deposition on the downstroke only (figure 9). *Z-type* multilayers are assembled on hydrophilic substrates by repeated deposition on the upstroke only (figure 10). There are two methods of *Y-type* multilayer deposition. In the first method a monolayer is transferred on to a hydrophilic substrate leaving the hydrophobic tails uppermost. Deposition then proceeds as for a hydrophobic substrate resulting in the hydrophilic head groups of the second layer being uppermost. Deposition continues as for a hydrophilic substrate and so on, producing a multilayer film with adjacent layers aligned in opposite directions (figure 11). The second method is the same as the first except that the first monolayer is transferred on to a hydrophobic substrate.

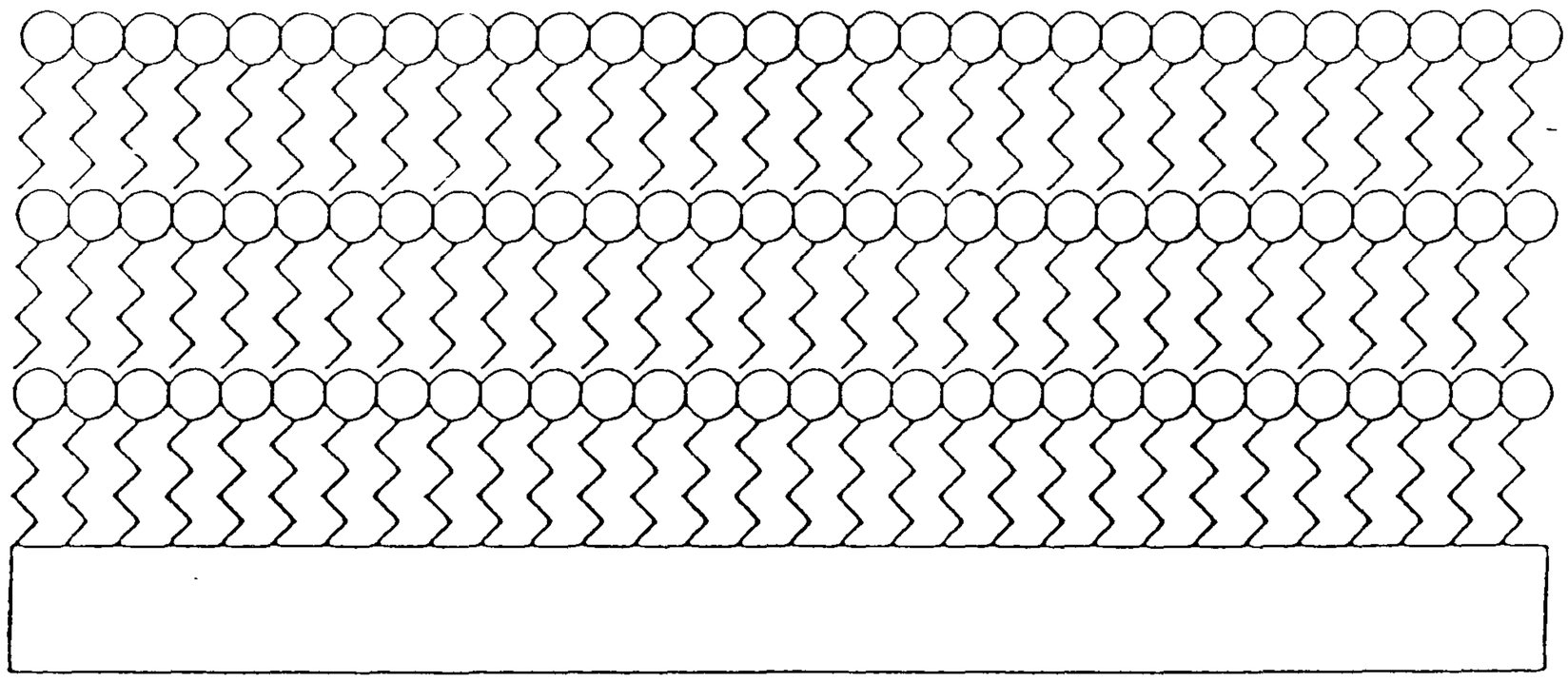

Figure 9. X-type deposition onto a hydrophobic substrate[41].

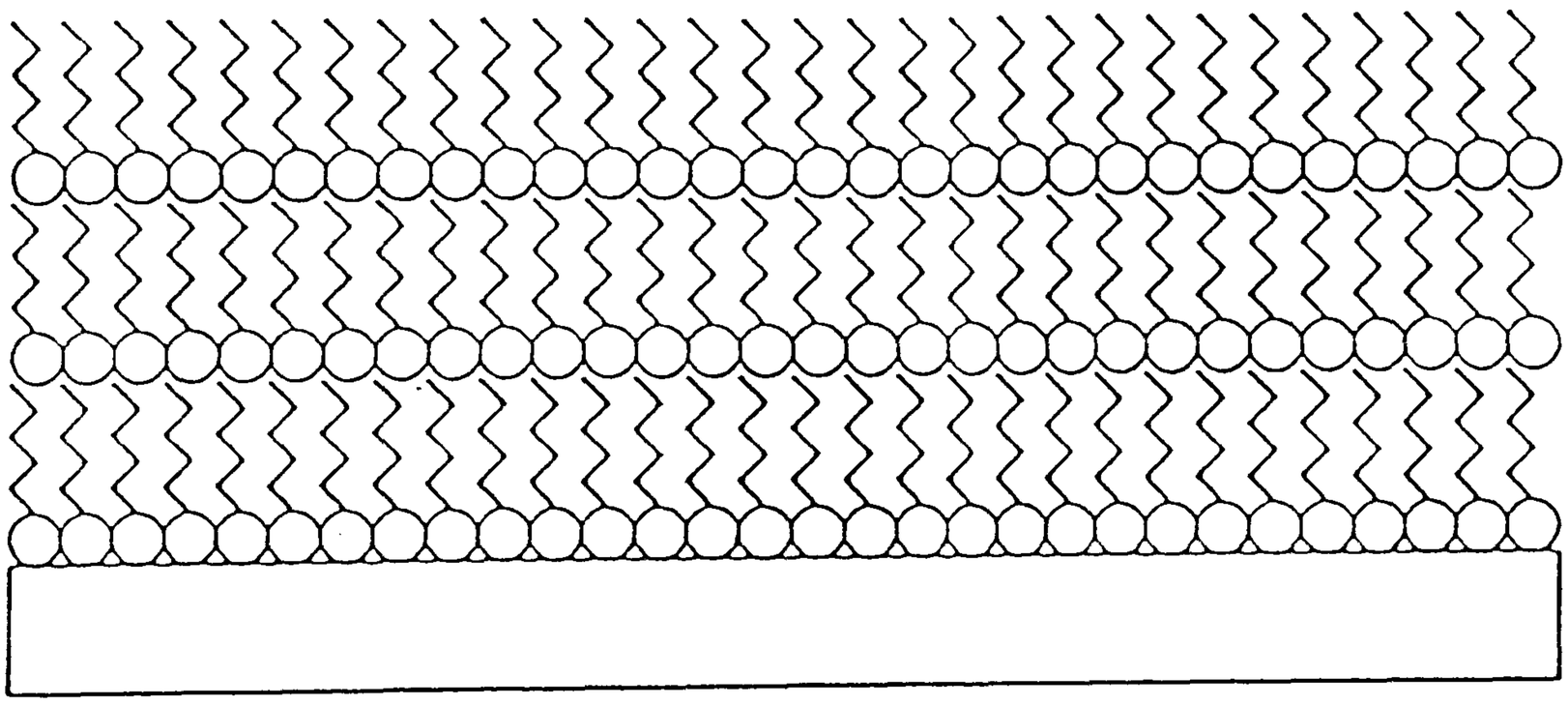

Figure 10. Z-type deposition onto a hydrophilic substrate[41].

X and Z-type multilayers are more difficult to fabricate. This is because the molecules are being forced to align with hydrophobic and hydrophilic parts adjacent to each other. If this type of deposition is successful it is often found that the multilayer is quite unstable. Y-type films, however, are energetically more favourable and therefore easier to fabricate.

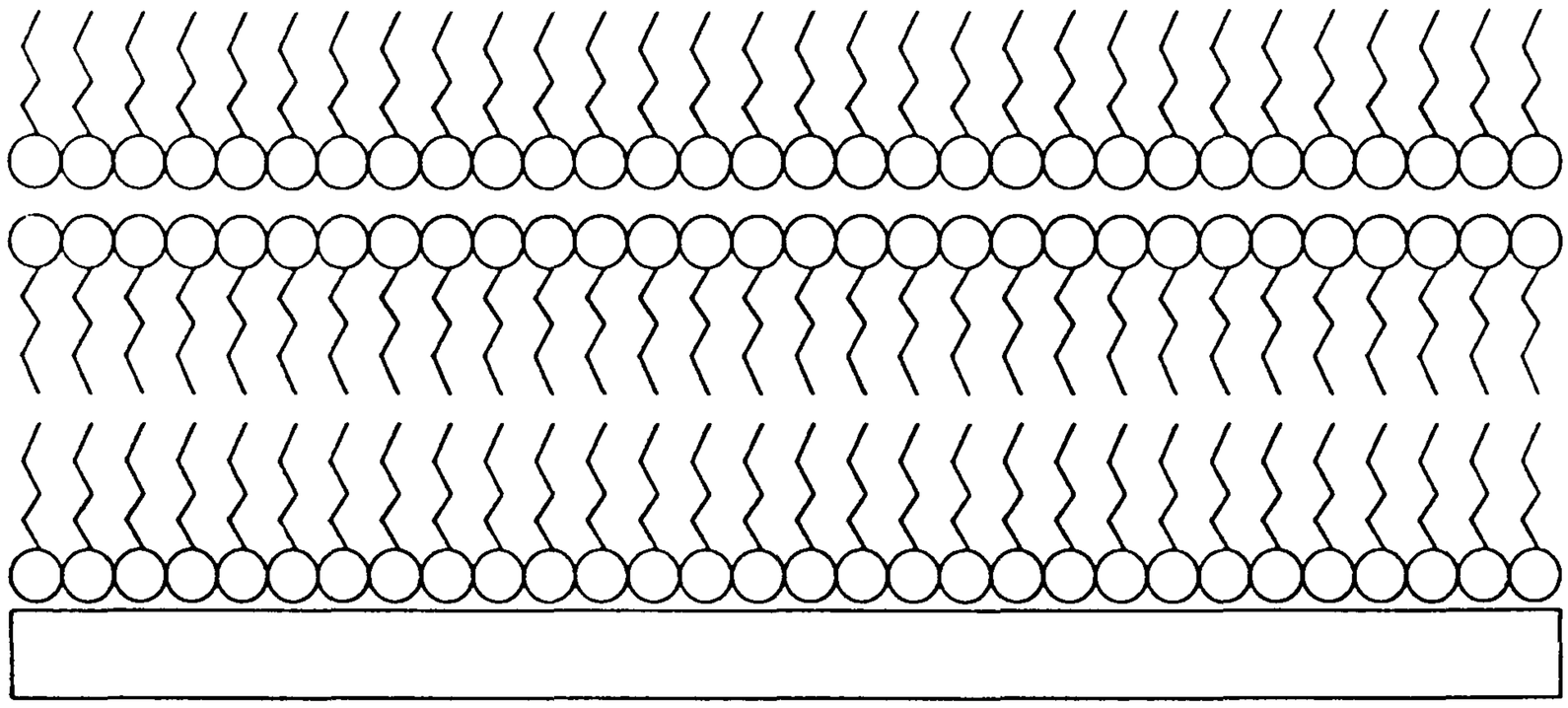

Figure 11. Y-type deposition onto a hydrophilic substrate[41].

Materials are usually transferred in the two-dimensional solid phase, although they can be deposited in the two-dimensional liquid phase or from the liquid expanded isotherm. There are few examples of deposition from pressures outside the range 10 to 40 mN m^{-1}. Constant pressure is maintained by a compression mechanism which is sensitive to the pressure drop as the material transfers to the substrate. The rate at which the substrate can be passed through the water depends on the dynamic properties of the monolayer. This is typically about 1 mm s^{-1}. It should be noted that there is an initial water layer between the substrate and film which must drain away or evaporate before transfer is complete.

A measure of the extent of deposition is the transfer ratio. This is the ratio of the area of monolayer removed from the water surface to the area of substrate covered by the material. If transfer ratios of unity are achieved one can assume that the orientation of molecules on the slide to be very similar to that on the water. Differences between the two orientations are indicated by large but consistent deviations from unity, poor film deposition is indicated by inconsistent transfer ratios.

1.5 Potential Applications of Langmuir-Blodgett Films

The majority of work published on LB films in the past fifteen years has focused on the possible uses for the resultant film. The following is a synopsis of the most important applications suggested for LB films in this period, but as this thesis concerns the characterization of optically nonlinear materials, the other areas are only outlined in the briefest detail.

1.5.1 Devices Utilizing Electrical or Electronic Properties

A number of properties have been studied in an attempt to improve upon the existing methods used in this field.

Conductivity. The enforced anisotropy of LB films makes any conductivity more attractive. Most reports concentrate on synthesising surface active analogues of known conducting materials[44,45,46]. The understanding of conductivity in LB films is complicated by the fact that difficulties arise from either imperfect electrodes or monomolecular assemblies containing a large number of defects. Extensive studies on charge transfer salts of tetracyanoquinodimethane (TCNQ) and tetrathiofulvalene (TTF) have resulted in LB films with conductivities in the range 10^{-2} to 10^{1} Scm^{-1}, in the plane of the film[47]. These values are comparable in order to weakly doped semiconductors. Polypyrrole and ferrocene LB films also exhibit a modest conductivity[48,49]. It has been shown that anthracene monolayers with short hydrophobic chains have a resistivity in the plane that is eight orders of magnitude higher than that in the film normal direction[50,51,52]. This exemplifies the way that LB films can enhance the properties of materials.

Insulation. Simple calculations based on applying a few volts across 100 $Å^2$ of organic material show the enormous charge storage capability of

metal-oxide | LB film | metal systems[53]. The criterion of thermal stability is very important for this application. Polymerised multilayers are therefore the most suitable materials. One approach involves the removal of the hydrophobic chain after deposition, in this way long alkyl amine salts are transferred then converted to polyamide[54]. To date, however, there are no reported LB films that can rival the thermal stability of established inorganic materials.

Photoelectronic. Studies of photoconductivity, photovoltaic and photomagnetic effects in LB films have not succeeded in producing applicable systems. They have, however, enabled further understanding of intermolecular interactions and photophysical and photochemical processes in organic materials. The studies on sensitizers by Kuhn are an example of this[36,37], so is the photopolymerisation of diacetylene films by surface active dyes in multilayer films[55]. The method by which sensitizing dyes work has been understood further by LB film studies of merocyanine, cyanine and oxonol[56-58].

Pyroelectric. The first report of pyroelectricity in LB films was an X-type multilayer of amphiphilic azoxy compounds[59]. At present the best reported LB film systems possess pyroelectric coefficients of less than 5 $\mu Cm^{-2}K^{-2}$ [60-62]. This contrasts with a value of 30 $\mu Cm^{-2}K^{-2}$ for poly(vinylidene fluoride)[63]. The consensus is that an increase in pyroelectric coefficient of approximately an order of magnitude will be needed before LB films become serious contenders for use in infrared imaging systems[64].

Rectification. Asymmetric current versus voltage behaviour has been recorded for a number of metal | LB film | metal structures[65,66]. This confirms the prediction by Aviram and Ratner that an asymmetric molecule containing the appropriate donor and acceptor groups separated by a short sigma-bonded bridge should exhibit diode characteristics[67].

Many reports of rectification are open to speculation because of the experimental method used. For example, observations using scanning tunnelling microscopy using a gold substrate are inconclusive because of the conducting surface[68]. Donor-acceptor materials that are bridged by a π-bond may also exhibit rectification as an LB film, although the observations may be due to permanent dipole moments[69]. As a result it has not yet been proven unequivocally that molecular rectification occurs in LB films.

1.5.2 Gas Sensors

Organic molecules can be synthesised so that they selectively recognise certain functions. To understand the use that LB films has in this field it is important to note the three distinct stages in a sensor[70].

A) Recognition - a specific interaction between a molecule and the sensing surface.

B) Change - the binding process must result in a detectable and systematic change in a physical parameter.

C) Transducing - the change must be converted to an observable signal.

Some examples of the methods by which LB films have been used to detect gases are given below.

Conductivity. LB multilayer films of phthalocyanine complexes have been shown to detect gases such as NO_x[71,72], NH_3[73,74], halogens and more recently, hydrazine[75] and organophosphorus vapours[76]. Porphyrins are able to detect NO_2 down to a few parts per million[77]. Both work by changes in conductivity upon exposure. The long response times of these have been improved upon by the use of the completely reversible system of TCNQ LB films, when exposed to NH_3[78].

Optics. Surface plasmon resonance is currently being studied extensively as a sensitivity tool[79-85]. Surface plasmons are electromagnetic waves at

the interface of a metal and a dielectric. Their excitation is influenced by changes in the properties of the dielectric layer in close proximity to the interface. Therefore LB films are ideally suited for this system. The most popular metal/dielectric is a silver/glass prism combination. Once parameters such as wavelength of incident light, refractive index of the glass, and thickness of the metal and organic layer have been optimised, the system can be exposed to the vapour being detected. Any changes in the resonance condition accompanying surface adsorption of the vapour results in the incident angle for peak resonance increasing. Substituted phthalocyanine LB films exhibit this property when exposed to acceptor gases[86].

Acoustoelectric. Quartz crystals coated with LB films of ω-tricosanoic acid and a substituted phthalocyanine have been shown to detect the presence of NH_3 and H_2S down to 1 ppm[87]. This was achieved by the change in resonant frequency that occurred upon interaction. Surface acoustic wave oscillators currently use quartz or lithium niobate. There is a possibility of using piezoelectric LB films to launch the surface waves, however all reported values of piezoelectric coefficients in monolayers are currently too small.

1.5.3 Biological Sensors.

Monomolecular films are very similar to biological membranes. Phospholipids, which constitute a significant proportion of biological structure, may form condensed monolayers at the air/water interface. It is even possible to build up LB multilayers of some of these compounds[88]. Some proteins have also being incorporated into multilayers[88]. Therefore the LB technique offers itself as a convenient means of building up artificial biological membrane structures. Stability requirements hinder many membrane analogues that have been studied. However some systems have shown great

potential[89-92] and the enzyme glucose oxidase (GOD) in LB film form has been used as the basis of a solid state glucose sensor[70]. Absorption of antibodies to membrane bound antigens alter the potential across the membrane. As a consequence biologically interesting species have been sensed on LB films. The enzyme is immobilised onto the head groups of a lipid. The LB technique is used to transfer the mixed layer onto chromium/gold electrodes. The electrode system is biased and the resulting current is a direct measure of the H_2O_2 concentration generated by the reaction:

$$C_6H_{12}O_6 + O_2 \xrightarrow{\text{GOD}} C_6H_{10}O_6 + H_2O_2$$

Changes in output current have been studied for the adsorption of enzyme glucose oxidase on two layers of cadmium arachidate[70]. Also, antigen concentration during deposition of an antibody can be detected by the fluorescence of the specific antibody[93].

1.5.4 Optics

There has been extensive work carried out in the field of LB films for applied optics. The three main areas of interest are detailed below.

Waveguide. In the simplest waveguide the guiding film is required to have a higher refractive index than those of the materials lying adjacent to it. This is so that light incident from within the film on to either of its boundaries will undergo total internal reflection. If the guiding film is thick enough for transverse constructive interference to occur, then light can be propagated over distances limited only by absorption of the field or by scattering due to defects, imperfections etc[93]. Loss due to scattering needs to be less than 1 $dBcm^{-1}$. Notable results for an LB waveguide have a measured attenuation of 11 $dBcm^{-1}$ in a relatively thick film of

preformed polymer[94]. Thick films of the DCANP material have achieved attenuation coefficients down to 12 $dBcm^{-1}$ measured at 633 nm[95]. There has been extensive studies of LB films of polydiacetylene, but they give enormous losses due to scattering[96,97].

Nonlinear optics. The property of fabricated single layer or multilayer films to generate nonlinear optical effects has created great interest. Second harmonic generation from LB films is of particular interest to this study and is discussed in detail in section 1.6. A substantial amount of work has been carried out investigating electro-optical effects from LB films[98,99], but the number of films exhibiting this is a small fraction of those studied. Success has been achieved with films of hemicyanine derivatives[100], stilbazolium dyes[101] and functionalised diarylalkynes[102]. In theory, third harmonic effects are much easier to study in LB films since the criteria of noncentrosymmetricity that constrains second order effects is not applicable. Diacetylene based LB films[103,104] exhibit cubic susceptibility that is larger than that of gallium arsenide, an established inorganic crystal for third harmonic generation (THG). Other materials such as merocyanine and stilbazonium dyes as LB films also exhibit THG[105,106].

Optical data storage. There are various elaborate mechanisms by which LB films may be employed for this process. One method exploits the photoelectrochemical properties of an LB film of 4-octyl-4'-(5-carboxypentamethyleneoxy)azobenzene[13]. The system can be converted photochemically or electrochemically between three chemical states. The system provides a potential storage process that allows for ultra high storage density, multi-function memory and non-destructive information readout. The *trans* form of the azobenzene is deposited as an LB film. The less stable *cis* form may be electrochemically reduced to hydrazobenzene; this is stable in an inert atmosphere but may be

electrochemically oxidised to the *trans*-azobenzene. Another method is to make use of the ability of some LB film forming aggregates. In one example the narrow absorption bands of red-shifted aggregates (J-aggregates) of some organic molecules are employed[107]. The LB film is a mixture of methyl stearate and dioctadecyl-dimethylammonium chloride. The laser light disorders the structure of the aggregates, thereby diminishing them and reducing the absorption band. When the film was deposited on to an aluminium reflective layer, the structural change could be restricted to a single recording layer. LB films of a novel zwitterion show promise as possible systems for photochromic data storage[14]. The absorption bands of LB monolayers of Z-ß-(1-hexadecyl-4-pyridinium)-α-cyano-4-styryldicyanomethanide and its quinolinium analogue are very sharp at 495 and 565nm respectively. These bleach when irradiated at wavelengths which overlap the bands, the process being reversible in solution but irreversible in the films. Thus they have a potential use as components of a multiple frequency write once/read many (WORM) memory.

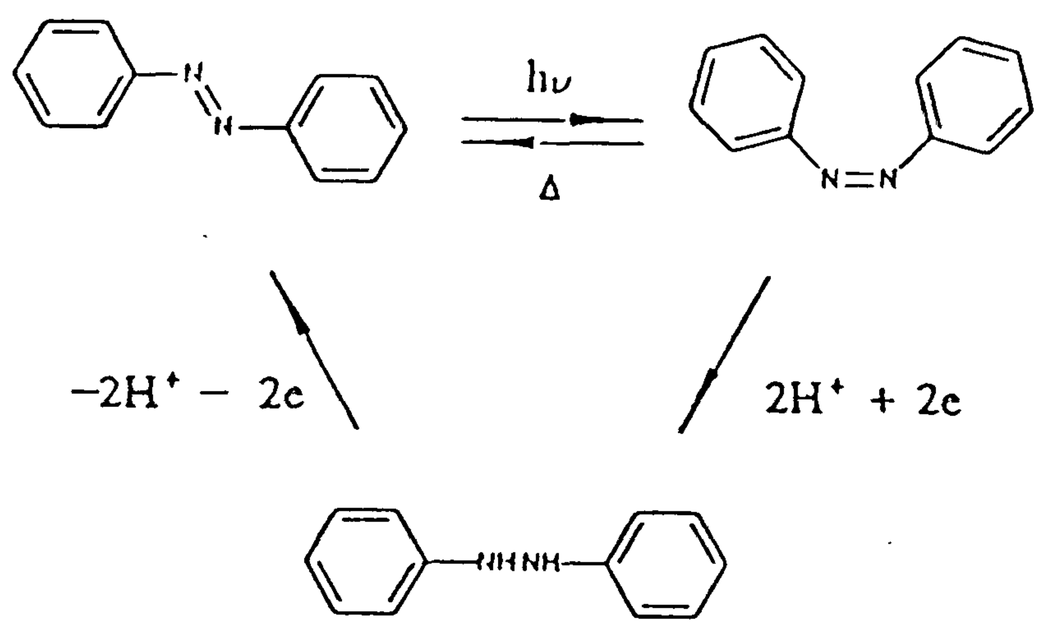

Figure 12. Photoisomerisation of an azobenzene followed by electrochemical reduction[13].

1.5.5 Other Potential Applications

The role of passive thin films in the electronics industry has been studied. In electron beam lithography a resolution better than 10 nm has been demonstrated for an LB film multilayer of a simple fatty acid salt[108]. These molecules disappear when irradiated due to sublimation and therefore the film is regarded as a positive resist. No organic systems are yet capable of challenging the established inorganic ones, however LB deposition will be well positioned once feature sizes reduce to 1μm in the semiconductor industry.

There are many other suggested applications of LB films and the most promising are summarised below.

LB films could be used to coat metal oxide layers thus sealing defects in the oxide layer[109]. The laser ablation of LB films of a phenylhydrazone dye, an amide and a prepolymerised polycondensate have been shown to be a clean and precise method that could be a viable technique for lithography[110]. Langmuir films of two component octadecanol/polymerised surfactant monolayers have been shown to control the evaporation of water[111]. Hemicyanine dye monolayers can be used to align nematic and smectic liquid crystals, although the thermal and mechanical stability of the system needs to be improved to produce a worthwhile lifetime[112]. Langmuir films of C_{60} have been deposited[113], and shown to be stable and rigid with a high degree of structural organisation[114]. LB films of C_{60}:$C_{18}H_{37}OH$ have been fabricated[115] and LB films of C_{60} on its own have recently been prepared although they are more stable when mixed with eicosanoic acid[116]. This is a good example of how the Langmuir-Blodgett technique can be used to enable the investigation of new materials.

At present the only LB film structure that is commercially available is a large area tritium standard source[64]. This is fabricated from monolayers of tritiated fatty acid deposited onto aluminium substrates.

1.6 Second Harmonic Generation from Langmuir-Blodgett Films

Many groups have investigated the second-harmonic (SH) intensity from LB films. The methods of fabrication vary slightly, as does the method of SH measurement, therefore direct comparison of different work is difficult. Section 2.2 details how SH response was measured in this work, which is similar to the general method that has been used in the majority of studies reported.

1.6.1 Early Reports of Monolayer SHG

I

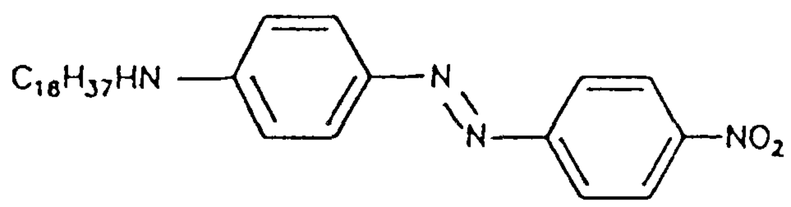

II

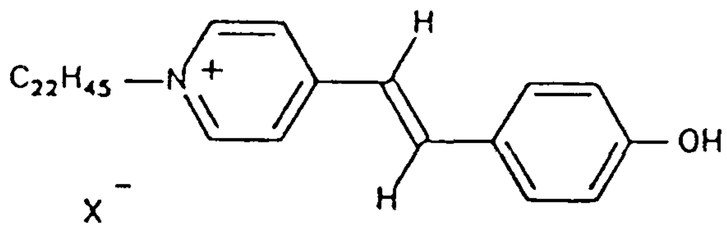

III

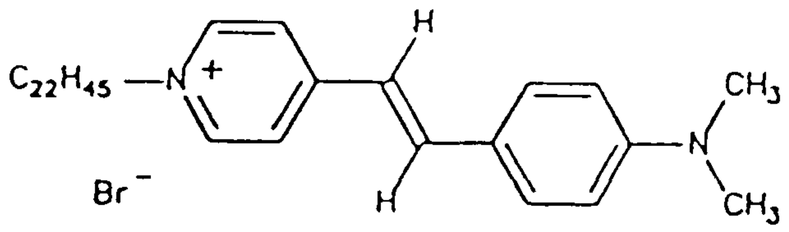

Figure 13. **(I)** 4-N-octadecylamino-4'-nitroazobenzene[117,118]; **(II)** E-1-docosyl-4-{2-(4-hydroxyphenyl)ethenyl}pyridinium halide[119,120]; **(III)** E-1-docosyl-4-{2-(4-dimethylaminophenyl)ethenyl}pyridinium bromide[121].

The first report of SHG from an LB film in 1983 gave a second order susceptibility $\chi^{(2)}$ of 4.2 x 10^{-8} esu for 4-(N-octadecylamino)-4'nitroazobenzene, **I**[117,118]. This has the same order of magnitude as lithium niobate crystals. A larger second order

response was later observed from LB monolayers of a merocyanine dye, **II**[119,120]. Unfortunately, the SHG is suppressed by protonation and it was necessary for the sample to be mounted in a cell containing ammonia vapour. An important early report of SHG was that of Girling et al[121] in 1985, in which a hemicyanine dye, **III**, was first used for LB film fabrication.

It is interesting to compare the SHG data for monolayers of **II** and **III**. **II** has a resonantly enhanced ß because its absorbance cut off is 650 nm. **III** also exhibits resonant enhancement but the effect is smaller because its absorbance cut off is at 590 nm. This makes the hemicyanine, **III**, more desirable for applications, especially since exposure to air does not cause deterioration of the signal.

Material	Type of LB film	Reported SHG data
I	Monolayer	$\chi^{(2)} = 1.8 \times 10^{-11}$ m V^{-1}
II	Monolayer	ß = 4.0×10^{-47} F m^3 V^{-1}
III	Monolayer	ß = 3.8×10^{-48} F m^3 V^{-1}

Table 1. Reported optical coefficients for **I**, **II** and **III**[117-121].

1.6.2 Molecular Structure and SH Response

There have been various attempts to correlate molecular structure with SH response from an LB monolayer. In one such study, analogues of the optically active hemicyanine **III** were prepared and their general structure is shown in figure 14[122]. They are stable to laser damage for a C_{14} chain or longer. Measurements indicate a large tilt angle leading to significant cancellation of separate molecular contributions. The SH

response is similar to that of **III**, as expected since the donor and acceptor parts are similar and the same distance apart.

IV

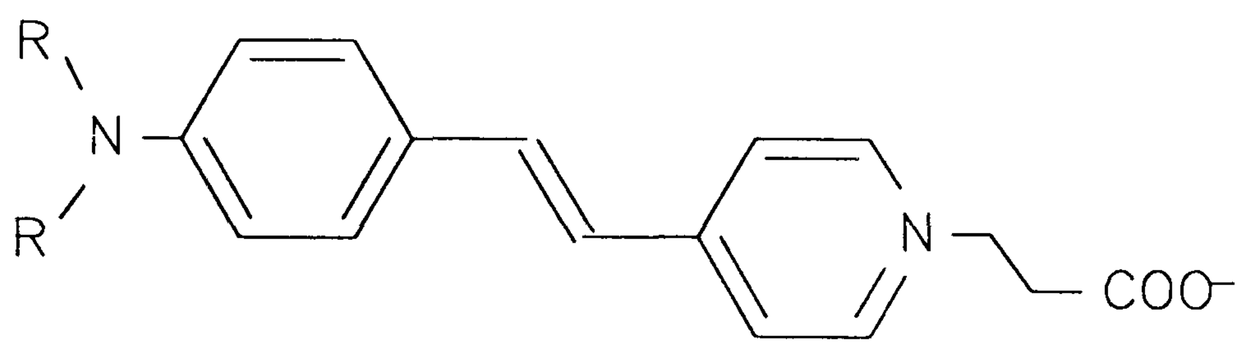

$R = C_6H_{13}; C_{10}H_{21}; C_{14}H_{29}; C_{18}H_{37}$.

Figure 14. Basic structure of **IV**: E-1-(2-carboxyethyl)-4-{2-(4-dialkylaminophenyl)ethenyl}pyridinium hydroxide dyes[122].

Material	Type of film	Reported SHG data
IV ($R = C_{18}H_{37}$)	Monolayer	$ß = 4.0 \times 10^{-50}$ F m^3 V^{-1}

Table 2. Approximate SH response of stable monolayers of **IV**[122].

Another study of this nature arose from the desire for molecules which have their donor-acceptor groups oppositely aligned to that of **III**[101]. Initial studies of the monolayers of **V** and **VI** have shown that one cannot simply predict the relative intensity of SH signals from the molecular structure. The N-stilbazene, **V**, unexpectedly has a SH response larger than hemicyanine; tilt angle studies show **III** to have a very similar alignment ($\theta = 22°$), and therefore, the difference must be due to deleterious local fields in the films that enhance the effective hyperpolarizability. Also, the larger dielectric constant at 532 nm for N-stilbazene should result in greater resonant enhancement. The difference in tilt angle between O-stilbazene and N-stilbazene probably causes the difference in their SH responses.

V

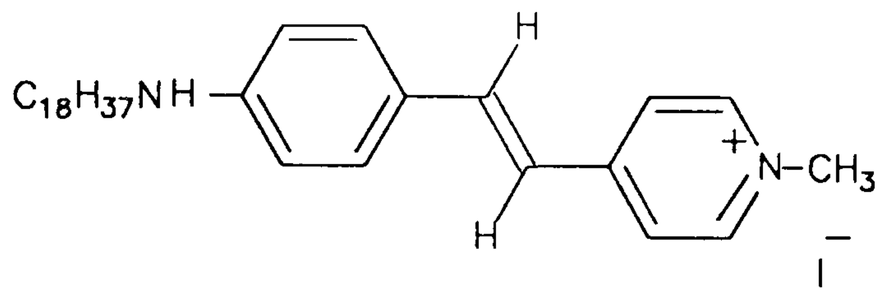

VI

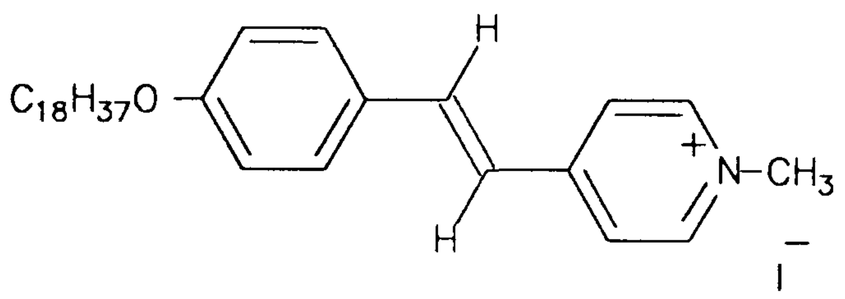

Figure 15. (**V**) E-1-methyl-4-{2-(4-octadecylaminophenyl)ethenyl}pyridinium iodide; (**VI**) E-1-methyl-4-{2-(4-octadecyloxyphenyl)ethenyl}pyridinium iodide.

Material	Type of film	Reported SHG data
V	Monolayer	SH intensity = 7.5 (x **III**) $\theta = 24°$
VI	Monolayer	SH intensity = 0.33 (x **III**) $\theta = 34°$

Table 3. SHG data for two stilbazene dyes[101].

These monolayer studies have been extended to include **VI** and four other phenylhydrazone or stilbazonium salt dyes, seen in figure 16[123-125]. Their monolayer SH response and estimated tilt angles are shown in table 4.

VII

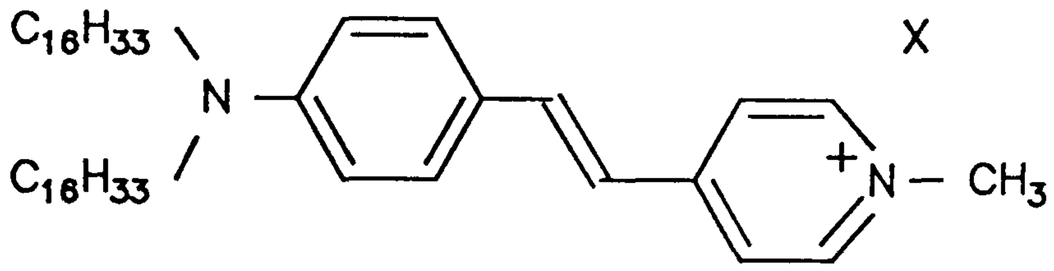

VIII

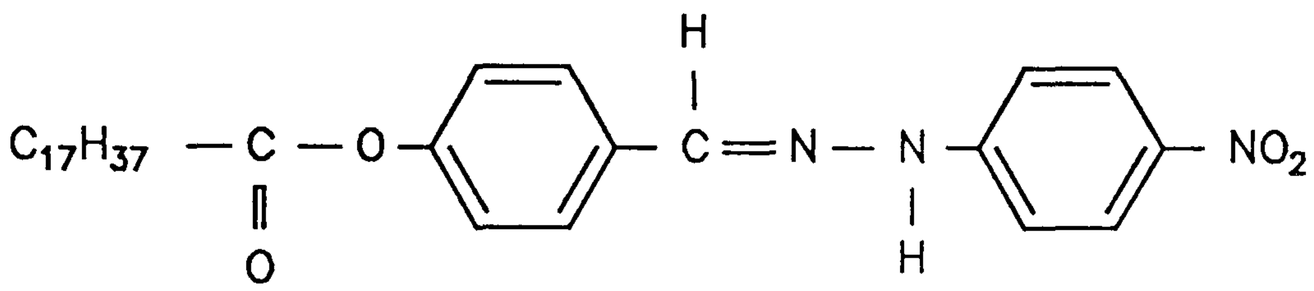

IX

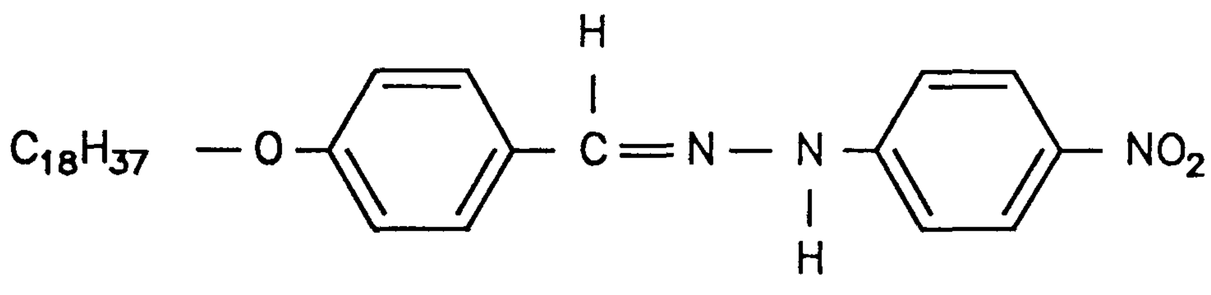

X

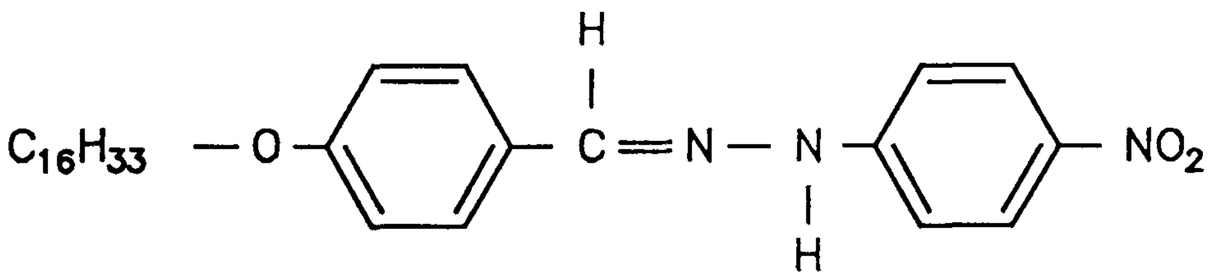

Figure 16. Phenylhydrazone and stilbazonium LB film forming materials[123-125].

The slightly larger response of **IX** to **X** may be explained by the slightly larger inductive effect of a $C_{18}H_{37}$ chain compared to a $C_{16}H_{33}$ chain. This is despite **IX** being inclined further away from the normal. The poor result of **VIII** compared to **IX** and **X** is indicative of the poor electron donor characteristics of the ester group.

Material	Type of film	Reported data ß / F m^3 V^{-1} $\chi^{(2)}$ / m V^{-1}	Tilt Angle
VI	Monolayer	ß = 5.6 x 10^{-49} $\chi^{(2)}$ = 2.1 x 10^{-10}	θ = 50°
VII	Monolayer	ß = 7.4 x 10^{-48} $\chi^{(2)}$ = 2.6 x 10^{-9}	θ = 50°
VIII	Monolayer	ß = 4.1 x 10^{-49} $\chi^{(2)}$ = 2.4 x 10^{-10}	θ = 65°
IX	Monolayer	ß = 1.5 x 10^{-48} $\chi^{(2)}$ = 7.6 x 10^{-10}	θ = 60°
X	Monolayer	ß = 1.2 x 10^{-48} $\chi^{(2)}$ = 7.2 x 10^{-10}	θ = 55°

Table 4. SHG data for phenylhydrazone and stilbazonium salt LB films[123-125].

The much larger response of **VII** compared to **X** is due to various factors:

1. better quality films result from molecules containing two chains;
2. the strong electron donor character of the dioctadecylamino group compared to the octadecyloxy group;
3. the lower electron donor character of the methyl group;
4. the absence of resonant enhancement between the SH and the first absorption peak of **X** which lies at 360 nm.

It is interesting to note that the SH intensity from **VII** is approximately 6 times that of **III** reported by Girling[121].

If all these results are assumed to be free of experimental variations then the classification of different chemical groups can be confirmed as:

electron donor character;

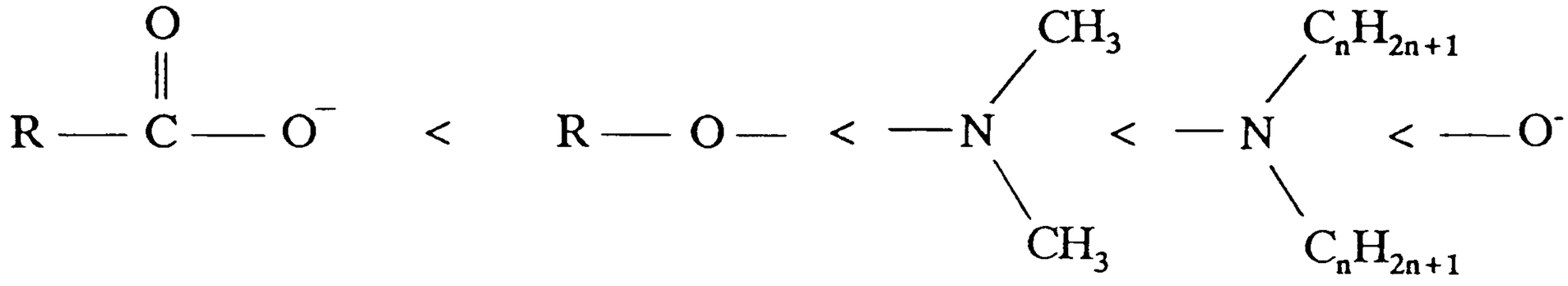

electron acceptor character.

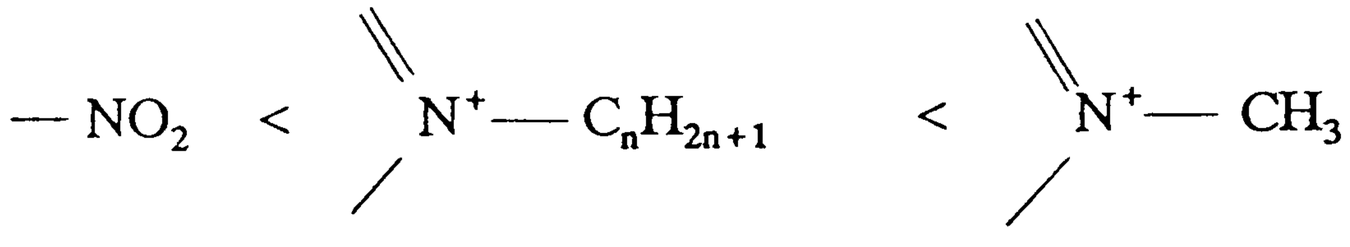

Rules governing SH response have been suggested as a result of a study of another set of amphiphiles, shown in figure 17[126,127]. Some ideas of how molecular structure effects nonlinearity are confirmed:

1. a substituent in the meta position decreases the molecular nonlinearity (**XVI** gave a larger responses than **XI** or **XII**);

2. increased planarity brought about by the interaction between an OH group and the nitrogen in the bridge improves SHG (**XVII** gave a larger response than **XVI**), and this occurs without a change in absorption band;

3. thioether instead of a simple ether bridge offers a significant improvement in nonlinearity (**XXIV** gave a larger response than **XVI** and **XX** gave a larger response than **XIX**).

Some theories are, however, contradicted:

1. the response is similar for **XV** and **XVIII** where one would expect the longer conjugated chain in the latter to give a larger response;

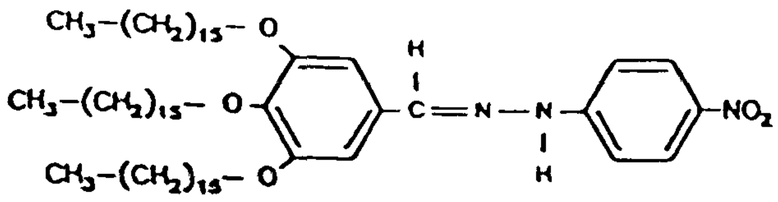

XI

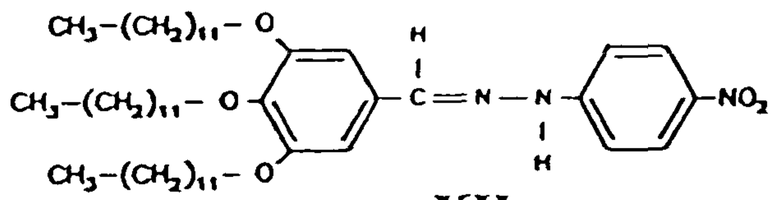

XII

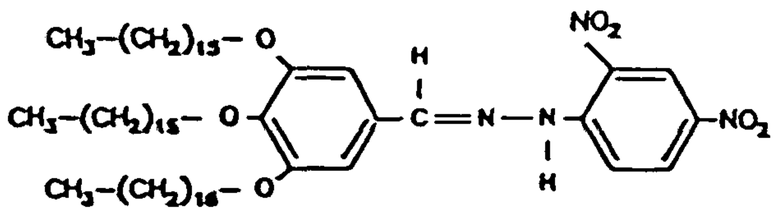

XIII

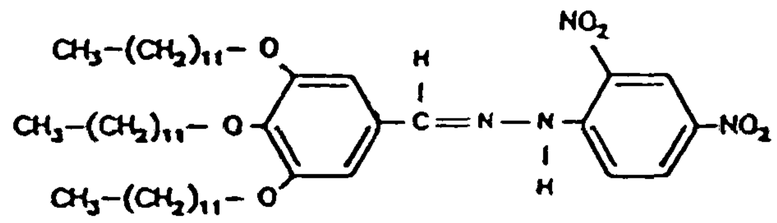

XIV

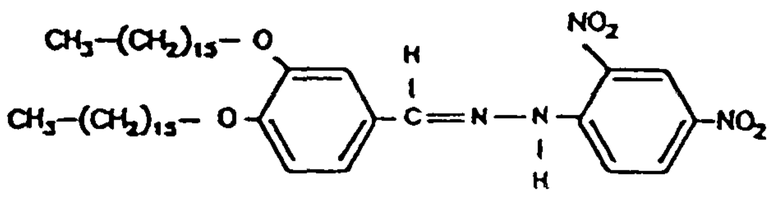

XV

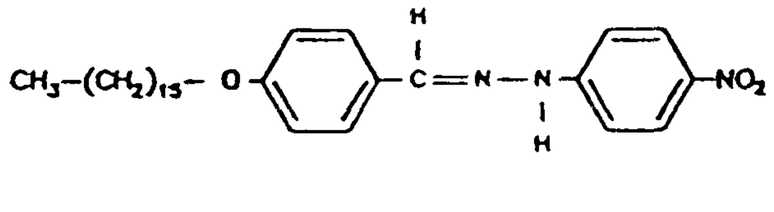

XVI

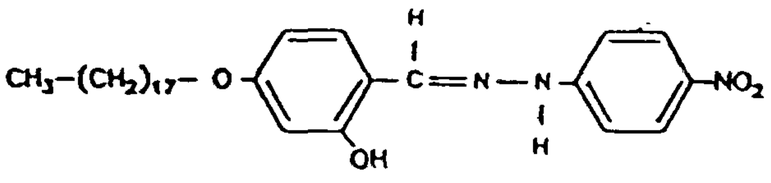

XVII

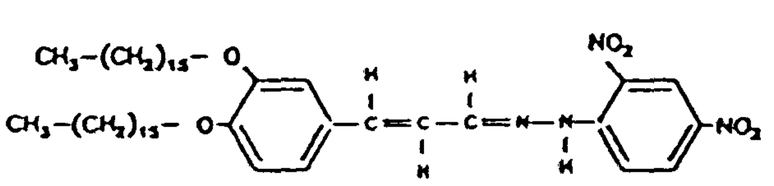

XVIII

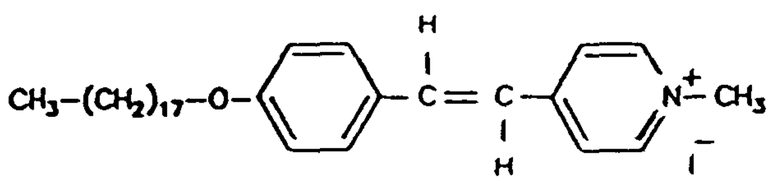

XIX

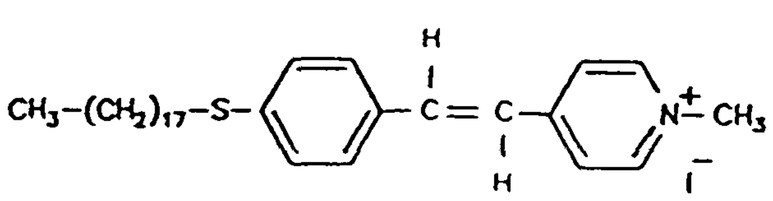

XX

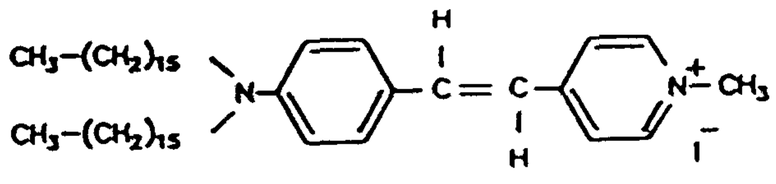

XXI

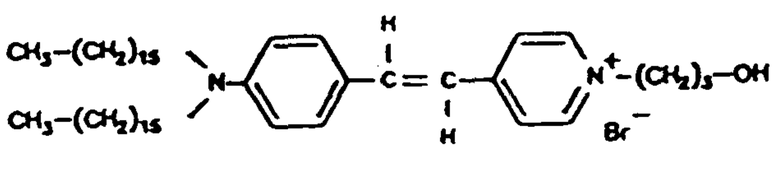

XXII

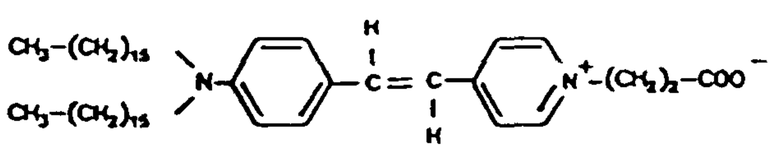

XXIII

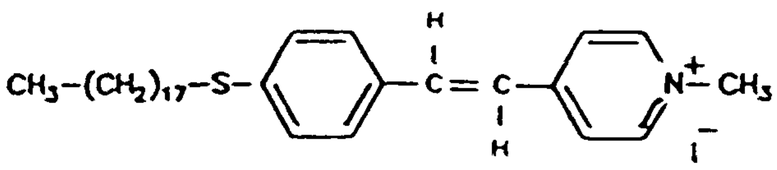

XXIV

Figure 17. Materials studied by Bubeck et al[126,127].

2. the presence of an extra alkyl chain does not improve the order in the film and therefore its SHG (the responses from **XI**, **XII**, **XIII** and **XIV** are no larger than that from **XV**), instead results are inconclusive.

More recently the same workers have approached the study of long substituted polyenes in the same way[128]. The experimental conditions were difficult to control and as a result the SH data was variable. It proved difficult, therefore, to assign any dependence of SH response on molecular configuration.

Finally some useful observations have been made for SHG studies of two azo dyes[129].

XXV

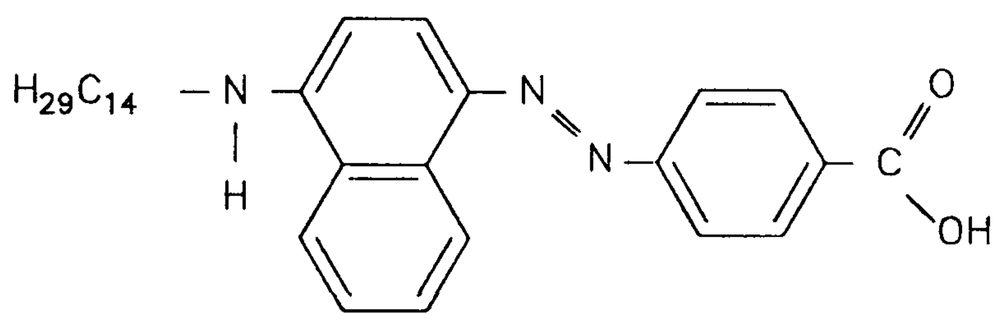

XXVI

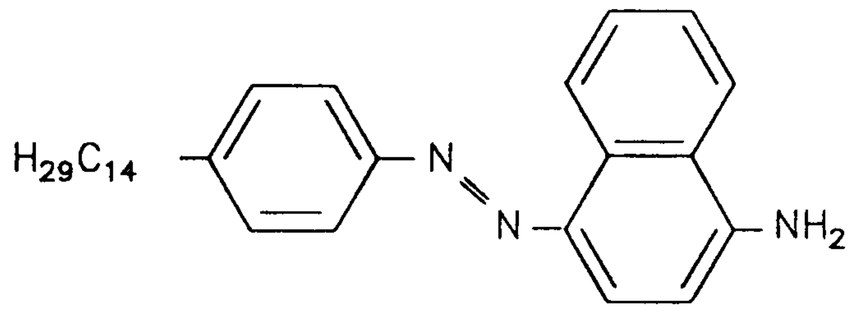

Figure 18. Two azo dyes with interesting SHG properties.[129]

Material	Type of film	Reported SHG data
XXV	Monolayer	$\beta = 2.8 \times 10^{-48}$ F m^3 V^{-1}
XXVI	Monolayer	$\beta = 1.2 \times 10^{-48}$ F m^3 V^{-1}

Table 5. SH response of materials **XXV** and **XXVI**[129].

The ß are reasonable since **XXVI** has no obvious acceptor group whereas **XV** has. In fact in **XXVI** it is possible that the azo linkage is acting as the acceptor group. By depositing from an acidified subphase the SH signal for a monolayer was five times greater in **XXVI** than when deposited normally, ie pH = 5.5. This may be due to protonation of the azo group which will shift the absorption band of the chromophore towards the SHG frequency, leading to resonant enhancement. In addition, protonation of the azo linkage may improve its electron accepting properties.

1.6.3 Multilayer films

The fabrication of multilayer films has been attempted for many materials which have a large SH response as a monolayer. Alternate layer films of **II** and ω-tricosanoic acid gave a signal greater than that from the monolayer[120]. In theory the signal should increase quadratically as the number of alternate layers increase but this was not observed. This departure was probably due to imperfect deposition.

Alternate layer films of **III** and ω-tricosanoic acid did not show quadratic behaviour either[121]. A reduction in the relative size of the s-signal indicated an increasing isotropic behaviour with thickness. As the number of layers increased the distribution of orientations may have changed also.

Alternating **III** with behenic acid resulted in a multilayer film exhibiting quadratic dependence for up to 6 bilayers[130]. The reason for this success compared with earlier attempts may be attributed to an improvement in experimental conditions. A single compartment trough was used and this meant that the surface had to be cleaned between every transfer, consequently cross-contamination of material was minimised.

Z-type layers of **III** have also been fabricated[131]. Subquadratic behaviour was observed for 1,2 and 3 layers and sublinear behaviour was observed for up to 12 layers.

An expected centrosymmetric Y-type bilayer of **III** demonstrated the different properties of layer 1 compared to subsequent layers. A signal of ≤ 25% of a monolayer was detected on layers 2 and upwards, on various samples. This indicates that the

molecules in the first layer are inclined at a different angle from those of the second layer. Incomplete transfer for one of the layers must not be ignored as a further possibility.

The inactive fatty acid used as a spacer molecule with **III** was replaced by a nitrostilbene, **XXVII** or **XXVIII**, in further studies[132]. These molecule have their donor-acceptor groups aligned in the opposite sense, with respect to the hydrocarbon chain, to those of **III.**

XXVII

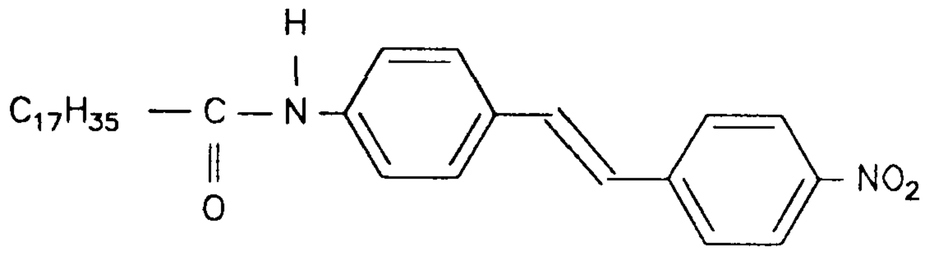

XXVIII

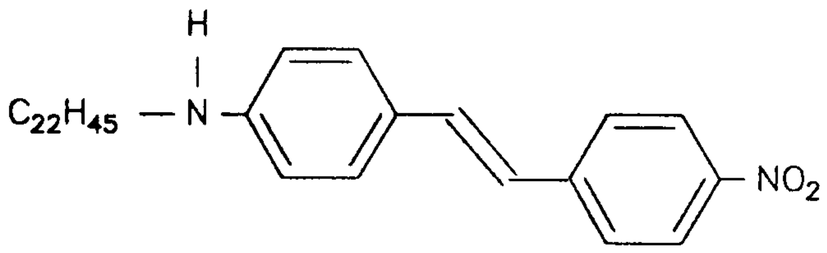

Figure 19. (**XXVII**) 4-N-heptadecylamido-4'-nitrostilbene[132]; (**XXVIII**) 4-N-heptadecylamino-4'-nitrostilbene[132].

Material	Film	Reported SHG data
III,XXVII	Alternate multilayer	ß(**III**) = 4.7 x 10^{-48} F m^3 V^{-1} ß(**XXVII**) = 8.6 x 10^{-49} F m^3 V^{-1} ß(**III,XXVII**) = 1.3 x 10^{-47} F m^3 V^{-1}

Table 6. Molecular coefficients for monolayers and bilayers of **III** and **XXVII**[132].

XXVII displayed excellent LB film forming properties, it had a linear relationship between absorbance and number of layers for up to 60 layers of a Y-type multilayer[133]. In theory an alternate multilayer of **III** and **XXVII** should have additive second order nonlinear molecular polarizabilities. Initial studies showed the first evidence of approximate quadratic behaviour for active-active multilayers for up to 3 bilayers. Molecular polarizability calculations for the hemicyanine were comparable to the monolayer[121].

The β coefficient of the bilayer is clearly greater than the addition of both individual polarizabilities. A thicker multilayer of ten layers was studied and the measured SH signal for this was still larger than an ideal model would predict[134]. This implies that there is some cooperative phenomenon occurring which renders the bilayer a much superior SH material than its individual components.

The idea that a bilayer can act as a discreet unit is perhaps to be expected, since the chromophores within it are in close proximity and are therefore likely to interact strongly. IR spectral data indicates two points that cause this effect:

1. **XXVII** molecules interact strongly by hydrogen bonding with each other, providing a rigid framework into which the **III** molecules may fit;

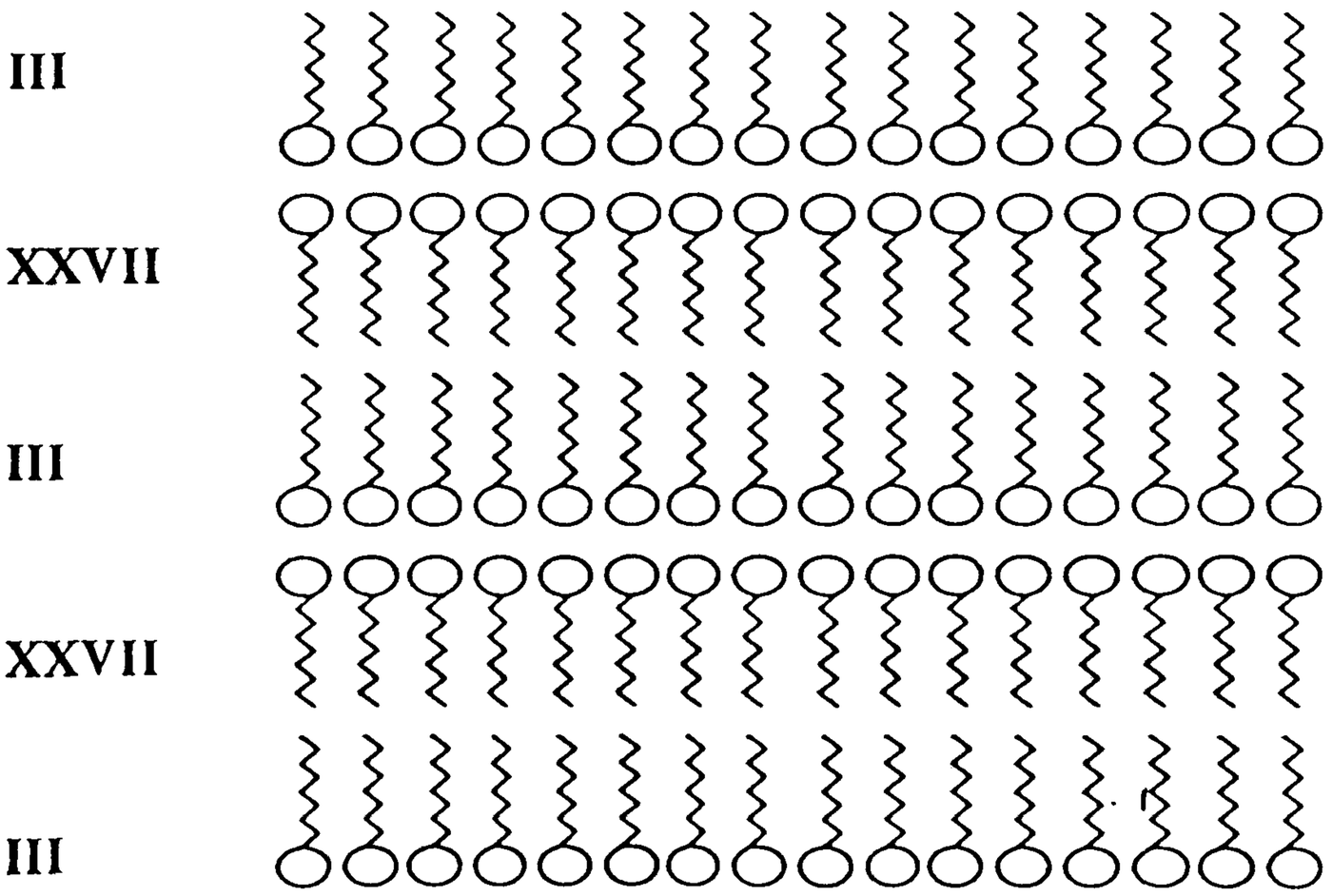

Figure 20. The nature of multilayer deposition of **III** and **XXVII**[132]

2. there is a degree of interdigitation of the **III** and **XXVII** molecules in the bilayers in such a way that the **III** molecules are held more rigidly and at least partly separated from each other. The separation probably reduces aggregation which affects SH response. This effect is discussed in more detail in section 1.6.4.

Material **XXVIII** was used instead of **XXVII** in attempt to improve the contribution from the nitrostilbene component. In **XXVIII** there is no carbonyl portion and this should increase the donor characteristics of the molecule. Unfortunately poor film quality rendered the SH signal similar to multilayers using **XXVII**. This is readily explained because the hydrogen bonding properties of the amide group are no longer available to provide the rigidity and alignment of the **III** molecules.

A large Y-type alternate multilayer of **XXVII** and a novel functional diarylalkyne showed SHG for 150 bilayers less than that of 49 bilayers. This may have been due to lack of phase matching since for thinner layers there is insufficient optical path length for this to become important[135]. Film deposition properties were excellent, further nonlinear optical experiments suggested ordering of molecules within the layer was low and decreased with an increasing number of layers.

Studies on the material 4-{4-(N-dodecyl-N-methylamino}phenylazo)-3-nitrobenzoic acid (DPNA), **XXIX**, demonstrated two properties common to LB films of a number of materials.[136]

Firstly, DPNA required the presence of Cd^{2+} in the subphase to stabilise it for LB deposition. Only layers deposited in the presence of Cd^{2+} produced multilayers with a near quadratic dependence. The λ_{max} in the presence of Cd^{2+} was 464 nm. Films deposited without Cd^{2+} present had slightly smaller $\chi^{(2)}$ and ß values but were less stable. This was probably because λ_{max} is 504 nm without Cd^{2+} which is closer to the SH frequency (532 nm) therefore resonant enhancement occurs.

Secondly, the SH response for the first layer of the Z-type multilayer was anomalously large compared to subsequent layers. This observation was mentioned earlier and merits more discussion. The environment of the first layer is very different

XXIX

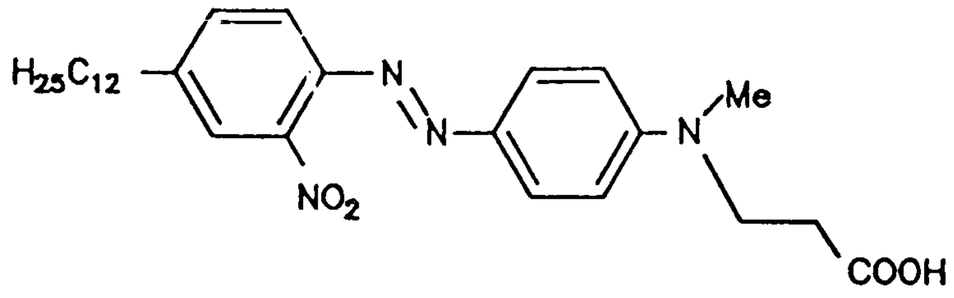

XXX

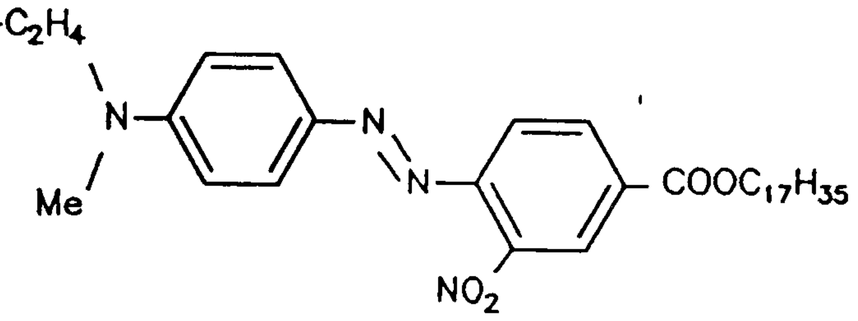

XXXI

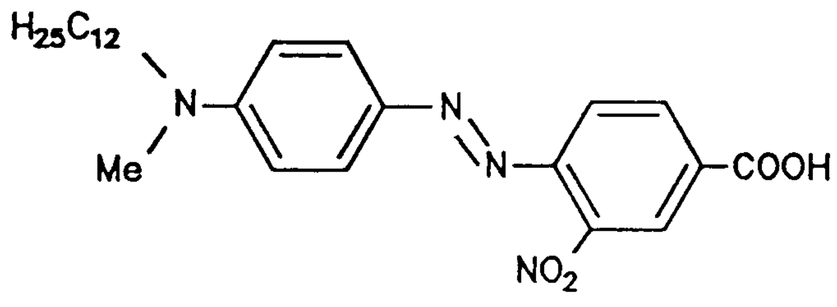

Figure 21. (**XXIX**) 4-{4-(N-dodecyl-N-methylamino)phenylazo}-3-nitrobenzoic acid (DPNA) and related materials for LB film fabrication[136].

Material	Type of film	Reported SHG data
XXIX	Monolayer	$\beta = 1.8 \times 10^{-46}$ F m^3 V^{-1}

Table 7. Reported SHG data for DPNA[136].

to that of the second, third etc layers because it is adsorbed to glass, not another molecular layer. IR studies of LB films of **III** and **XXVII** indicated that the influence of the substrate in disordering the initial monolayer was gradually lost as more layers were deposited[137]. Therefore both the structure and the orientation become more uniform.

It may be that the interaction between the substrate and the molecular layer causes the molecular layer to align at a different tilt angle to that formed when two molecular layers are adjacent. The difference in tilt angles causes a difference in SH response. The molecules in the first layer usually orientate their charge transfer axis more towards the input beam thereby giving a larger signal. In material **XXIX** the $\chi^{(2)}$ for Y-type layers was only 3 or 4 times smaller than those of Z-type layers with equal active layers[137-141]. This is partially accounted for by the predominance of the first layer. The deposition of up to 6 passive layers of arachidic acid before the first active layer of **XXIX** showed a signal smaller than that from a monolayer of **XXIX** alone, supporting this theory. Other experiments have indicated that upper layers of these LB films bind less strongly than lower ones, giving rise to a significant decrease in ß. Thermodesorption experiments confirm a reduction in binding energy of upper layers, ellipsometry and surface plasmon resonance studies have confirmed this[134]. In fact the binding energy enhancement is thought to cover the first 3 to 4 layers, which would certainly explain the subquadratic behaviour of this material.

The same workers have investigated the effect of confirmation changes in molecules on SH activity by studying **XXX** and **XXXI**. **XXXI** had a smaller ß value than either **XXIX** or **XXX** because of the lack of an electron attracting group in the para position. **XXX** had a ß value slightly less than **XXIX**, probably because the ester is a weaker electron attracting than the acid. In addition the propionic acid form is a weaker electron donor than the alkyl chain.

Alternate "active-active" Y-type multilayers of molecules **XXX** and **XXXI** were deposited and a sharp increase in SH response was observed where N (number of layers) > 5. Other combinations of passive-active multilayers were also deposited using **XXX**, **XXXI** and arachidic acid (see table 8). The results show that two active species eliminate the dilution effect of the passive species, in addition the similarity in their molecular configuration improves the stability of the multilayer. It is noted, however, that quadratic behaviour over a significant number of layers was not achieved due to the

increased disorder in the layers moving away from the substrate. The ideas presented have, however, proven a stimulus for many others in the field.

Nature of active materials	**XXXI**	**XXXI**	**XXXI** **AA**	**XXX**	**XXX** **XXXI**	**XXX** **XXXI**	**XXX** **XXXI**
Film	Z	Z	Y + 4	Y	Y	Y	Y
Active layers	7	12	11	1	3	7	11
$\chi^{(2)}$ x 10^{10} (SI)	2.16	1.93	0.88	3.3	1.43	1.91	3.4

Table 8. Reported SHG data for various LB layers of **XXX** and **XXXI**[138]. Note that AA denotes arachidic acid and that Y + 4 indicates the deposition of four Y-type layers of arachidic acid followed by the transfer of the alternate bilayers.

Materials **XXXII** and **XXXIII**, shown overleaf, were specifically designed to have opposite polarizabilities. The monolayer signal from **XXXII** was relatively large on a hydrophilic substrate, as one might expect from a molecule where charge transfer occurs through a relatively large conjugated system[142,143].

Material	Type of film	Reported SHG data
XXXII	Monolayer	$ß = 3.1 \times 10^{-48}$ F m^3 V^{-1}

Table 9. SHG data for **XXXII**[142].

XXXII

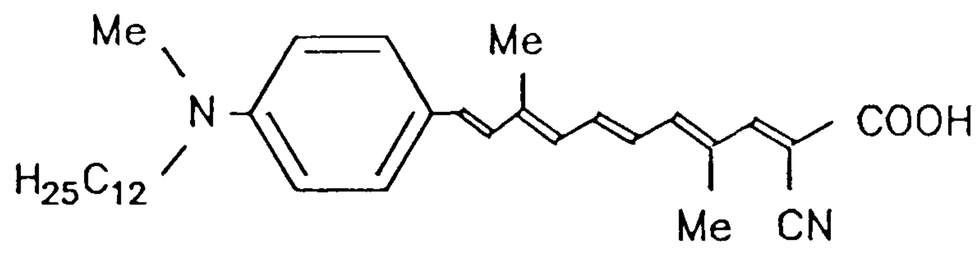

XXXIII

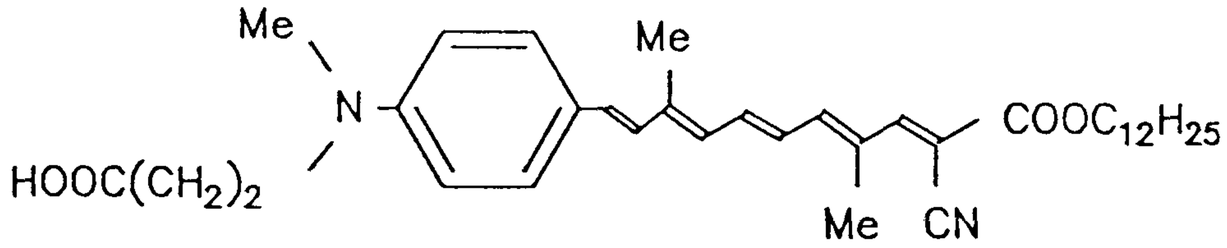

Figure 22. Two LB film forming materials (**XXXII** and **XXXIII**) designed to have opposite polarizabilities[142].

Mixed bilayers deposited with either as layer 1 exhibited considerably higher SH responses compared to their monolayer signals. Further bilayers showed a significant decrease in nonlinear susceptibility reflecting a decrease in molecular order with increasing layers. An important observation from these results is that the SH response of **XXXII** on a hydrophilic substrate is much larger than when it is deposited onto a hydrophobic substrate. There appears no significant first layer anomaly for a hydrophobic substrate. This is indicated by the near total cancellation for a bilayer. The monolayer deposited on the hydrophilic substrate has its nonlinear part situated nearest to the substrate. This infers that the interaction between this and the substrate must be the cause of the "first layer effect". Observations of the frequency dependence of **XXXII** and **XXXIII** show that both these materials have resonant enhancement at $2\omega = 532$ nm although the effect is much more marked for **XXXIII**[144].

1.6.4 Aggregates

Marked improvements in SH response have been observed when active materials have been mixed with inactive ones and then deposited as a monolayer. One of the first reports of this observed SHG enhancement by mixing hemicyanine with arachidic

acid[134]. A full range of hemicyanine molar ratios were deposited and their monolayer SH responses are shown in figure 23.

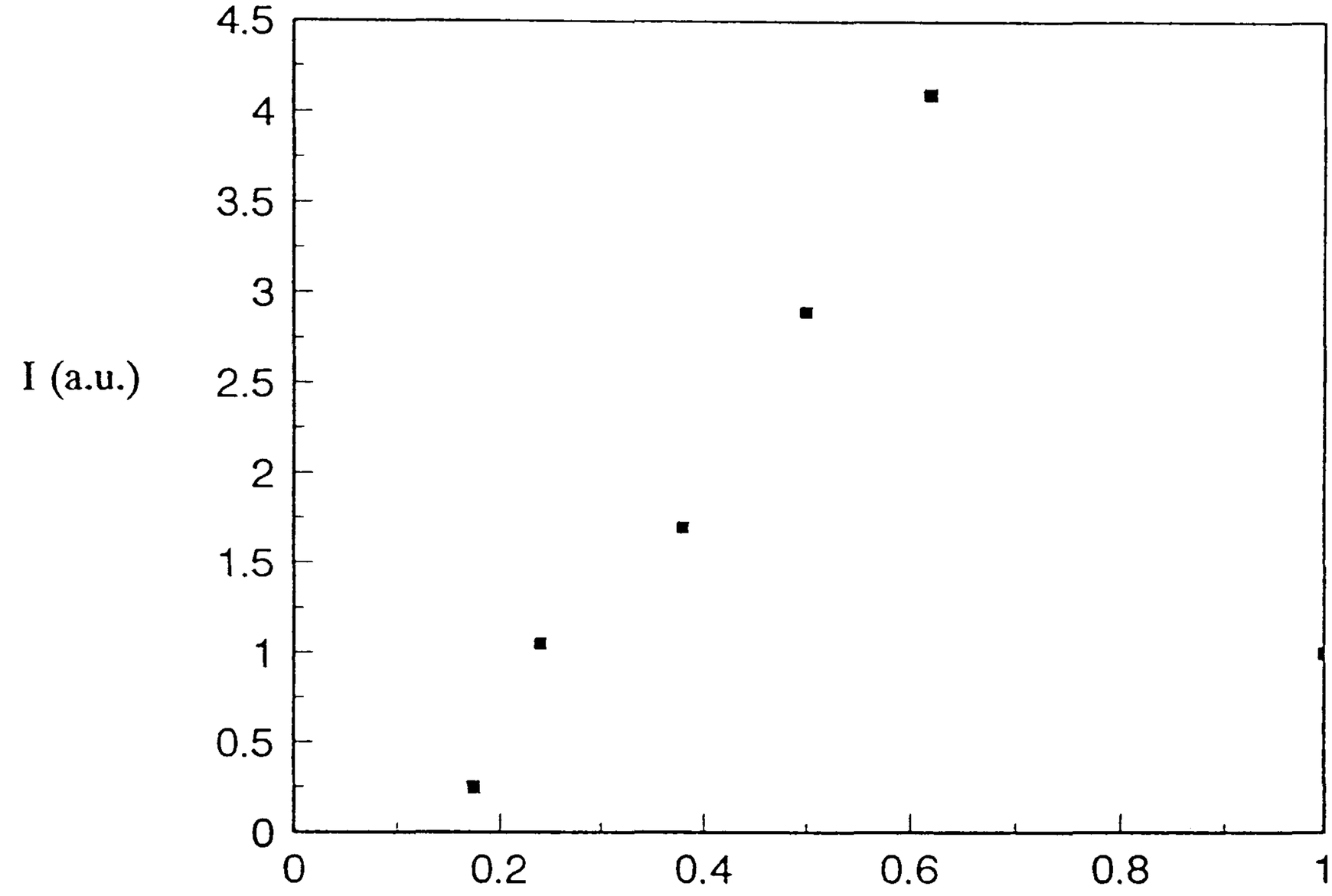

Figure 23. Second harmonic signal from mixtures of **III** and arachidic acid[134].

The fractional area of hemicyanine of approximately 0.62 where maximum 4-fold enhancement of pure hemicyanine occurs is equivalent to a 50:50 mixture of hemicyanine and acid. This enhancement can be accounted for by two possible mechanisms:

1. a change in packing results in better alignment relative to the incident and second harmonic electric fields, this is supported by the fact that enhancement is not perfectly uniform for all geometries and polarizations;

2. enhancement of the local optical fields is experienced by the hemicyanine because of the decreased shielding from more distant neighbouring dye molecules and evidence for this derives from the fact that the phenomenon is observed for all geometries and polarizations.

A more detailed investigation of the same species is shown in figure 24[145]. The data supports the observation of optimum enhancement between 0.5 - 0.7 fractional area, and a constant film structure in the region 0.2 - 0.6 fractional area.

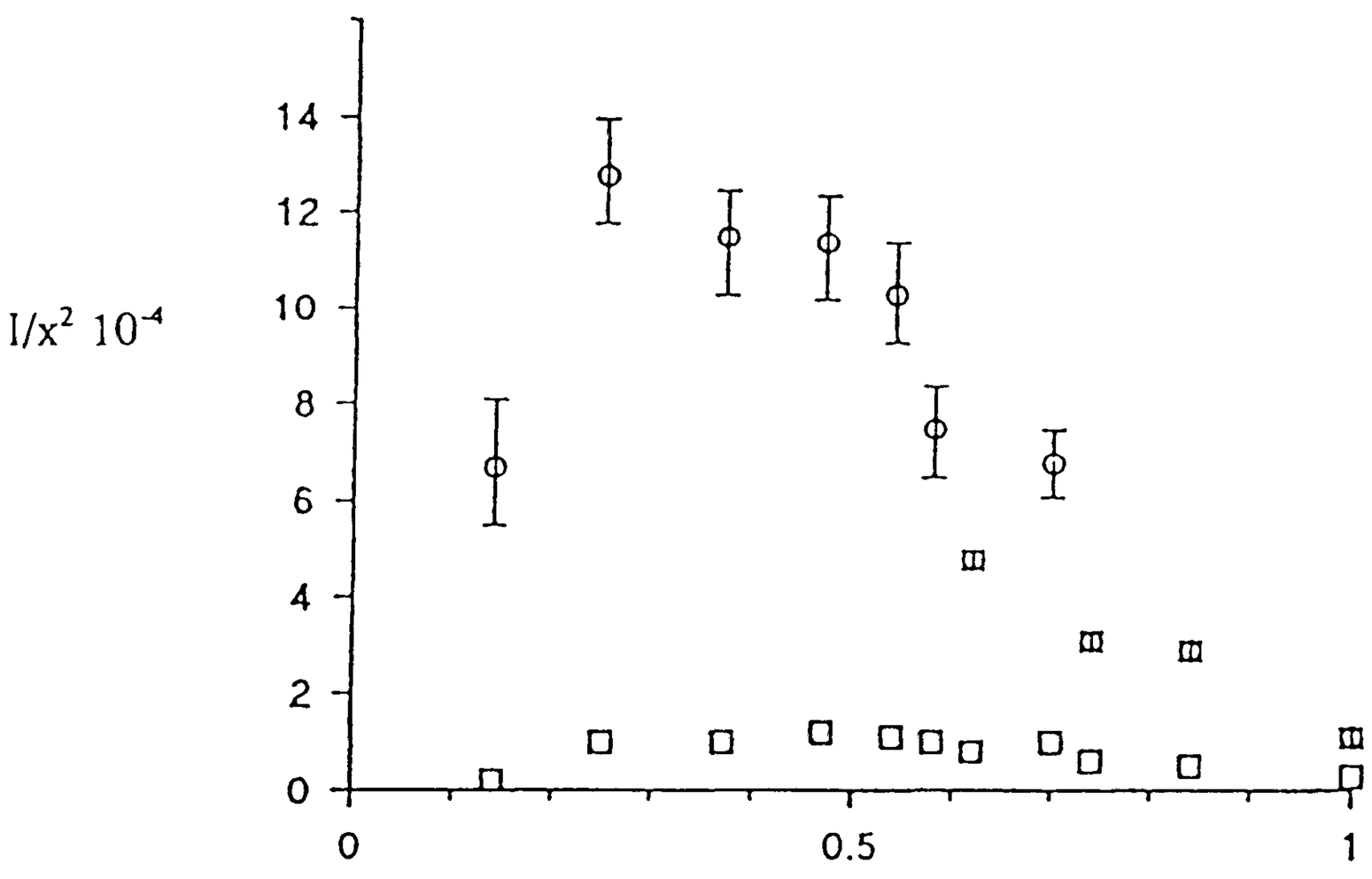

Figure 24. Second harmonic signal from transmission (O) and reflection (□) of mixtures of **III** and arachidic acid[145].

The value of ß for **III** was derived as 3.3×10^{-48} F m^3 V^{-1}, this is similar to that observed previously[121]. At concentrations greater than 50%, β decreases and this is most probably the result of changes in the distribution of inclinations. It is possible that at lower concentrations there are fewer chromophores lying flat, thus making the observed signal larger. At higher concentrations there are relatively more chromophores inclined

at angles that do not contribute as largely to the overall SH signal. Evaluation of the tilt angle of the chromophore for each monolayer was reported to be almost constant therefore having little effect on the SH response.

This early work on monolayer mixtures highlighted two fundamental points:

1. efficiency of SHG is found to be greater for mixed dye-arachidic acid films than for a pure-dye film;

2. efficiency of SHG does not increase quadratically with the number of layers in noncentrosymmetric multilayer films.

The absorption spectrum and SHG of LB monolayers of both pure **III** and a 1:4 mixture of **III** and arachidic acid indicate possible reasons for these observations[146].

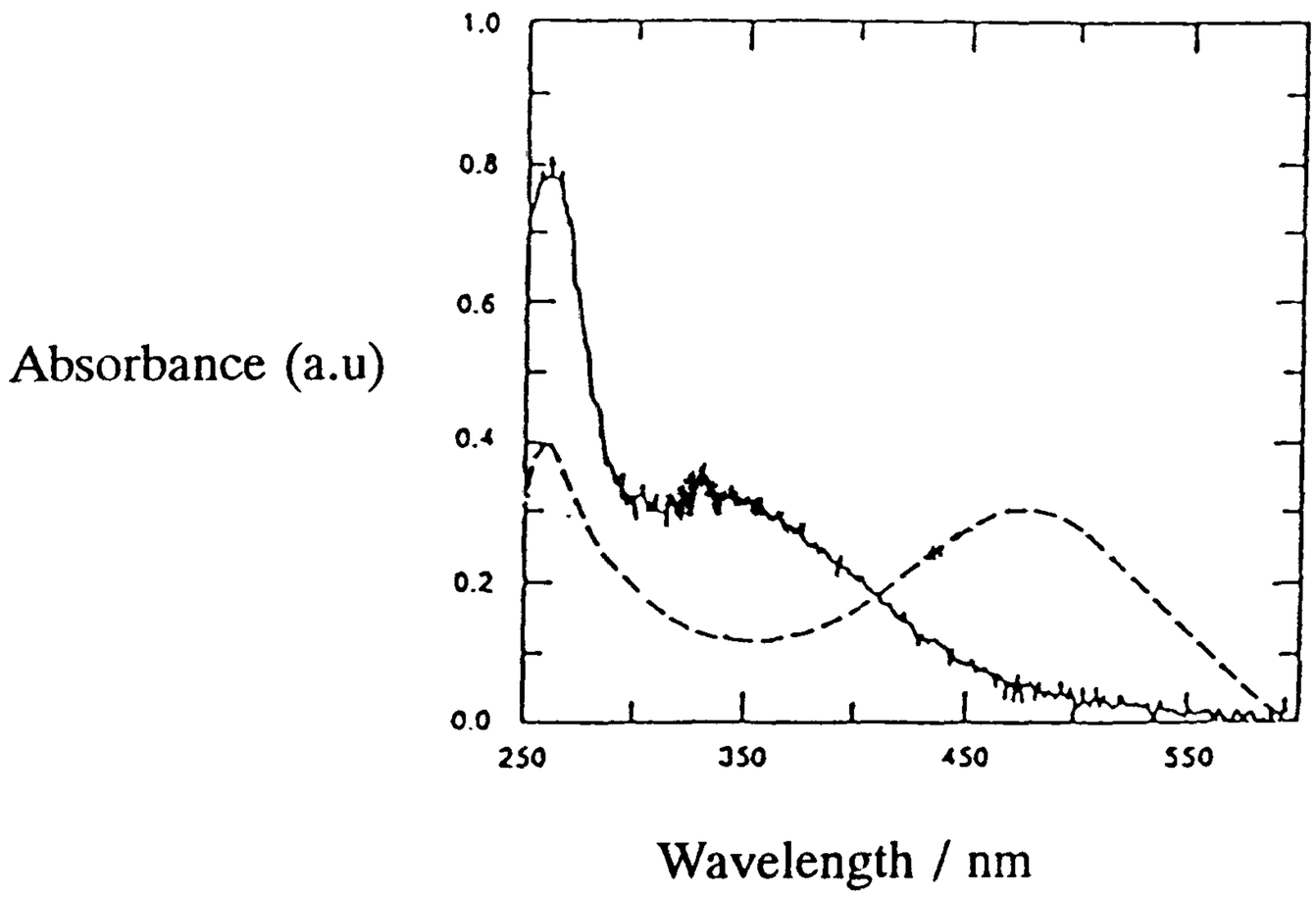

Figure 25. Absorption spectrum of pure **III** (—) and 1:4 mixture of **III** and arachidic acid (---)[146].

Both films have an absorption band at 263 nm and one at a higher wavelength. The high wavelength band of the mixed film is at 477 nm, which is close to the monomer band in chloroform solution (494 nm). The high wavelength band of the pure

III film at 339 nm is blue shifted more than 150 nm from the monomer band. These observations are a clear indication of H-aggregate formation in the pure **III** film.

SHG measurements of both films confirmed an almost completely p polarised output beam from a p and s polarised 1064 nm incident beam. This indicates that in both films the molecular orientation distribution is uniaxial, with the symmetry axis normal to the film.

The SH signal from the mixed film is 44 times greater than that of the pure **III** film. Therefore the second order susceptibility of the mixed film is 6.6 times higher than that of the pure film. The enhanced signal observed here and previously[121,134] is also evidence of H-aggregate formation. Resonant enhancement of SHG will occur in the mixed film because of the spectral overlap of the monomers absorption band and the 532 nm beam. The pure **III** film will not exhibit this because of the blue shift in absorbance.

The ratio of the SH intensity for p and s polarised input beams at an incident angle of 45° is 5.9 ± 0.5 for pure **III** and 4.6 ± 0.5 for the mixed film. This indicates that the monomer and the aggregate dye have nearly the same orientation in the film. Therefore orientational effects do not play a major role in the difference in SHG efficiency of the monomer and aggregate.

Further studies have indicated that the monomer dye is three times as active as the aggregate dye[147-149]. This could be due to antiparallel molecular alignment, which minimises electrostatic energy, resulting in cancellation of individual second-order susceptibilities. In addition, electronic coupling of separate molecules may diminish the molecular hyperpolarizability.

As reported earlier, the Z-type multilayer film reported by Hayden et al[131] failed to achieve quadratic dependence of SH response with number of layers. This may be due to the instability of Z-type structures. It can also be explained by the differing relative amounts of aggregate and monomer dye in each layer of the film[150]. This could occur through a change in the monomer-aggregate equilibrium with time at the air/water interface during multilayer deposition. Alternatively it may be a result of interlayer

interaction of the transferred films. Also, polarised IR spectroscopy studies show that the layers lose their registration with the surface of the substrate after only a few layers are deposited.

Temperature studies of SHG, absorption and X-ray diffraction have shown that H-aggregation occurs when the concentration of **III** exceeds 50% in a **III**:arachidic acid film[151]. As the temperature increases for a 50:50 film the molecular hyperpolarizability, ß, increases because some of the aggregated molecules dissociate to monomers. At 60°C, ß decreases because the arachidic acid melts, allowing aggregate formation again.

More azobenzene structures have been studied as mixtures with acids[152]. They have been investigated extensively as LB films for nonlinear optical applications for various reasons. They have extended conjugated π systems, onto which electron-donating and electron-accepting groups may be easily attached during synthesis. In addition the synthetic pathways for azobenzenes allow flexibility in the attachment of amphiphilic substituents. They also exhibit high chemical and thermal stabilities, which is desirable if these materials are to be used as integral components in working optoelectronic devices.

XXXIV

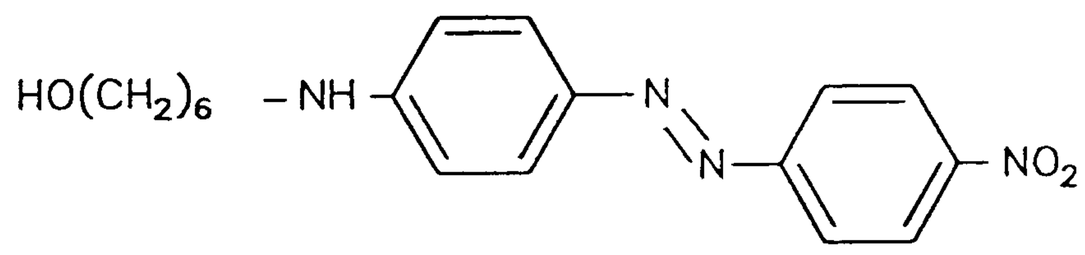

XXXV

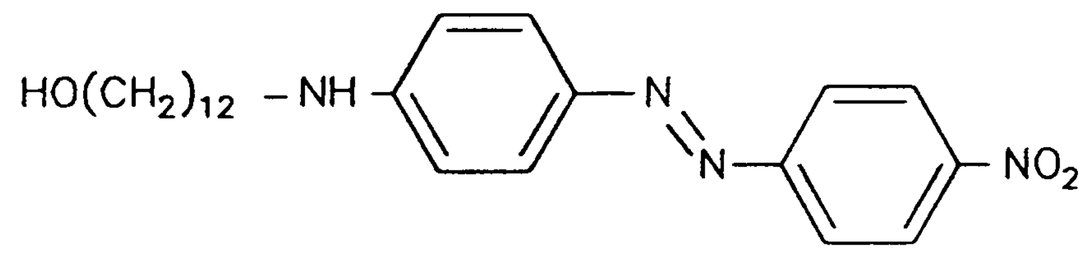

Figure 26. LB film forming azobenzenes: (**XXXIV**) 4-(N-hydroxyhexyl)amino-4'-nitroazobenzene[152] (**XXXV**) and 4-(N-hydroxydodecyl)amino-4'-nitroazobenzene[152].

They did not form stable monolayers unless they were mixed with stearic acid and the subphase had to be doped with bivalent cations (ie Cu^{+} or Cd^{2+}). Absorption

effects were minimal (1.5% at 532 nm for **XXXIV**). The best multilayer film fabricated from these materials was a Y-type "passive-active" film using 2:1 stearic acid:**XXXIV** with stearic acid interleaved. The second harmonic dependence was only just subquadratic for 1,2 and 3 layers. This is considerably better than other systems reported, as well as contradicting the theory of anomalous first layer behaviour. Similar studies for **XXXV** were less successful; this could simply be explained as a carbon chain length mismatch since **XXXIV** matches the length of stearic acid very closely and **XXXV** does not.

Material	Type of film	Reported SHG data
XXXIV	Mixed monolayer	$\beta = 2.4 \times 10^{-49}$ F m^3 V^{-1}
XXXV	Mixed monolayer	$\beta = 1.3 \times 10^{-49}$ F m^3 V^{-1}

Table 10. Reported SHG data for **XXXIV** and **XXXV**[152]

1.6.5. Quadratic SHG Enhancement from Y-type Films.

A large SH signal from a Y-type multilayer film of a simple chromophore and spacer material was reported by Japanese workers[153]. Noncentrosymmetric LB films of more than 200 bilayers, with thickness of more than 1 μm, were successfully fabricated with an alternating deposition of a phenylpyrazine derivative, **XXXVI**, and arachidic acid monolayers.

The alternate layers were deposited consistently from a subphase containing $BaCl_2$ to stabilise the materials. The films were transparent from the visible to the near IR region so the SH response was not increased by resonant enhancement of the output beam at 532 nm. The LB multilayer absorption spectrum was blue shifted by 50 nm, indicating the formation of H-aggregates. The multilayer showed a quadratic dependence

of SH intensity with film thickness for up to 200 bilayers. The average tilt angle of **XXXVI** was estimated as 30°. This was supported by X-ray diffraction data which demonstrated that **XXXVI** was orientated predominantly normal to the film plane in the LB film. The second order nonlinear susceptibility was very large compared to other organic LB films.

XXXVI 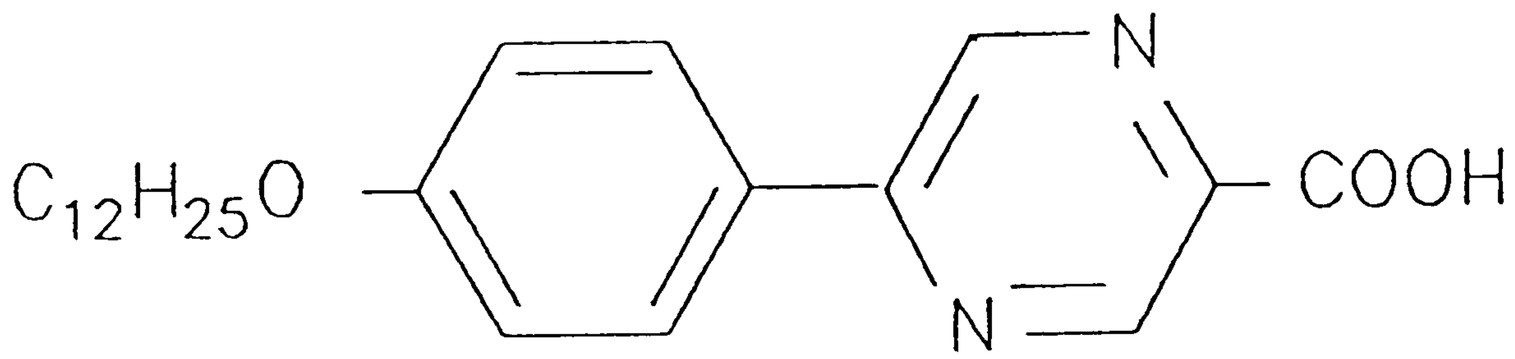

Figure 27. **XXXVI**: 5-(p-dodecyloxyphenyl)pyrazine-2-carboxylic acid[153].

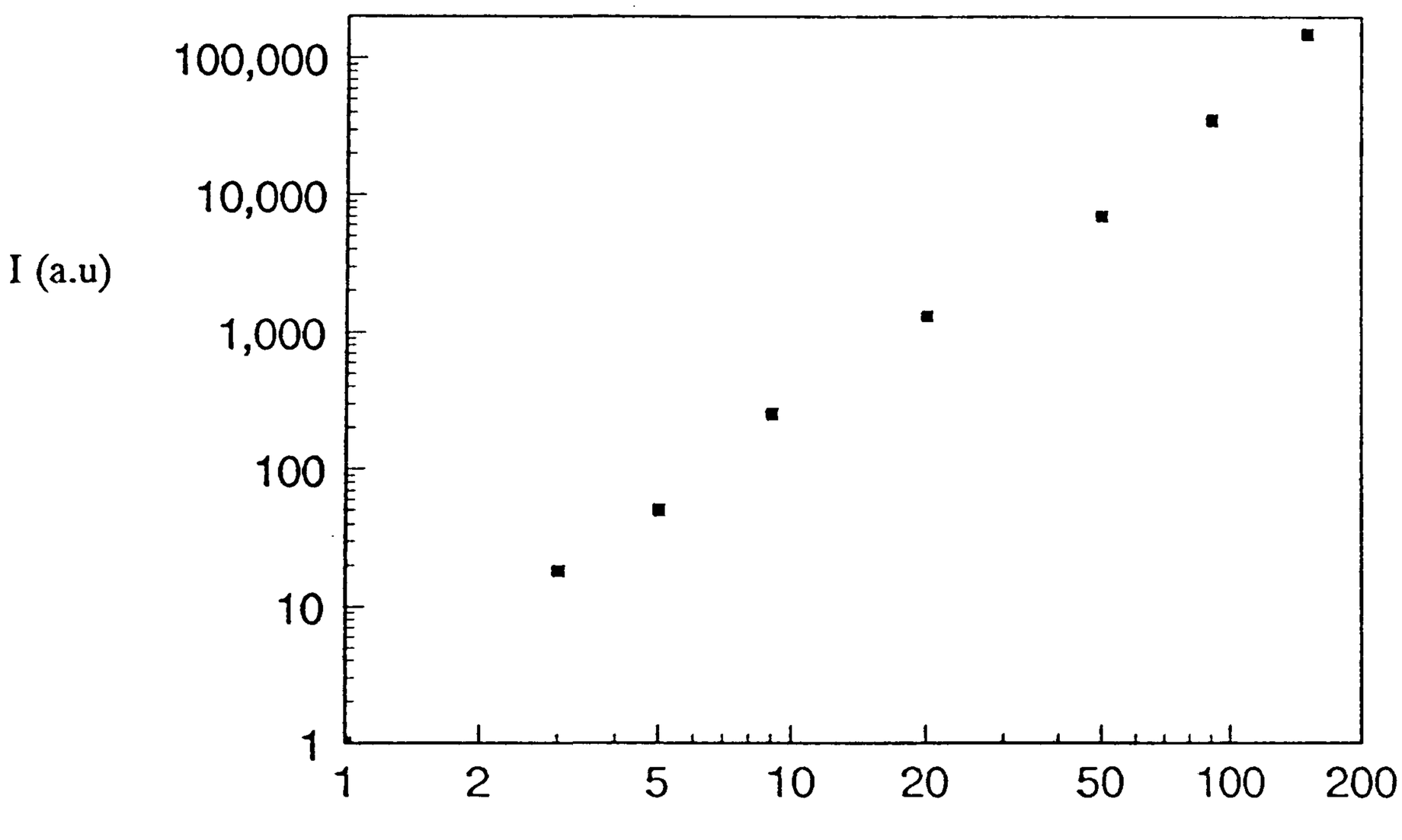

Figure 28. SH intensity versus number of bilayers for an alternating multilayer film of **XXXVI** and arachidic acid[153].

Material	Type of film	Reported SHG data
XXXVI	200 bilayers	$\chi^2 = 4.2 \times 10^{-11}$ m V^{-1}

Table 11. Reported SHG data for **XXXVI**[153]

Further to this work, two new pyrazine derivatives were studied (figure 29) that also form thick noncentrosymmetric LB films[154]. **XXXVII** and **XXXVIII** have similar hyperpolarizabilities to **XXXVI**.

Material	Type of film	Reported SHG data
XXXVI	Monolayer	ß = 3.3×10^{-50} F m^3 V^{-1}
XXXVII	Monolayer	ß = 7.2×10^{-50} F m^3 V^{-1}
XXXVIII	Monolayer	ß = 2.8×10^{-50} F m^3 V^{-1}

Table 12. Reported SHG data for pyrazine derivatives[154].

XXXVII

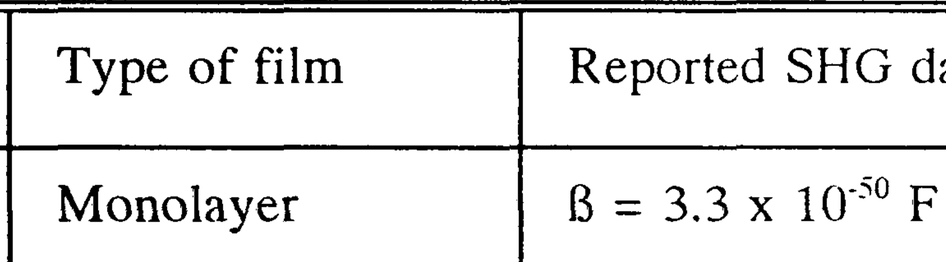

XXXVIII

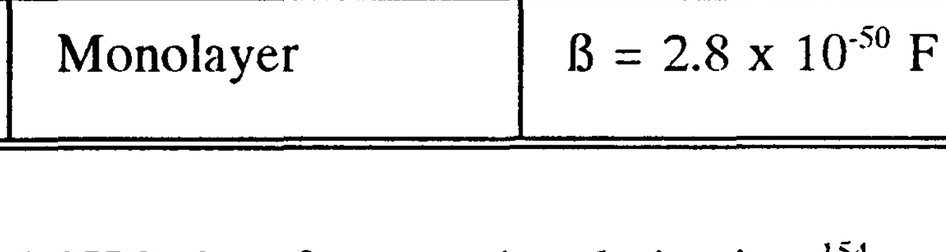

Figure 29. Two new pyrazine materials for LB film applications[154]

Fifty bilayer films were successfully fabricated using either **XXXVII** or **XXXVIII**. They were deposited from subphases containing either Ba^{2+} or Cd^{2+} ions. All the films exhibited an approximate quadratic dependence of SH intensity with number of bilayers.

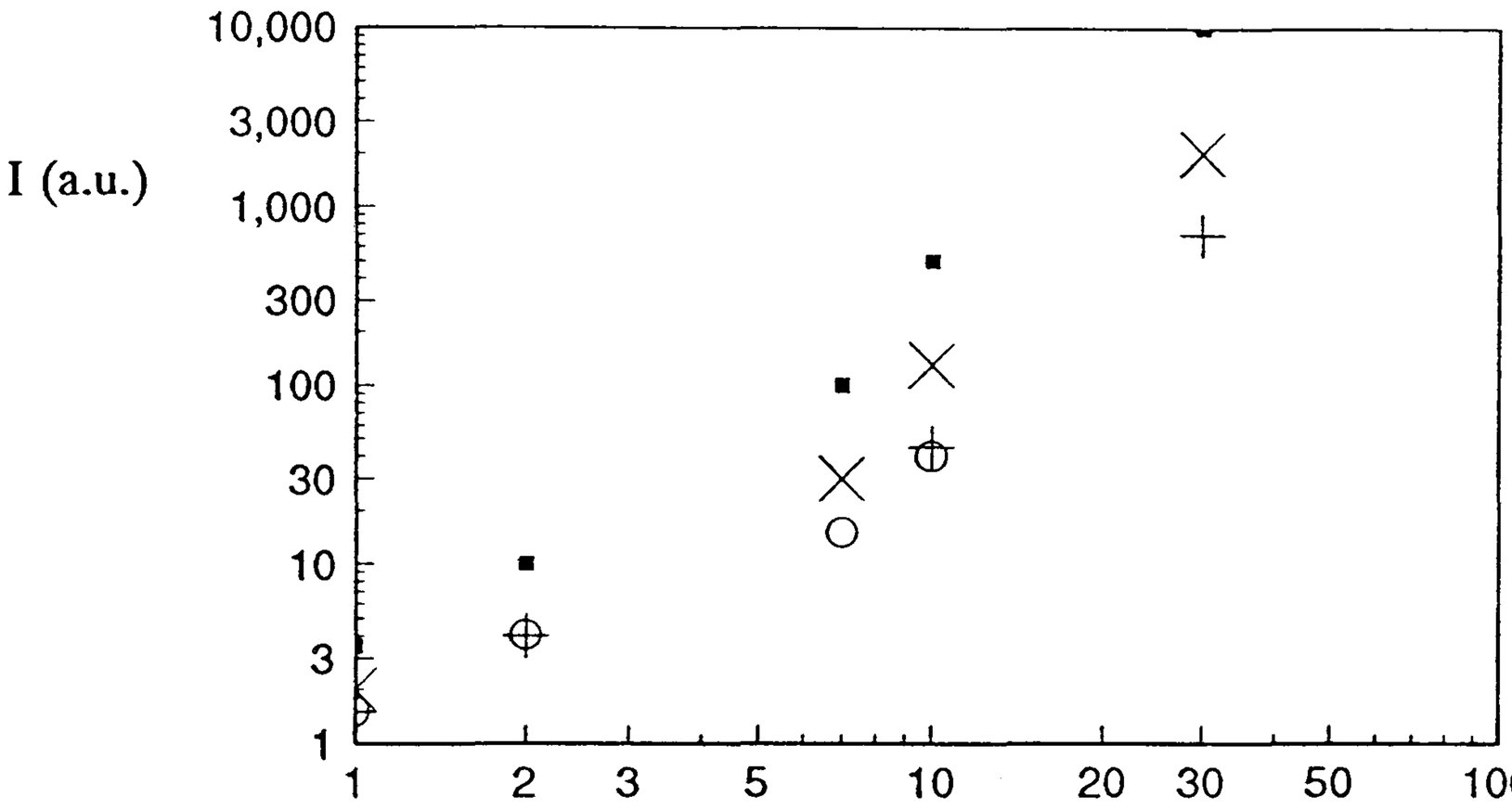

Figure 30. SH intensity versus number of bilayers for 50 bilayer films of **XXXVII** and **XXXVIII** with arachidic acid[154]. (o) **XXXVII** Ba salt, (+) **XXXVIII** Ba salt, (X) **XXXVIII** Cd salt, (■) **XXXVII** Cd salt.

The SH responses for the 50 bilayer films are listed in table 13 and it is worthwhile noting that the multilayer film of **XXXVII** Cd^{2+} salt possessed the largest second order susceptibility. The absorption bands of the Cd^{2+} salt LB films were closer to the second harmonic wavelength than those of the corresponding Ba^{2+} salt LB films. This probably explains why their susceptibility was larger.

Material	Type of film	Reported SHG data
XXXVII Cd^{2+}	50 bilayers	9.6 x 10^{-11} m V^{-1}
XXXVIII Ba^{2+}	50 bilayers	3.4 x 10^{-11} m V^{-1}
XXXVII Cd^{2+}	50 bilayers	4.6 x 10^{-11} m V^{-1}
XXXVIII Ba^{2+}	50 bilayers	2.9 x 10^{-11} m V^{-1}

Table 13. Reported SHG data for new pyrazine derivatives **XXXVII** and **XXXVIII**[154].

1.6.6. Quadratic SHG Enhancement from Z-type Films

Materials suitable for LB deposition are very often unsuitable for Z-type multilayer fabrication. The requirement for hydrophilic head groups to transfer onto a layer of hydrophobic tails is usually too difficult. In fact in systems where this has occurred the resulting multilayer is usually quite unstable compared to a Y-type film of the same material. Interlayer rearrangement can drastically affect the consistency of each layer, and this has been shown to occur for Z-type films of **III**[130].

Z-type multilayers can be fabricated if the hydrophobic end groups are positioned along the chain[155]. Similar molecules with hydrophobic end groups at the end of the chain do not deposit Z-type because the criterion of < 90° advancing contact angle and approximate 0° receding contact angle is not met[156].

A novel method of achieving stable Z-type layers is to deposit materials that prefer this alignment energetically. In the molecules **XXXIX** and **XL** centrosymmetric alignment does not occur because the negative ends have a columbic repulsion[157-159]. Multilayer films of **XL** were fabricated using a two component trough with a floating monolayer in one side only. Continual rotation through both compartments allowed

repetitive upstroke transfer. Figure 32 shows that quadratic behaviour was achieved for up to 50 layers.

XXXIX

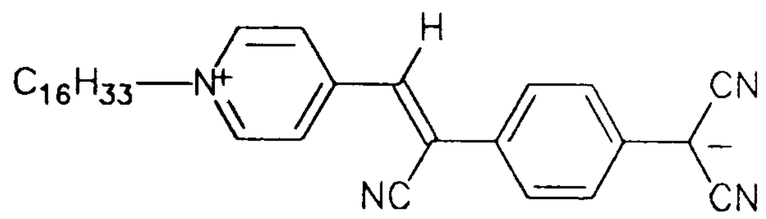

XL

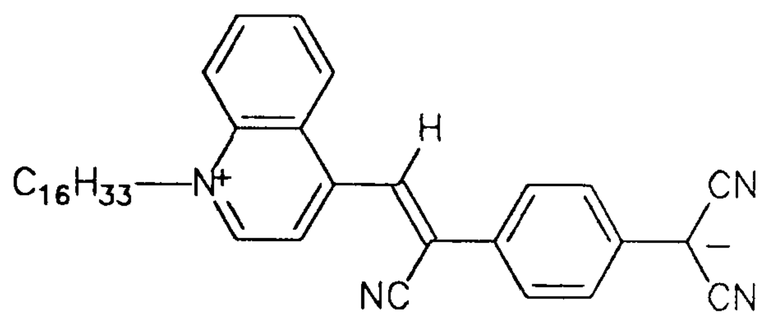

Figure 31. Zwitterionic LB film forming materials: (**XXXIX**) Z-ß-(1-hexadecyl-4-pyridinium)-α-cyano-4-styryldicyanomethanide; (**XL**) Z-ß-(1-hexadecyl-4-quinolinium)-α-cyano-4-styryldicyanomethanide[157-159].

Material	Type of film	Reported SHG data (theoretical)
XXXIX	Monolayer	ß = 4.7 x 10^{-48} F m^3 V^{-1}

Table 13. Reported SHG data for **XXXIX**[157].

Mixtures of **XXXIX** and **XL** also showed interesting behaviour[159]. The signal from **XL** was approximately 30 times that of **XXXIX**. Various mixtures indicated that SH response increased with increasing **XL**. The absorbance spectrum showed that the mixture was, in fact, an organic "alloy" having only one absorbance peak instead of the two component peaks. A plot of SH intensity vs λ_{max} of the mixture showed that SH response increased towards 2ω (532 nm). In fact the pure film of **XL** provided the

optimum conditions for SHG; the harmonic is on the leading edge of the sharp charge transfer band with an absorbency at 532 nm of less than 0.002 per layer.

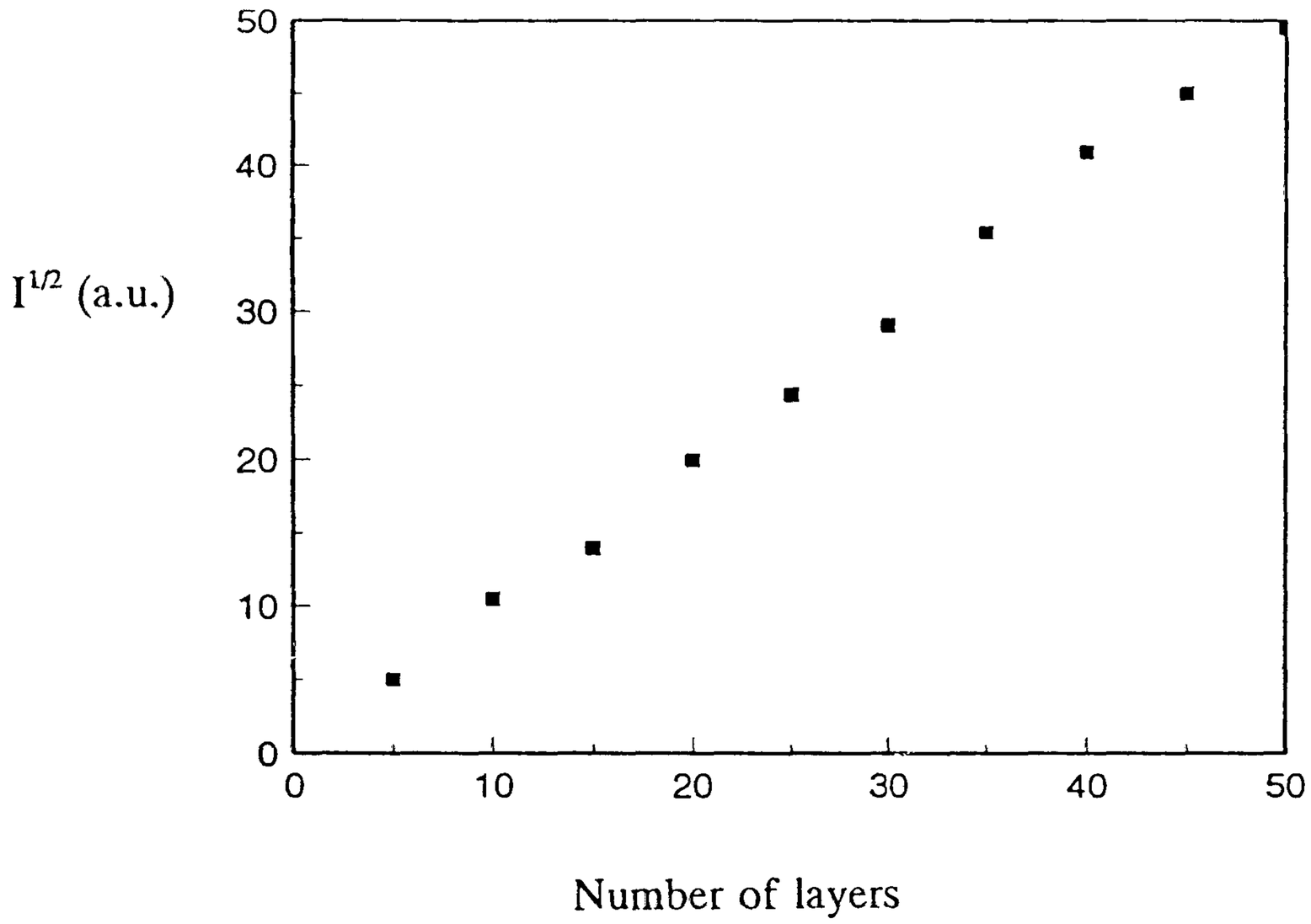

Figure 32. SH response versus number of layers for a multilayer of **XL**[157]

1.6.7 Polymers

The stability of organic polymers make them ideal materials as LB films for SHG. Simple polymers such as polymethylmethacrylate and polyvinylacetate and block copolymers can be transferred to a solid substrate but defect free multilayers have not yet been fabricated[160].

Polymerisation of an amphiphile, after deposition, has been studied. Multilayer films of poly(benzothiazole) prepolymer showed a quadratic dependence of SHG with number of layers for up to 20 layers[161]. A multilayer film of the polymer was obtained by heating the prepolymer film to 300°C. The SH response of the polymer multilayer

was 0.025 times as intense as the prepolymer. This indicates that alteration of the molecular structure and the disorder of layers has taken place.

A multilayer film consisting of alternating layers of poly(N-(p-heneicosafluorodecylsulfonyphenyl)-L-prolinol acrylate and poly(2-(p-(1-oxy-1-trifluoromethyl-2,2-diheptafluoroisopropylethylene)phenyl)-2-oxazoline) was prepared[162]. Up to 80 layers of the multilayer showed a steady increase in SH response although this was not quadratic.

A novel method is to incorporate a known nonlinear optically active chromophore along the backbone of a polymer and fabricated it into a Y-type multilayer[163,164]. Molecules **XLI** and **XLII** were deposited alternately and the SHG for the first four bilayers increased quadratically. Although no absolute SH signals were reported it is interesting to note that the chromophores absorb visible light with a λ_{max} = 390 nm and an absorption edge near 500 nm in chloroform. This makes them transparent to Nd:YAG laser light at 532 nm, however no spectrophotometry of the resultant LB film, was reported.

In an attempt to reduce the effect of interaction between layers, a double spacer was used to fabricate an ABCC structure where A,B = polymers **XLI** and **XLII**, C = behenic acid and **XLI** is the first layer[165]. The acid was incorporated to prevent hydrophilic-hydrophobic interactions between polymer-dye bilayers and to insulate against interlayer local field effects. For comparison a non interleaved structure was studied. The results, shown in figure 34 indicated that the non-interleaved structure was not as SH responsive when two films of similar thickness were compared. This cannot be attributed to poor deposition, ionization of chromophores[166], local field effects[145], or successive disordering because of imperfect registry between bilayers. It can be concluded that through control of the film architecture it is possible to obtain quadratic enhancement of SHG intensity when the optically active bilayers are interleaved with an optically inert material.

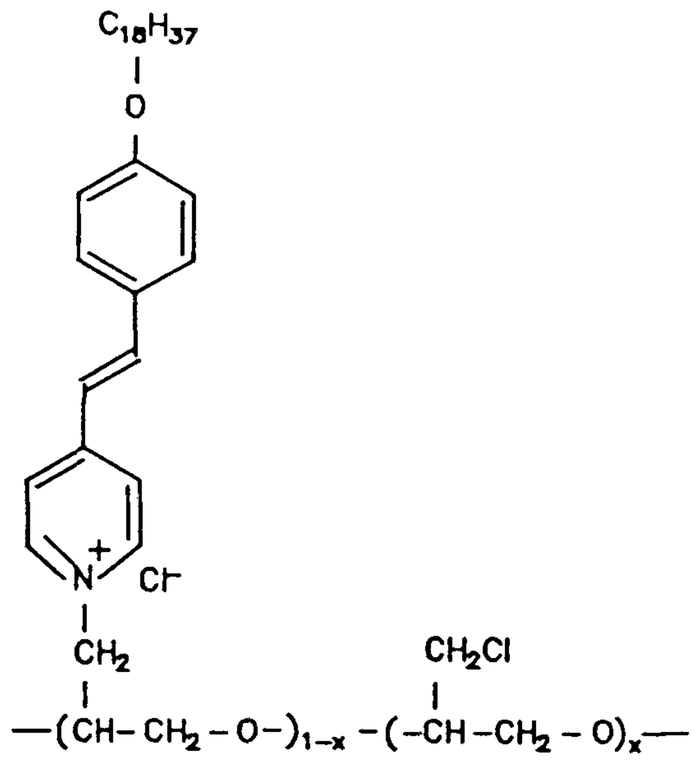

XLI

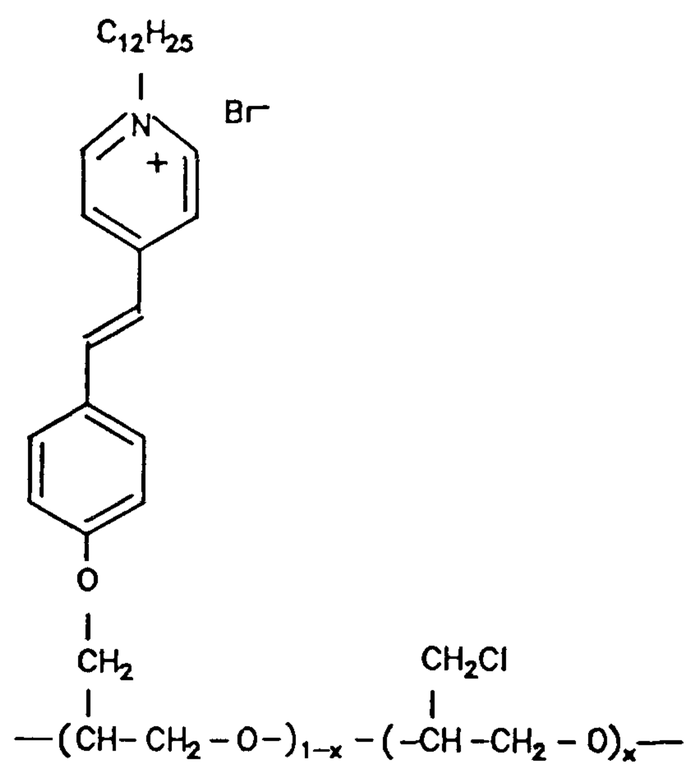

XLII

Figure 33. Chromophores incorporated onto polymeric backbones[163,164].

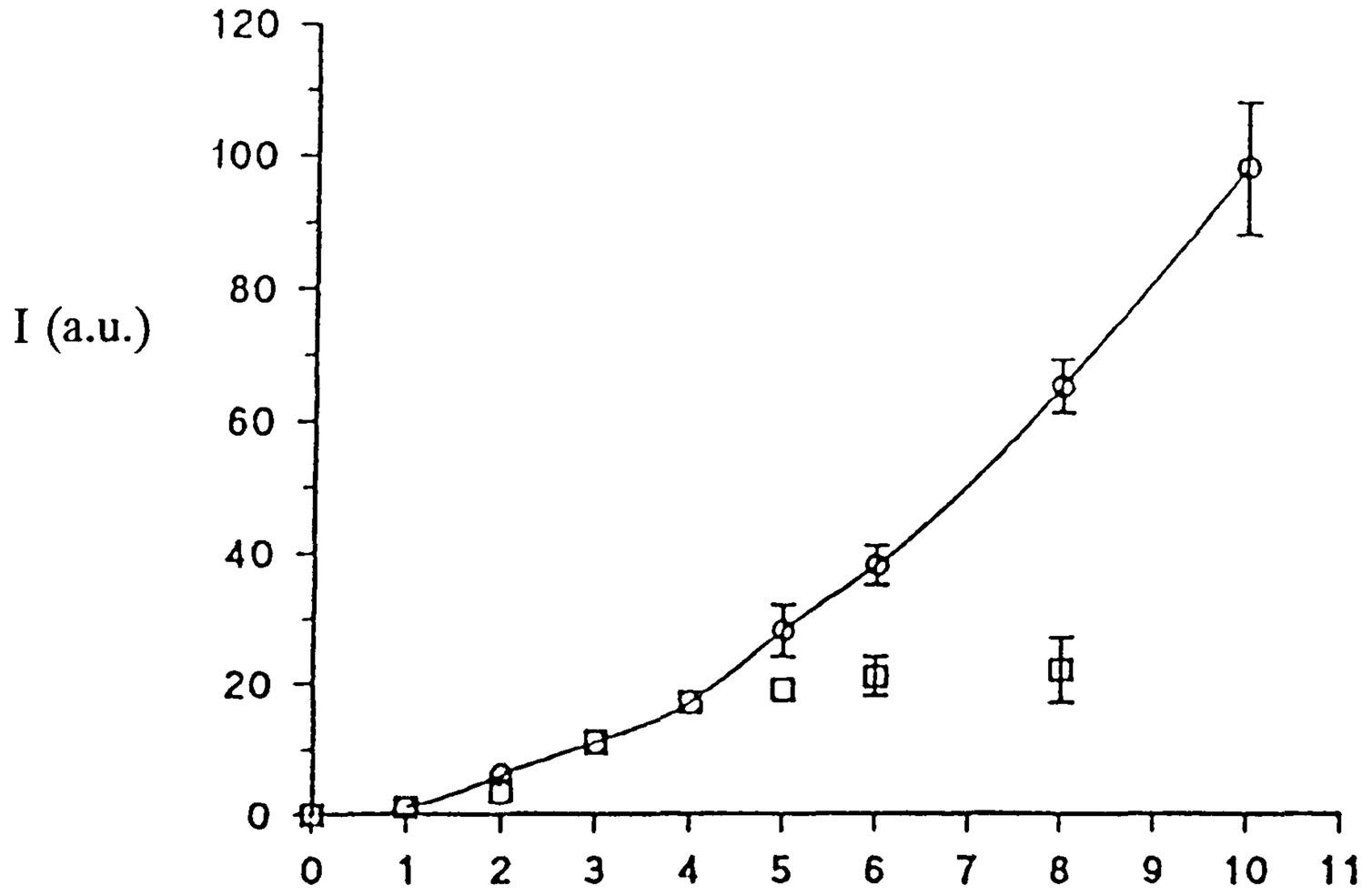

Figure 34 SH response versus number of bilayers of **XLI** and **XLII**;
○ interleaved structure, □ non-interleaved structure.

Anderson and coworkers extended these studies by using material, **XLIII**, which has a larger second order polarizability[167]. This polymer has a hemicyanine type chromophore with a hydrocarbon tail covalently bonded to a polyether backbone. Its susceptibility is of the same order as the hemicyanine dye, the spacer was behenic acid again.

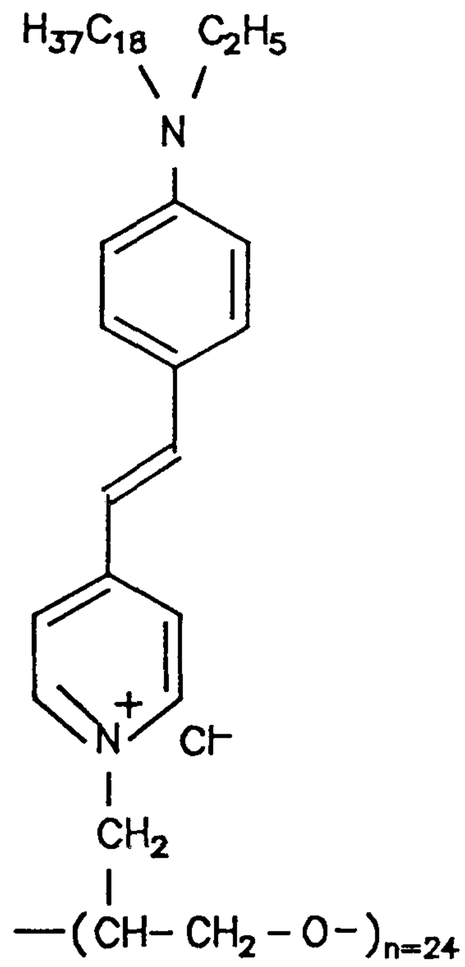

XLIII

Figure 35. An improved chromophore incorporated onto a polymeric backbone[167].

The increase in SHG with number of layers of the interleaved multilayer is shown in figure 36. The results were normalized to the intensity of a 5 layer film thereby diminishing the effect of the anomalous first layer response.

The response was subquadratic, however it should be noted that the 25 layer film had a SHG signal approximately 265 times stronger than a hemicyanine monolayer.

Absorbance data showed consistent deposition and a slight shift of λ_{max} with increasing layers. In fact for 10 to 25 layers λ_{max} was blue shifted, therefore resonant enhancement was reduced slightly, reducing the relative SHG. This may explain the subquadratic behaviour. The effect of the spacer layer was investigated by SHG and optical absorbance measurements, however results were contradictory.

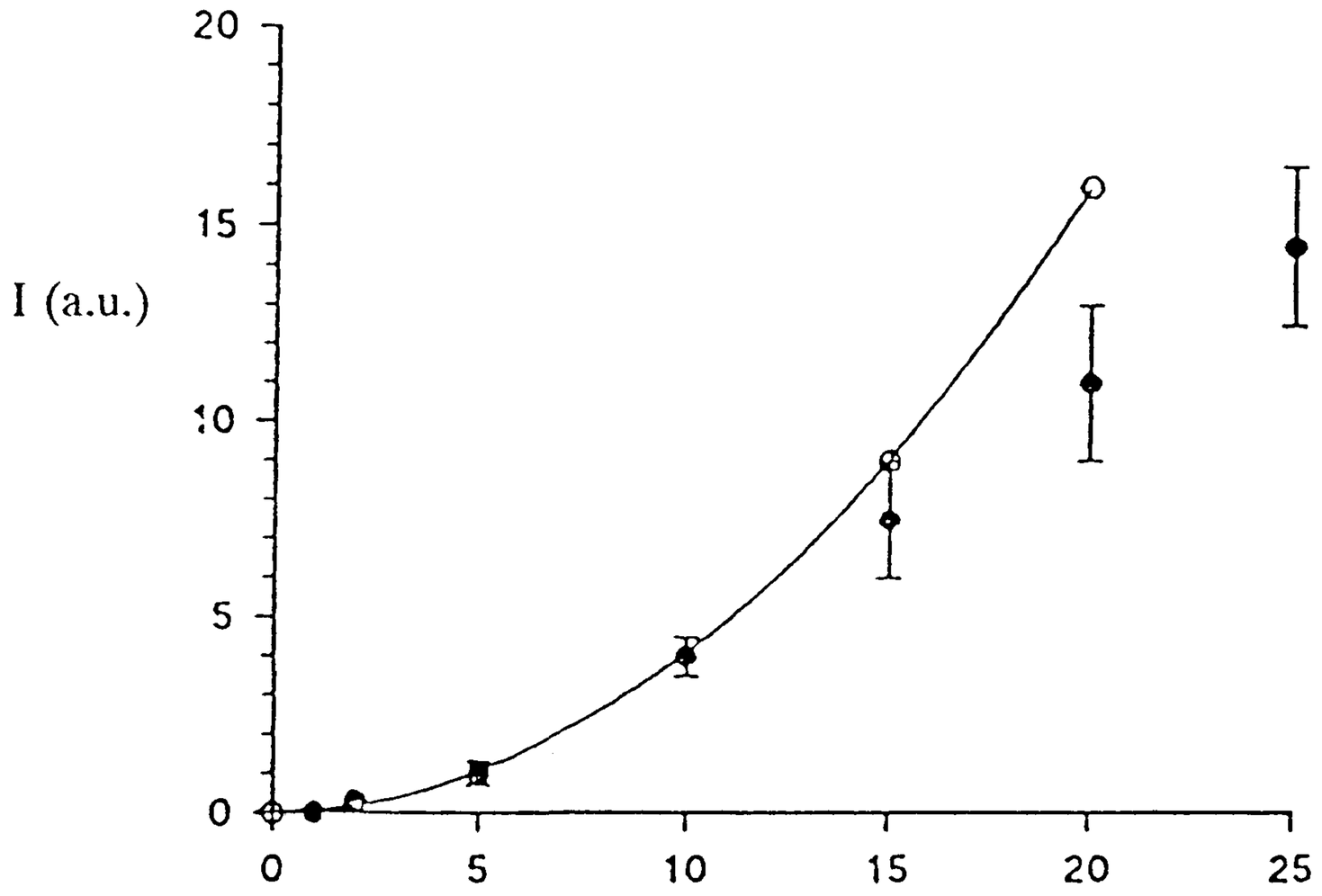

Figure 36. SH response versus number of bilayers for a **XLIII**:behenic acid interleaved multilayer film; (O) quadratic dependence, (●) actual dependence.

Similarly, **XLIV** and polymer **XLV** were deposited[166]. Since merocyanine was used it was necessary to enclose the samples in a cell containing ammonia vapour to prevent protonation. The Y-type structure produced multilayers of various thicknesses up to 70 bilayers, which still appeared uniform when viewed through a microscope.

The SHG did not increase in a linear fashion with thickness. A possible explanation is that most nonlinear organic molecules have permanent dipole moments of about 5 debye units or larger so that they produce an electric potential of approximately 1 volt in this film. The energy required to transfer an electron from one

chromophore to another is 10 eV. Hence for films with more than 10 layers, some of the chromophores can be ionised and the charge transferred from one side of the system to the other. The larger the film the greater the effect on SHG.

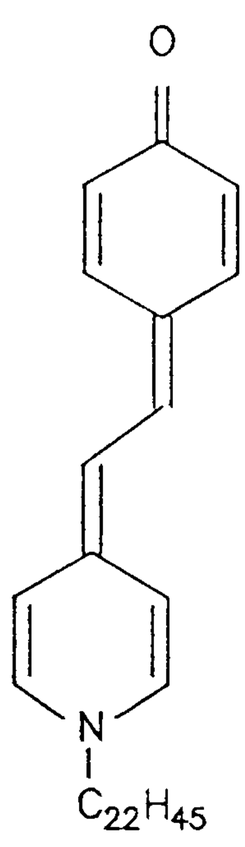

XLIV

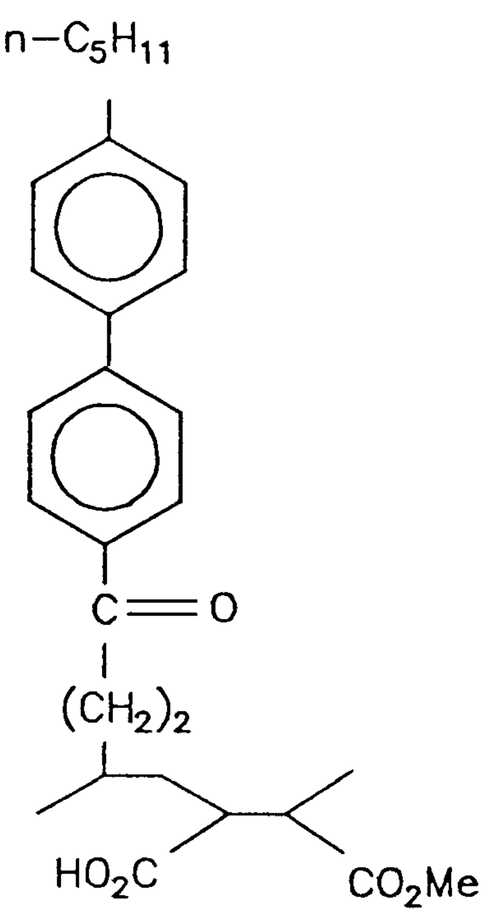

XLV

Figure 37. Two chromophores with their nonlinearity aligned in the opposite sense, relative to the hydrophobic chain[166].

Further investigations used a hemicyanine chromophore instead of merocyanine[168]. A 120 layer film was deposited, as well as a film with a double spacer layer of arachidic acid deposited every ten layers. The latter film exhibited much better SH characteristics but was still not quadratic. A larger monolayer signal, from polymer **XLVI**, was observed and an alternating multilayer film of good optical quality was also fabricated[169].

Alternating Y-type multilayers using arachidic acid and a polyacrylate containing a 4-amino-4'-sulfonylazobenzene chromophore exhibited quadratic dependence of SH response with increasing layers[170].

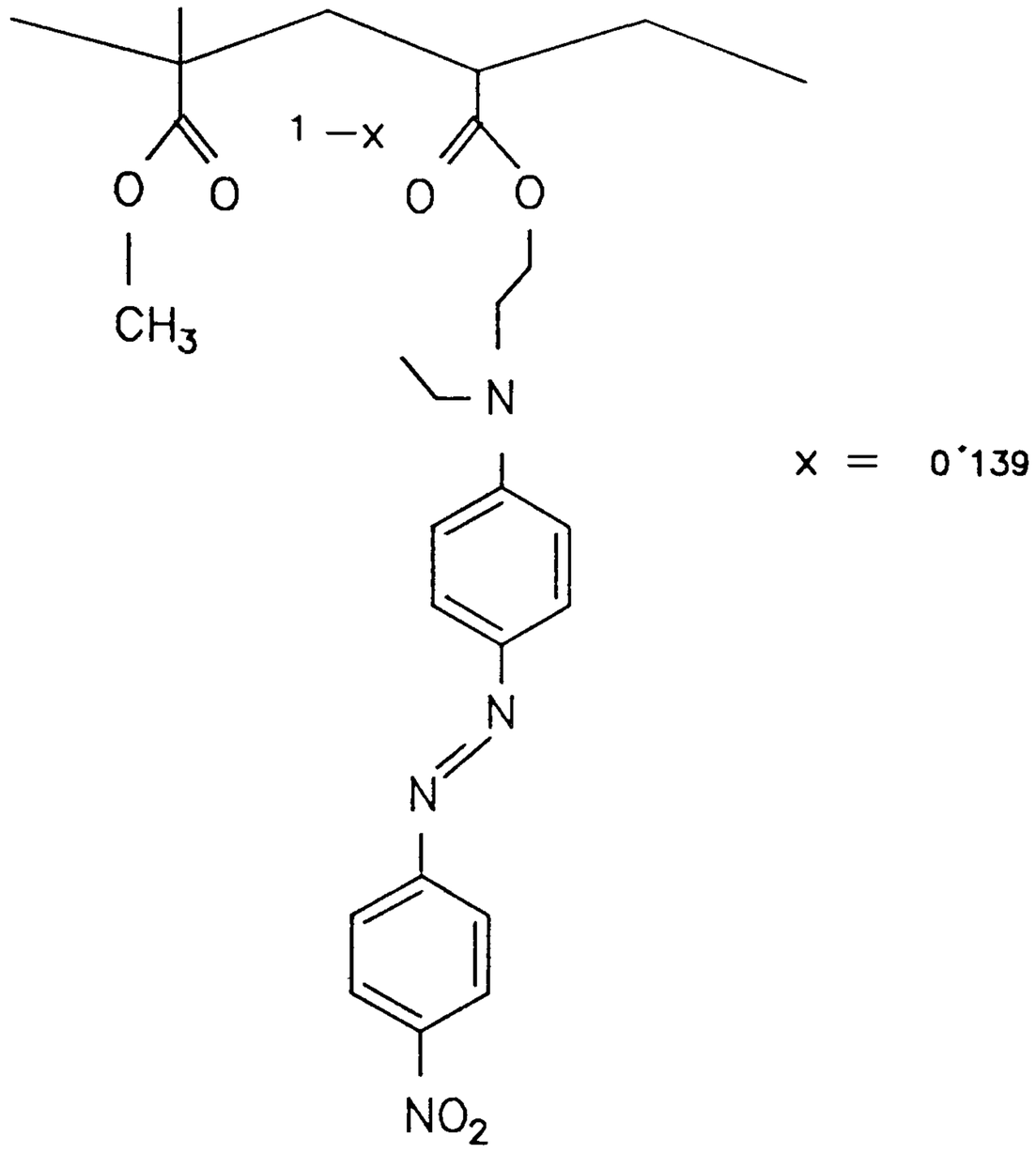

Figure 38. **XLVI** Copoly(2-(N-ethyl-N-(4-nitrophenylazo)phenyl)amino)ethyl acrylate/methyl methacrylate[169].

Material	Type of film	Reported SHG data
XLVI	Multilayer	$\chi^{(2)} = 9.8 \times 10^{-12}$ m V^{-1}

Table 14. Reported SHG data for material **XLVI**[169].

One group fabricated 262 layers of a noncentrosymmetric structure that had a quadratic dependence of SHG with film thickness[171], using the random copolymer

XLVII. Alternating multilayer films were deposited using ω-tricosanoic acid as a spacer. The chromophore absorbed up to 580 nm therefore some resonant enhancement was responsible for the SH signal.

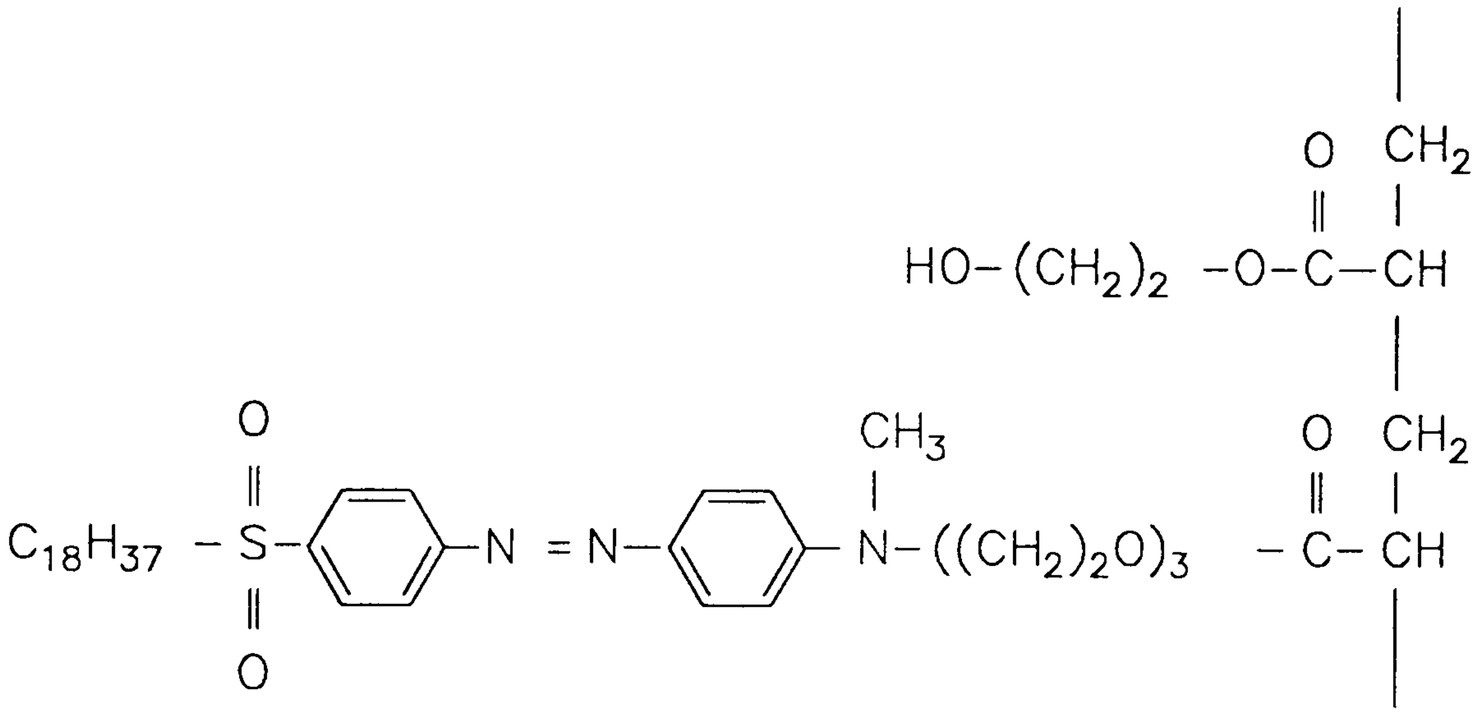

Figure 39. **XLVII**, a copolymer capable of fabrication into a thick alternate multilayer[171].

The stability of the polymer as an LB film was in contrast to the lack of thermal or mechanical stability of the acid. Ellipsometry measurements indicated that the film was thicker than 1000 **Å**. Polarisation studies of the SHG indicated that the chromophores were highly ordered. The value of $\chi^{(2)}$ for the multilayer of **XLVII** not only represents that largest signal recorded for a polymeric LB film, but is also one of the largest documented for any type of LB film.

Material	Type of film	Reported SHG data
XLVII	Multilayer	$\chi^{(2)} = 4.2 \times 10^{-11}$ F m^3 V^{-1}

Table 15. Reported SHG data for **XLVII**[171].

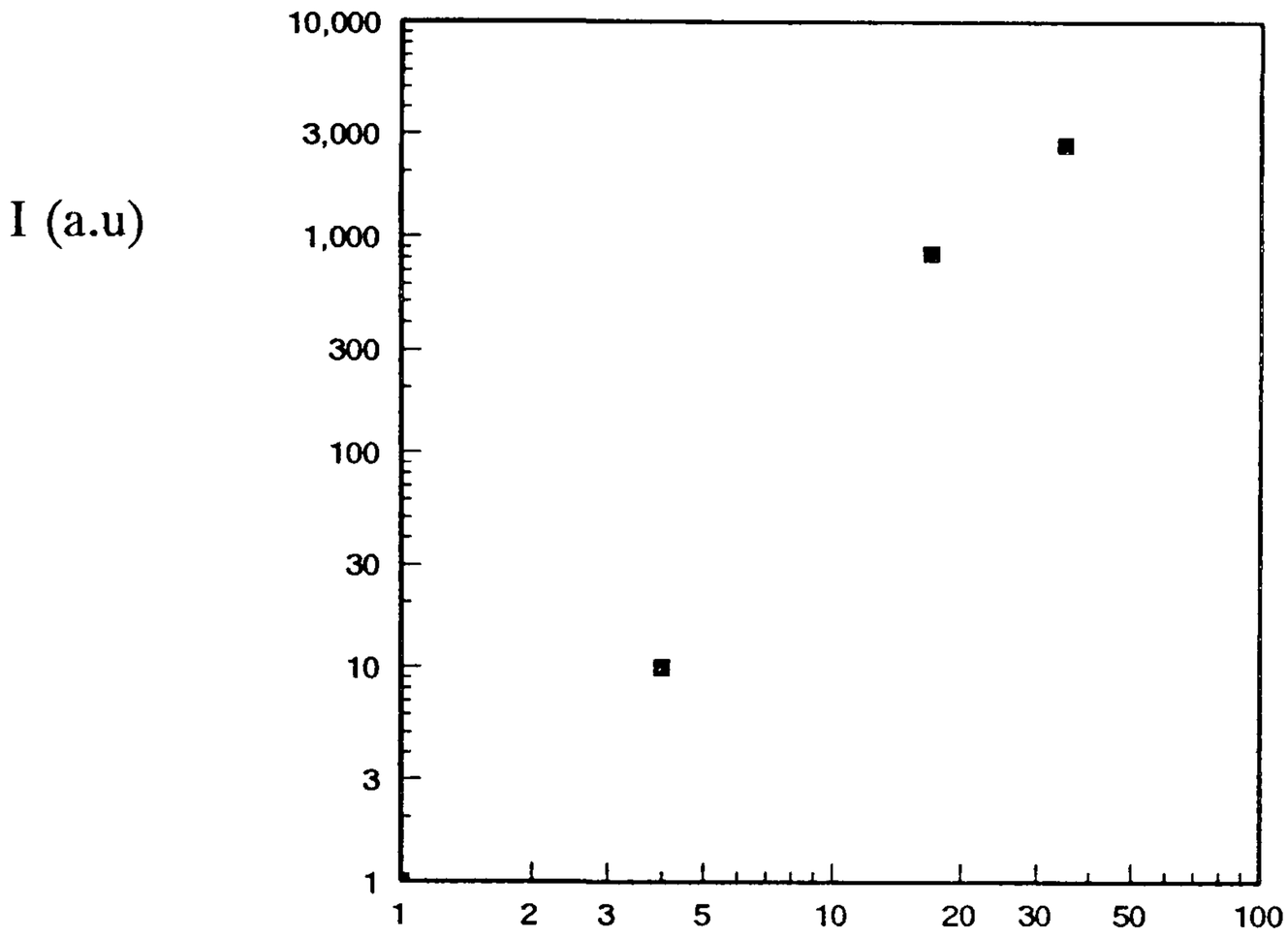

Figure 40. SH response versus number of layers for a multilayer film of **XLVII**[171].

A novel analogue of the material 2-docosylamino-5-nitropyridine (DCANP), described in section 1.6.8., was polymerised as an LB film[172]. Multilayer films of 2-(21-docosenyl)amino-5-nitropyridine, **XLVIII**, were polymerised by X-ray irradiation. The UV/vis and IR spectrum before and after polymerisation were identical and it was found that polymerisation had no effect on the nonlinear optical coefficient of the film.

1.6.8 Herringbone or Intercalated Y-type Multilayer Films

A novel multilayer structure was deposited that derived its quadratic nonlinear properties from its alignment[173-176]. Initially a group of materials were investigated as monolayers in an attempt to identify optimum LB film parameters, ie chain length, nature of substituent etc. The materials contained either a pyridine or a benzene ring.

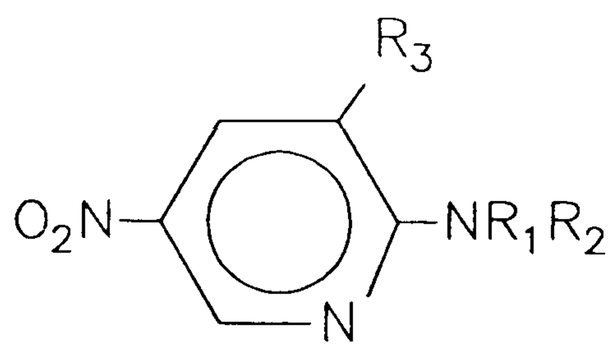

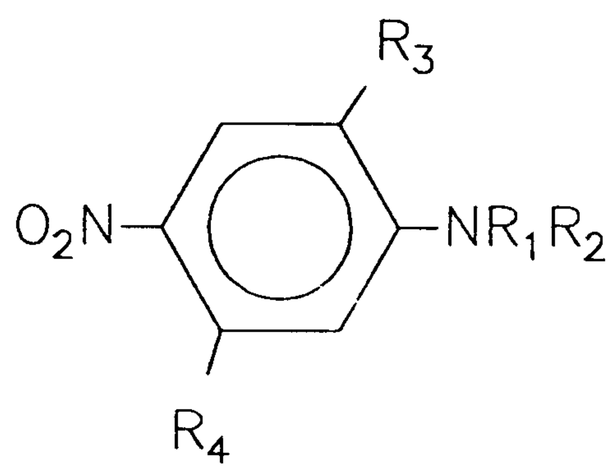

Figure 41. General formula of pyridine and benzene derivatives fabricated as LB films for SHG[173].

Multilayer films of the pyridine derivatives, $R_1 = C_{18}H_{37}$ to $C_{26}H_{53}$ and R_2, R_3 = H were fabricated. The molecules were transferred on the upstroke and downstroke until 36 deposition cycles had taken place. The SH response from each film was investigated (figure 42) and it was found that the $C_{22}H_{45}$ analogue provided the largest signal.

An investigation into the orientation of the chromophores indicated that local field effects of intermolecular interactions reduced the nonlinear optical activity of the C_{24} and C_{26} analogues. The C_{22} analogue was most likely the optimum chain length because it counteracted this effect with its improved molecular alignment. It is possible, therefore, that slight changes in the hydrophobic part of a LB film significantly influence the orientation of the hydrophilic part and the associated material parameters.

A large multilayer film of 2-docosylamino-5-nitropyridine (DCANP) exhibited a quadratic nonlinear dependence of SH response for up to 270 bilayers. This behaviour indicates that the nonlinearities of each layer were directed in the same direction, this

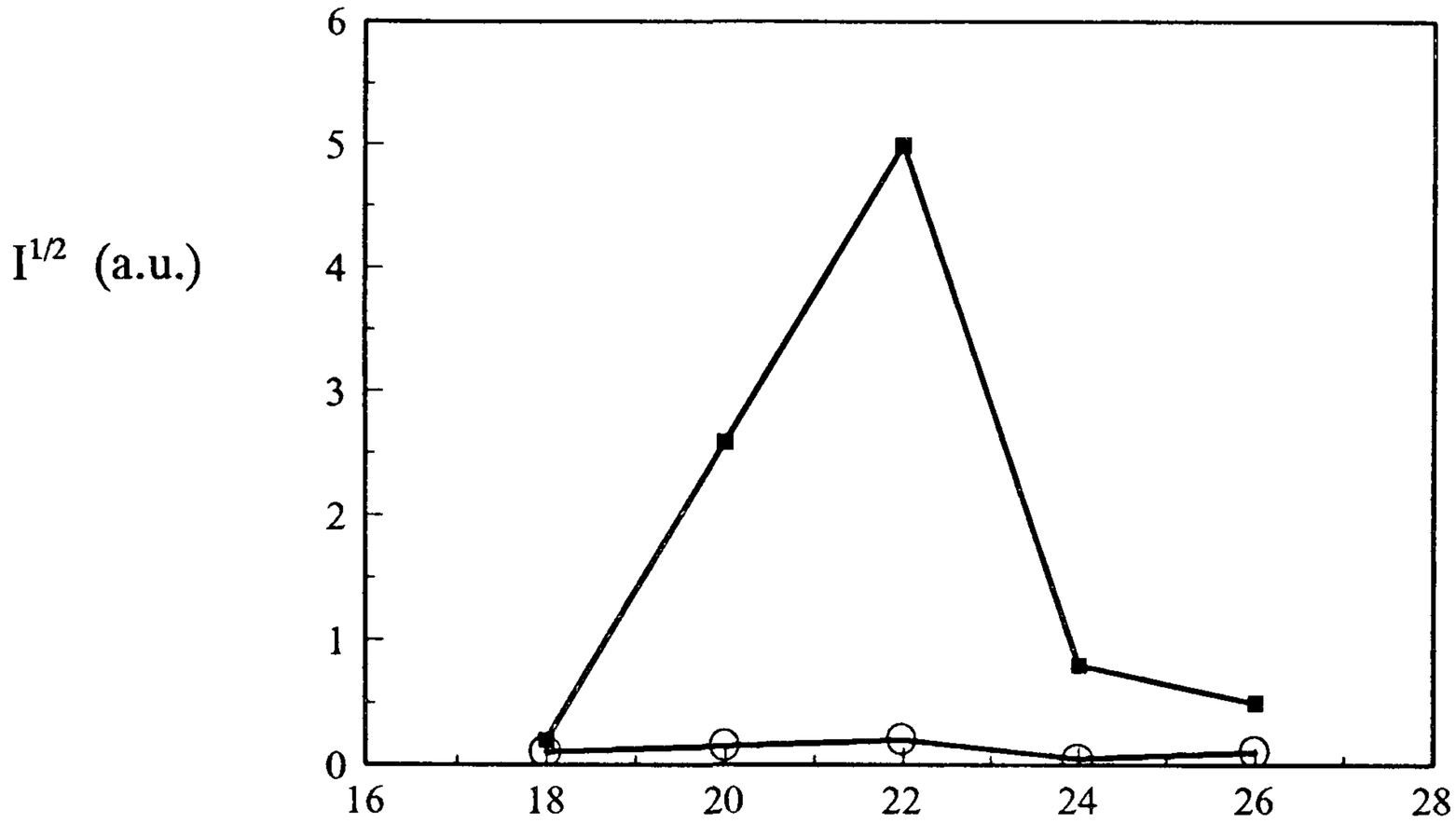

Figure 42. SH response versus chain length for multilayer films of the homologous materials, 2-alkylamino-5-nitropyridine[173]. (■) I parallel to dipping direction, (o) I perpendicular to dipping direction.

alignment infers a X-type or Z-type structure. However X-ray diffraction studies indicated that the molecules in the film were highly ordered and centrosymmetric thus eliminating the feasibility of such film types. The layers must therefore be arranged in a novel Y-type arrangement, either:

1. a polar Y-type structure with a herringbone-type arrangement;
2. an intercalated structure with the alkyl chains orientated nearly perpendicular to the substrate.

In both cases the noncentrosymmetricity results from a unique alignment of the chromophore in a single direction. The chromophore arrangement is probably enhanced or stabilised by interlayer hydrogen bridging between the amino and nitro substituents of adjacent molecules. This is similar to how it occurs in single crystals of 2-

cyclooctylamino-5-nitropyridine[176]. Intercalation requires a phase transition during or after film transfer and this makes it less likely than the "herringbone" structure.

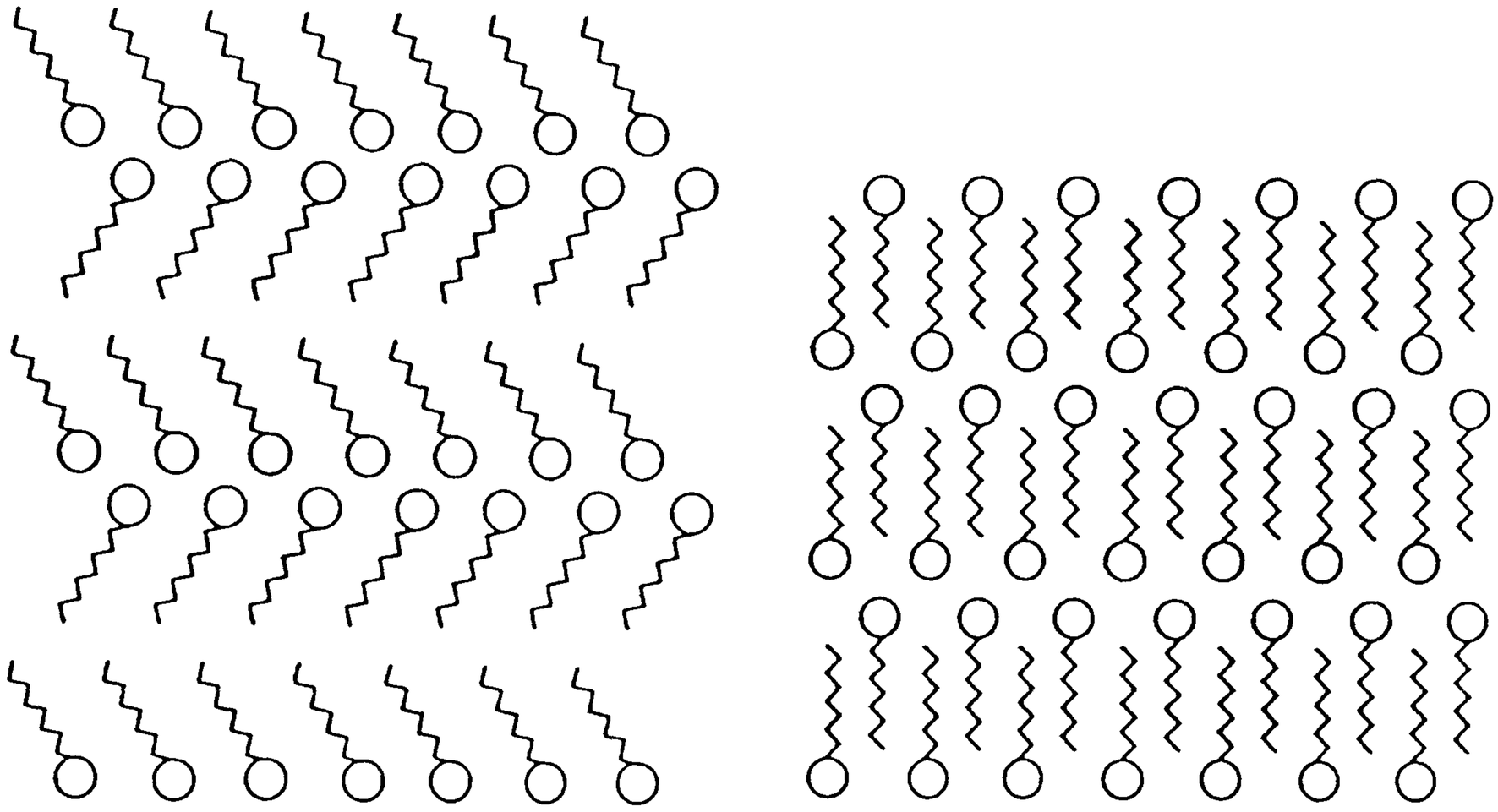

A B

Figure 43. Possible configurations for the multilayer structure of 2-dialkylamino-5-nitropyridine: (A) "herringbone", (B) intercalated[174,175].

The nonlinear response for a 80 layer film of DCANP was calculated in terms of d, where $d = \frac{1}{2} \chi^{(2)}$.

Material	Type of film	Reported SHG data
DCANP	80 layers	$d_{333} = 6.8 \times 10^{-12}$ m V^{-1} $d_{311} = 0.9 \times 10^{-12}$ m V^{-1}

Table 16. SHG data for DCANP[173-175].

1.6.9 Summary of Findings

It is evident that a huge number of very different molecules have been studied and as a result some simple prerequisites are apparent for the fabrication of organic LB films for SHG. Firstly, materials must be synthesised that are:

1. stable at the air/water interface, preferably without requiring the presence of counterions;
2. uniform and tightly packed at deposition;
3. stable as a monolayer LB film, with their molecules aligned in parallel along the molecular layer.

Secondly the molecules should contain a chromophore capable of nonlinear response upon irradiation from an intense light source. It is noted that a considerable number of the materials reported contain a conjugated, hydrophobic head group attached to a saturated aliphatic chain. Upon transfer to the substrate the chromophore should align at an angle that maximises its SH response in the direction of the light source. In order to generate a large SH response the material must be capable of forming stable multilayers having the nonlinear functions of each layer aligned in the same direction. If each layer has transferred perfectly then the thick film should have a quadratic relationship between SHG and the number of layers.

It is important to achieve these ambitions with materials that are neither difficult or expensive to prepare, and ones that have a structure that can be altered slightly in configuration in order to improve performance. If so then a lot can be learned about all aspects of LB films, the surface properties of materials and SHG, as well as progressing towards the goal of assembling LB films for commercial applications.

2.0 Experimental

The preparation of all the materials studied are presented, as well as the apparatus used for the LB investigations and the optical equipment used for the study of second harmonic generation (SHG).

2.1 Synthesis

2.1.1 Quinolinium Hemicyanines

E-1-hexadecyl, E-1-octadecyl, E-1-eicosyl, and E-1-docosyl-4-{2-(4-dimethylaminophenyl)ethenyl}quinolinium bromide and E-1-octadecyl-4-{2-(4-dimethylaminophenyl)ethenyl}quinolinium iodide were synthesised in similar fashion. The synthesis of E-1-octadecyl-4-{2-(4-dimethylaminophenyl)ethenyl}quinolinium bromide is presented.

To a solution of N-octadecyl-4-methylquinolinium bromide (1.13 g, 2.37 mmol) and 4-dimethylaminobenzaldehyde (0.34 g, 2.25 mmol) in hot ethanol was added one drop of piperidine. The solution was refluxed for four hours during which time it turned purple, it was then cooled to room temperature and yielded a purple precipitate. Recrystallisation from a 50:50 methanol:water mixture produced purple crystals.

Yield 21% Melting point 237-240°C. $C_{37}H_{55}N_2Br$ requires C,73.2; H,9.1; N,4.6% Found C,73.0; H,9.4; N,4.4% IR: 2960, 2920, 2845, 1620, 1605, 1525, 1450, 1430, 1377, 1328, 1170, 976, 940, 875, 834, 812 and 712 cm^{-1}. ^1H NMR (DMSO): 0.9 (3H, t, $-CH_3$); 1.3 (32H, br s, $(CH_2)_{16}$; 3.0 (6H, s, $(CH_3)_2N$-); 4.9 (2H, t, CH_2N^+); 6.8 (2H, d, J = 5.9 Hz, -CH=CH-); 7.9 - 8.5 (9H, m, Ar-H), 9.0 - 9.4 (1H, m, Ar-H).

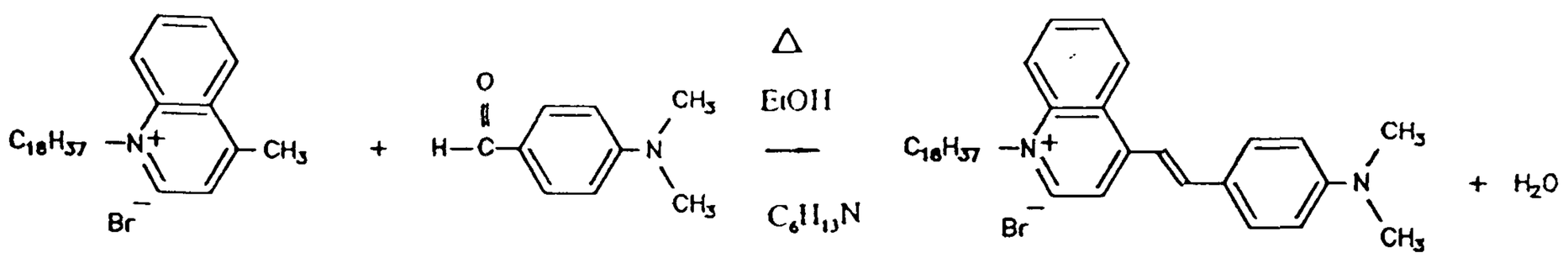

Figure 44. Synthesis of *E-1-octadecyl-4-{2-(4-dimethylaminophenyl) ethenyl}quinolinium bromide* (2.1.1).

E-1-hexadecyl-4-{2-(4-dimethylaminophenyl)ethenyl}quinolinium bromide:

Purple powder, 22% yield. Melting point 238-240°C.

E-1-docosyl-4-{2-(4-dimethylaminophenyl)ethenyl}quinolinium bromide:

Purple powder, 20% yield. Melting point 237-238°C. $C_{41}H_{63}N_2Br$ requires C,74.2; H,9.5; N,4.2% Found C,74.0; H,9.8; N,4.1%

E-1-eicosyl-4-{2-(4-dimethylaminophenyl)ethenyl}quinolinium bromide:

Purple powder, 62% yield. Melting point 241-244°C.

E-1-octadecyl-4-{2-(4-dimethylaminophenyl)ethenyl}quinolinium iodide:

Purple powder, 80% yield. Melting point 221-222°C. $C_{37}H_{55}N_2I$ requires C,67.9; H,8.4; N,4.3; I,19.4% Found C,67.3; H,8.5; N,3.9; I,19.8% IR: 2958, 2919, 2844, 1625, 1605, 1523, 1449, 1430, 1380, 1333, 1166, 976, 941, 875, 830, 812 and 717 cm^{-1}. ^1H NMR (DMSO): 0.9 (3H, t, $-CH_3$); 1.3 (32H, br s, $(CH_2)_{16}$; 2.9 (6H, s, $(CH_3)_2N$-); 4.8 - 5.1 (2H, t, CH_2N^+); 6.9 (2H, d, J = 5.9 Hz, -CH=CH-); 7.8 - 8.6 (9H, m, Ar-H), 9.0 -9.4 (1H, m, Ar-H).

2.1.2 Pyridinium Hemicyanines

E-1-hexadecyl, E-1-octadecyl and E-1-docosyl-4-{2-(4-dimethylamino-phenyl)ethenyl}pyridinium bromide, E-1-octadecyl-4-{2-(4-dimethylamino-phenyl)ethenyl}pyridinium iodide and E-1-docosyl-4-{2-(4-methylphenyl)ethenyl}pyridinium bromide were synthesised in similar fashion. The

synthesis of E-1-octadecyl-4-{2-(4-dimethylaminophenyl)ethenyl}pyridinium iodide is presented.

To a solution of N-octadecyl-4-methylpyridinium iodide (0.28 g, 0.6 mmol) and 4-dimethylaminobenzaldehyde (0.089 g, 0.6 mmol) in hot ethanol was added one drop of piperidine. It was refluxed for two and a half hours during which time it turned red, it was then cooled to room temperature and yielded an orange/red precipitate. Recrystallisation from a 50:50 methanol:water mixture produced red crystals.

Yield 46% Melting point 194-195°C. $C_{33}H_{53}N_2Br$ requires C,65.5; H,8.8; N,4.6% Found C,65.2; H,8.5; N,4.3% IR: 2958, 2915, 2845, 1637, 1590, 1525, 1465, 1430, 1365, 1328, 1162, 976, 946, 875, 829, 810 and 717 cm^{-1}. ^1H NMR (DMSO): 0.9 (3H, t, $-CH_3$); 1.3 (32H, br s, $(CH_2)_{16}$); 2.9 (6H, s, $(CH_3)_2N$); 4.7 (2H, t, CH_2N^+); 6.7 (2H, d, J = 5.9 Hz, -CH=CH-); 7.0 (1H, s, Ar-H); 7.5 (2H, d, Ar-H); 7.7 (1H, s, Ar-H); 8.0 (2H, d, Ar-H) and 8.4 (2H, d, Ar-H).

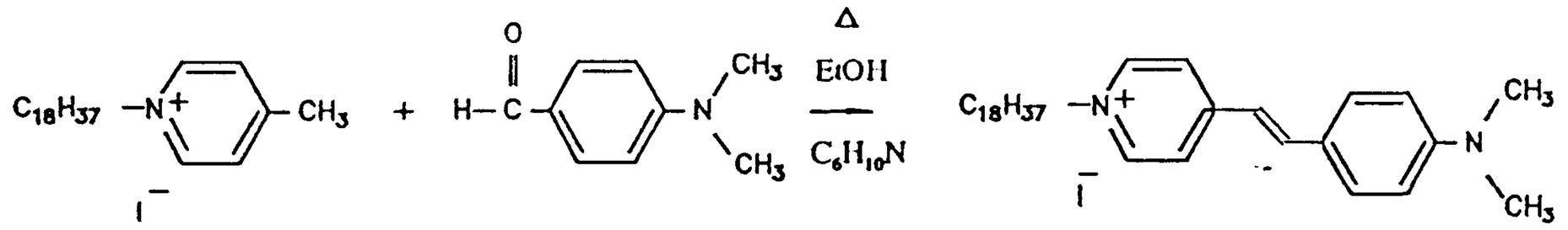

Figure 45. Synthesis of *E-1-octadecyl-4-{2-(4-dimethylaminophenyl) ethenyl}pyridinium iodide* (2.1.2).

E-1-hexadecyl-4-{2-(4-dimethylaminophenyl)ethenyl}pyridinium bromide:

Red powder, 45% yield. Melting point 190-192°C.

E-1-octadecyl-4-{2-(4-dimethylaminophenyl)ethenyl}pyridinium bromide:

Red crystals, 37% yield. Melting point 207-209°C. IR: 2960, 2920, 2848, 1637, 1605, 1525, 1455, 1430, 1380, 1330, 1162, 975, 943, 875, 826, 808 and 715 cm^{-1}.

^{1}H NMR (DMSO): 0.9 (3H, t, -CH_3); 1.3-1.8 (32H, br s, $(CH_2)_{16}$); 3.1 (6H, s, $(CH_3)_2$N-); 4.7 (2H, t, CH_2N^+); 7.0 (1H, s, C=CH); 7.1 (4H, doublet of doublet, Ar-H); 7.7 (1H, s, HC=C); 8.4 (4H, doublet of doublets, Ar-H).

E-1-docosyl-4-{2-(4-dimethylaminophenyl)ethenyl}pyridinium bromide:

Red powder, 21% yield. Melting point 210-211°C.

E-1-docosyl-4-{2-(4-methylphenyl)ethenyl}pyridinium bromide:

Red crystals, 38% yield. Melting point 73-76°C. IR. 2960, 2920, 2844, 1625, 1605, 1514, 1455, 1377, 1333, 1170, 980, 882, 828, 820 and 717 cm^{-1}.

2.1.3 E-1-alkyl-4-{2-(4-dimethylaminonaphthyl)ethenyl}quinolinium or pyridinium bromide.

E-1-octadecyl and E-1-docosyl-4-{2-(4-dimethylaminophenyl)ethenyl} quinolinium and E-1-octadecyl and E-1-docosyl-4-{2-(4-dimethylaminophenyl) ethenyl}pyridinium bromide were prepared by the same method. The synthesis of E-1-docosyl-4-{2-(4-dimethylaminonaphthyl)ethenyl}quinolinium bromide is presented.

N-docosyl-4-methylquinolinium bromide (1.0 g, 0.22 mmol) was dissolved in refluxing ethanol and added to 4-dimethylaminonaphthaldehyde (0.45 g, 2.24 mmol). Two drops of piperidine were added and the mixture refluxed for twelve hours to produce a deep purple solution. This was filtered to leave a purple residue. The residue was recrystallised from a 50:50 methanol:water mixture.

Yield 42% Melting point 285-290°C. $C_{45}H_{65}N_2Br$ requires C,75.8; H,9.1; N,3.9% Found C,76.0; H,9.5; N,4.1% IR: 2955, 2915, 2848, 1614, 1603, 1528, 1455, 1430, 1375, 1328, 1160, 972, 940, 872, 834, 818 and 717 cm^{-1} ^{1}H NMR (DMSO): 0.9 (3H, t, -CH_3); 1.3 (40H, br s, $(CH_2)_{20}$; 3.1 (6H, s, $(CH_3)_2$N-); 4.9 (2H, t, CH_2N^+); 6.7 (2H, d, J = 5.9 Hz, -CH=CH-); 7.7 - 8.7 (11H, m, Ar-H), 9.0 - 9.4 (1H, m, Ar-H).

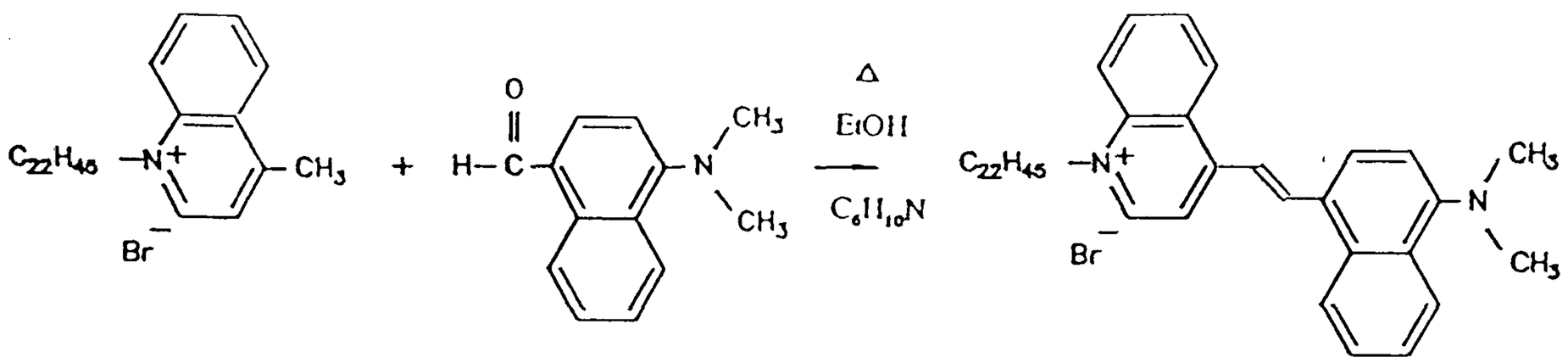

Figure 46. Synthesis of *E-1-docosyl-4-{2-(4-dimethylaminonaphthyl)ethenyl} quinolinium bromide.* (2.1.3).

E-1-octadecyl-4-{2-(4-dimethylaminonaphthyl)ethenyl} quinolinium bromide:

Purple powder, 36% yield. Melting point 285-288°C.

E-1-octadecyl-4-{2-(4-dimethylaminonaphthyl)ethenyl} pyridinium bromide:

Red powder, 71% yield. Melting point 249-253°C.

E-1-docosyl-4-{2-(4-dimethylaminonaphthyl)ethenyl} pyridinium bromide:

Red powder, 60% yield. Melting point 251-255°C.

2.1.4 E-1-alkyl-4-{4-(4-dimethylaminophenyl)-1,3-butadienyl}pyridinium bromide.

E-1-octadecyl and E-1-docosyl-4-{4-(4-dimethylaminophenyl)-1,3-butadienyl}pyridinium bromide were prepared in the same manner as the other hemicyanines described in sections 2.1.2, 2.1.3 and 2.1.4 only using 4-dimethylaminocinnamaldehyde.

E-1-octadecyl-4-{4-(4-dimethylaminophenyl)-1,3-butadienyl}pyridinium bromide.

Red powder, 28% yield. Melting point 275-280°C.

E-1-docosyl-4-{4-(4-dimethylaminophenyl)-1,3-butadienyl}pyridinium bromide.

Red powder, 8% yield. Melting point 279-281°C $C_{39}H_{63}N_2Br$ requires C,73.2; H,9.9; N,4.4% Found C,73.7; H,9.6; N,4.6%

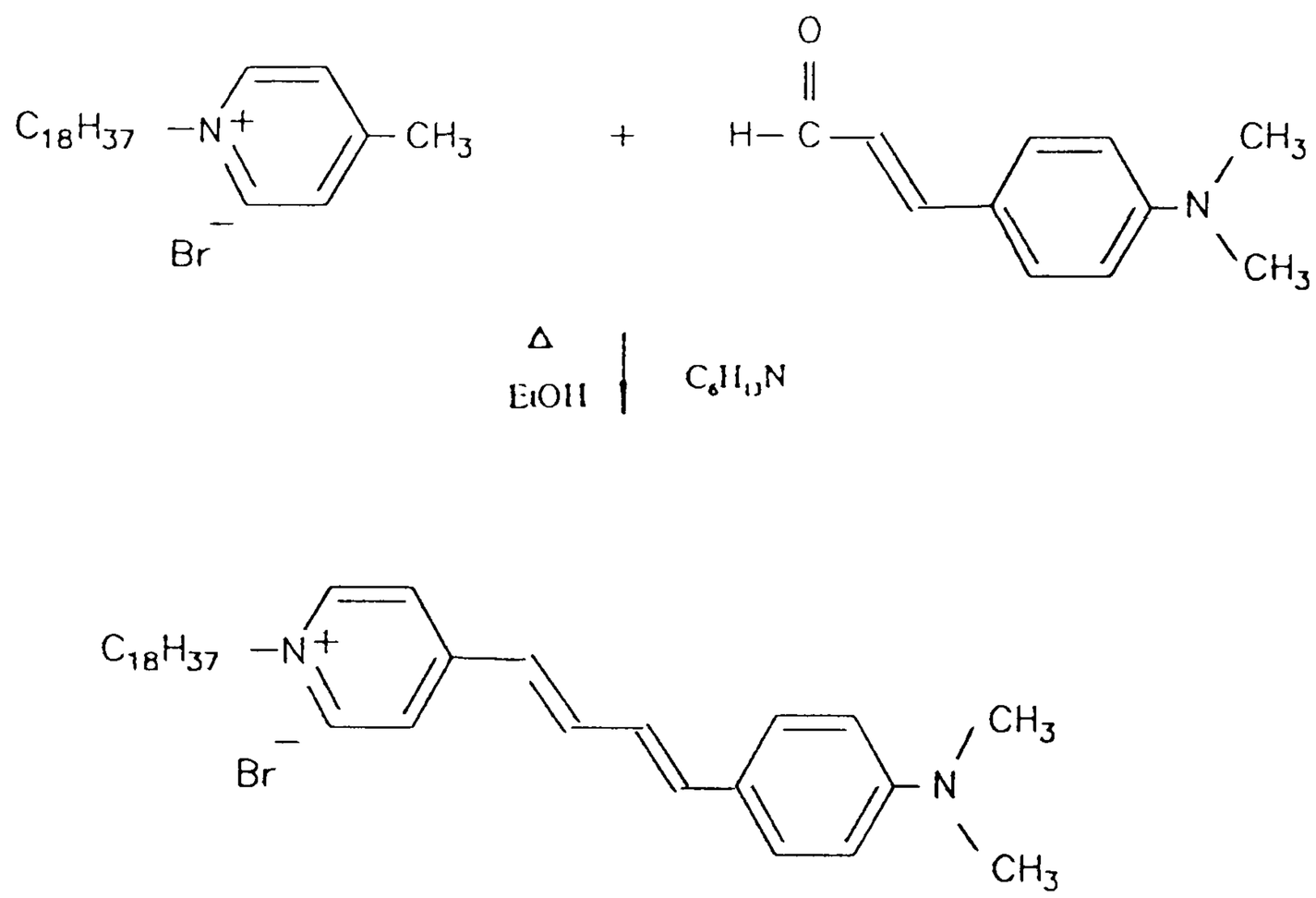

Figure 47. Synthesis of *E-1-octadecyl-4-{4-(4-dimethylaminophenyl)-1,3-butadienyl} pyridinium bromide (2.1.4).*

2.1.5 E-1-docosyl-4-{2-(4-{2-(4-dimethylaminophenyl)ethenyl}benzyl)ethenyl} pyridinium bromide.

This material was synthesised in the same manner as the other hemicyanines, using E-1-docosyl-4-{2-(4-methylphenyl)ethenyl}pyridinium bromide and 4-dimethylaminobenzaldehyde.

Yield 7% Melting point 180-182°C. $C_{45}H_{67}N_2Br$ requires C,75.5; H,9.4; N,3.9% Found C,75.0; H,9.0; N,3.8% IR: 2952, 2912, 2845, 1625, 1610, 1525, 1464, 1432, 1380, 1330, 1162, 975, 945, 875, 825, 808 and 715 cm^{-1}.

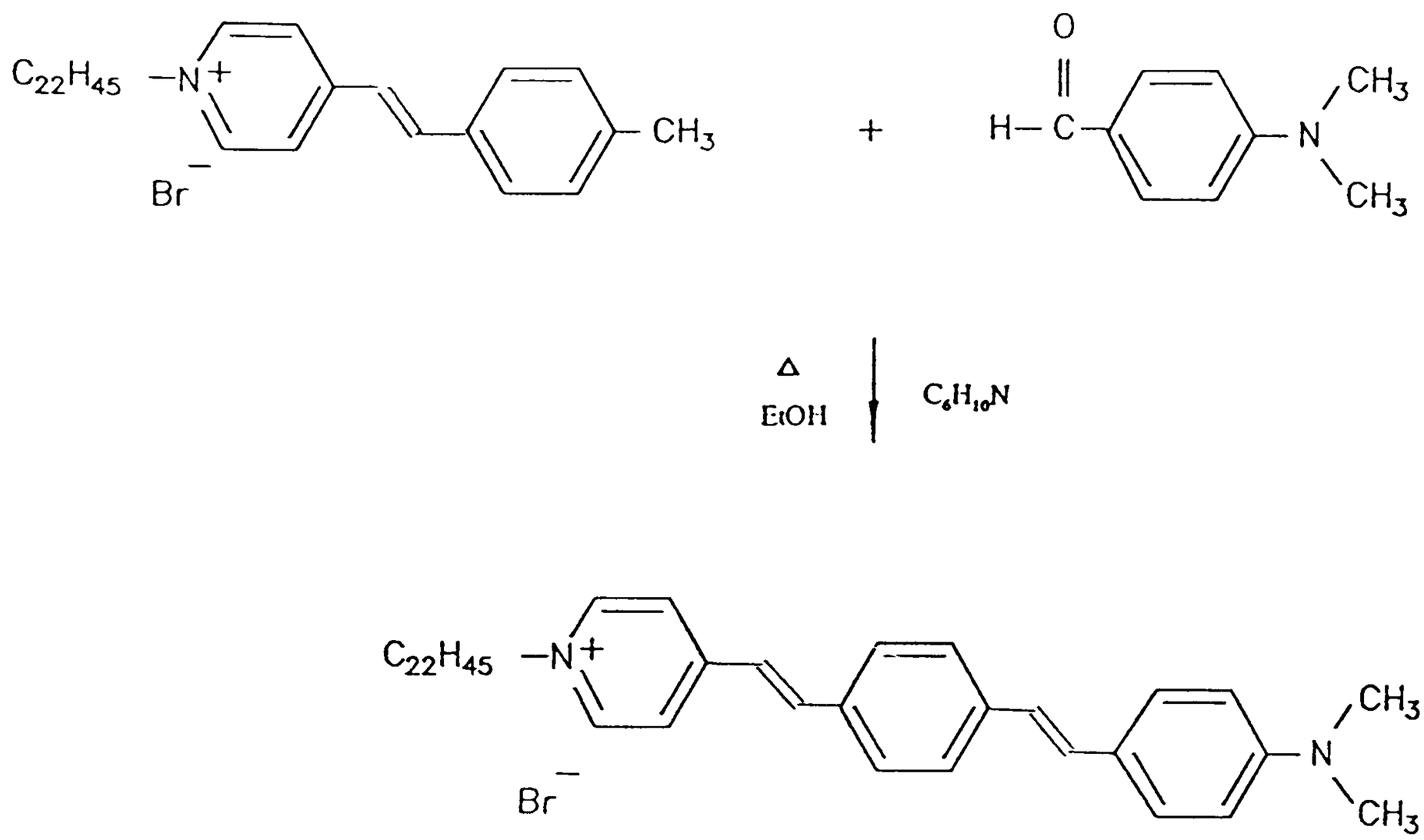

Figure 48. Synthesis of *E-1-docosyl-4-{2-(4-{2-(4-dimethylaminophenyl)ethenyl}benzyl)ethenyl}pyridinium bromide* (2.1.5).

2.1.6 E-1-alkyl-4-{2-(4-alkoxystyryl)ethenyl}pyridinium iodide.

E-1-octadecyl and E-1-docosyl-4-{2-(4-methoxystyryl)ethenyl}pyridinium iodide and E-1-docosyl-4-{2-(4-butoxystyryl)ethenyl}pyridinium iodide were prepared. The materials were synthesised in the same manner as other hemicyanines only using 4-methoxybenzaldehyde or 4-butoxybenzaldehyde.

E-1-docosyl-4-{2-(4-methoxystyryl)ethenyl}pyridinium iodide.

Yellow powder, 62% yield. Melting point 170-172°C.

E-1-octadecyl-4-{2-(4-methoxystyryl)ethenyl}pyridinium iodide.

Yellow powder, 60% yield. Melting point 170-176°C. $C_{32}H_{50}NOI$ requires C,64.9; H,8.5; N,2.4% Found C,65.2; H,8.1; N,2.5% IR: 2955, 2918, 2845, 1620, 1611, 1595, 1510, 1461, 1377, 1170, 1038, 980, 840, 810 and 720 cm^{-1}. ^1H NMR (DMSO): 0.9 (3H t, -

CH_3); 1.3-1.6 (32H, br s, $(CH_2)_{16}$); 2.7 (3H s, $-OCH_3$) 4.6 (2H, t, CH_2N^+); 7.0 (1H, s, C=CH); 7.3 (4H, doublet of doublet, Ar-H); 7.9 (1H, s, HC=C); 8.8 (4H, doublet of doublets, Ar-H).

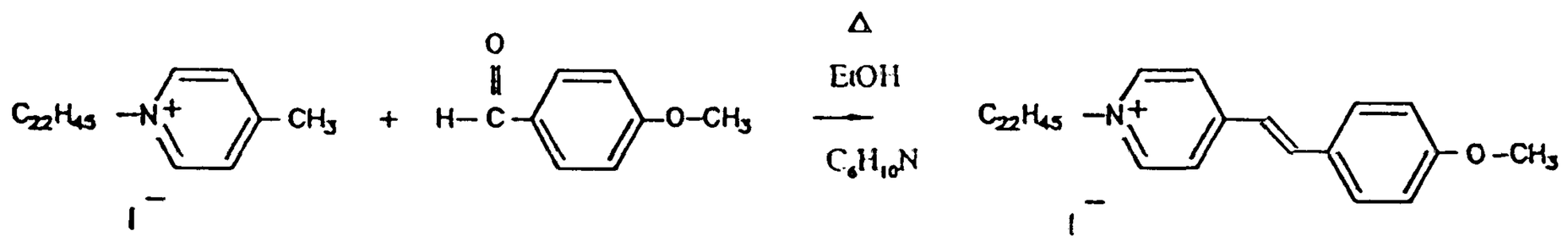

Figure 49. Synthesis of *E-1-docosyl-4-{2-(4-methoxystyryl)ethenyl}pyridinium iodide* (2.1.6).

E-1-docosyl-4-{2-(4-butoxystyryl)ethenyl}pyridinium iodide.

Yellow powder, 35% yield. Melting point 165-166°C.

2.1.7 4-octadecyloxybenzaldehyde

To a solution of sodium (0.84 g, 37 mmol) in ethanol (19ml) was added hydroxybenzaldehyde (4.44 g, 3.7 mmol). The mixture was heated to give an orange solution. Bromooctadecane (12.12 g, 3.6 mmol) was added and the mixture refluxed for 24 hours. On cooling a white precipitate formed which was dried at 80°C for a total of five hours. Recrystallised from ethanol produced a white powder.

Yield 52% $C_{25}H_{42}O_2$ requires C,80.2; H,11.2% Found C,77.4; H,11.4; IR: 2960, 2918, 2840, 1705, 1605, 1505, 1465, 1365 and 810 cm^{-1}

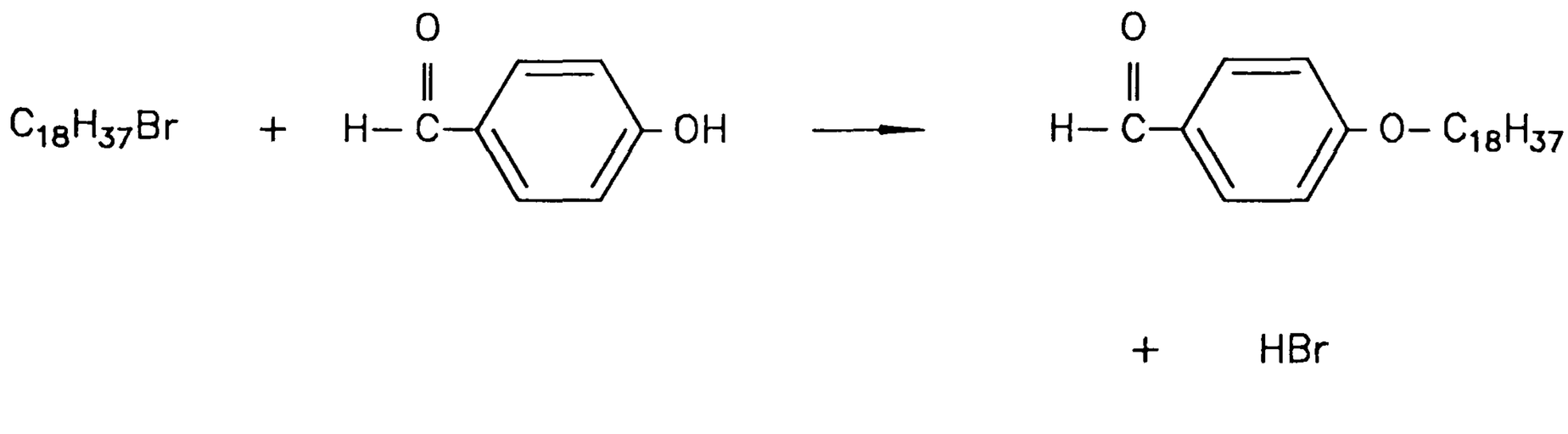

Figure 50. Synthesis of *4-octadecyloxybenzaldehyde* (2.1.7).

2.1.8 E-1-methyl-4-{2-(4-octadecyloxystyryl)ethenyl}pyridinium iodide.

To a solution of 4-octadecyloxybenzaldehyde (0.41 g, 1.1 mmol) and N-methyl-4-pyridinium iodide (0.12 g, 1.1 mmol) in ethanol was added 1 drop of piperidine. It was refluxed for 24 hours during which the solution turned orange and on cooling to room temperature a yellow precipitate formed. Recrystallisation from a 50:50 methanol:water mixture produced a yellow powder.

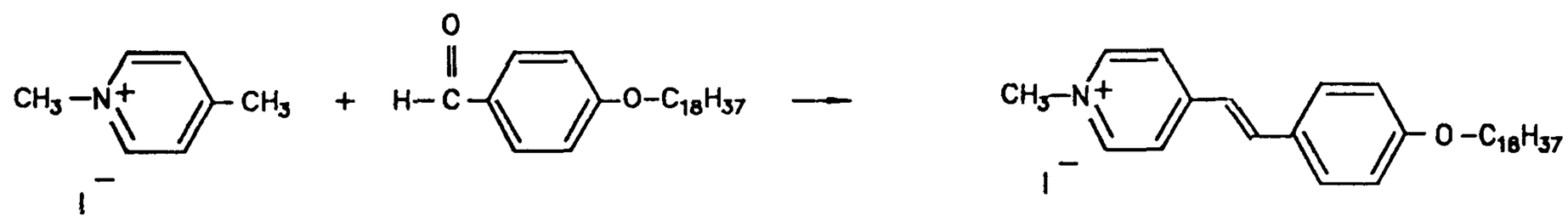

Figure 51. Synthesis of *E-1-methyl-4-{2-(4-octadecyloxystyryl)ethenyl}pyridinium bromide.*(2.1.8)

Yield 9% Melting point 190-191°C. $C_{32}H_{50}NOI$ requires C,64.9; H,8.5; N,2.4% Found C,65.0; H,8.7; N,2.2% IR: 2962, 2922, 2841, 1628, 1604, 1595, 1510, 1455, 1375 , 1170, 1040, 975, 832, 815 and 715 cm^{-1} ^1H NMR (DMSO): 0.9 (3H, t, $-CH_3$); 1.3-1.6 (32H, br s, $(CH_2)_{16}$); 2.7 (2H t, $-OCH_2$) 4.3 (3H s, CH_3N^+); 7.0 (1H, s, C=CH);

7.2 (4H, doublet of doublet, Ar-H); 7.9 (1H, s, HC=C); 8.8 (4H, doublet of doublets, Ar-H).

2.1.9 Mechanism of Hemicyanine Synthesis

The hemicyanines were synthesised by the method described by Girling et al[121] and the following mechanism is proposed.

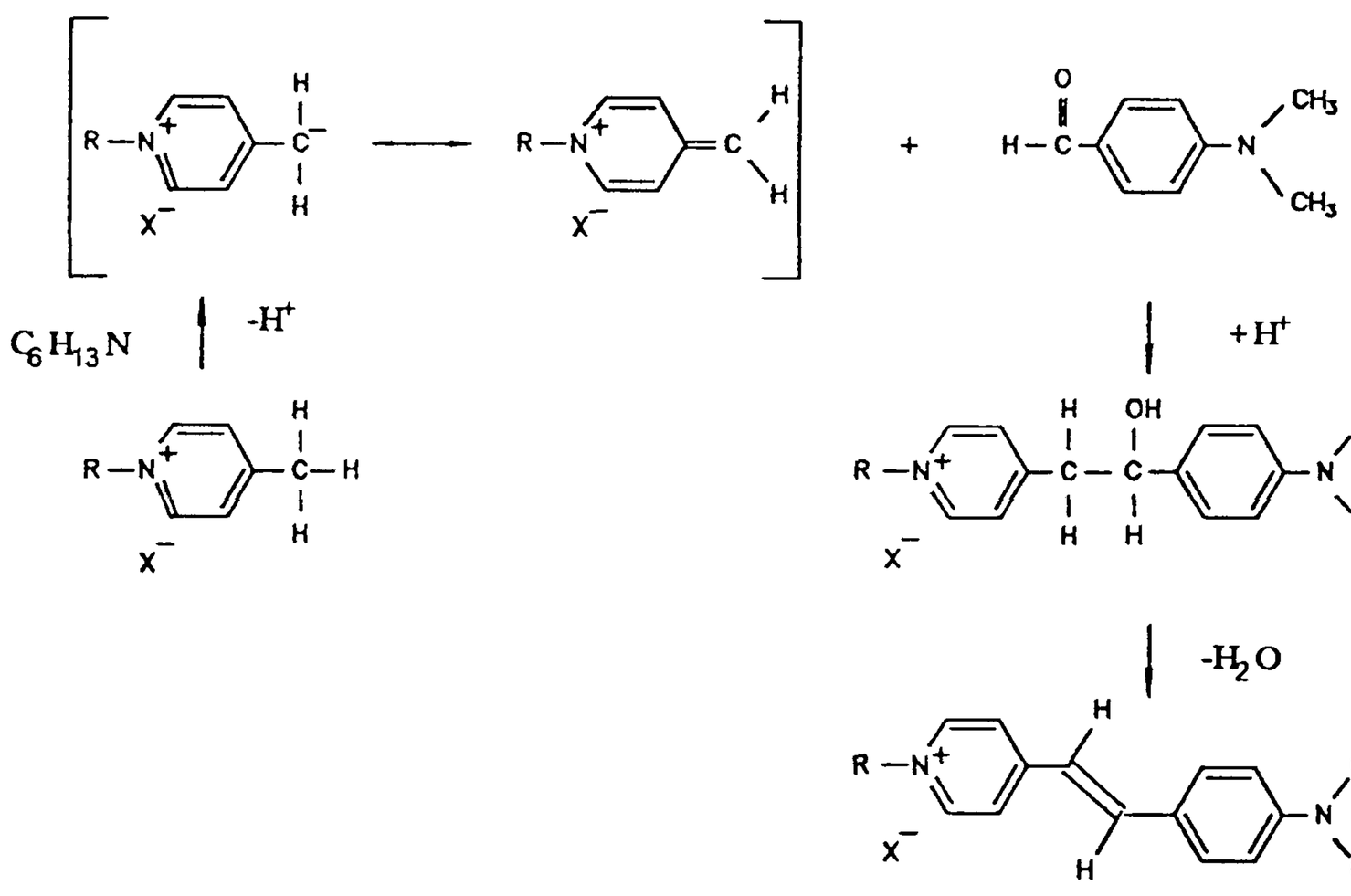

Figure 52. Mechanism of a typical hemicyanine synthesis.

The piperidine acts as a base catalyst and extracts a proton from the cation. This deprotonated form is stabilised because of its resonant quinoidal form. The polar carbonyl carbon then attacks the olefinic carbon on the cation to form a σ-bonded structure. The acidified ethanol solution then extracts the hydroxyl group to leave a carbocation. This is easily stabilised by the loss of another proton to form the fully conjugated, trans bridged molecule.

2.1.10 Zwitterion Adducts

Z-ß-(N-hexadecyl-4-quinolinium)-α-cyano-naphthalenyldicyanomethanide and Z-ß-(N-hexadecyl-4-pyridinium)-α-cyanonaphthalenyldicyanomethanide and their corresponding benzylmethyl analogues were synthesised in the manner described by Ashwell[178]. The synthesis of Z-ß-(N-benzylmethyl-4-quinolinium)-α-cyano-naphthyldicyanomethanide is presented.

N-benzylmethyl-4-methylquinolinium bromide (0.06 g, 0.2 mmol) and the naphthyl analogue of 7,7,8,8,-tetracyanoquinodimethane (0.05 g, 0.2 mmol) were dissolved in hot ethanol and two drops of N-methylpiperidine added. The resultant blue solution was refluxed for three hours and the cooled to room temperature to give a blue/green precipitate. Recrystallisation from an ethanol:water solution produced blue crystals.

Yield 21% Melting point. 211-212°C. $C_{32}H_{20}N_4$ requires C,83.5; H,4.3; N,12.2% Found C,83.1; H,4.6; N,12.3% IR: 2160, 2120, 1625, 1610. ^{1}H NMR (DMSO): 4.9 (2H broad d, CH_2N^+); 6.8 (1H d, Ar-H); 7.8 (1H d, Ar-H), 8.0 - 8.9 (15H m, Ar-H); 9.7 (1H d -HC=C(CN)-).

Z-ß-(N-hexadecyl-4-quinolinium)-α-cyano-naphthyldicyanomethanide.

Green microcrystals, 19% yield. Melting point 235-238°C.

$C_{41}H_{44}N_4$ requires C,82.8; H,7.7; N,9.4% Found C,82.5; H,7.8; N,9.5%

Z-ß-(N-benzylmethyl-4-pyridinium)-α-cyano-naphthyldicyanomethanide.

Green microcrystals, 4% yield. Melting point 181-186°C.

Z-ß-(N-hexadecyl-4-pyridinium)-α-cyano-naphthyldicyanomethanide.

Green microcrystals, 10% yield. Melting point 233-234°C

The mechanism for this reaction has been well documented[157]. It has been reported using either piperidine or N-methylpiperidine as a catalyst. Greater yields result

using the latter. This could be due to there being no amine-TCNQ addition products formed because TCNQ does not react with tertiary amines.

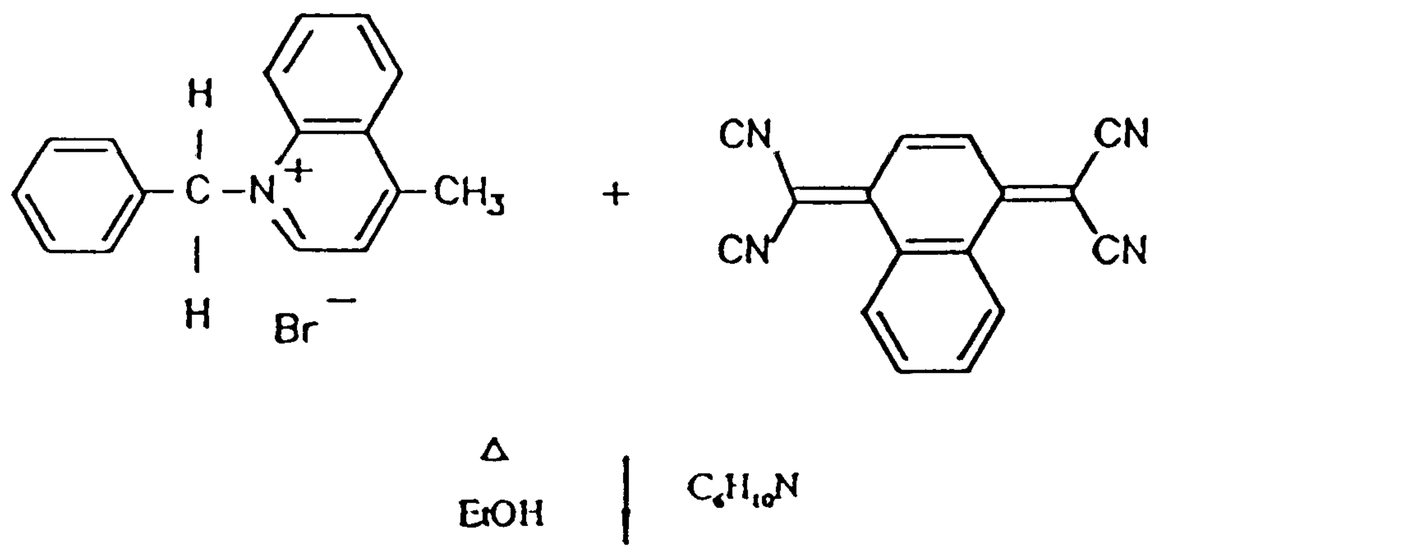

Figure 53. Synthesis of *Z-β-(N-benzylmethyl-4-quinolinium)-α-cyano-naphthyldicyanomethanide* (2.1.10).

2.2 Langmuir-Blodgett Films

2.2.1 The Nima Technology Langmuir-Blodgett Trough

All Langmuir film studies and LB film depositions were performed on a Nima Technology System 2000 L-D2-25 trough. The main body of the trough, shown in figure 54, is machined from PTFE mounted on an aluminium base.

It has two compartments, A and B, separated by a fixed surface barrier and two mobile barriers. Pressure measurement is made by two sensors using the Wilhelmy plate method, one for each of the two compartments. The mobile barriers separate the compartments and a dipper mechanism acts as a carrier for the substrate as well as

acting as part of the barrier. The system is fully computer controlled through an interface unit.

Compartments A and B have a maximum area of 500 cm^2 when the barriers are fully open. This is relatively small compared with many other troughs and reduces contamination inherent in large depths of water.

The *pressure sensors* (figure 55) operate using the Wilhelmy plate method, i.e. when a strip of high grade filter paper is suspended at an air/water interface it is pulled down into the bulk of the subphase by the surface tension of the water. The force acting on the paper is measured by a displacement transducer. The total error in the pressure reading is quoted as being less than 1%[41].

The *dipper mechanism* (figure 56) houses a substrate holder attached to two chain belts. These allow the substrate to be passed down through the air/water interface of one compartment and up through the other. A complete barrier is maintained by the two flexible PTFE sealing blocks.

2.2.2 LB Trough Cleanliness

The subphase needs to be as pure as possible therefore contaminants such as dust particles, ions or surface active impurities must be kept to a minimum. The following procedures are undertaken to ensure a dust free environment free from external vibrations:

(a) the trough is situated in a clean room at a positive air pressure with the air intake filtered through Bassair micropore filters to remove any dust present;

(b) clean room overalls, hoods and overshoes are worn to prevent contamination from airborne cloths and hair;

(c) the trough is housed on a Wentworth Laboratories AVT-700 anti-vibration table;

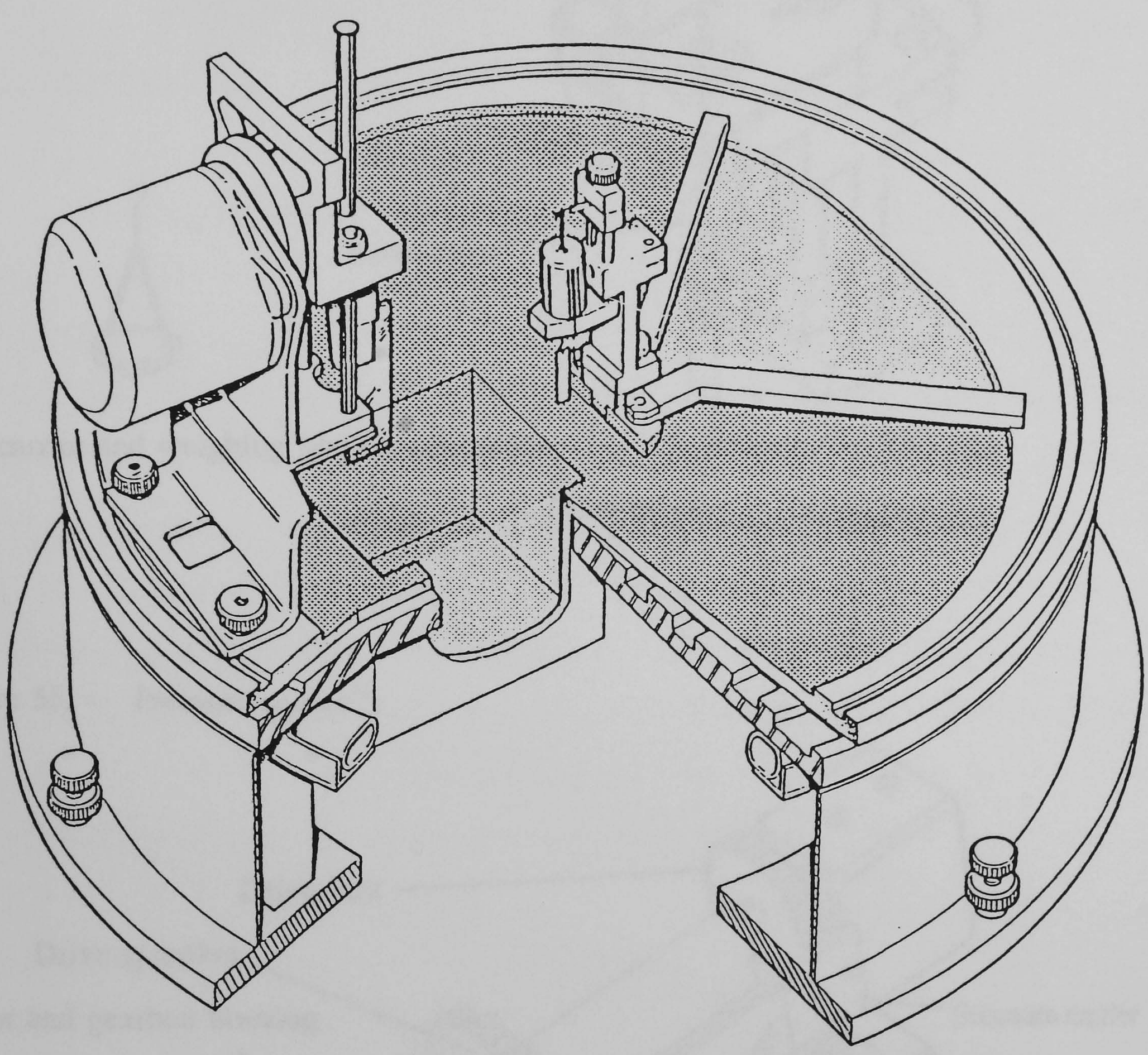

Figure 54. Nima Langmuir-Blodgett Trough (with dipper mechanism and pressure sensors removed)[41]

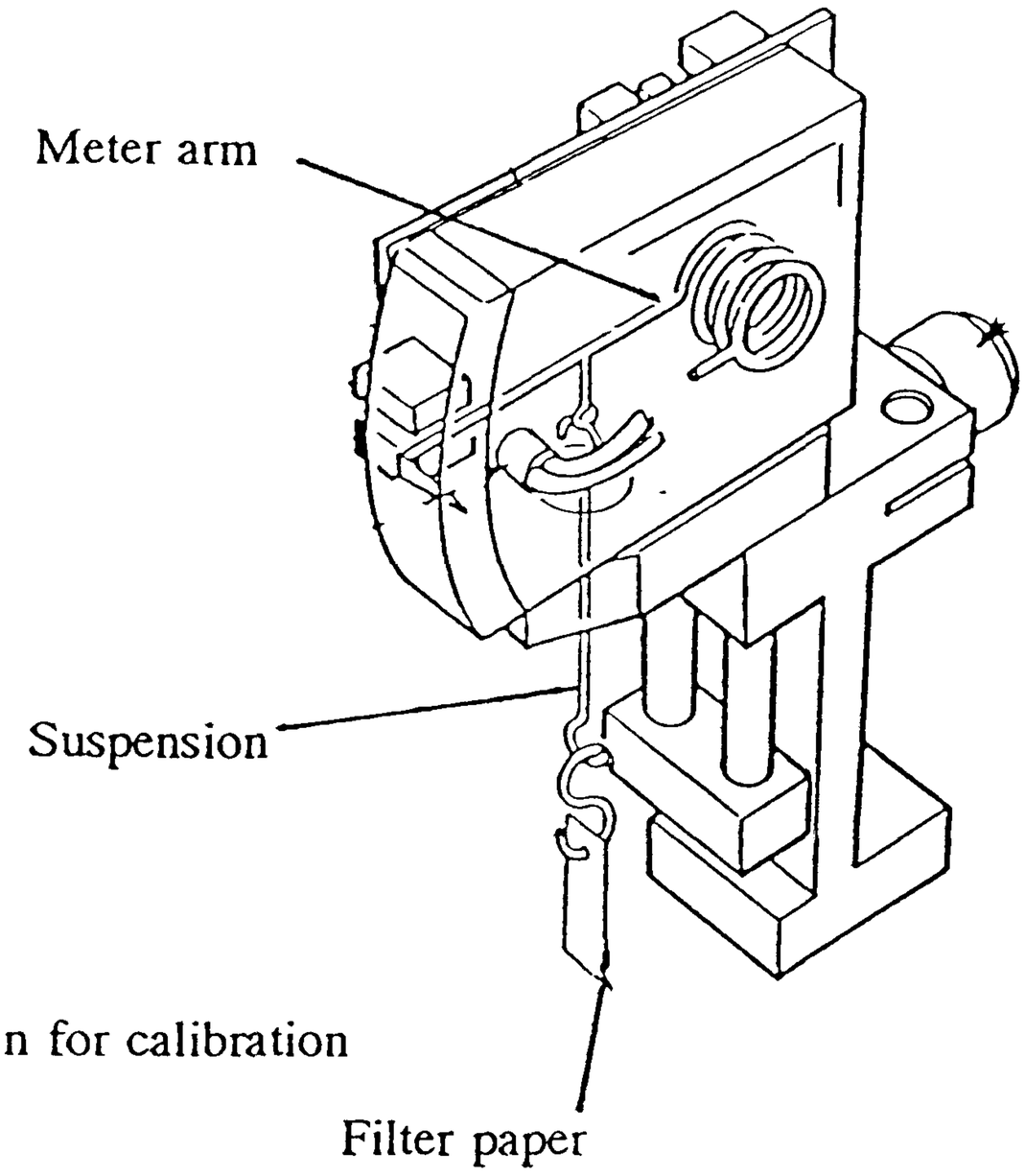

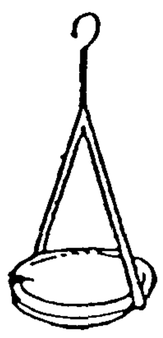

Pan carrier and weighing pan for calibration

Figure 55. Pressure sensor[41].

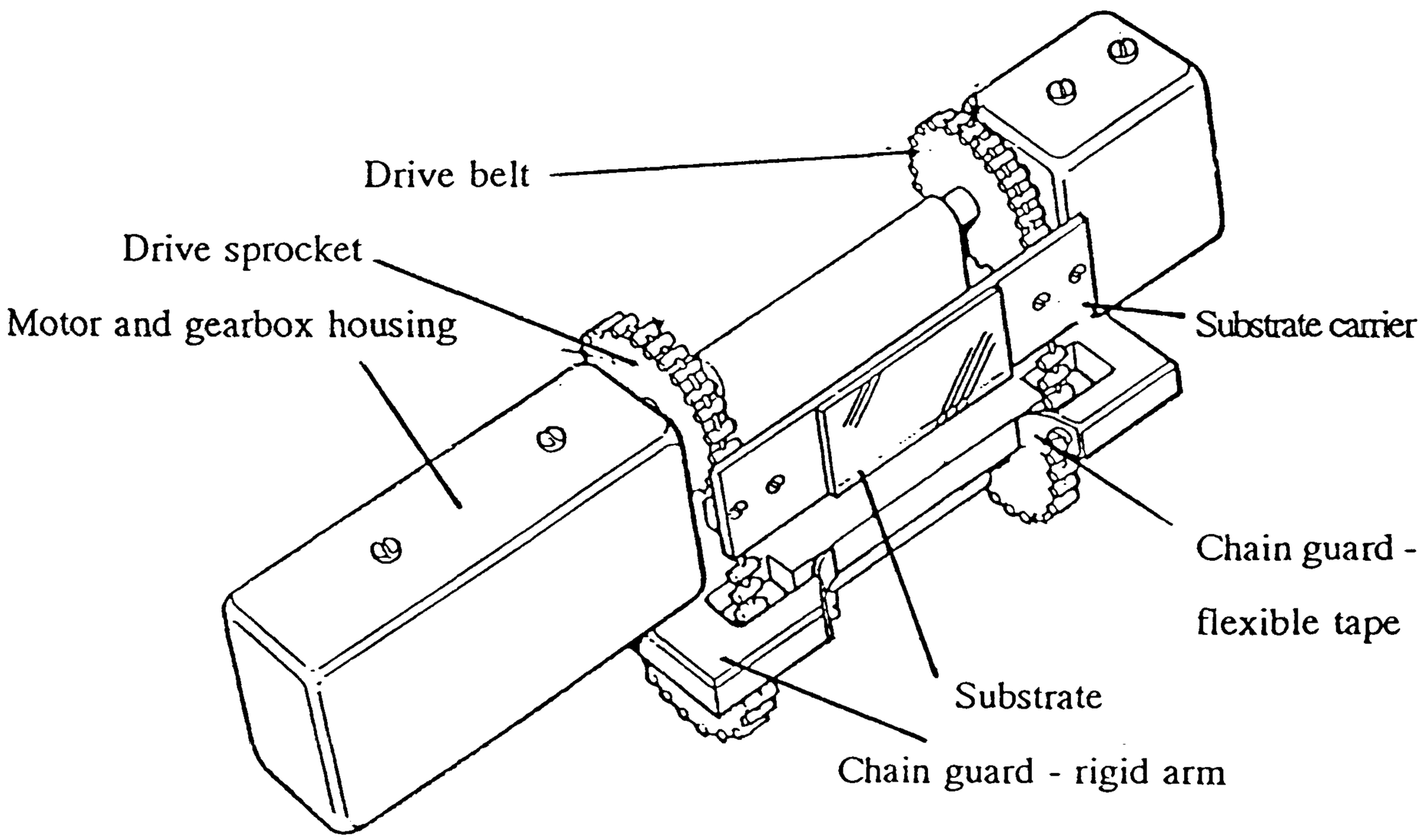

Figure 56. The dipper mechanism during deposition[41].

(d) all the surfaces of the trough, including the detachable barriers and dipper mechanism, are cleaned with organic solvents before and after use;
(e) a lid is placed over the surface as further protection from any air-born contaminants.

2.2.3 The Subphase

The subphase used for all experiments was ultrapure water. Organic contaminants were removed by reverse osmosis, then the water was passed through an Elgastat C240 purification unit to produce 5 MΩ deionised water. This was further purified using a MilliQ-plus purification system. This system contains an activated carbon filter, three mixed bed filters, an Organex polishing unit and a final filter unit which contains a microporous filter to remove micro-organisms and particulate matter larger than 0.22 μm, resulting in 18.2 MΩ water at 25°C. The purity of the water subphase was confirmed by measuring its surface pressure (72.8 mNm^{-1} at 25°C). Surface active contaminants were identified by compressing the barriers and observing any significant increases in surface pressure. The subphase was replaced every time the material of study was changed and at the end of each working day.

2.2.4 Solvents

All materials were deposited from organic solvents that met the criteria described earlier (section 1.4.2). The solubility of the material studied is important since solutions of less than 0.1 mg/ml require too large a volume to form a reasonable layer. The purity of the solvent is crucial, therefore only Aristar grade was used. The purity was tested by spreading the solvent on the subphase and compressing it. A solvent was discarded or further purified if it produced a significant increase in surface pressure upon compression.

2.2.5 Substrates

Either quartz slides or glass microscope slides were used. They were handled with plastic tweezers and treated hydrophilically, as described below.

1. Wiped with a solvent that dissolved any existing film, using surfactant-free tissues.
2. Wiped with Aristar grade chloroform until clean to the naked eye.
3. Sonication for 15 minutes in a bath of chloroform.
4. Sonication for 15 minutes in a bath of isopropanol.
5. Sonication for 15 minutes in a bath of fresh 18.2 MΩ water.
6. Sonication for 15 minutes in a bath of isopropanol.
7. Rinsed with fresh 18.2 MΩ water.
8. Left overnight in a bath of freshly prepared hydrogen peroxide solution (20% v/v).
9. Rinsed with fresh 18.2 MΩ water.
10. Blow dried with nitrogen.

2.2.6 Treatment and Storage of LB Films.

Once deposition had taken place the LB film was returned to the horizontal position by the dipper mechanism. Deposition was always on one side of the substrate only, therefore the other side was dried with a surfactant-free tissue. The LB films were stored vertically in an air-tight box.

2.3 Measurement of Second Harmonic Generation.

To record the SHG from an LB film the experimental apparatus shown below was used. The monochromatic source was a Q-switched Nd:YAG laser (1.064 μm; pulse width 10 ns; repetition rate 2 Hz).

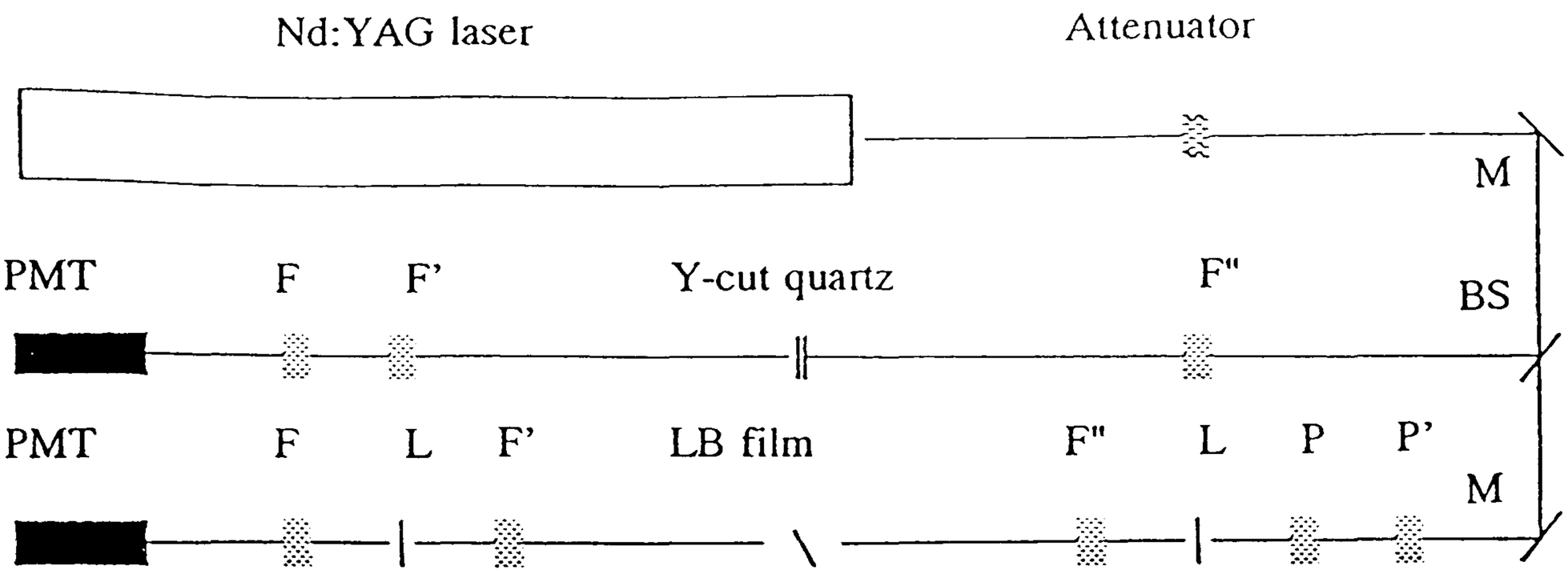

Figure 57. Schematic representation of the standard SHG apparatus: PMT, fast rise-time photomultiplier tube (Philips XP 20202); F, 532nm narrow bandpass filter; F', infrared blocking filters; F", visible blocking filters; P, halfwave plate; P', Glan Thompson polariser; L, lens; M, infrared mirror; BS, beam splitter.

The beam is p-polarised and incident to the film at 45°. A Hewlett-Packard 54111D digitising oscilloscope recorded the signals from the photomultiplier tubes. The signal from the LB film was compared to that from the Y-cut quartz. The LB film was mounted in a stand that allowed vertical and lateral movement. Parts of the slide where no deposition was known to have taken place were analysed, and if the signal from these positions was zero then it was assumed that any signals measured were due only to that film. Several locations on the LB film were analysed, in order to identify consistent deposition. When the actual signal was recorded the average of five positions on the film was taken. These positions were constant so that a multilayer film could be periodically analysed under identical conditions.

The apparatus was also used to estimate chromophore tilt angles. The angle of polarisation of the incident beam was rotated in conjunction with the polariser, P'. A sheet polariser set for p-polarised light was placed in front of the detector. Tilt angles were calculated using the equations:

$$\chi_1/\chi_0 = (4I_{pp}/I_{sp})^{½} - 3 \qquad (11)$$

and

$$\psi = \tan^{-1}(2\chi_0/\chi_1)^{½} \qquad (12)$$

where I_{pp} is the intensity of the SH response from the film when irradiated with p-polarised light, I_{sp} is the intensity of the SH response from the film when irradiated with s-polarised light and ψ is the average angle of inclination of the chromophores relative to the normal of the substrate[39].

3.0 Results and Discussion

3.1 Standard Quinolinium and Pyridinium Hemicyanines

3.1.1 Absorbance Spectra of Solutions

The spectra of typical quinolinium and pyridinium hemicyanines in chloroform are shown in figures 58 and 59. It was observed that the solutions decomposed upon sonication. Both groups of hemicyanine solutions exhibited high molar absorption coefficients.

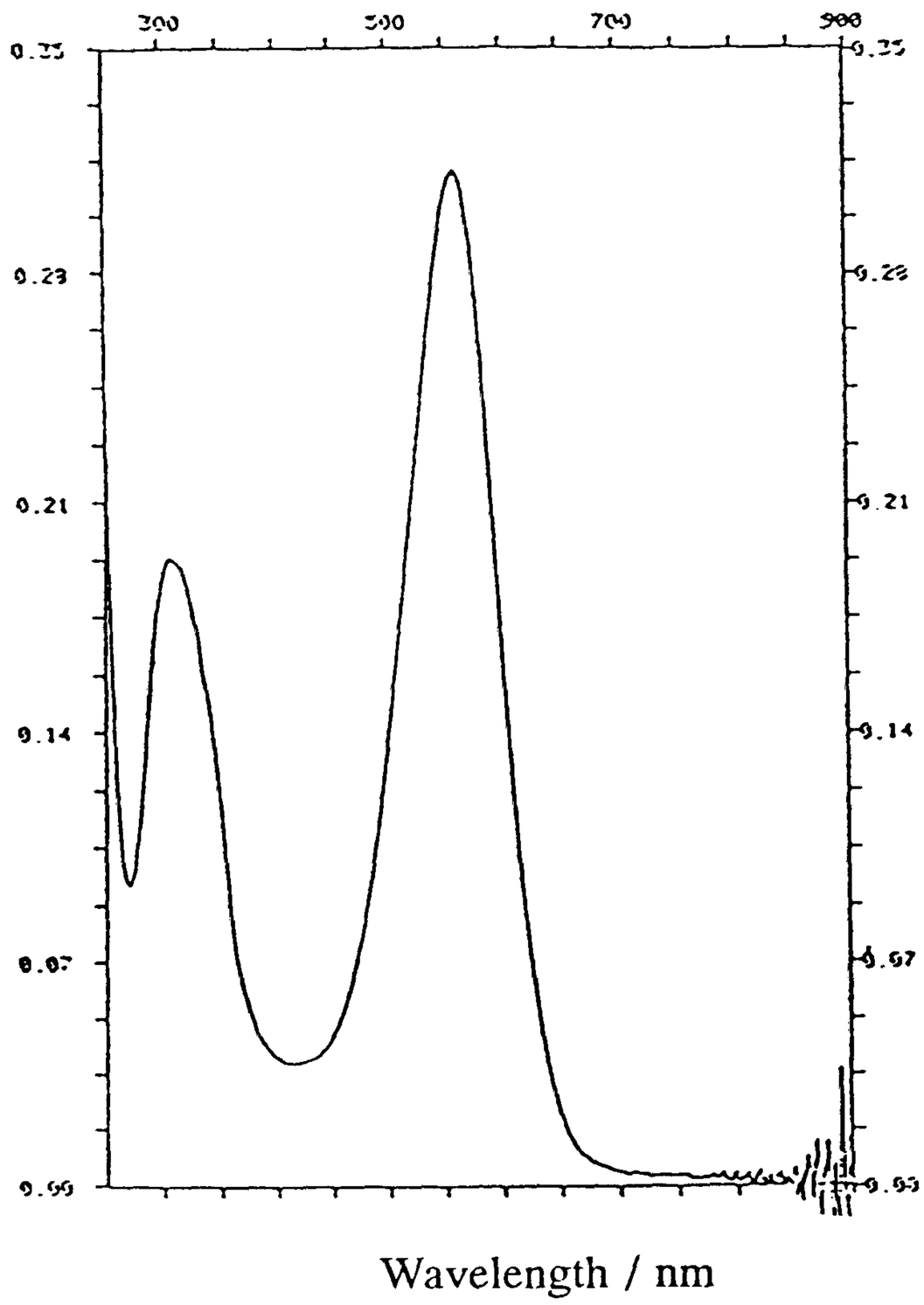

Figure 58. Absorbance spectrum of E-1-docosyl-4-{2-(4-dimethylamino phenyl)ethenyl}quinolinium bromide ($C_{22}H_{45}QHBr$) in chloroform. A list of the systematic nomenclature abbreviations is given in section 6.1.

The quinolinium hemicyanines exhibit a strong absorption peak at 560 nm, corresponding to a charge transfer band between the donor and acceptor parts of the molecule. The intensity is largely dependent on two factors: (a) the probability of interaction between the radiation energy and the electronic system and (b) the difference between the ground and excited state. The probability of transition is proportional to the square of the transition moment (or dipole moment of transition), which in turn is proportional to the change in the electronic charge distribution occurring during excitation. Intense absorption occurs when a transition is accompanied by a large change in transition moment. It was seen in section 1.3 that this can be achieved upon excitation of charge transfer complexes. The absorbance in the 300 nm region can be assigned to π-π^* transitions in the aromatic part of the molecule. The peak at 498 nm in the pyridinium hemicyanine is also due to charge transfer.

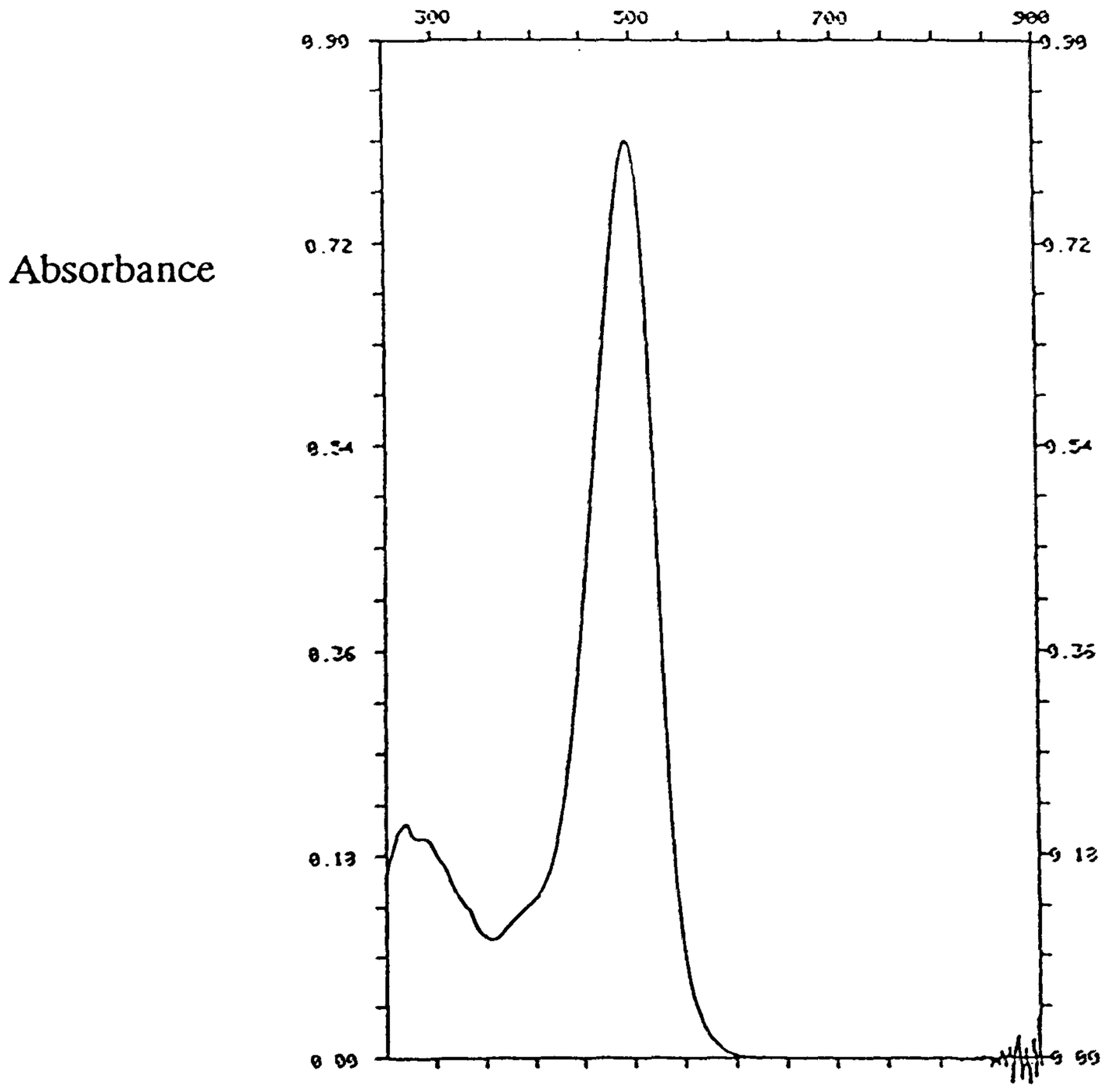

Figure 59. Absorbance spectrum of E-1-octadecyl-4-{2-(4-dimethyl aminophenyl)ethenyl}pyridinium iodide ($C_{18}H_{37}PHI$) in chloroform.

The alkyl chain has no effect on the wavelength of transition, nor does the halide ion. Therefore the only relevant structural difference between the two sets of materials is the heterocycle. The energy of the transition is crudely given by:

$$E_{CT} = (I_D - E_A) - C \qquad (13)$$

where I_D and E_A are the ionisation energy and electron affinity of the donor and acceptor ends of the molecule respectively and C is the coulomb energy. The donor ionisation energy and intramolecular charge separation are assumed to be equal. The quinolinium heterocycle is a stronger electron acceptor than pyridinium therefore the wavelength of the charge transfer transition is bathochromically shifted.

The effect of solvent on the solution spectra is shown overleaf, the behaviour being similar for the quinolinium and pyridinium dyes. The aprotic solvents cause a hypsochromic shift of λ_{max} with increasing polarity of solvent. This effect has been noted previously for highly polar complexes which undergo a reduction in dipole moment on charge transfer[178]. The polar protic solvents show the same effect but the differences are reduced, probably because of hydrogen bonding. Dichloromethane and ethanol have similar polarity's but their λ_{max} is not as similar as expected. This may be due to hydrogen bonding between ethanol and the solute which will result in an increased difference between the neutral and excited state thus lowering λ_{max}.

3.1.2 Molar Absorption Coefficient

The molar absorption coefficient of $C_{22}H_{45}QHBr$ was calculated using the Beer-Lambert Law,

$$\mathrm{Log}_{10}\, I_o/I = \varepsilon.l.c \qquad (14)$$

where I_o and I are the intensities of the incident and transmitted light respectively; l is the path length of the absorbing solution; c is the concentration; $\log_{10} I_o/I$ is the absorbance and $\mathscr{E}$ is the molar absorption coefficient. Given a path length of 1 cm, $\mathscr{E}(C_{18}H_{37}QHI) = 2.33 \times 10^4\ mol^{-1}m^2$ and $\mathscr{E}(C_{22}H_{45}PHBr) = 8.25 \times 10^4\ mol^{-1}m^2$ (see figures 60 and 61 respectively). The results for the other quinolinium and pyridinium hemicyanines were similar, showing that a change in alkyl chain length has no effect.

Solvent	Dipole moment[179], debyes	$C_{22}H_{45}QHBr$ λ_{max}	$C_{18}H_{37}PHI$ λ_{max}
$C_6H_5CH_3$	0.36	536	461
C_2H_5OH	1.7	545	477
CH_3OH	1.7	548	479
$CHCl_3$	1.01	560	496
CH_2Cl_2	1.6	578	504
$(CH_3)_2O$	2.8	538	473
CH_3CN	3.8	537	468

Table 17. The effect of solvent on standard hemicyanines.

3.1.3 Isotherms

Surface pressure-area (π - a) isotherms of the quinolinium hemicyanines were obtained by spreading the dye from dilute chloroform solution on the pure water subphase of the LB trough, then the surface layer was compressed at 50 cm^2min^{-1}. Representative isotherms are shown in figures 62 and 63.

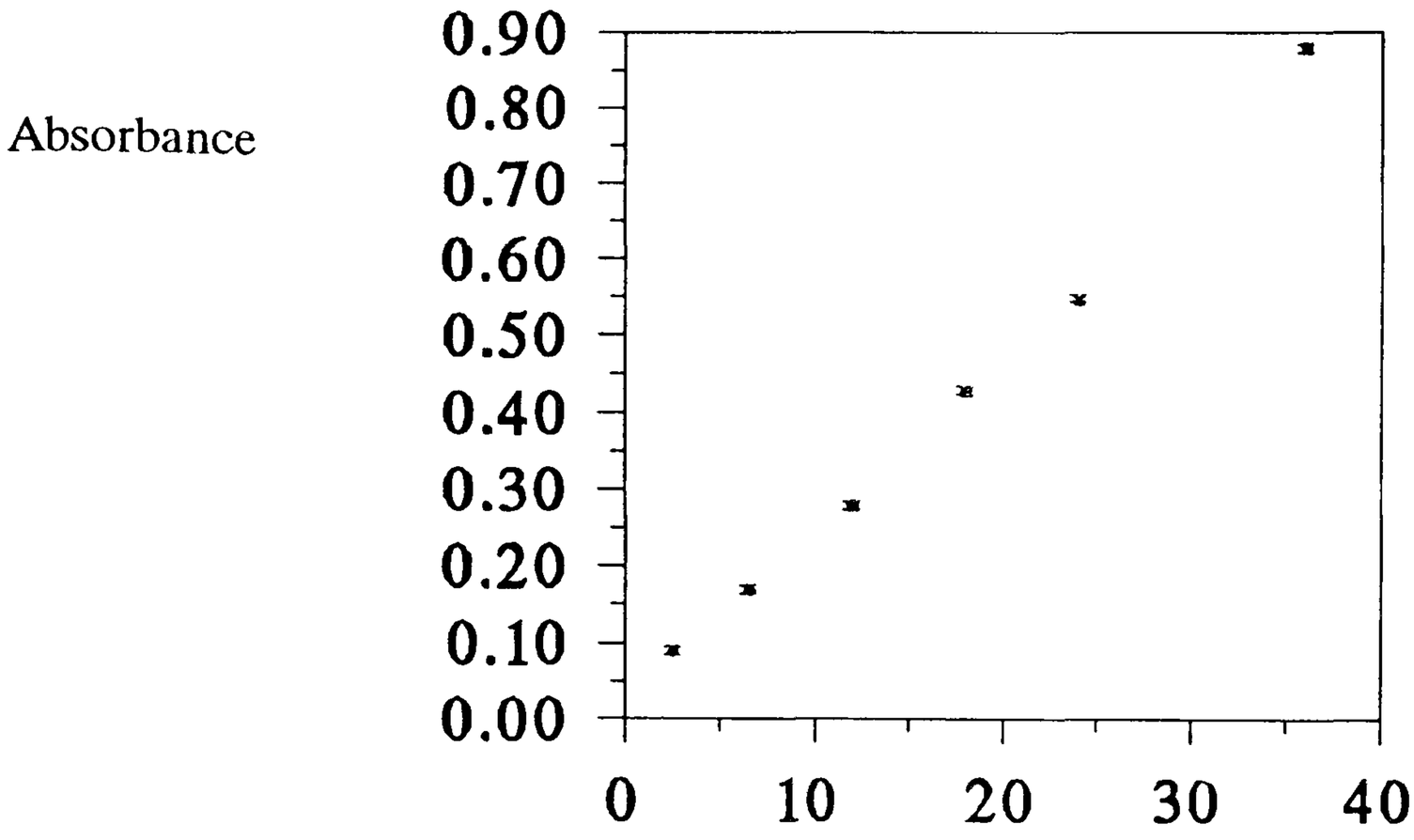

Figure 60. Absorbance versus concentration for $C_{18}H_{37}QHI$

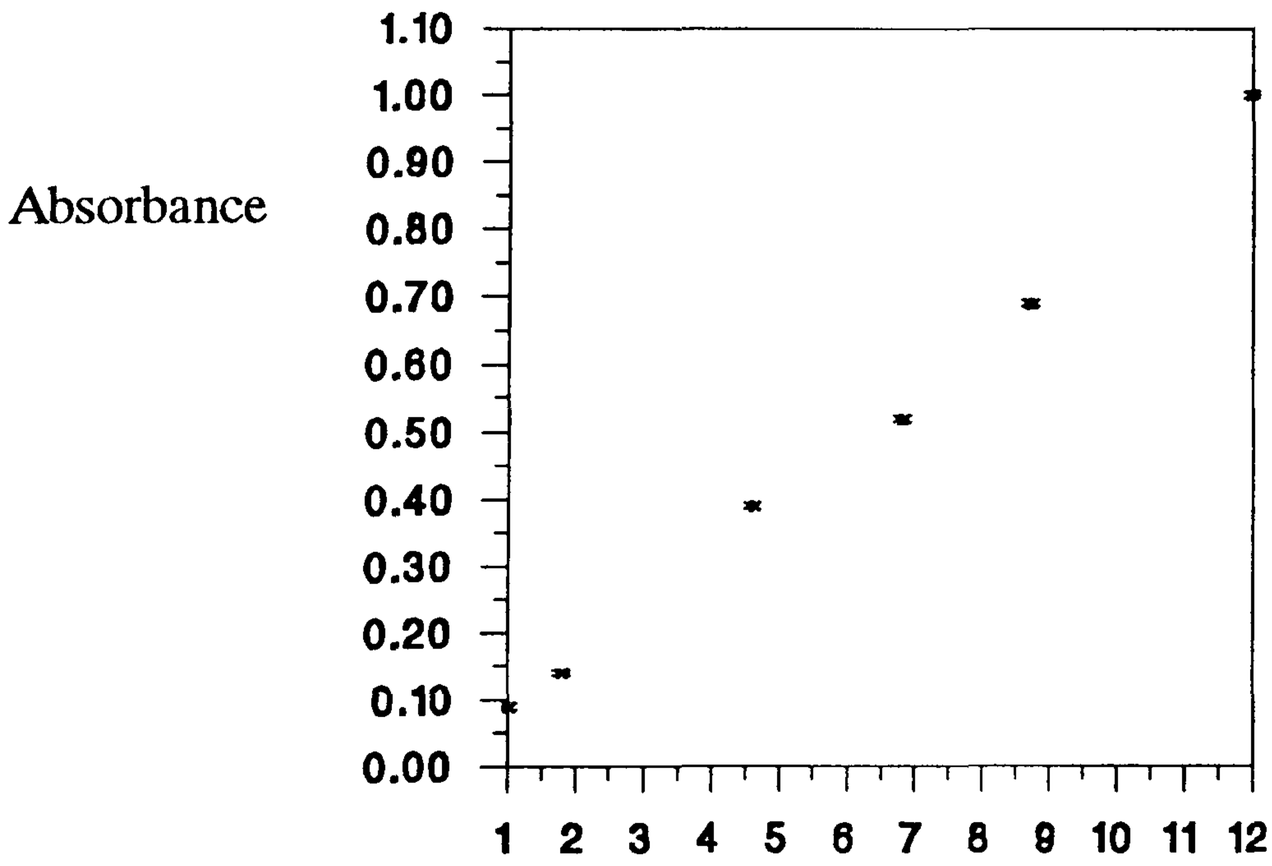

Figure 61. Absorbance versus concentration for $C_{22}H_{45}PHBr$

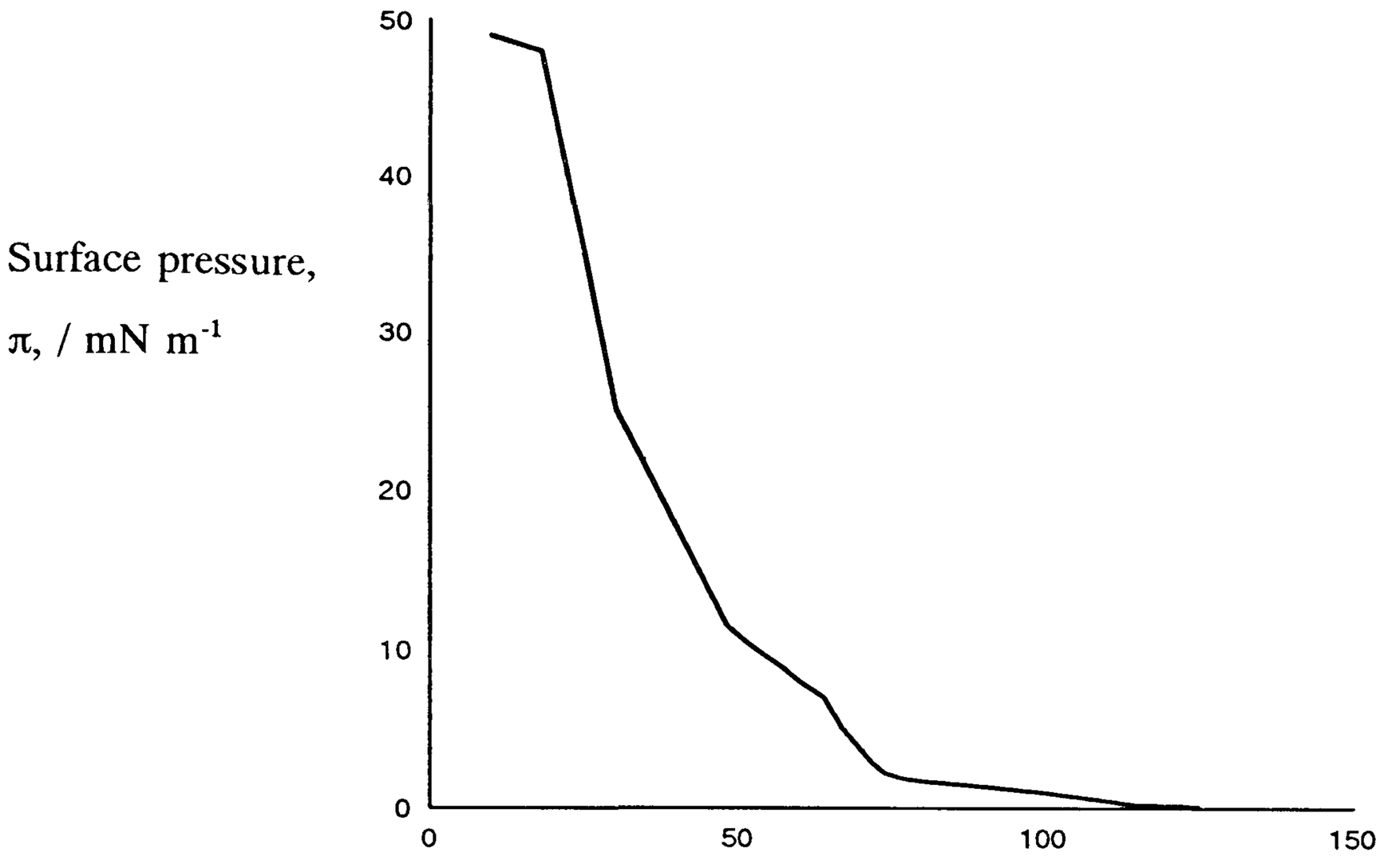

Figure 62. Π - a isotherm of $C_{22}H_{45}QHBr$.

The first pressure increase for $C_{22}H_{45}QHBr$ is observed at an area per molecule of 120 Å^2. The face area of the hemicyanine chromophore has been estimated as approximately 100 Å^2 and therefore, it appears that the chromophore is lying flat on the water surface at this point. Extrapolation at zero pressure of the steep part of the isotherm gives an area per molecule of approximately 38 Å^2. The cross-sectional area of the quinolinium hemicyanine chromophore has been estimated at 30 Å^2 . It therefore appears that the hemicyanine is orientated close to the vertical. Collapse occurs at about 50 mN m^{-1}. It was observed that isotherms of all quinolinium hemicyanines were similar.

The first pressure increase for $C_{22}H_{45}PHBr$ is observed at an area per molecule of 120 Å^2, which agrees with the theory that the molecules are lying flat. Extrapolation to zero pressure of the steep part of the isotherm gives an area per molecule again of about 38 Å^2. Collapse occurs at a pressure of 40 mN m^{-1}. The pyridinium hemicyanines

were also very similar to each other. It can be seen that isotherms of quinolinium and pyridinium hemicyanines are similar in shape.

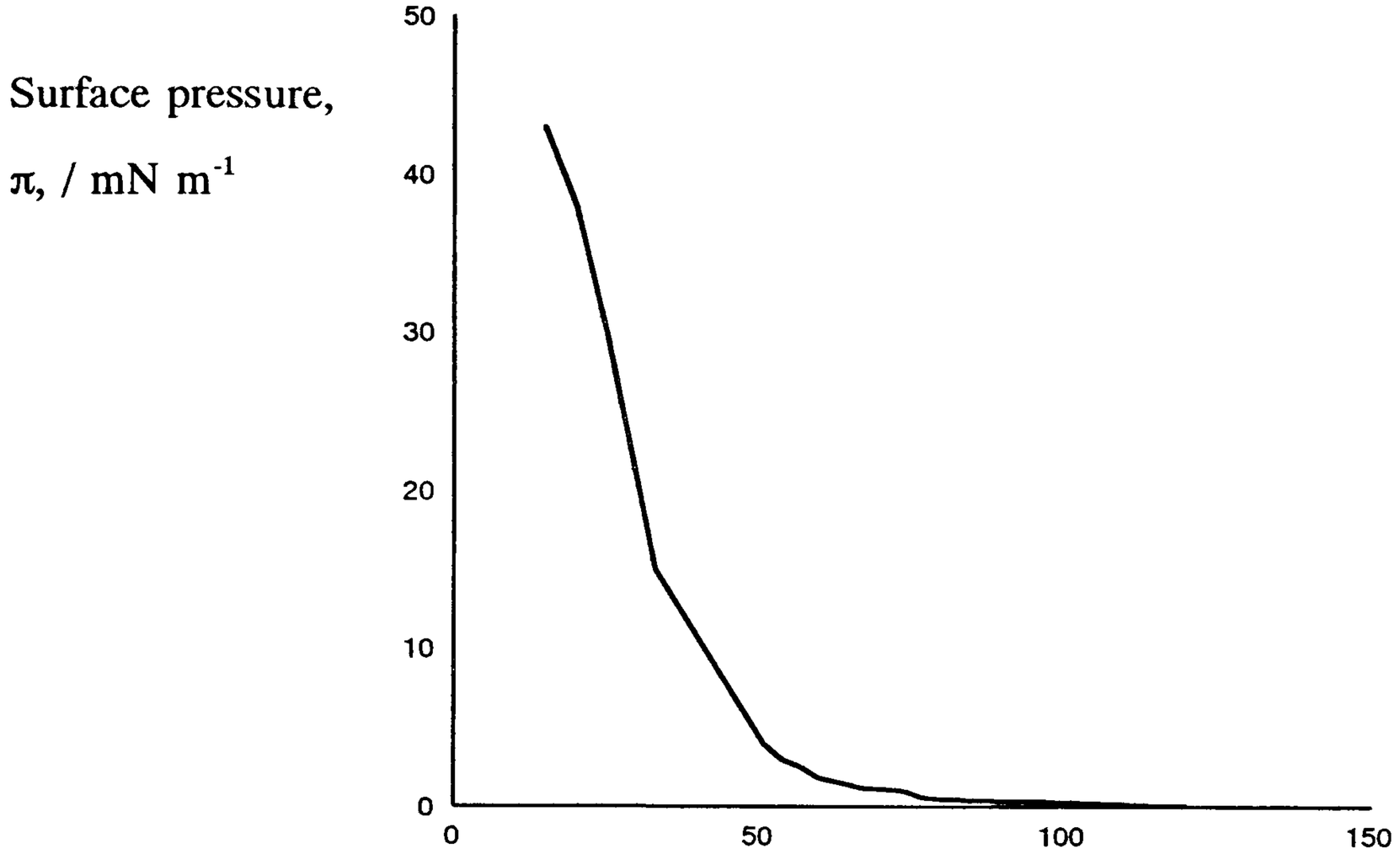

Figure 63. Π - a isotherm of $C_{22}H_{45}PHBr$.

The isotherms of these materials showed a "kink" at about 70 mN m^{-1}. This can be attributed to the molecules moving from being almost flat on the surface to being aligned towards the vertical. When the hemicyanines were compressed fifteen minutes after being transferred onto the subphase the isotherm shape was slightly steeper and the kink was less marked.

The results of an experiment to illustrate the alignment changes in the films are shown in figure 64. It can be seen that, from right to left, the langmuir film does not return to a completely two dimensional gaseous state after being compressed, expanded and then compressed again 10 minutes later. Repeat compressions show the same phenomena. In conclusion:

1. the film forms a semi-ordered state after compression and does not return to its original orientation at zero pressure;

2. the area per molecule at high pressure is almost exactly the same irrespective of the history of the film (as long as it has not previously collapsed).

This means that for meaningful comparison of behaviour at the air/water interface, great care must be taken to achieve identical conditions. In addition, the conditions required for compression up to deposition pressure are not critical, because at 30 mN m^{-1} and above the film always occupies the same area per molecule.

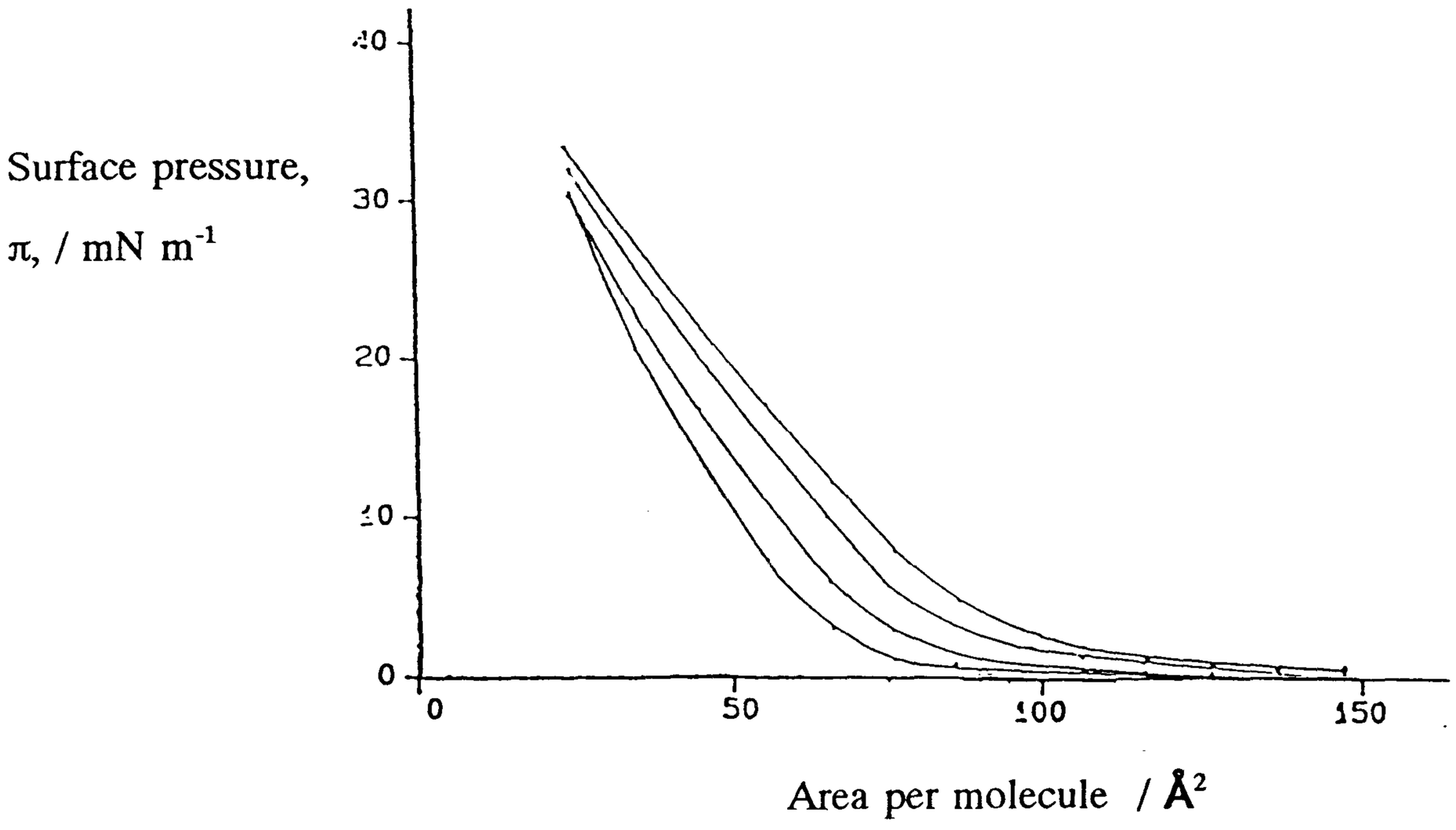

Figure 64. The effect of four consecutive compressions on the same film of $C_{22}H_{45}PHBr$. From right to left, isotherms after 0 minutes, 10 minutes, 20 minutes and 45 minutes.

The π - a isotherms of both hemicyanines are quite steep in the "two-dimensional solid" region and there is a difference of about 13 mN m^{-1} between the area at zero

pressure and the area at 30 mN m^{-1}. For example at 30 mN m^{-1} $C_{22}H_{45}QHBr$ occupies an area per molecule of 28 $Å^2$ compared to 41 $Å^2$ at extrapolated zero pressure.

The estimated value for a reported pyridinium hemicyanine orientated vertically at the surface has been reported as between 25 to 30 $Å^2$ [130,167,180]. This suggests that $C_{22}H_{45}PHBr$ is inclined slightly away from the vertical at the same pressure, as in figure 65. A quinolinium hemicyanine orientated vertically at the surface should occupy a larger area by virtue of its extra benzene ring, therefore $C_{22}H_{45}QHBr$ is inclined significantly closer to the vertical.

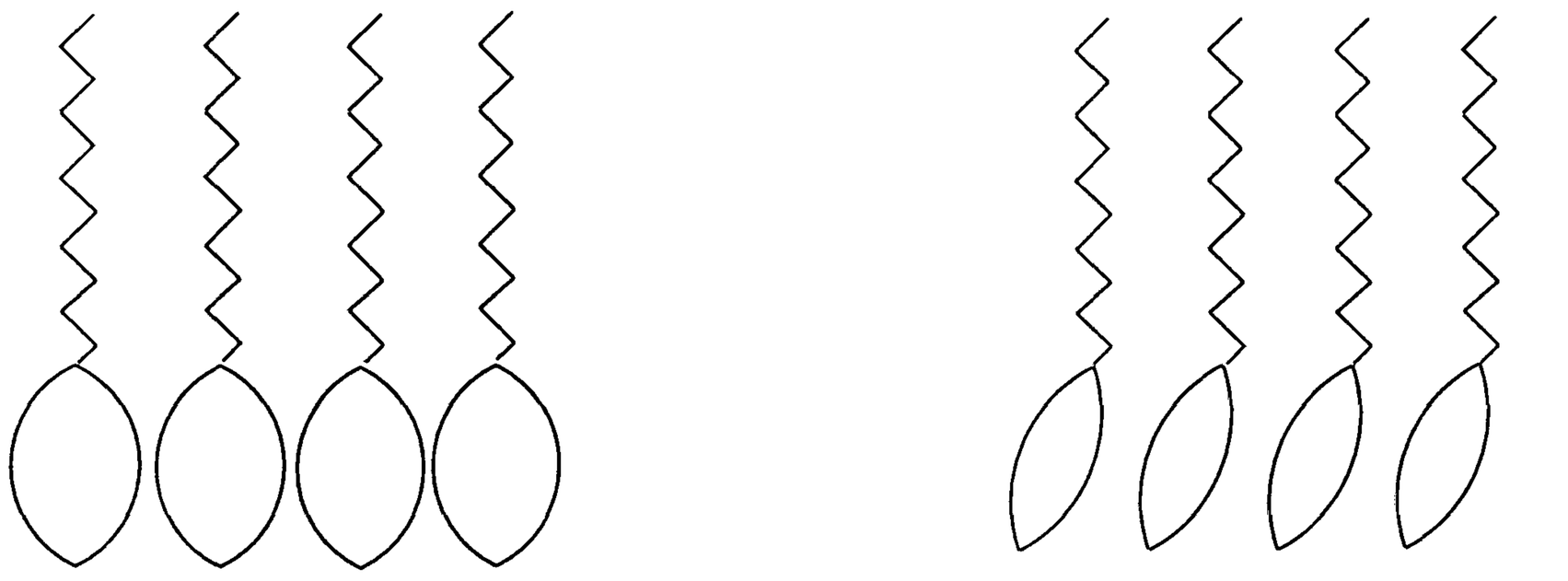

Quinolinium hemicyanine

Pyridinium hemicyanine

Figure 65. Diagrammatic representation of how hemicyanines are orientated at the air/water interface at deposition pressure.

Some slight differences in isotherm shape were observed for $C_{16}H_{37}$ analogues of both hemicyanines. The shorter chain materials had shallower curves indicating some material dissolving into the subphase. This was confirmed by some simple solubility tests whereas the other materials gave no evidence of solubility in water.

3.1.4 Stability of Langmuir Films

A hemicyanine dye was spread onto the pure water subphase and compressed to 25 mN m^{-1}; the film was kept at constant pressure by the barriers and the reduction in area that occurred over twenty minutes was recorded.

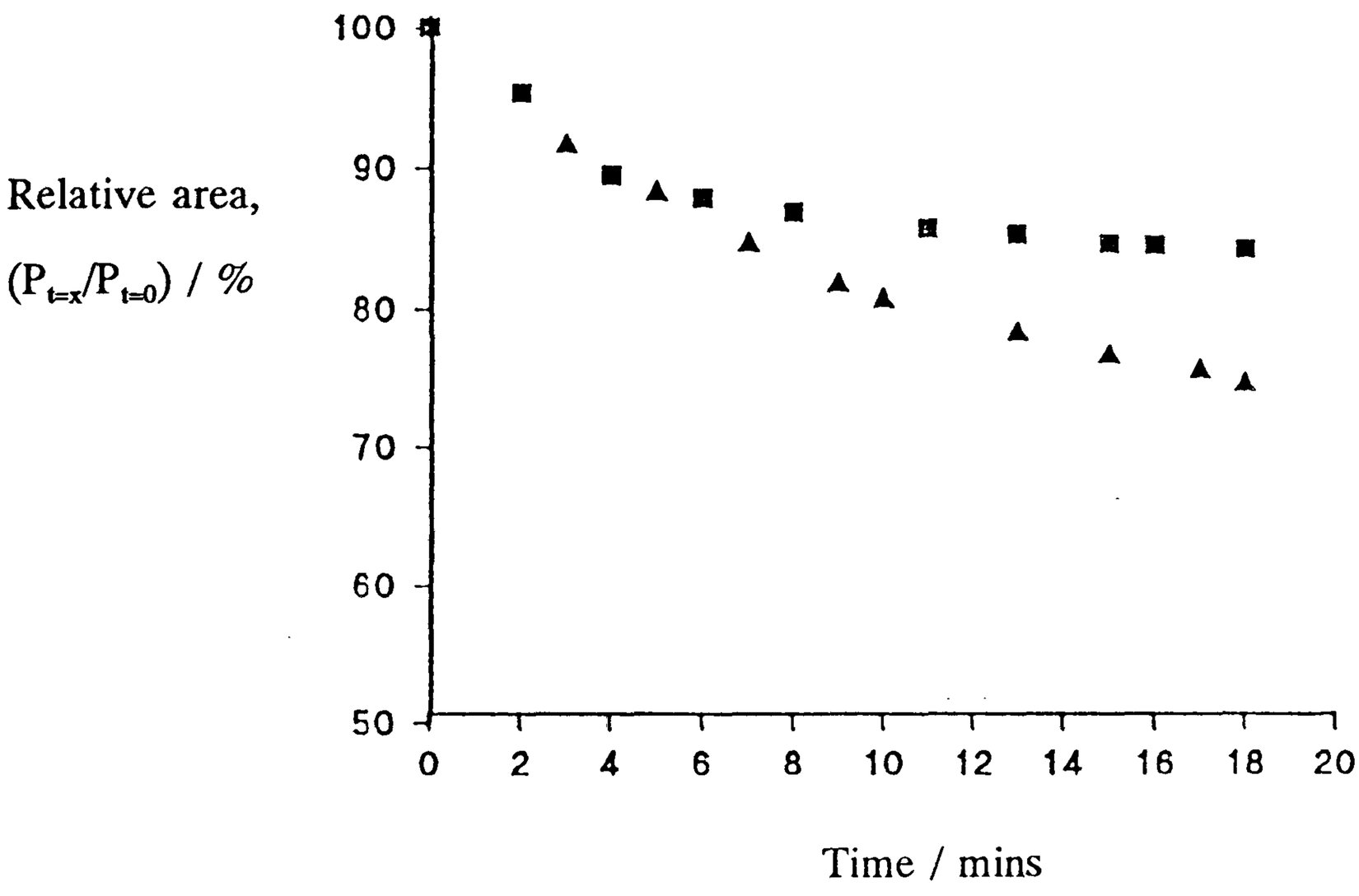

Figure 66. Drop in area, at constant pressure, over time for $C_{18}H_{37}QHI$ (■) and $C_{16}H_{33}PHBr$ (▲).

$C_{18}H_{37}QHI$ underwent layer rearrangement for approximately six minutes and thereafter stayed in the same state. This is representative of all quinolinium and pyridinium hemicyanines of chain length $C_{18}H_{37}$ and greater. $C_{16}H_{33}PHBr$ is not capable of reaching such an equilibrium, probably because of its slight solubility in water. Some material dropped into the subphase at higher pressures, shown by its continual drop in area at constant pressure.

A layer of $C_{16}H_{33}PHBr$ was completely removed from the surface by suction and the barrier opened to maximum area. Compression five minutes later indicated the presence of material at the surface, this had probably diffused to the surface from within the subphase, this is further evidence of dissolution especially since the other hemicyanines did not exhibit this characteristic.

3.1.5 Monolayer Deposition

Hemicyanines were deposited by the method described in section 1.4.2. Solution concentrations in the range 0.1 to 1 mg/ml, dipping pressures in the range 30 to 35 mN m^{-1} and dipping speeds in the range 3.6 to 10 mm min^{-1} were used. No deposition was found to occur on the downstroke, therefore all monolayers discussed are the result of upstroke deposition.

Analysis of the respective isotherms shows the steepest parts to be above 25 mN m^{-1}, therefore deposition was carried out at pressures in this region. The steep 2D "solid" regions in the isotherms are indicative of a compact phase. The molecules are aligned near to the vertical at the surface which aids deposition since the repulsion of the hydrophobic chain to the hydrophilic substrate is minimised.

The slight solubility of $C_{16}H_{33}QHBr$ and $C_{16}H_{33}PHBr$ make area per molecule deductions at 30 mN m^{-1} erroneous. These analogues were deposited as quickly as possible to avoid further dissolution and to minimize error.

In general, all the materials transferred to the substrate easily. None of the problems associated with poor LB film forming materials were encountered, ie the requirement of counterions in solution, columbic repulsions, high dissolution, formation of micelles etc. The transfer ratios for monolayer deposition were consistent for repeated experiments, inferring consistent and reproducible behaviour at the water surface and during transfer. The transfer ratios for the $C_{16}H_{37}$ analogues were higher which is symptomatic of slight dissolution.

3.1.6 Absorbance Spectra of LB Films

The high molar absorption coefficients of these materials renders a glass slide slightly coloured after transfer of the monolayer.

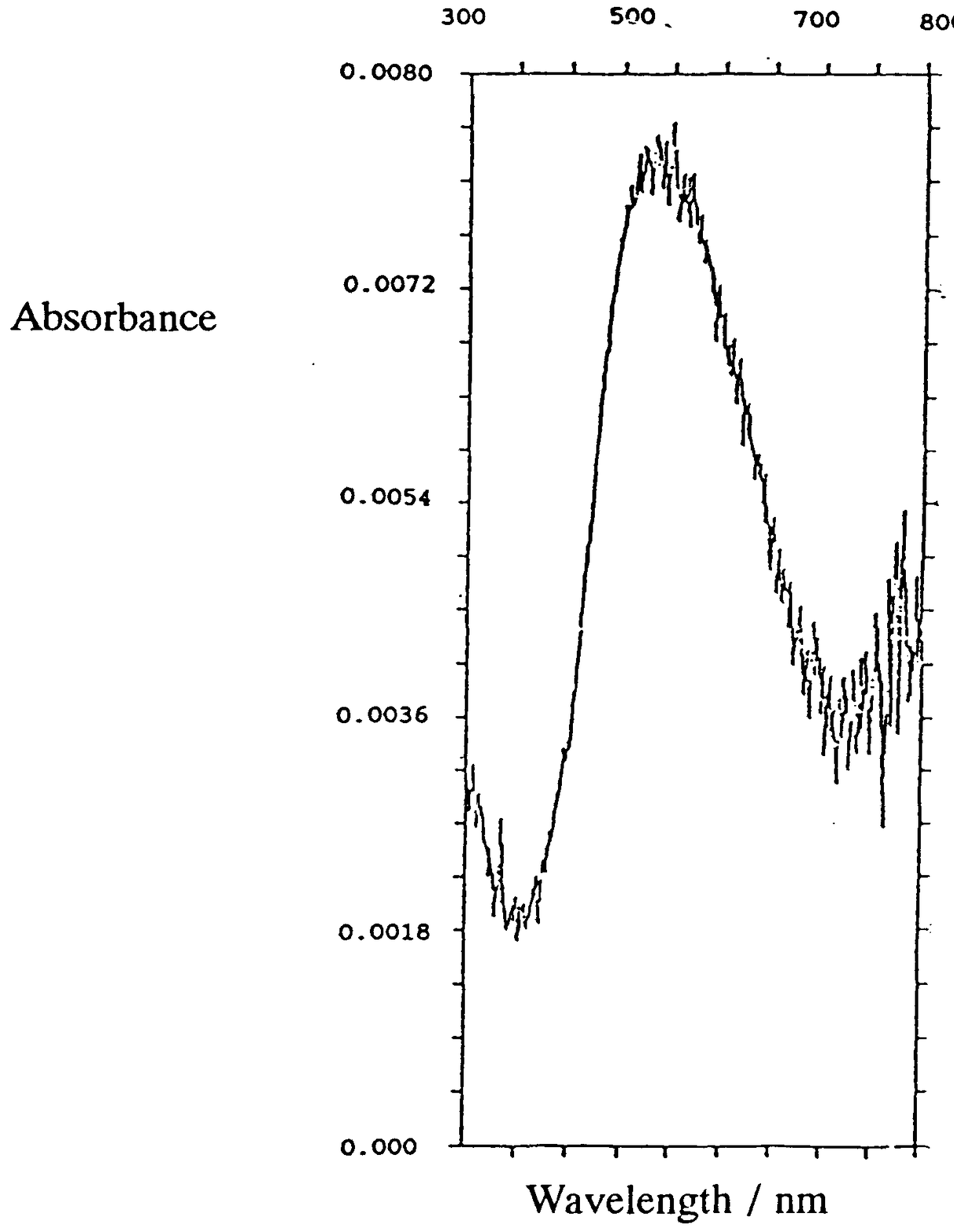

Figure 67. Absorbance spectrum of a monolayer of $C_{22}H_{45}QHBr$.

The charge transfer peak of a monolayer of $C_{22}H_{45}QHBr$ is hypsochromically shifted compared to its solution spectrum, but the shape is very similar. The shape of the spectrum is typical of all quinolinium hemicyanines studied, and since the molecular environments affect the shape and position of the peak in the monolayer, it can be deduced that neither differences in chain length or anion affect the molecular packing or overlaps. Similar properties were noted for the pyridinium analogues.

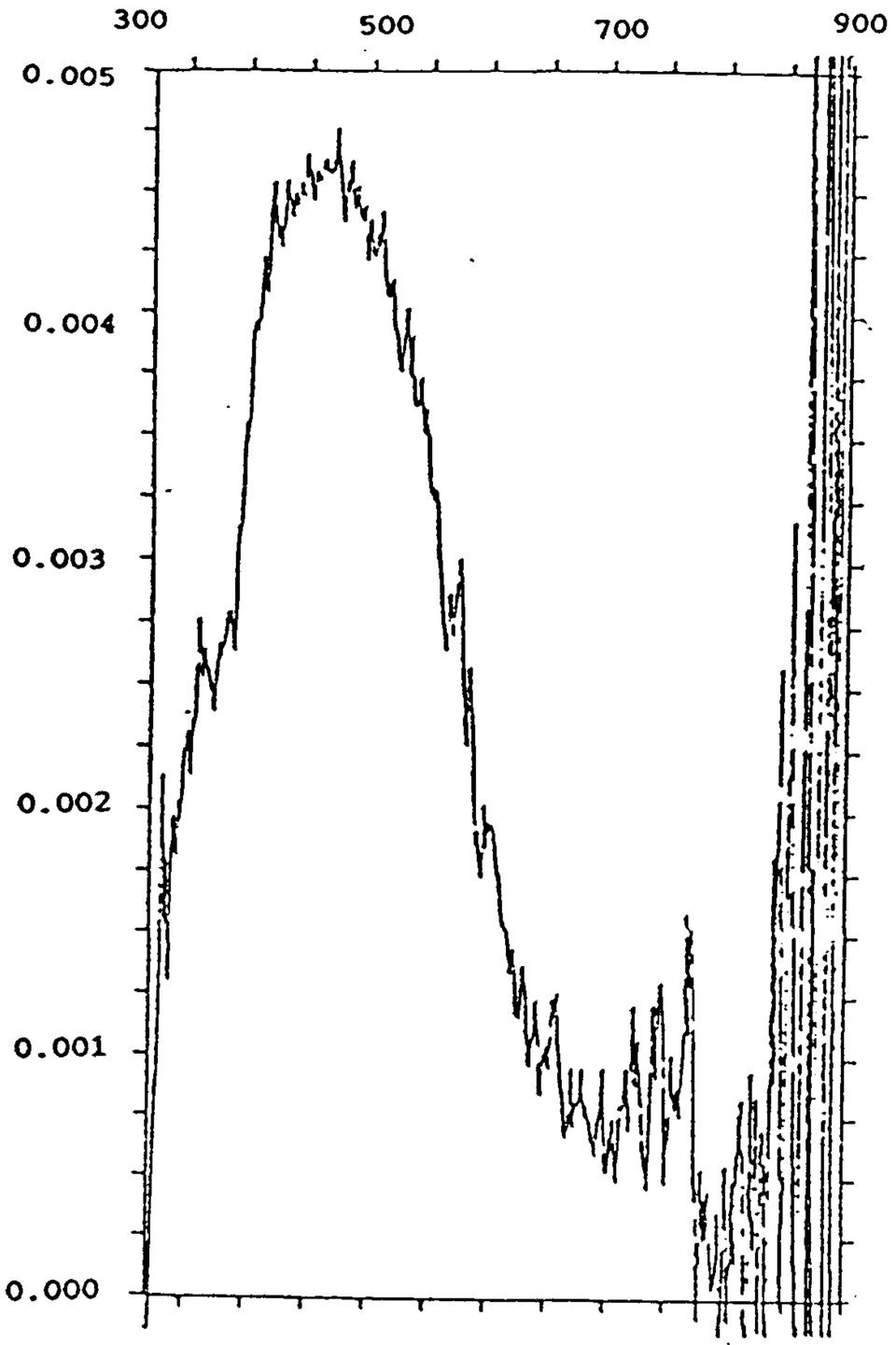

Figure 68. Absorbance spectrum of a monolayer of $C_{18}H_{37}PHBr$.

Various workers have reported evidence of aggregation in hemicyanine LB films in the form of shoulders or separate peaks in the absorbance spectra[134,146-152]. The monolayer films shown here contain one peak representing the charge transfer of the chromophore, consequently there is no spectroscopic evidence of any aggregation.

The spectra are physical evidence that deposition has taken place. One should observe consistent, reproducible absorbance intensities if a material produces consistent, reproducible monolayers. Transfer ratios of unity and subsequent SHG studies indicate monolayer formation. Evidence for consistent monolayer formation across the film is

derived from taking spectra at various positions on the slide and observing similar results. The intensities of both groups of materials varied, this is noted in table 18.

Hemicyanine	Absorbance, λ_{max}	Hemicyanine	Absorbance, λ_{max}
$C_{16}H_{33}QHBr$	0.006 ± 0.0005	$C_{16}H_{33}PHBr$	0.002 ± 0.0005
$C_{18}H_{37}QHBr$	0.009 ± 0.0005	$C_{18}H_{37}PHBr$	0.006 ± 0.0005
$C_{20}H_{41}QHBr$	0.003 ± 0.0005		
$C_{22}H_{45}QHBr$	0.008 ± 0.0005	$C_{22}H_{45}PHBr$	0.004 ± 0.0005
$C_{18}H_{37}QHI$	0.008 ± 0.0005	$C_{18}H_{37}PHI$	0.010 ± 0.0005

Table 18. Absorbance for hemicyanine monolayers.

The intensity of absorbance of these LB monolayers is an indication of the number of molecules per unit area. This is because the intensity depends on the probability of interaction which will be greater for a film with a greater molecular density.

The values represent typical absorbance for each material and it is obvious that there is no simple configurational trend. The experimental conditions were kept as similar as possible. It appears possible, however, that experimental error present in the precarious technique of Langmuir-Blodgett deposition, is too great to allow sensitive comparison of monolayers.

It is reasonable to deduce that the low absorbance of $C_{16}H_{33}PHBr$ is due to its slight solubility in water, which has resulted in imperfect deposition. $C_{16}H_{33}QHBr$ is slightly less soluble than its pyridinium analogue, however the relative absorbance for this material is not as low as expected.

3.1.7 Second Harmonic Generation from Monolayers

Each monolayer was analysed for second harmonic generation using the apparatus described in section 2.3, with the monolayer inclined at 45° to the normal. The values are reported relative to $C_{22}H_{45}PHBr$ (arbitrarily assigned as unity) for each experiment.

Hemicyanine	SHG	Hemicyanine	SHG
$C_{16}H_{33}QHBr$	1.17 ± 0.02	$C_{16}H_{33}PHBr$	0.06 ± 0.00
$C_{18}H_{37}QHBr$	3.54 ± 0.02	$C_{18}H_{37}PHBr$	1.92 ± 0.04
$C_{20}H_{41}PHBr$	0.81 ± 0.03		
$C_{22}H_{45}QHBr$	8.20 ± 0.01	$C_{22}H_{45}PHBr$	1.00 ± 0.01
$C_{18}H_{37}QHI$	2.74 ± 0.02	$C_{18}H_{37}PHI$	6.09 ± 0.01

Table 19. SHG from monolayers of hemicyanines.

Girling et al studied the SH response of a LB monolayer of $C_{22}H_{45}PHBr$ and reported a signal (1.17×10^{-4}) x quartz[146]. This value has been used as a benchmark in recent years by workers in the same field. In this experiment the SH response from a monolayer of $C_{22}H_{45}PHBr$ was recorded as (1.0×10^{-4}) x quartz.

It is noted that each material exhibited second harmonic generation. It can be seen that there is no obvious relationship between the length of the hydrophobic chain and SHG, or between the counterion and SHG and it is difficult to deduce if different heterocycles have an effect on SH response. Therefore the absorbance and SHG were compared regardless of configuration. The values reported in tables 18 and 19 were used as well as values gathered from similar experiments where different absorbance occurred.

The graph illustrates the wide variation in absorbance and emphasises the dependence of the SHG intensity on absorbance. It is worth noting that the highest absorbance was not as a result of bilayer formation since a bilayer would be centrosymmetric and a reduction in SH signal would be observed.

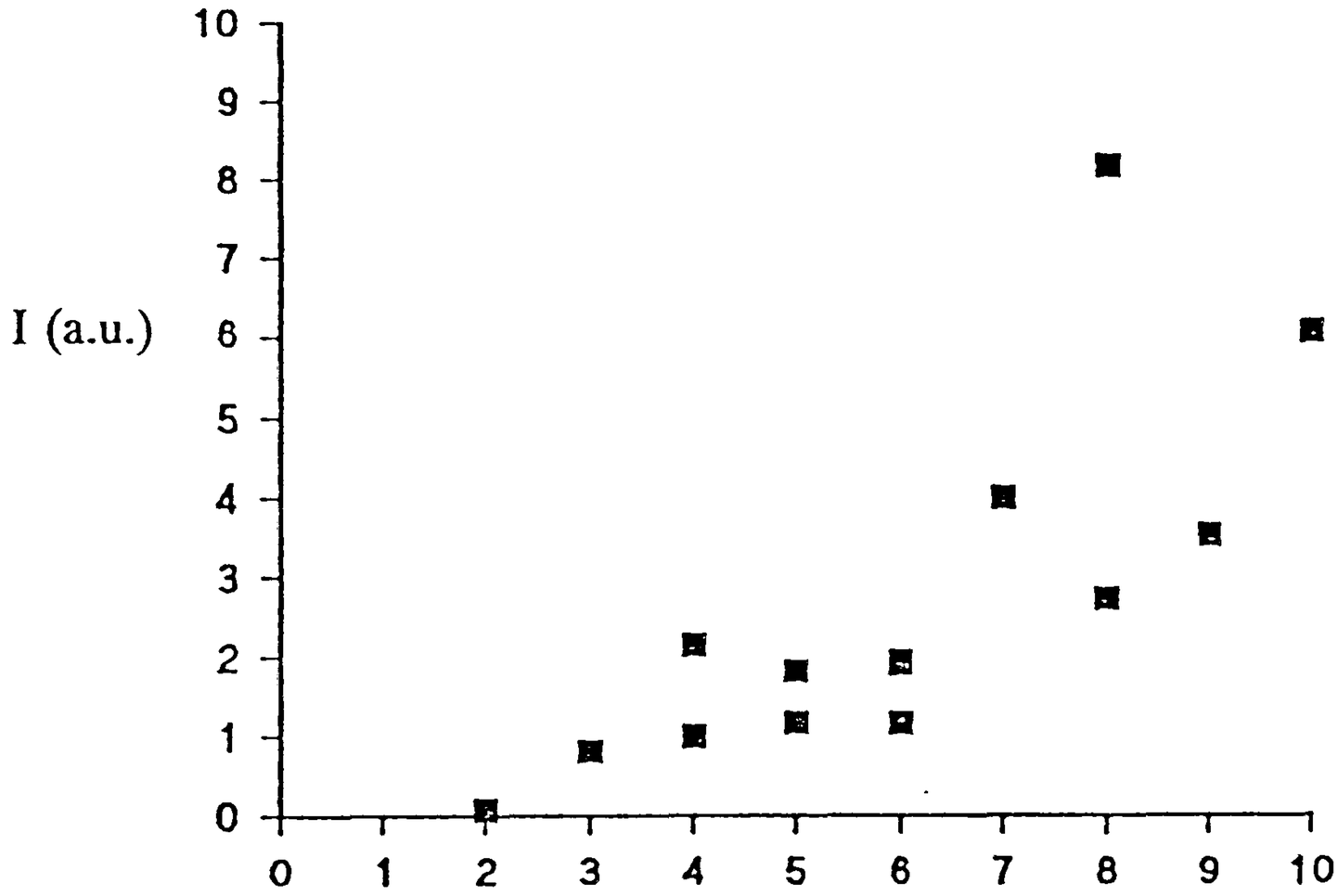

Figure 69. SHG versus absorbance of LB monolayers of hemicyanines.

3.1.8 Multilayer LB films

A monolayer of $C_{22}H_{45}PHBr$ was deposited on the upstroke from compartment B of the LB trough. A second layer of $C_{22}H_{45}PHBr$ was deposited on the downstroke from compartment A, and a third on the upstroke from compartment B and so on. Various films of up to 9 layers were fabricated and the resulting SHG indicated a Y-type structure.

A large multilayer assembly was fabricated using the same material. Standard conditions were used and it was noted that deposition was generally more successful on the upstroke.

This material had a monolayer absorbance of 0.005, therefore, assuming molecule-molecule absorbance equals glass-molecule absorbance, a perfect 40 layer assembly should have an absorbance of 0.200. It can be seen that absorbance does not have a linear dependence with number of depositions as proposed for Y-type deposition. This can be attributed to imperfect deposition, especially on the downstroke. Molecule-molecule deposition never achieved the same absorbance as glass-molecule absorbance. This may be a function of differing tilt angles giving different absorbance.

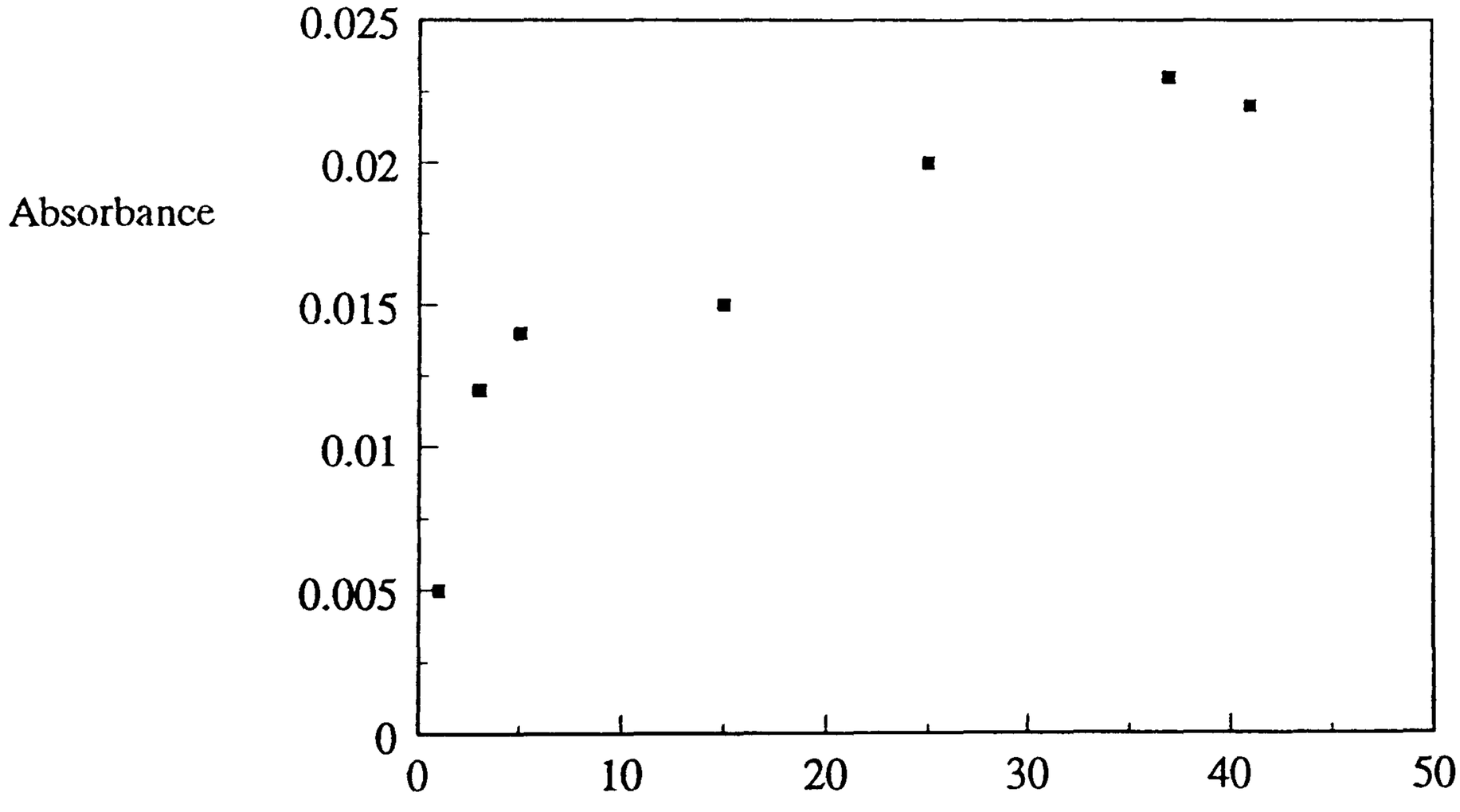

Figure 70. Absorbance versus number of depositions for a Y-type multilayer of $C_{22}H_{45}PHBr$.

The absorbance data alone (table 20), is inconsistent. Absorbance is related to SH response in the form $y = ax^n$, where y = absorbance and x = SH response, and for a quadratic relationship, n = 2. Logarithms of each side of the equation give the straight line form log y = n.log x + log a. Absorbance and SH response were recorded relative to layer one and plotted in this form (figure 71). The regression data gives a R-squared value of 0.943 for n = 1.44, however when the data for layer one is ignored, R-squared = 0.967, for n = 2.08, the latter is a good fit for only 4 data points. Firstly, this confirms the anomolous behaviour of the first layer, and secondly the SH response is related quadratically to absorbance.

Layer	Absorbance	(I/I_1)
1	0.005 ± 0.0005	1.00 ± 0.01
3	0.012 ± 0.0005	2.47 ± 0.01
5	0.014 ± 0.0005	2.96 ± 0.02
25	0.020 ± 0.0005	7.90 ± 0.01
37	0.023 ± 0.0005	8.35 ± 0.01

Table 20. Absorbance and SHG from a Y-type multilayer of $C_{22}H_{45}PHBr$.

Various hemicyanines were deposited in an attempt to fabricate Y-type bilayers. The SH signal was seen to drop for the second layer in each case. Perfect noncentrosymmetric bilayers should have no nonlinear susceptibility because the properties of each layer should cancel out. A signal, smaller than that for the monolayer, was recorded in each film. This may have been because of the anomalous behaviour of the first layer, but transfer ratios indicated that imperfect deposition on the downstroke had occurred.

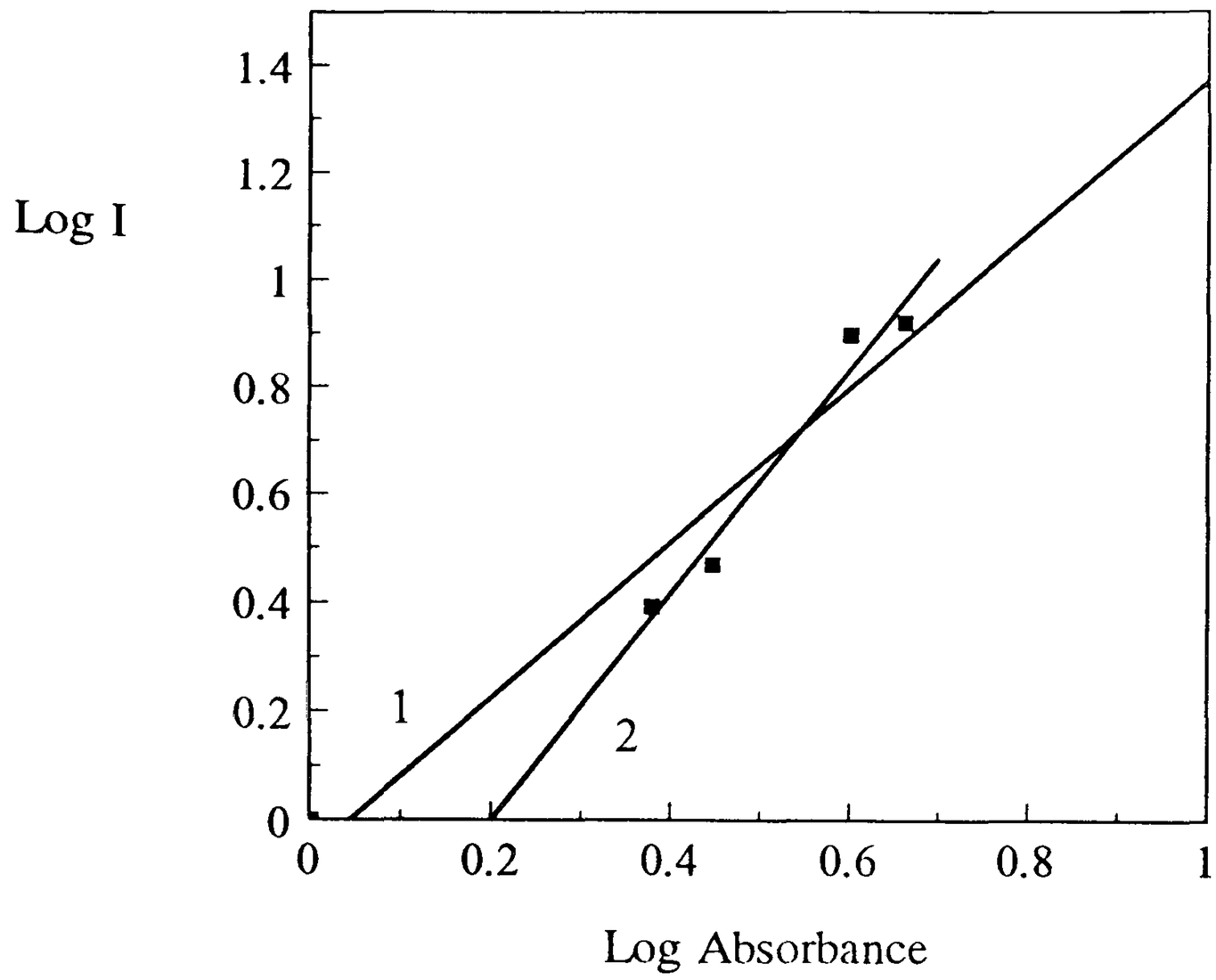

Figure 71. Log (SH response) versus Log (Absorbance) of a $C_{22}H_{45}PHBr$ multilayer. (1) including first layer data, (2) not including first layer data.

Z-type deposition has been observed previously by Hayden although no attempt at explaining the method of deposition was made[131]. Therefore deposition of $C_{22}H_{45}PHBr$ was attempted by transferring six times on the upstroke only. Transfer ratios were similar for each layer.

Number of layers	Absorbance	$(I/I_1)^{1/2}$
1	0.004 ± 0.0005	1.00 ± 0.01
6	0.012 ± 0.0005	1.50 ± 0.01

Table 21. Optical data for an attempted Z-type multilayer of $C_{22}H_{45}PHBr$.

One would expect a signal approximately six times higher than that of layer 1 for a perfect film. The absorbance indicates the equivalent of approximately 3 layers. This, coupled with a poor SHG response indicates incomplete deposition.

The SHG from these films is large compared to others reported in the literature. The fabrication of stable, multilayer films would therefore be useful, however attempts at constructing homomolecular Y-type or Z-type multilayer films has proven difficult. Alternating multilayer were consequently studied, in which all active molecules are aligned in the same direction. The hemicyanine, $C_{22}H_{45}QHBr$, was studied in detail.

Common materials used as interleaving passive layers are stearic acid and stearate salts. These do not exhibit SHG and therefore enable the fabrication of multilayers with each active layer orientated in the same direction. When alternating multilayer of these and $C_{22}H_{45}QHBr$ were studied they showed poor transfer ratios for the interleaving layers as well as inconsistent absorbance for each alternate layer of hemicyanine, probably because of imperfect transfer of the alternate layers.

An alternative material was chosen, N-docosyl-4-methylquinolinium bromide ($C_{22}H_{45}QBr$). This is the cation precursor in the preparation of $C_{22}H_{45}QHBr$ and has a similar molecular configuration. Monolayers of $C_{22}H_{45}QBr$ had transfer ratios of unity but absorbance characterisation was not possible because of its transparency in the visible region of the spectrum.

Initially $C_{22}H_{45}QHBr$ was transferred on the upstroke. After this, bilayers of $C_{22}H_{45}QBr/C_{22}H_{45}QHBr$ transferred at 30 mN m^{-1}/35 mN m^{-1} respectively were deposited on the downstroke/upstroke. An initial study indicated that collapse of the structure was occurring above five bilayers, shown by the reduction in absorbance per bilayer. A second study focused on replenishing the cation for each revolution of the dipper mechanism. This considerably improved the quality of the film and a film of eight bilayers was deposited.

A third study mirrored the conditions of the previous study and a multilayer film of twenty bilayers was deposited. The absorbance of the film was measured at regular intervals and the results are shown in figure 72. Clearly, an absorbance of 0.07 for 20

layers of $C_{22}H_{45}QHBr$ is a large increase on that achieved for the Y-type multilayer of $C_{22}H_{45}PHBr$. The graph indicates that deposition onto the glass substrate (layer 1) has been more successful than deposition onto a molecular layer. Taking this into account the multilayer has an approximate linear relationship between absorbance and number of layers. This is a strong indication that consistent deposition has occurred. The SH signal dependence on number of bilayers is seen in figure 73.

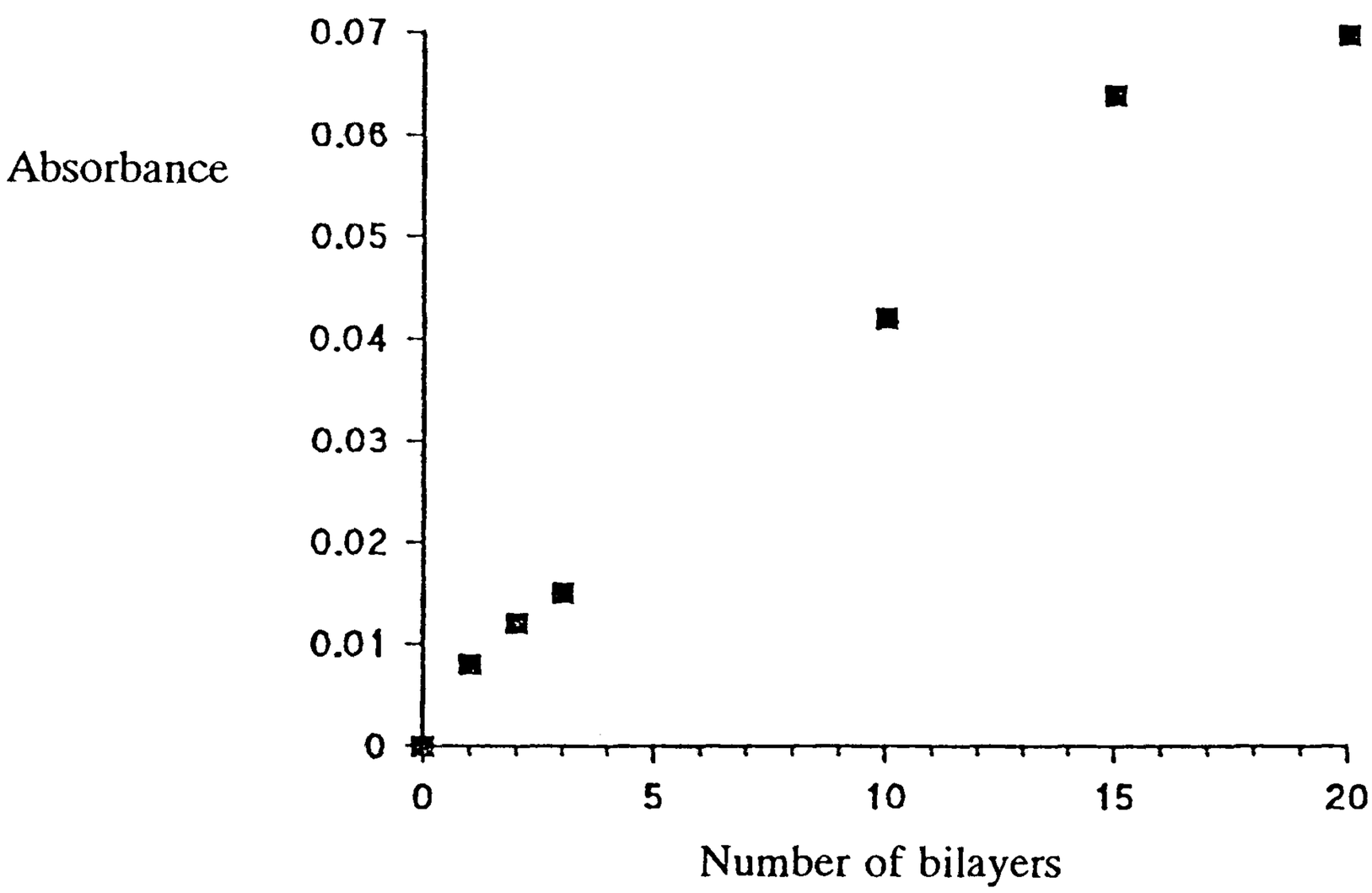

Figure 72. Absorbance versus number of bilayers for a multilayer film of $C_{22}H_{45}QHBr/C_{22}H_{45}QBr$.

It is common to compare the rise in SHG with the theoretical quadratic dependence normalised to layer 1. In this study the experimental data has been compared to a quadratic dependence normalised to layer 3, similar to the approach taken by Anderson et al[167]. Many reports have shown the signal from the first layer is disproportionably large and this has led to subquadratic behaviour being concluded[130,131,134,138-140,142,143]. The multilayer is known to have an anomalous absorbance for layer 1 therefore it appears reasonable to approach the comparison in this way. The

graph suggests, however, that an approximate quadratic dependence for up to 20 bilayers has still not been achieved.

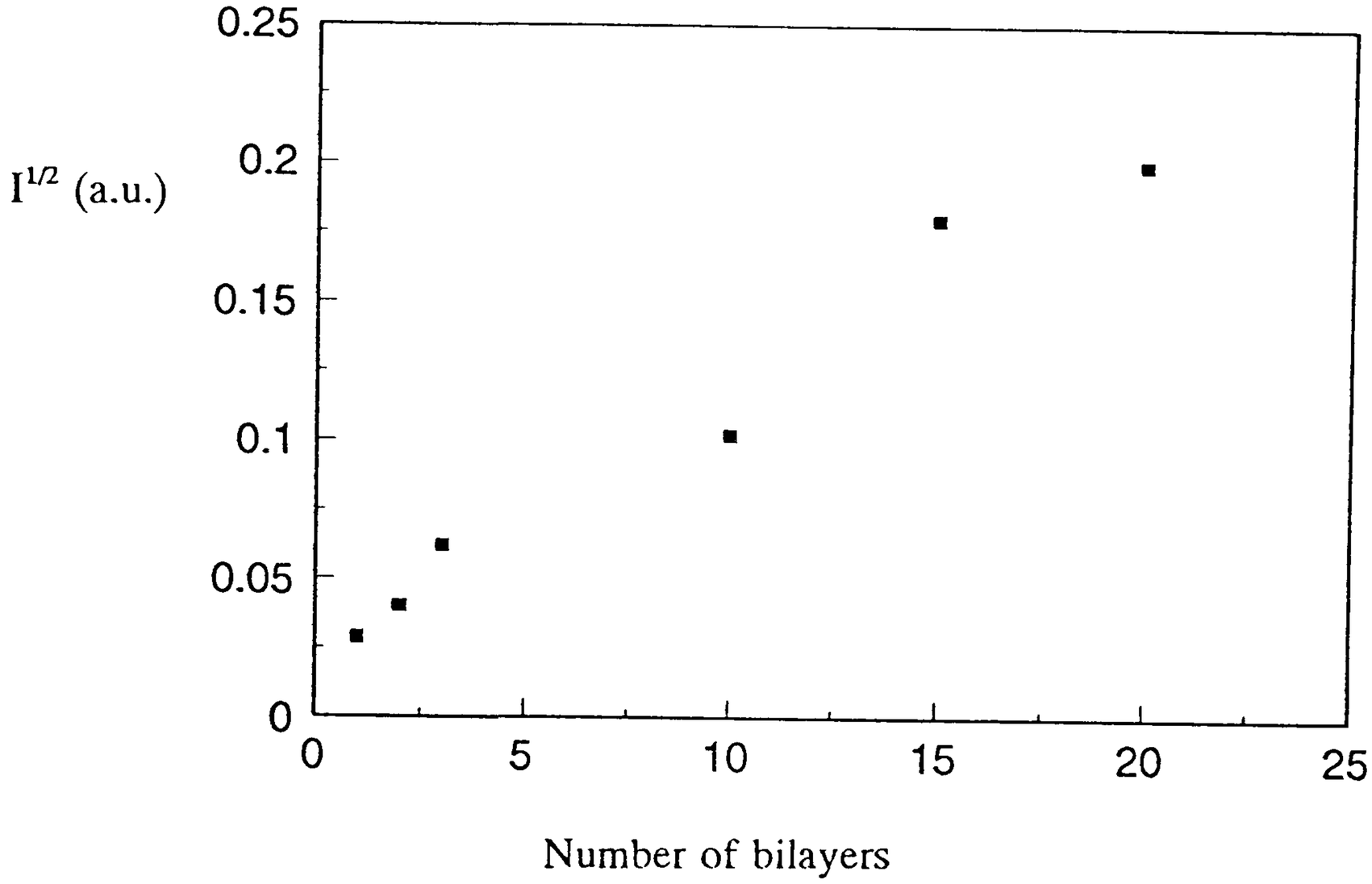

Figure 73. SH response versus number of bilayers for a multilayer film of $C_{22}H_{45}QHBr/C_{22}H_{45}QBr$.

The absorbance spectra from a 20 bilayer film is shown in figure 74. It is nearly identical in shape to that of a monolayer of $C_{22}H_{45}QHBr$. There is no optical evidence for aggregate formation in the form of shoulders on the charge transfer peak. The cation has no absorbance in the visible region of the spectrum and is therefore not seen.

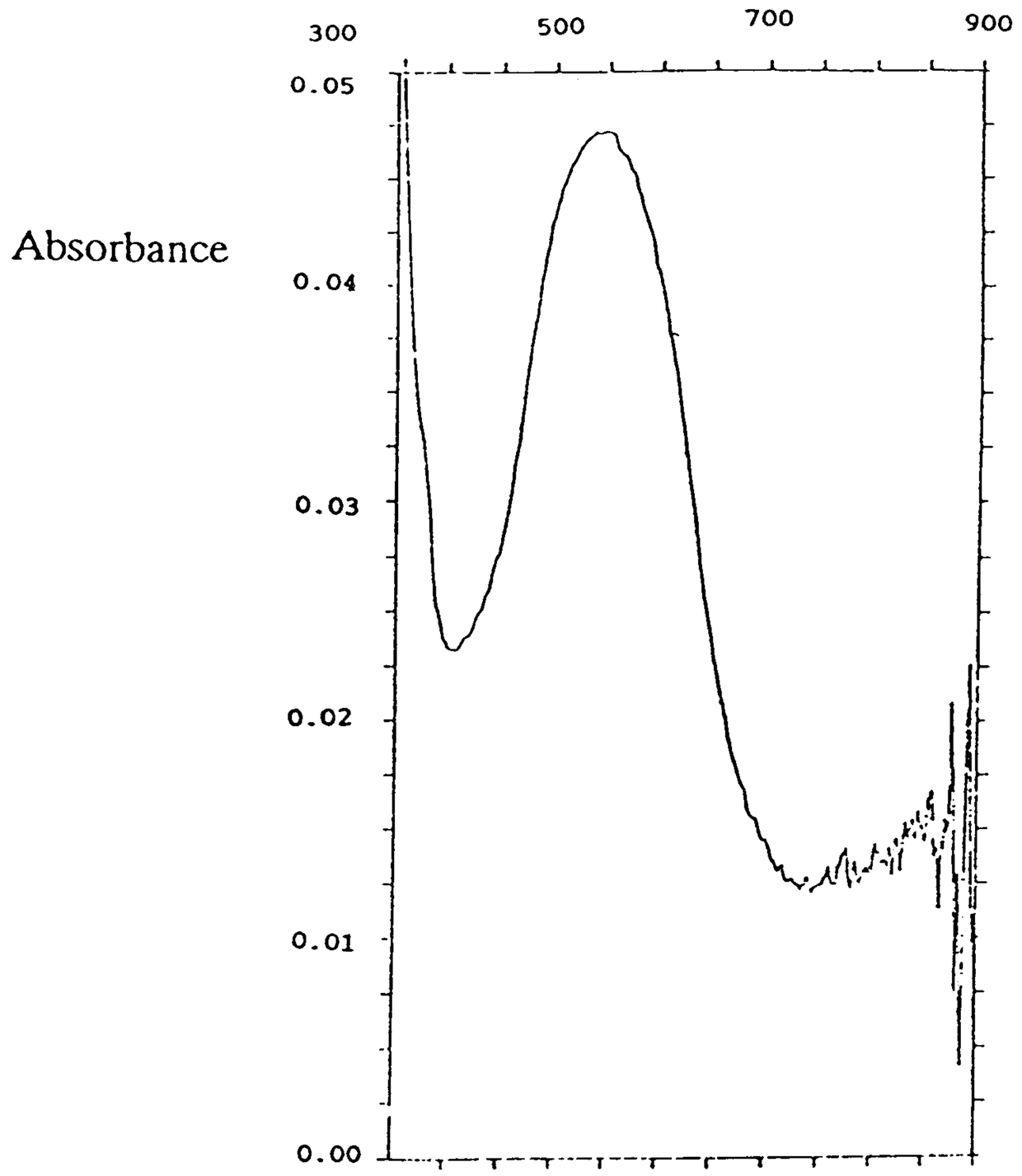

Figure 74. Absorbance of a twenty bilayer film of $C_{22}H_{45}QHBr/C_{22}H_{45}QBr$.

In section 3.1.7 the proportionality between absorbance and SHG for various monolayers was established. There is also a proportionality between absorbance and SHG for multilayer films. Figure 75 clearly shows a quadratic dependence of SHG on absorbance. It also illustrates that some layers in the multilayer were not transferred perfectly. When a layer has a lower than average absorbance in the multilayer the subsequent SH signal is also lower than average. It is noted that the absolute SH signal from the twenty bilayer film is 0.04 x quartz.

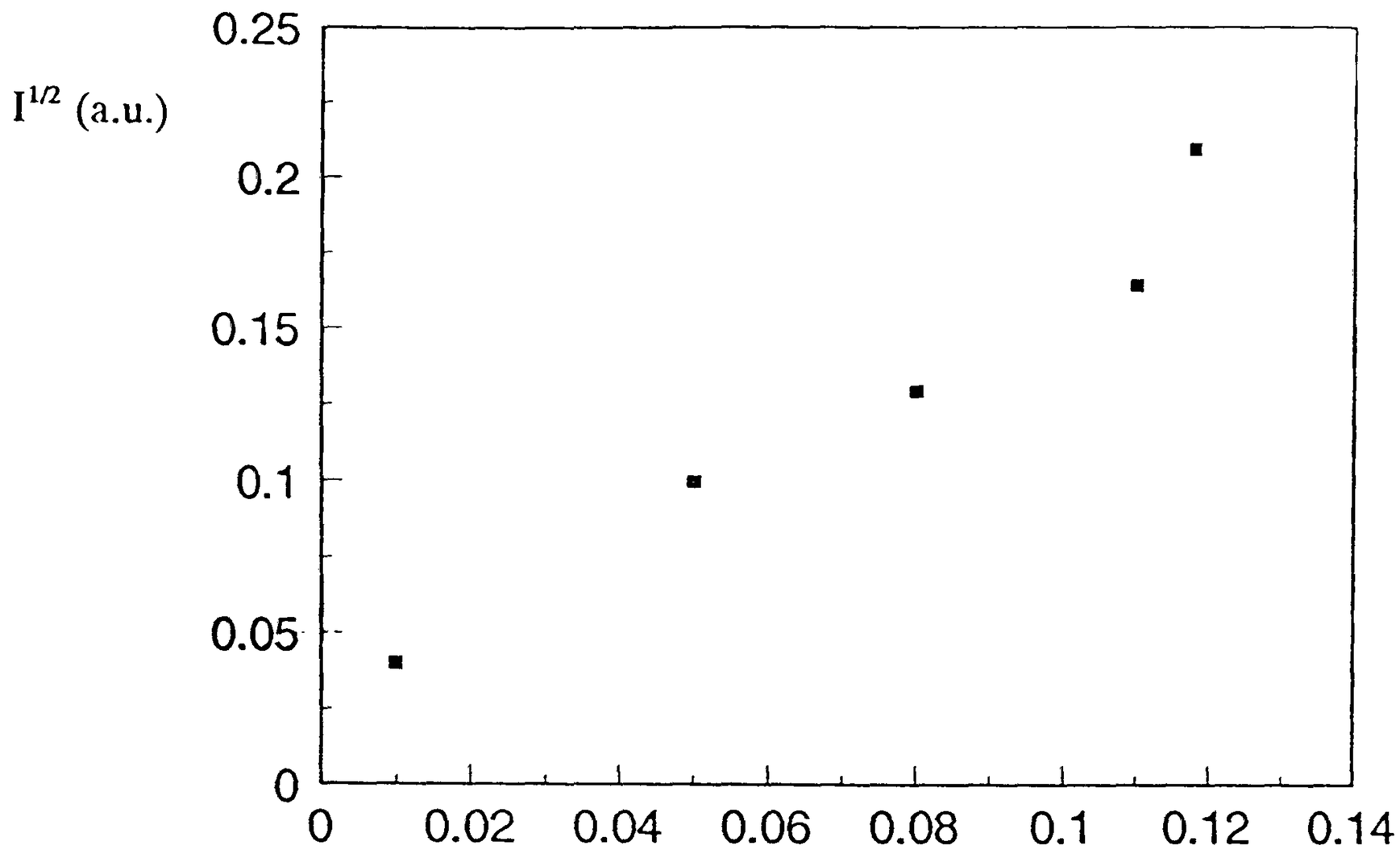

Figure 75. SH response versus absorbance for a multilayer film of $C_{22}H_{45}QHBr/C_{22}H_{45}QBr$.

Another material investigated as a suitable interleaved layer was 4,4'-dioctadecyl-3,5,3',5'-tetramethyldipyrrylmethenehydrobromide. This was synthesised specifically for LB film fabrication[182,183].

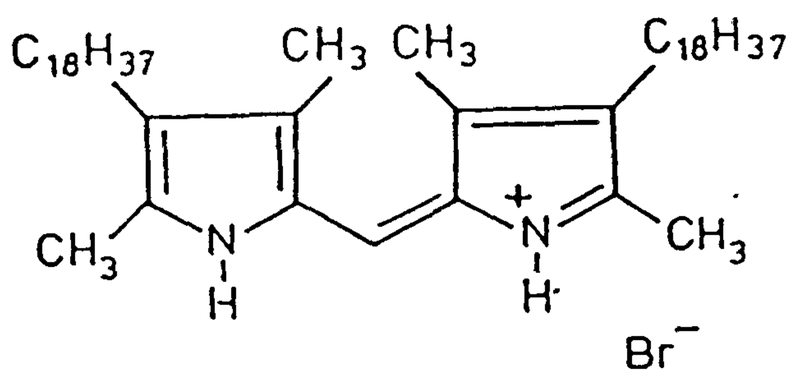

Figure 76. A molecular engineered spacer material for LB multilayer film fabrication, 4,4'-dioctadecyl-3,5,3',5'-tetramethyldipyrrylmethenehydrobromide (DPM).

The two hydrophobic chains of this molecule are sterically very compatible with $C_{22}H_{45}QHBr$. It is possible that alternate layers might deposit with the chain of the hemicyanine positioned inside the two chains of the spacer molecule. This would make individual bilayers very stable and may maintain long range order.

The spacer material was sufficiently surface active to allow compression above 35 mN m^{-1} without collapse. A multilayer of $C_{22}H_{45}QHBr$/DPM was deposited using identical conditions to those used for the $C_{22}H_{45}QHBr/C_{22}H_{45}QBr$ system.

The SH signal dropped below the quadratic dependence line as layers increased. This may be due to imperfect deposition on some transfers. The relationship between SH response and absorbance was quadratic though, shown in figure 77.

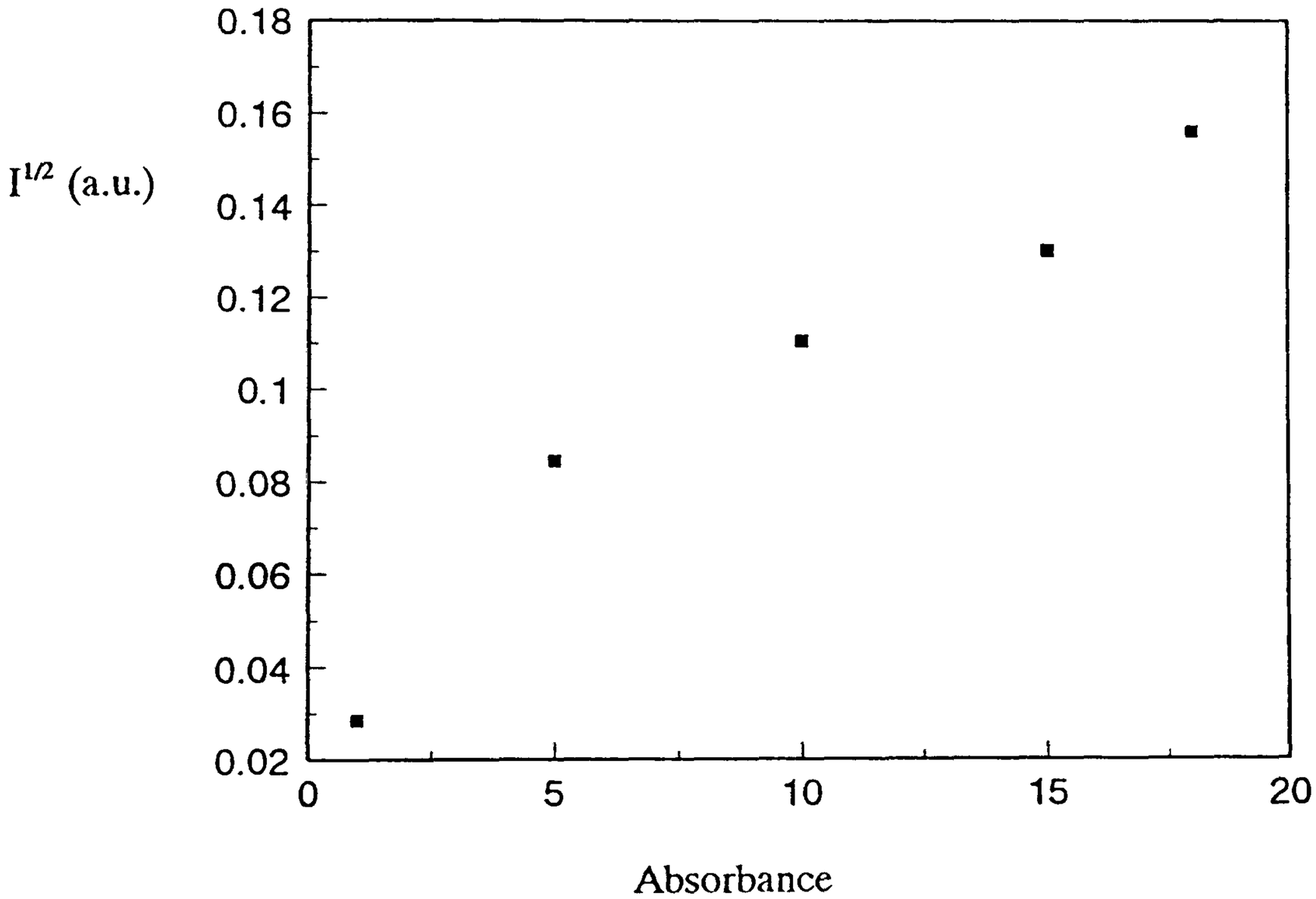

Figure 77. SH response versus number of bilayers for a multilayer film of $C_{22}H_{45}QHBr$/DPM.

Figure 77 indicates clearly that the relationship between absorbance and SH response is not quadratic, probably because of poor deposition. The final signal was large (0.04 x quartz) therefore if the deposition characteristics were improved a useful system could be fabricated. The interdigitation that may have occurred between the two layers may be made easier by using chain lengths that are equal. Therefore two hemicyanines containing $C_{18}H_{37}$ hydrophobic chains were used, ie $C_{18}H_{37}$QHI and $C_{18}H_{37}$PHI. A detailed description of this work can be found in the papers by Ashwell et al[181-183].

3.2 Novel Hemicyanines

The relationship between conjugation and nonlinear activity has been studied by many workers (see section 1.6.2). The materials studied in section 3.1 were chosen partly because molecular modifications are relatively simple. Therefore novel hemicyanine materials were designed, in which the level of conjugation differed. The effect that these alterations had on the LB film deposition characteristics and the subsequent nonlinear properties are discussed below. Figure 78 shows the general formula of the materials that were synthesised.

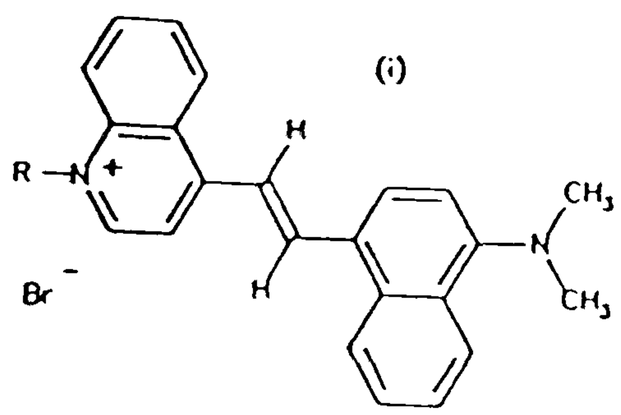

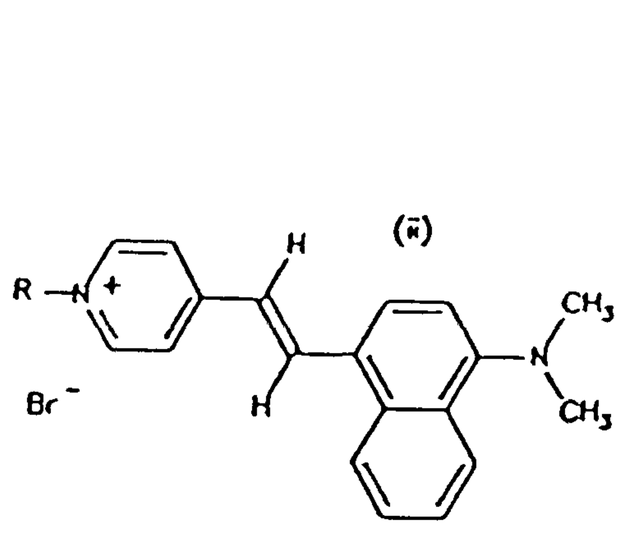

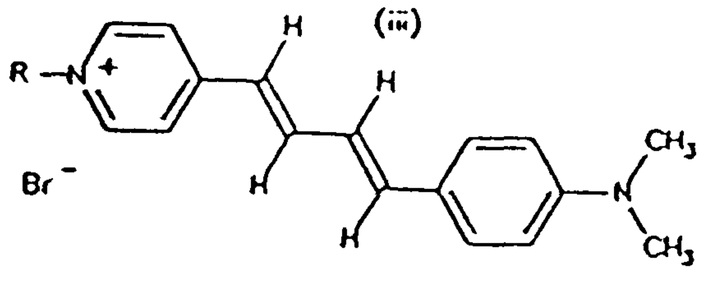

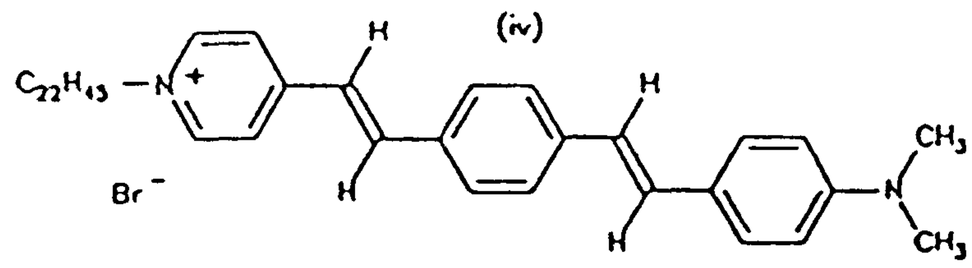

Figure 78. Novel hemicyanines prepared for LB studies. (i) E-1-alkyl-4-{2-(4-dimethylaminobenzylphenyl)ethenyl}quinolinium bromide, $C_nH_{2n+1}QNBr$ (ii) E-1-alkyl-4-{2-(4-dimethylaminobenzylphenyl)ethenyl}pyridinium bromide, $C_nH_{2n+1}PNBr$ (iii) E-1-alkyl-4-{4-(4-dimethylaminophenyl)-1,3-butadienyl} pyridinium bromide, $C_nH_{2n+1}PEHBr$ (iv) E-1-docosyl-4-{2-(4-{2-(4-dimethylaminophenyl)ethenyl}benzyl)ethenyl}pyridinium bromide, $C_{22}H_{45}PBHBr$.

3.2.2 Isotherms

The materials were compressed under the same conditions as their analogues in section 3.1.3. The isotherms of $C_{22}H_{45}QNBr$ and $C_{22}H_{45}PNBr$ were similar, the former is shown in figure 79. The important features of both, plus their analogues, are summarised in table 22.

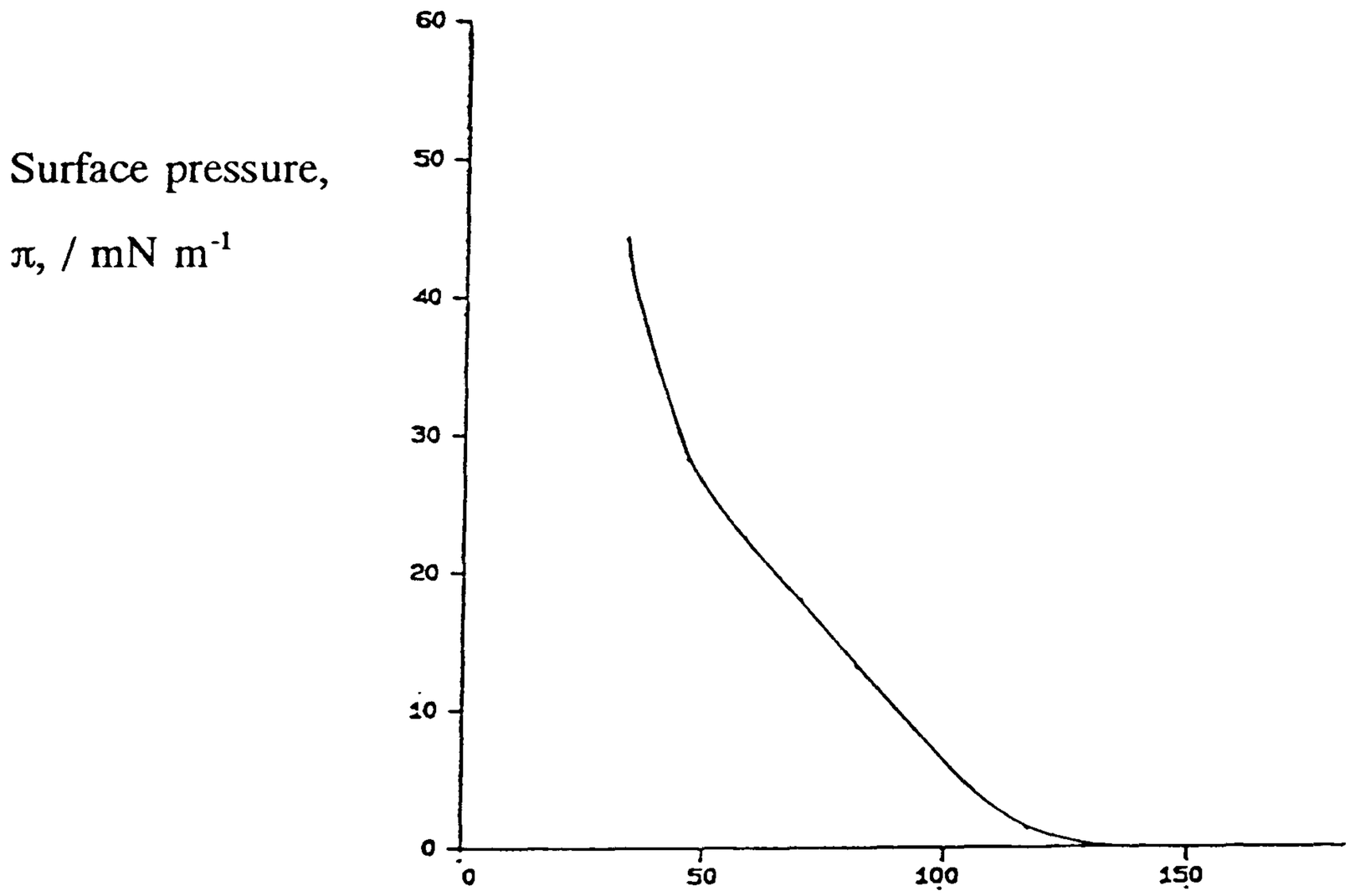

Figure 79. Π - a isotherm of $C_{22}H_{45}QNBr$.

The area per molecule that $C_{22}H_{45}QNBr$ occupies as it begins to exert a surface pressure is slightly larger than that of $C_{22}H_{45}QHBr$. The former contains an extra benzene ring therefore it has a larger face area, about 110 Å^2, compared to approximately 100 Å^2. The figures indicate that both materials lie with their chromophore flat on the air/water interface before compression. A slight kink at

approximately 60 Å^2 for $C_{22}H_{45}QNBr$ indicates an alignment phase change similar to that evident for $C_{22}H_{45}QHBr$. The minimum cross-sectional area for $C_{22}H_{45}QNBr$ is determined by the two double aromatic rings therefore it should be slightly larger than $C_{22}H_{45}QHBr$. In the two-dimensional solid phase the area per molecule of $C_{22}H_{45}QNBr$ is approximately 40 Å^2, for $C_{22}H_{45}QHBr$ the corresponding area per molecule is 30 Å^2, confirming this theory. It is noted that these figures indicate that the molecules are aligned nearly vertical to the interface.

Hemicyanine	Area per molecule / Å^2	Area per molecule / Å^2	Area per molecule / Å^2
	1 mN m^{-1}	Phase change	30 mN m^{-1}
$C_{22}H_{45}QHBr$	120 ± 0.5	70 ± 0.5	30 ± 0.5
$C_{22}H_{45}QNBr$	130 ± 0.5	60 ± 0.5	40 ± 0.5
$C_{22}H_{45}PHBr$	120 ± 0.5	70 ± 0.5	30 ± 0.5
$C_{22}H_{45}PNBr$	125 ± 0.5	60 ± 0.5	35 ± 0.5

Table 22. A comparison of the isotherm characteristics of four hemicyanines.

The π - a isotherm characteristics of $C_{22}H_{45}PNBr$ confirms the similarities found in these materials. The relationship between $C_{22}H_{45}PNBr$ and $C_{22}H_{45}PHBr$ is similar to that for the quinolinium analogues.

$C_{22}H_{45}PEHBr$ exhibited no noticeable phase change in its π - a isotherm. It has an estimated chromophore face area of 105 Å, therefore it appears to be lying flat at the water surface. Its area in the two-dimensional solid phase is approximately 50 Å, indicating a larger angle of tilt away from the vertical than has been seen for other hemicyanines.

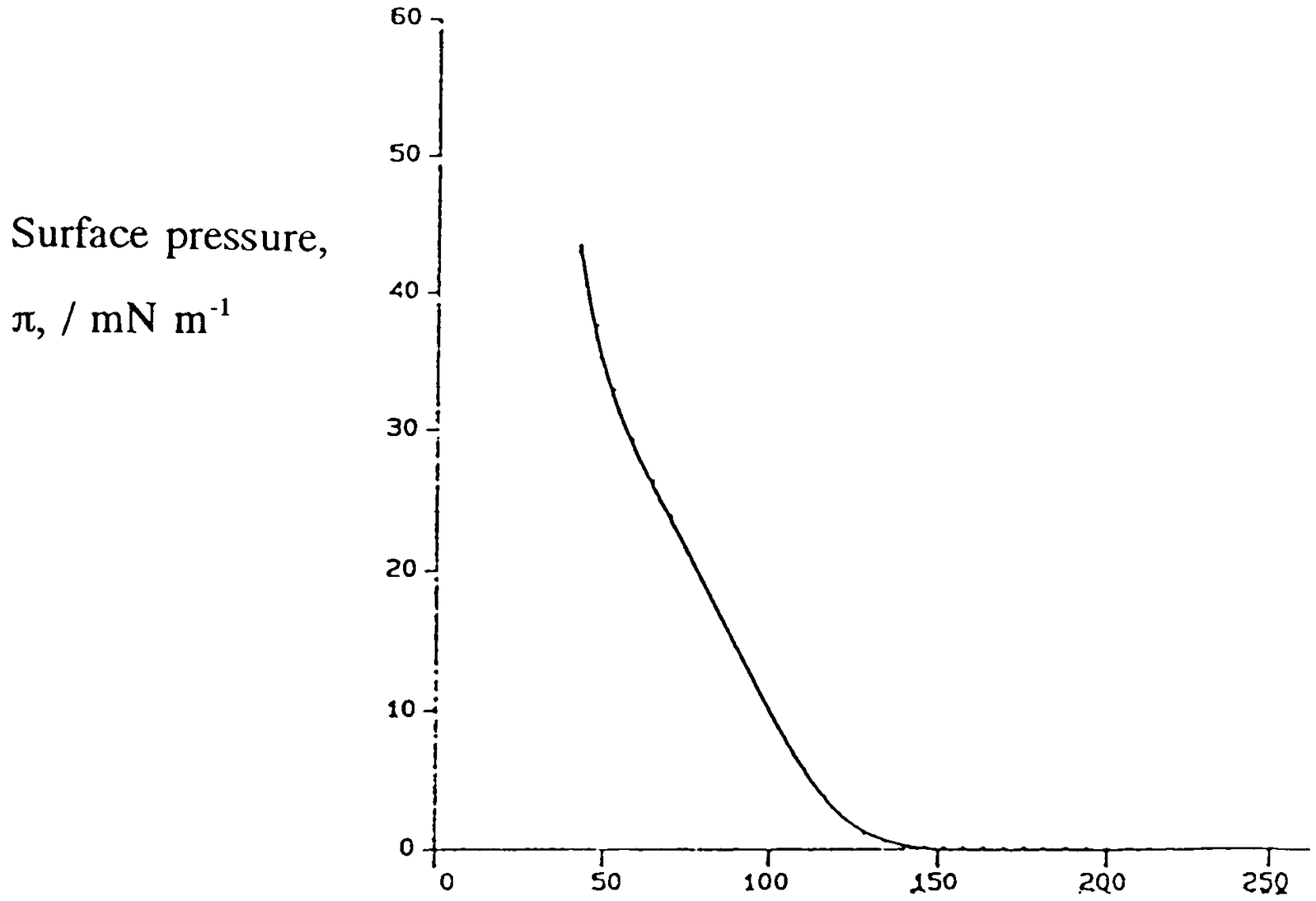

Figure 80. Π - a isotherm of $C_{22}H_{45}PEHBr$.

The pressure-area isotherm of $C_{22}H_{45}PBHBr$ is seen in figure 81. It is interesting to compare this material to an isotherm of $C_{22}H_{45}PHBr$ (figure 63), since the only difference between the two is that the former has an extra benzene ring along the length of the chromophore. At 30 $Å^2$ both exert a surface pressure of approximately 30 mN m^{-1}. The area that the molecules would occupy at zero surface pressure is significantly greater for the longer molecule (approximately 60 $Å^2$ compared to 38 $Å^2$), this suggests that $C_{18}H_{37}PBHBr$ is tilted further away from the vertical.

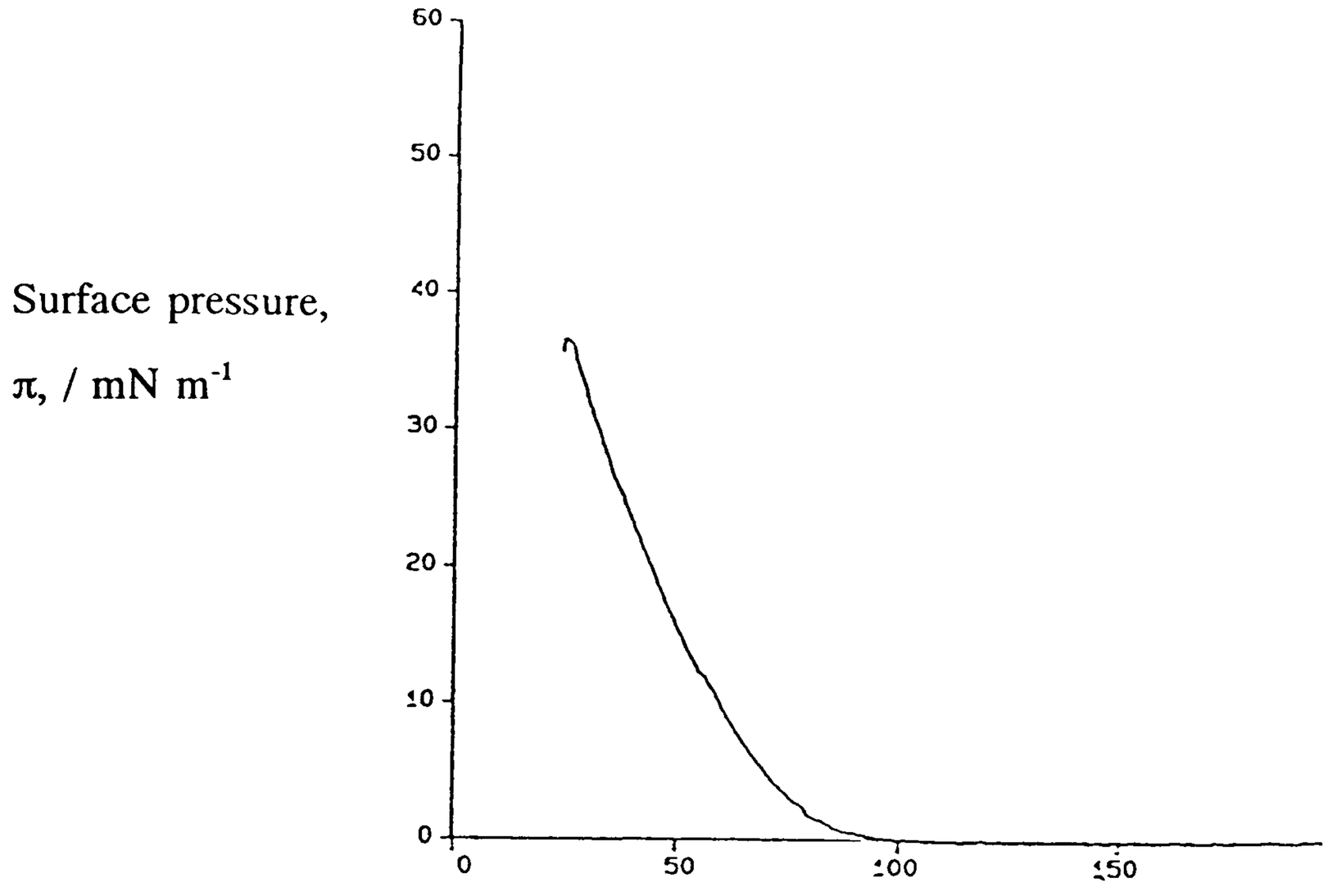

Figure 81. Pressure-area isotherm of $C_{22}H_{45}PBHBr$.

3.2.3 LB Films of $C_{22}H_{45}QNBr$

LB films were transferred at 35 mN m^{-1}. Monolayers, transferred on the upstroke, had consistent transfer ratios indicating reproducible films. Absorbance spectra was consistent and the film was visible to the naked eye after deposition.

The charge transfer peak was hypsochromically shifted to 535 nm compared to its peak in chloroform solution. The spectrum was the same all over the substrate, indicating consistent coverage of the slide. It was noted that the absorbance decreased to 25% of its original value after four days. This drop may be due to a gradual rearrangement of the molecules on the slide to a tilt angle that is aligned further away from the normal of the irradiating beam in the spectrometer. It may also have resulted from some interaction with the laser beam when tested for second harmonic generation. SHG from the freshly prepared monolayer film was 1.6 x 10^{-4} x quartz.

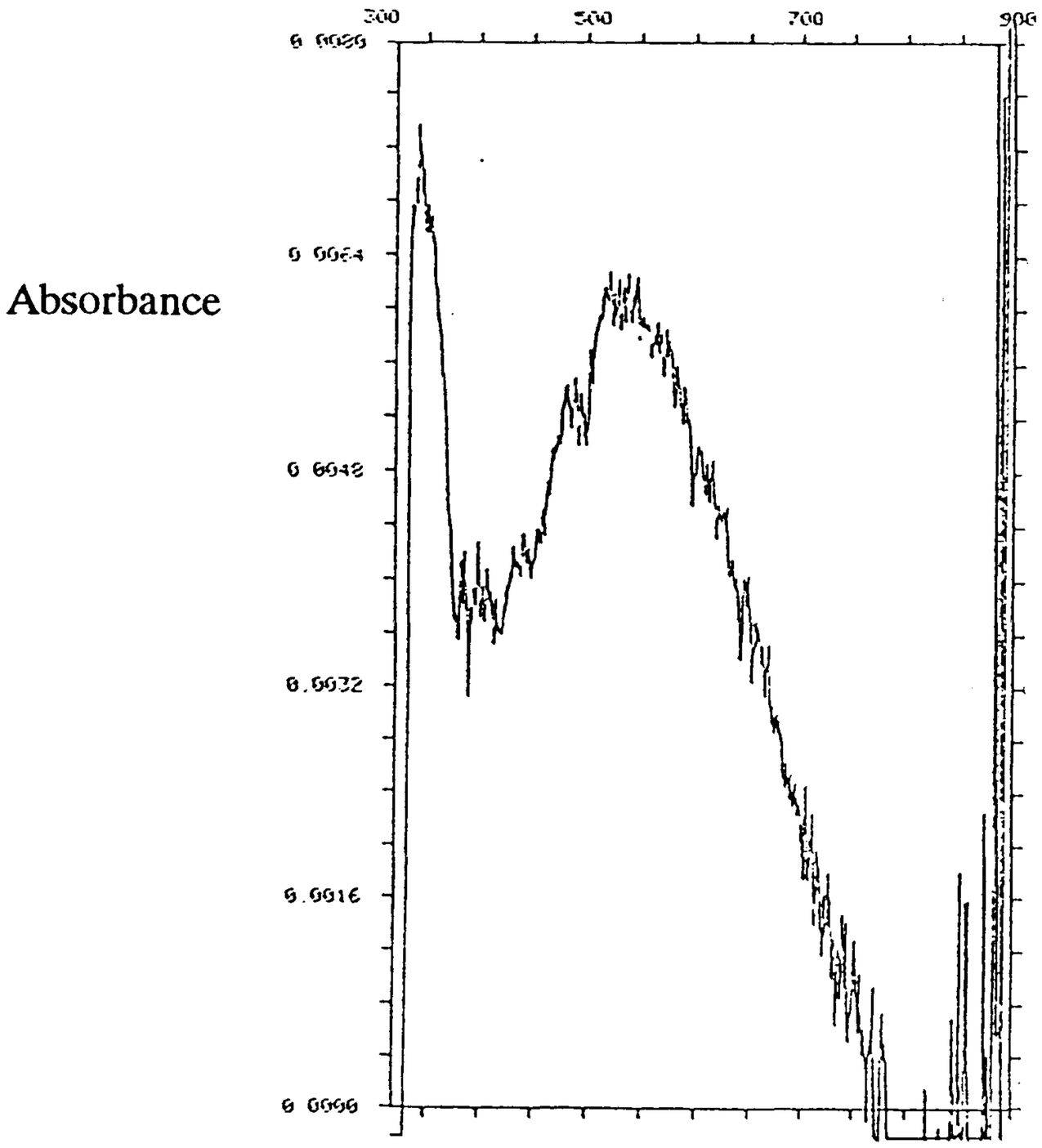

Figure 82. Absorbance of an LB monolayer of $C_{22}H_{45}QNBr$.

An alternating multilayer film of $C_{22}H_{45}QNBr$ and $C_{22}H_{45}QBr$ was fabricated. $C_{22}H_{45}QBr$ was deposited on the downstroke at a pressure of 30 mN m^{-1} followed by $C_{22}H_{45}QNBr$ on the upstroke at a pressure of 35 mN m^{-1}. The Langmuir film at the water surface was replaced for each transfer because this has been noted to improve subsequent film properties. The transfer ratios were consistent for both materials. After 5 bilayers the film was purple, and after 10 bilayers there were no visible defects and absorbance was confirmed as consistent over the whole of the multilayer.

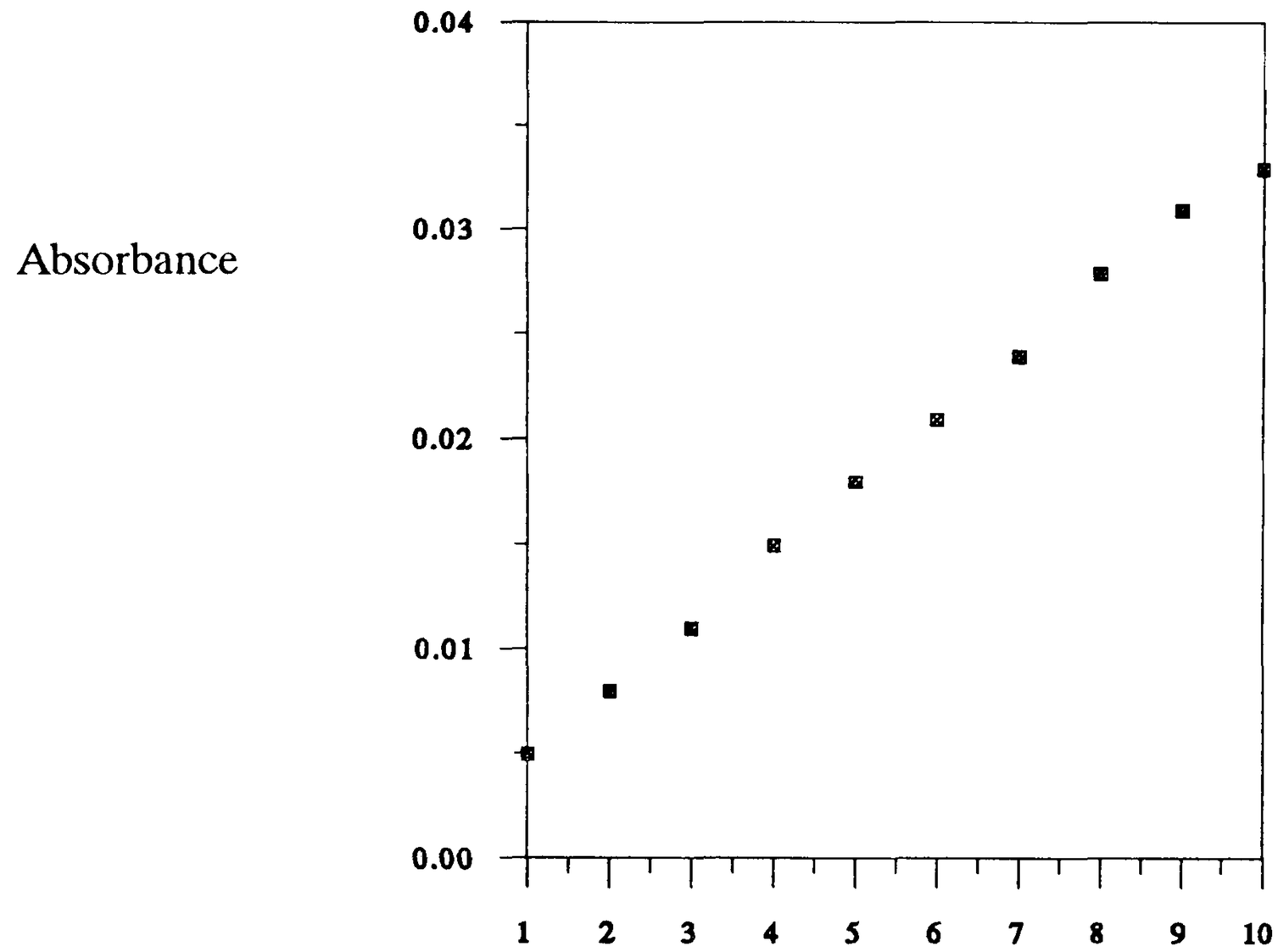

Figure 83. Absorbance versus number of bilayers for a multilayer LB film of $C_{22}H_{45}QNBr/C_{22}H_{45}QBr$.

The dependence of SH response on number of bilayers is shown in figure 84, when normalised to the signal from layer 3 the response is quadratic up to ten bilayers. The SH signal from the ten bilayer LB film was 0.01 x quartz.

The tilt angle of the chromophore relative to the normal of the substrate was calculated from the polarisation-dependent intensities of the second harmonic generation (figure 85). It was observed that $I_{2\omega}(ps) \approx I_{2\omega}(ss) \approx 0$ and $I_{2\omega}(pp) \approx 9.8I_{2\omega}(sp)$, corresponding to a tilt angle of 38°. The refractive index and thickness of the film, obtained using a Nanofilm 1000 ellipsometer equipped with a diode laser (λ = 670 nm), was 1.59 and 4.5 nm respectively. The two molecules have a combined length equalling

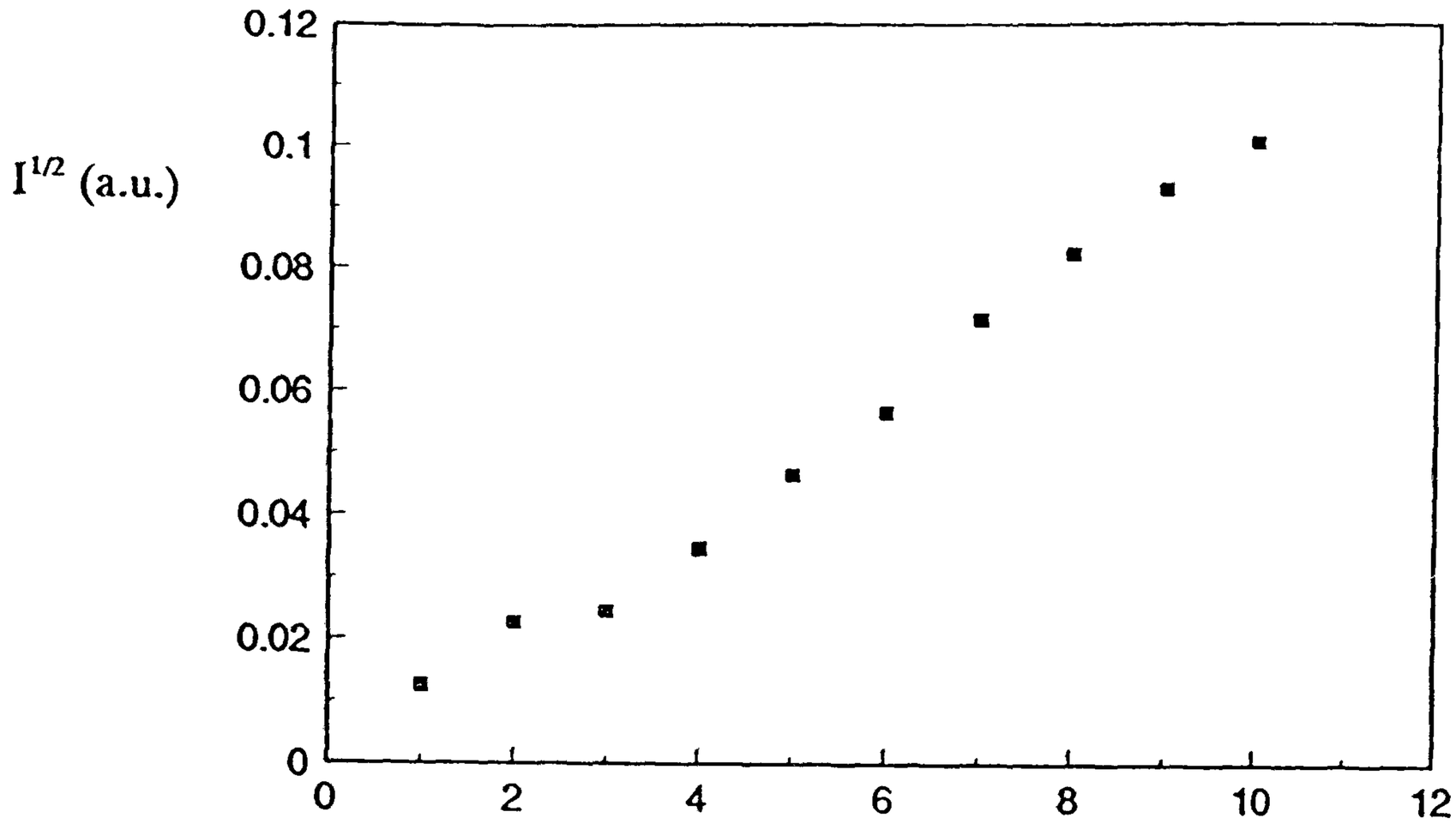

Figure 84. SH response versus number of bilayers for a multilayer LB film of $C_{22}H_{45}QNBr/C_{22}H_{45}QBr$.

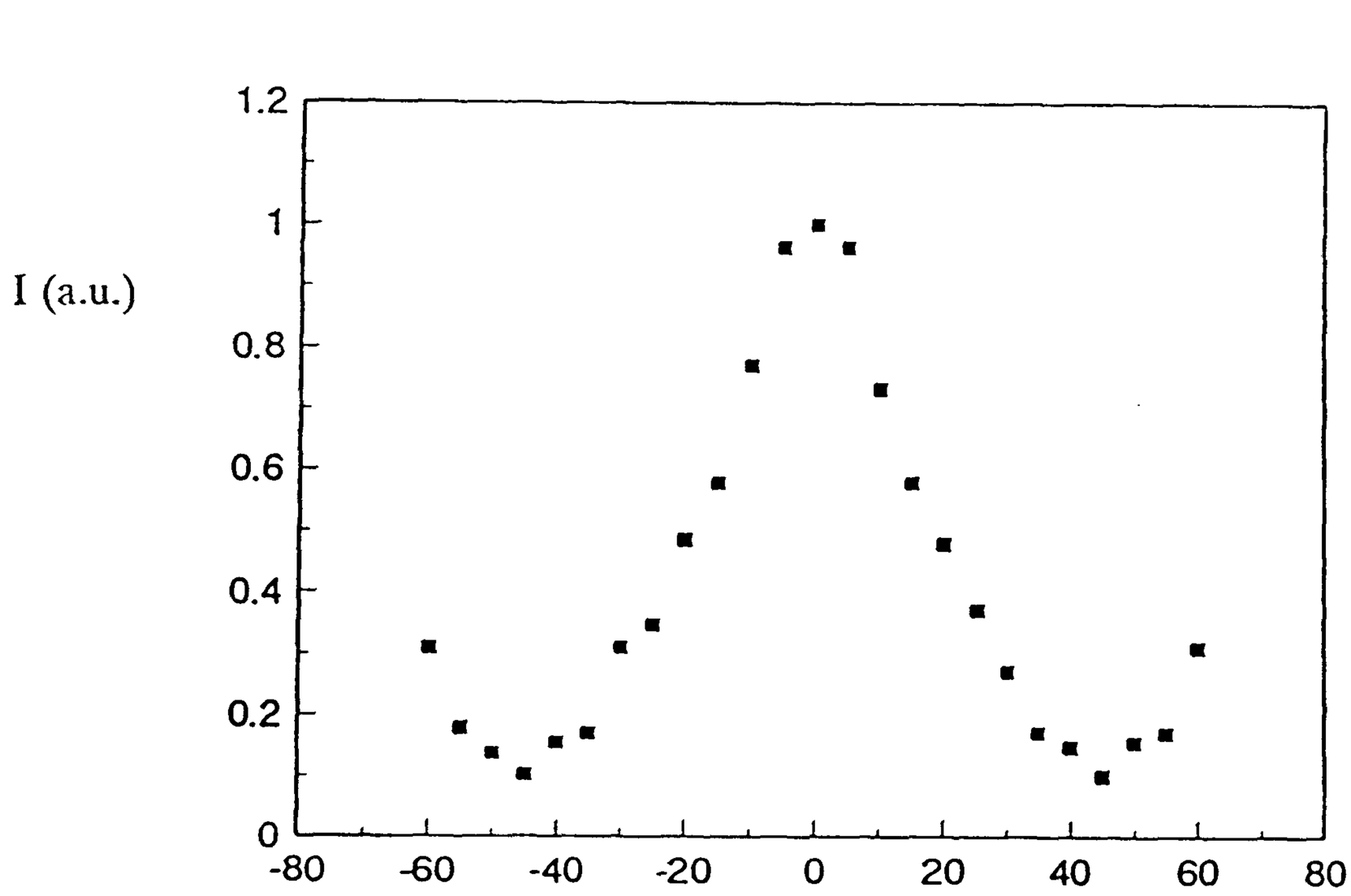

Figure 85. Polarisation dependence of SHG of a multilayer film of $C_{22}H_{45}QNBr/C_{22}H_{45}QBr$.

7.8 nm and this enables a calculation of the theoretical bilayer thickness of ca 6.0 nm. The observed bilayer thickness of 4.5 nm is explained if the hydrophobic chains of $C_{22}H_{45}QHBr$ and $C_{22}H_{45}QBr$ interdigitate. The proposed molecular arrangement for the multilayer is shown in figure 86.

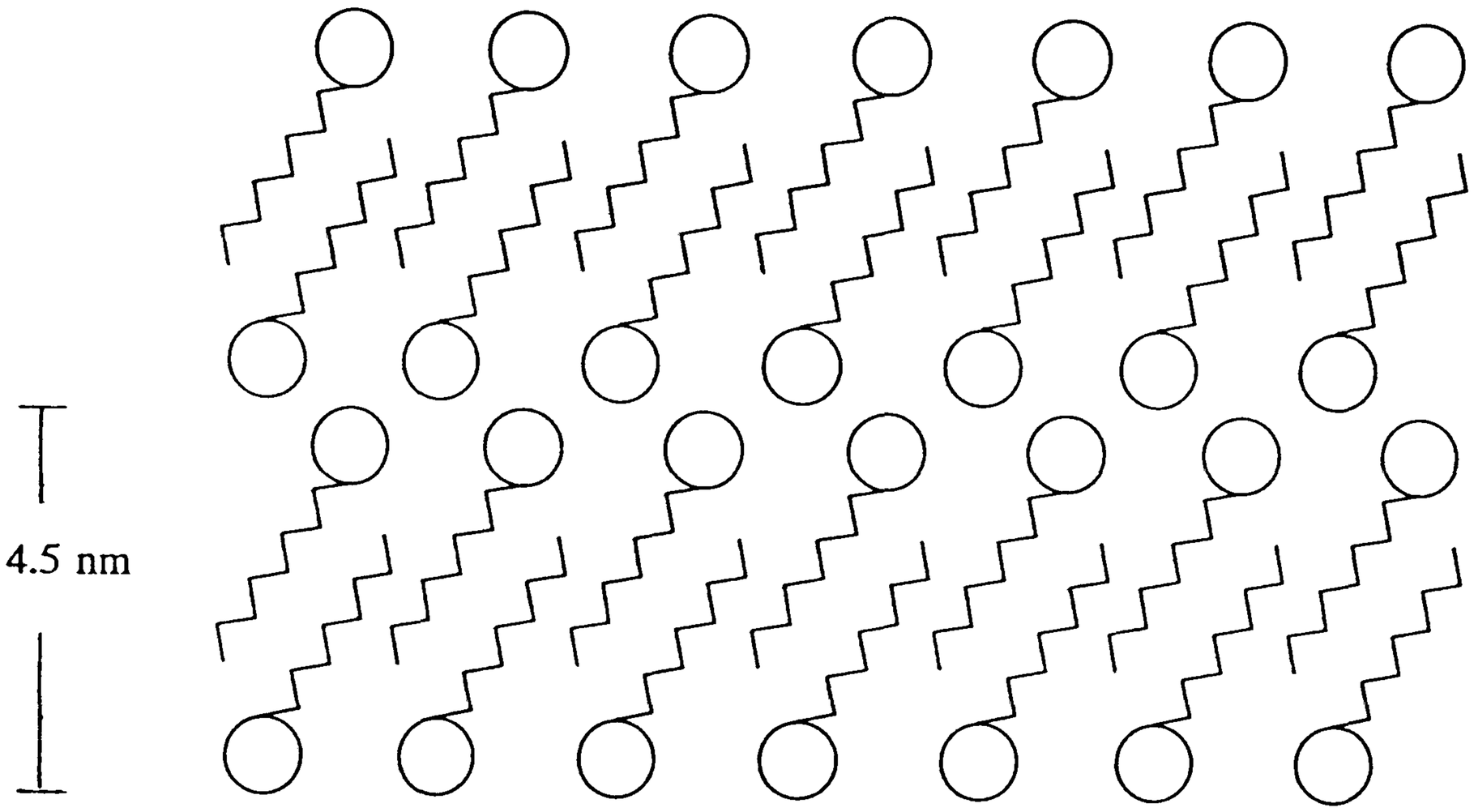

Figure 86. Interdigitation of $C_{22}H_{45}QNBr$ and $C_{22}H_{45}QBr$ bilayer.

3.2.4 LB Films of $C_{18}H_{37}PNBr$ and $C_{22}H_{45}PNBr$

Monolayers of $C_{18}H_{37}PNBr$, deposited in the usual manner, gave an absorbance of 0.004 for the charge transfer peak, hypsochromically shifted compared to its spectrum in chloroform solution. The SHG from monolayers of this material was surprisingly small, approximately 2.5 x 10^{-5} x quartz; an order less than the standard hemicyanines reported in section 3.1.7.

Alternating multilayer films were deposited in the same manner as the multilayer film of $C_{22}H_{45}QNBr$. Transfer ratios were consistent, however absorbance data for up to

5 bilayers was very poor. The SH signal for the five bilayer film was less than that for a monolayer. The π - a isotherm indicates a collapse pressure slightly less than that of other hemicyanines and simple solubility tests show the material to be slightly soluble in water. This may cause the molecules in the Langmuir film at the air/water interface to go into the aqueous phase instead of on to the substrate. This produces imperfect films of poor absorbance, as seen, which will become worse with subsequent layers. This inconsistency was supported by analyzing the whole of the film in detail and observing erratic and inconsistent results for both absorbance and SHG.

Number of bilayers	Absorbance	$I^{1/2}$ (a.u)
1	0.004 ± 0.0005	1.00 ± 0.01
2	0.006 ± 0.0005	1.14 ± 0.01
3	0.008 ± 0.0005	1.39 ± 0.02
4	0.010 ± 0.0005	1.19 ± 0.01
5	0.013 ± 0.0005	1.43 ± 0.02
6	0.015 ± 0.0005	1.18 ± 0.01

Table 23. Absorbance and SHG data for a multilayer film of $C_{22}H_{45}PNBr/C_{22}H_{45}QBr$.

Monolayers of $C_{22}H_{45}PNBr$ showed a charge transfer peak at the same wavelength as $C_{22}H_{45}PHBr$, its analogue, as expected. Interestingly the intensity of this absorbance is also 0.004. Since it is totally insoluble in water it appears that solubility has less of an effect on the first deposition than it does on later ones. This may be because the glass-molecule adsorption is a stronger interaction than the molecule-molecule adsorption. The SH response from the monolayer was 1.4 x 10^{-4} x quartz,

larger than $C_{18}H_{37}PNBr$ and similar to that of a monolayer of $C_{22}H_{45}PHBr$. A multilayer film of $C_{22}H_{45}PNBr$ was fabricated using the spacer $C_{22}H_{45}QBr$, and standard conditions for transfer as described earlier. Transfer ratios were inconsistent which is a clear indication of poor deposition. Although the absorbance was consistent for bilayers 2 to 6 the SHG from the film indicates that imperfect deposition occurred.

3.2.5 LB films of $C_{22}H_{45}PEHBr$

One would expect this material to exhibit the same monolayer absorbance spectra as $C_{22}H_{45}PHBr$ if their alignment were equal. This is because the only difference in chromophore groups is an extra double bond. The charge transfer peak is actually slightly hypsochromically shifted compared to that of $C_{22}H_{45}PHBr$. The transfer ratio and monolayer absorbance for various monolayers were consistent. The absorbance value, 0.0026 is about 60% of the absorbance of $C_{22}H_{45}PHBr$ and indicates that the packing is less efficient. This may account for the slight difference in λ_{max} since less molecules per unit area may be due to a different angle of alignment. The SH response was 1.1×10^{-4} x quartz, approximately equal to $C_{22}H_{45}PHBr$ (1×10^{-4} x quartz). This supports the observation that SH response is dependent on absorbance. One can assume that for an absorbance of 0.004 (ie equal to that of $C_{22}H_{45}PHBr$) the SH response would be noticeably larger. This is as expected because of the increased conjugation length between donor and acceptor.

Two layers were deposited on the upstroke only. The study was done in duplicate and is shown in table 24. The transfer ratios indicated coverage on each pass through the air/water interface. The SHG indicates that the film was not aligned Z-type, but was probably a poorly deposited Y-type film.

Sample	Layer 1	Layer 1	Layer 2	Layer 2
	Absorbance	SH response*	Absorbance	SH response*
1	0.003 ± 0.0005	1.10 ± 0.01	0.010 ± 0.0005	0.55 ± 0.01
2	0.003 ± 0.0005	1.03 ± 0.01	0.009 ± 0.0005	0.49 ± 0.01

Table 24. Absorbance and SHG data for 3 layers of $C_{22}H_{45}PEHBr$.

* relative to a monolayer of $C_{22}H_{45}PHBr$

Alternating multilayer films of $C_{22}H_{45}PHBr/C_{22}H_{45}QBr$ and $C_{22}H_{45}PEHBr/C_{22}H_{45}QBr$ were compared. The transfer ratios for $C_{22}H_{45}PHBr/C_{22}H_{45}QBr$ were consistent.

Hemicyanine multilayer	No. of bilayers	Absorbance	SH response*
$C_{22}H_{45}PHBr$	5	0.020 ± 0.0005	1.00 ± 0.01
$C_{22}H_{45}PEHBr$	5	0.013 ± 0.0005	0.18 ± 0.02
	8	0.018 ± 0.0005	0.22 ± 0.01

Table 25. A comparison of LB alternate multilayer characteristics for $C_{22}H_{45}PHBr/C_{22}H_{45}QBr$ and $C_{22}H_{45}PEHBr/C_{22}H_{45}QBr$. * - relative to the signal from the 5 bilayer film of $C_{22}H_{45}PHBr/C_{22}H_{45}QHBr$.

A multilayer film was fabricated using $C_{22}H_{45}PBr$ as a spacer because this matched the configuration of $C_{22}H_{45}PEHBr$ more closely and the results are shown in figure 87. The SH response did not show a quadratic dependence on the number of layers but it did show a dependence of SHG on absorbance.

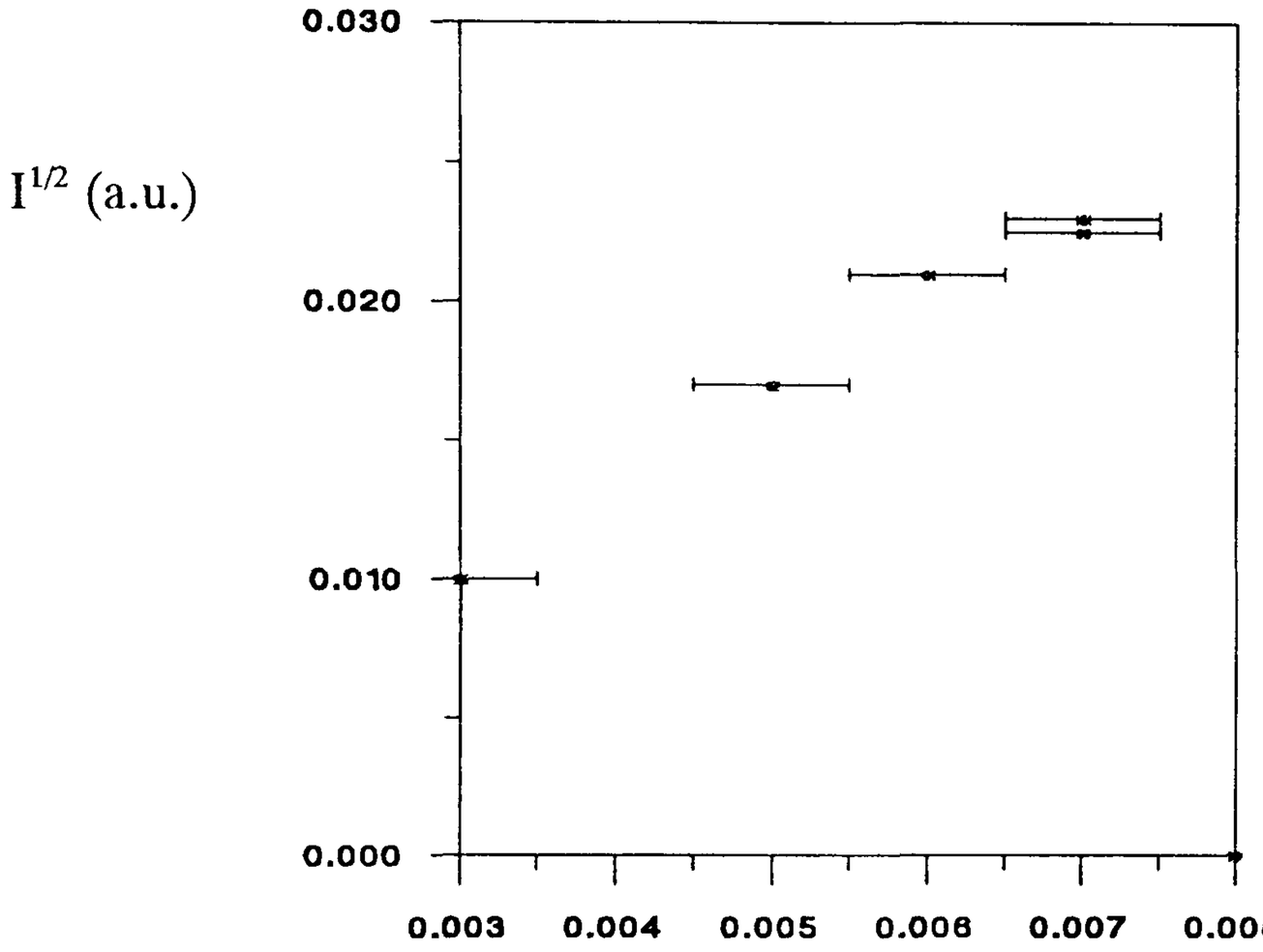

Figure 87. SH response versus absorbance for each layer of a five bilayer film of $C_{22}H_{45}PEHBr/C_{22}H_{45}PBr$.

3.2.6 LB films of $C_{22}H_{45}PBHBr$

Langmuir films were stable and transfer on the upstroke occurred successfully. The absorbance of a monolayer was poor compared to $C_{22}H_{45}PHBr$, but the characteristic charge transfer peak in the 470 nm region was clearly evident. The SH response was small as expected for a poorly deposited film, ie 3.6×10^{-6} x quartz. This result was reproducible so a multilayer was deposited. The spacer chosen was E-1-docosyl-4-{2-(4-methylphenyl)ethenyl}pyridinium bromide ($C_{22}H_{45}PT$) since it was similar in

configuration. $C_{22}H_{45}PBHBr$ was deposited on the upstroke, followed by nine bilayers of $C_{22}H_{45}PT/C_{22}H_{45}PBHBr$ and the resulting film was yellow. The absorbance of ten layers was still poor but the SHG did increase with each layer.

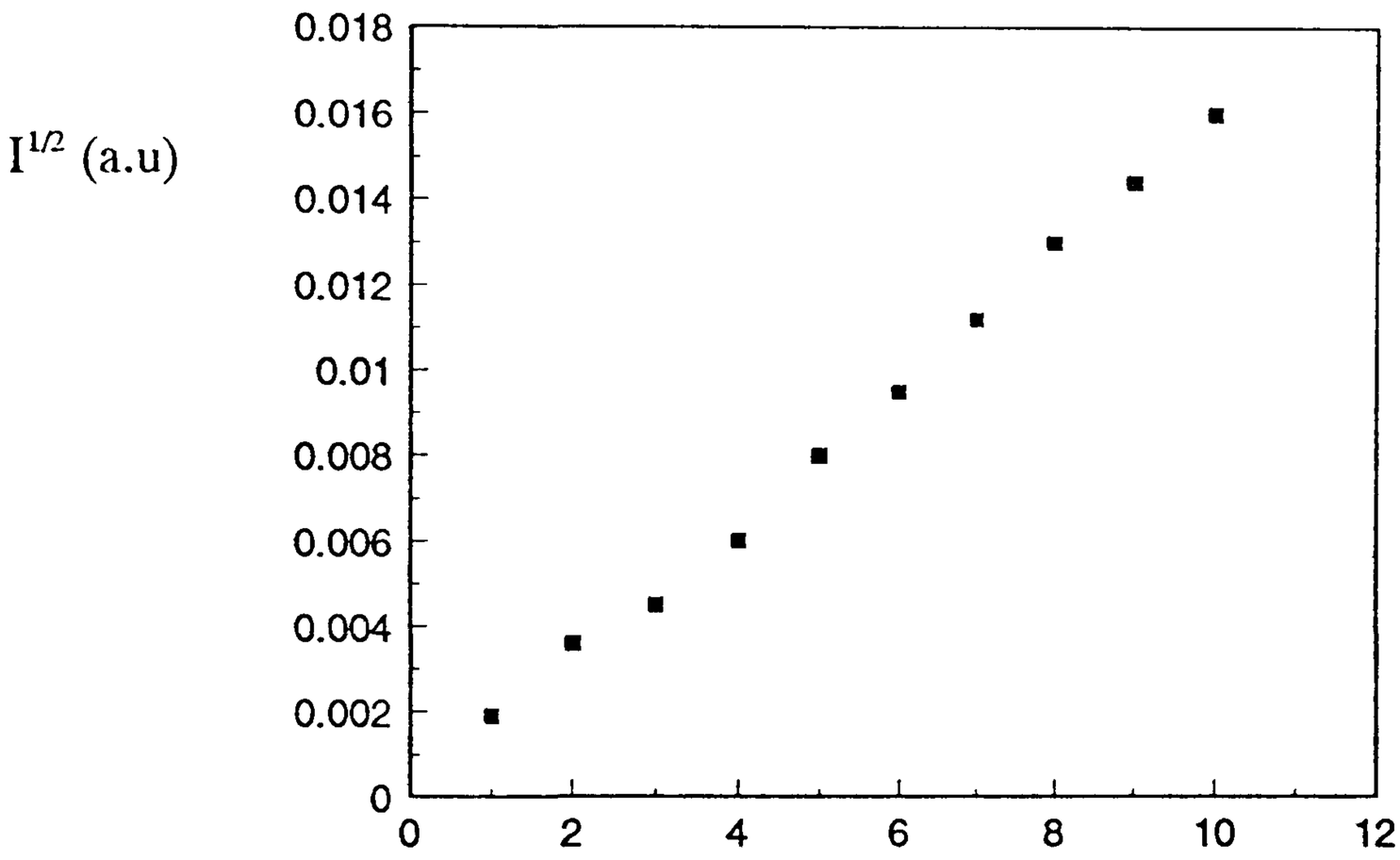

Figure 88. SH response versus number of bilayers for a multilayer film of $C_{22}H_{45}PBHBr/C_{22}H_{45}PT$.

$C_{22}H_{45}PBHBr$ has therefore been shown to produce multilayers with a quadratic dependence of SHG to the number of layers. The SHG signal is not as large as a similar film of $C_{22}H_{45}QNBr$, however extrapolation of the data indicates that if a much thicker film were fabricated, a very large signal could be achieved.

3.3 Transparent Materials for Nonlinear Optics.

The common criteria for organic molecules exhibiting second harmonic generation is a donor and acceptor part linked by a conjugated chain, through which charge transfer occurs. Characteristically these materials have relatively low transition energies and maximum absorptions in the visible region. This limits the useful operating range for the material, as well as allowing resonant enhancement if the absorption occurs at the fundamental or second harmonic frequency. This has been called the "transparency-efficiency" trade off[26], and most reported LB films that give large SHG signals absorb at one of these frequencies.

The hemicyanine materials reported in sections 3.1 and 3.2 have intense absorptions in the visible region. A number of these materials show excellent film forming properties and very high SH responses. Therefore a material with a similar molecular configuration that does not absorb in the visible region is desirable. Two materials, E-1-octadecyl-4-{2-(4-methyloxyphenyl)ethenyl}pyridinium iodide (A) and E-1-methyl-4-{2-(4-octadecyloxyphenyl)ethenyl}pyridinium iodide (B), have been identified, synthesised, and studied in detail, they are shown in figure 89.

3.3.1 Absorbance Spectra of Solutions

The part of the molecule giving rise to charge transfer in both molecules is the same. Therefore the λ_{max} due to charge transfer occurs at identical wavelengths and the two materials have indistinguishable absorbance spectra. The absorbance spectrum of material (A) is shown in figure 90. Note that the tail of the charge transfer peak does not infringe on the second harmonic wavelength (532 nm) from the Nd:YAG source (1064 nm).

(A)

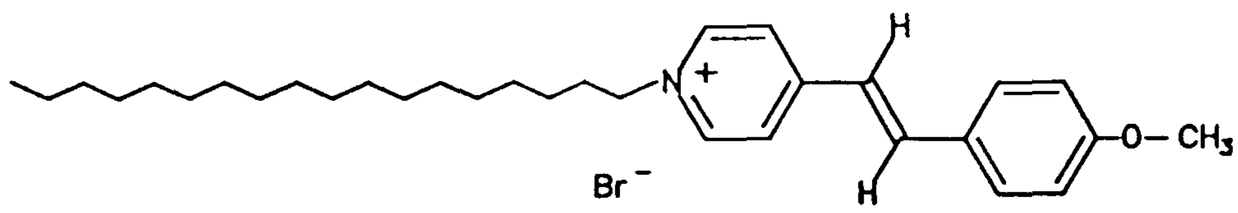

(B)

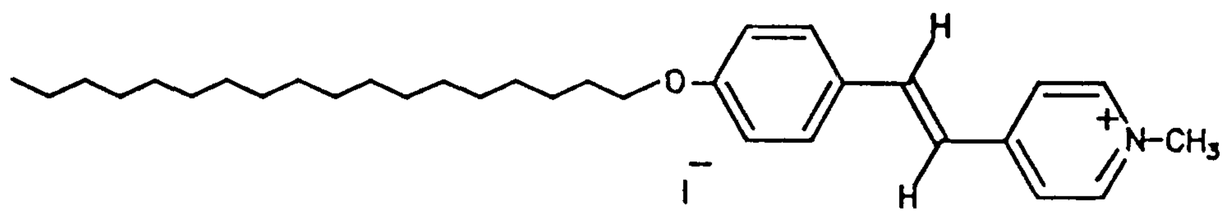

Figure 89. (A) E-1-octadecyl-4-{2-(4-methyloxyphenyl)ethenyl}pyridinium iodide and (B) E-1-methyl-4-{2-(4-octadecyloxyphenyl)ethenyl}pyridinium iodide.

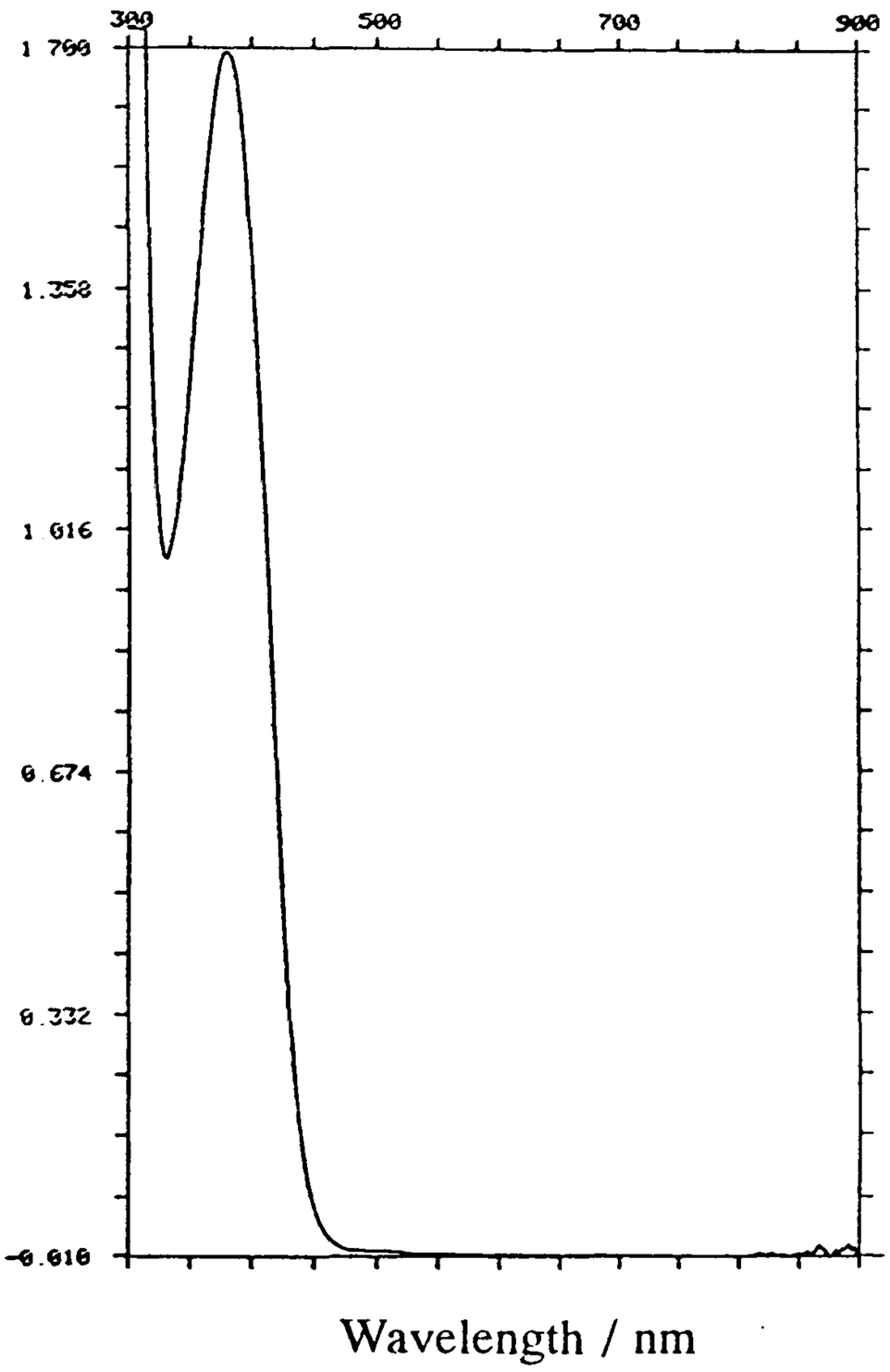

Figure 90. Absorbance spectrum of (A) in ethanol.

3.3.2 Isotherms

The shape of the π - a isotherm of (A) indicates that the molecules are lying flat on the air/water interface before compression. The gradient of the isotherm increases gradually upon compression up to about 15 mN m^{-1} as the molecules align more closely, however the gradient then decreases slightly, which may be caused by dissolution of some molecules into the subphase.

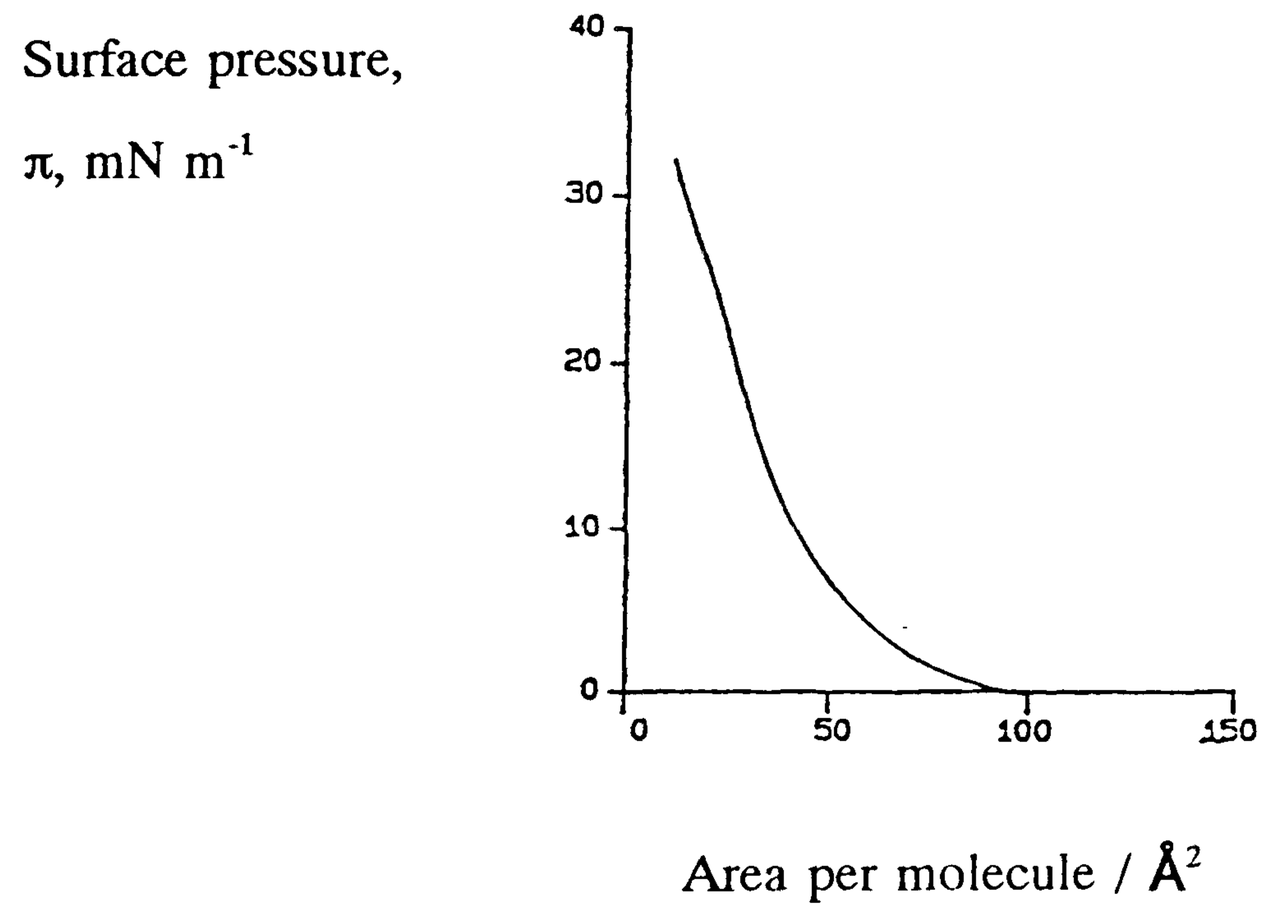

Figure 91. Π - a isotherm of (A)

The shape of the isotherm of (B) is more reminiscent of a classic Langmuir film, eg stearic acid. It has a steep pressure gradient and increases to pressures in the region of 45 mN m^{-1}. There is little evidence of a kink. An understanding of the reason for the differences between (A) and (B) may be gained by visualising the molecules at the air/water interface (figure 93).

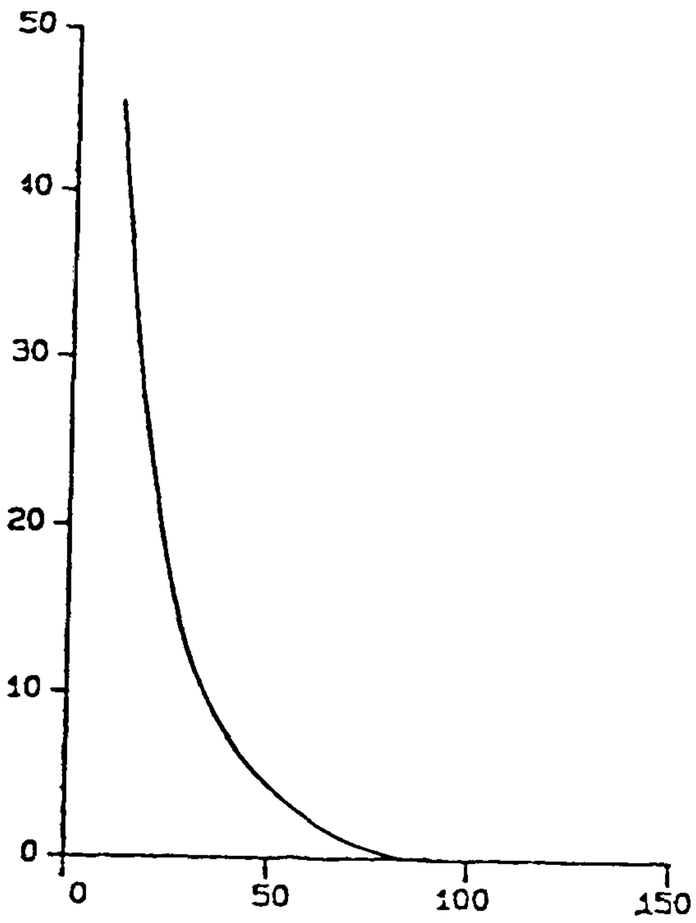

Figure 92. Π - a isotherm of (B)

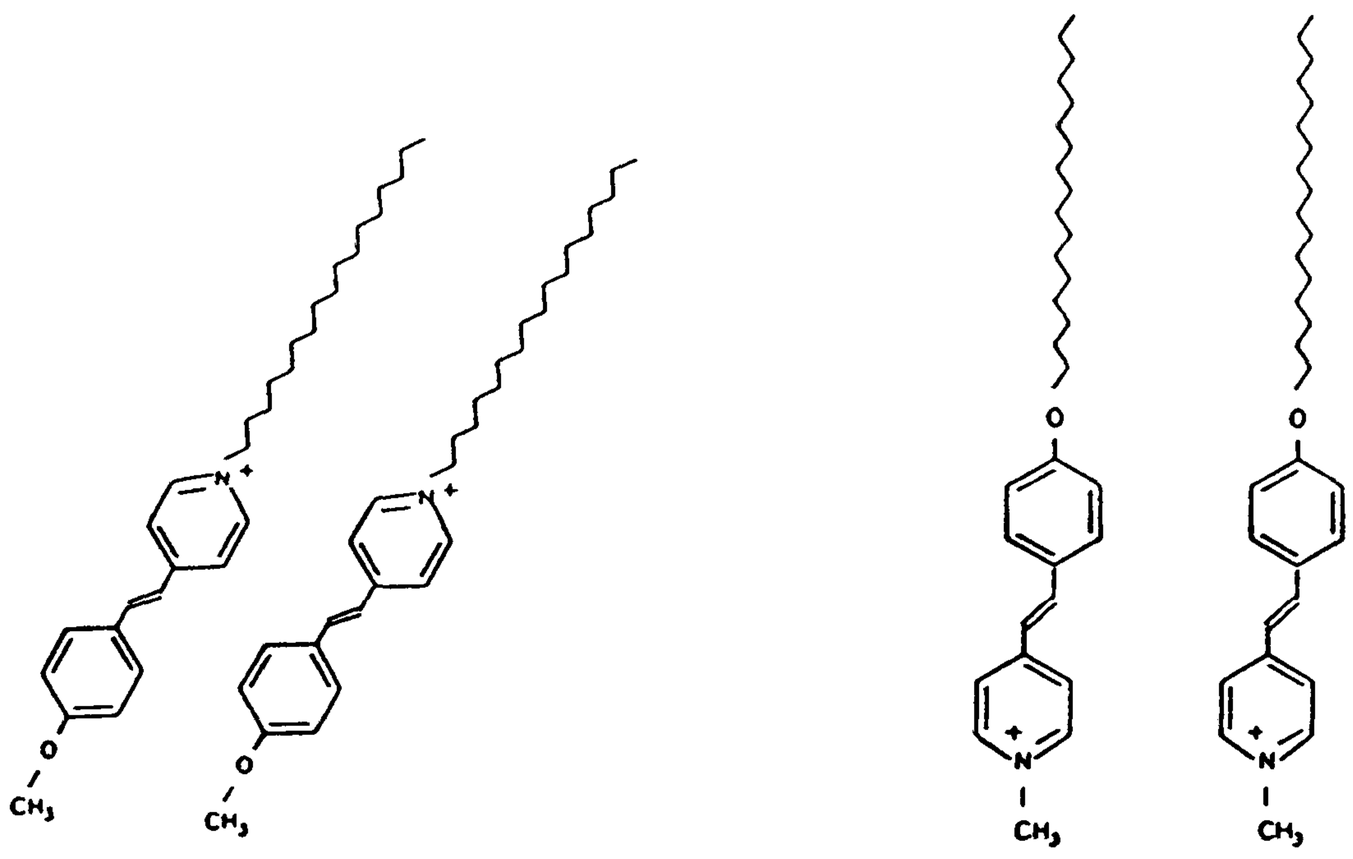

(A) (B)

Figure 93. Illustration of the molecular arrangement of (A) and (B) at the air/water interface.

In both molecules the pyridinium nitrogen will be attracted towards the water subphase. In (A) this movement is restricted by the adjacent proximity of the hydrophobic chain which is repelled from the water. In (B) the chain is separated from the pyridinium nitrogen by the chromophore part of the molecule, therefore the molecule will tend more towards the vertical. This allows more efficient packing. Thus, the shallower curve in the π - a isotherm of (A) corresponds to the molecules realigning to a more vertical position. In (B) the molecules start compression in this position therefore a steeper gradient is observed. A $C_{22}H_{45}$ analogue of (A) was prepared and its π - a isotherm was steeper than (A), this was probably due to its greater hydrophobicity.

3.3.3 Stability of Langmuir Films.

Solutions of (A) and (B) in Aristar grade chloroform were spread on the pure water subphase and compressed to 30 mN m^{-1}. Some dissolution of (A) was noted when the surface area was studied at constant pressure. In contrast, (B) was stable at this surface pressure. The $C_{22}H_{45}$ analogue of (A) was, as expected, stable at 30mN m^{-1}.

3.3.4 Monolayer Deposition.

Both materials were deposited at 30 mN m^{-1} from chloroform solutions (1 x 10^{-3} mol dm^{-1}) and studied. The resulting monolayer films of (A) were not consistent in transfer ratio or absorbance. This is most likely due to its slight solubility in the subphase. Monolayer films of (B) were much more consistent. In fact (B) was also deposited at a surface pressure of 35mN m^{-1} since the Langmuir film was perfectly stable at this pressure.

Monolayers of the $C_{22}H_{45}$ analogue of (A) were also deposited. The resulting LB films were more reproducible than similar films of (A) and had a larger absorbance. It was noted that good deposition of all these materials only occurred when the solution was freshly prepared.

3.3.5 Absorbance Spectra of LB films

The absorbance spectra of monolayers of (A) and (B) and the $C_{22}H_{45}$ analogue of (A) were identical in shape. They are characterised by a charge transfer peak at 380 nm, with no absorbance above 450 nm. This is because the chromophore responsible for the charge transfer is identical in each material.

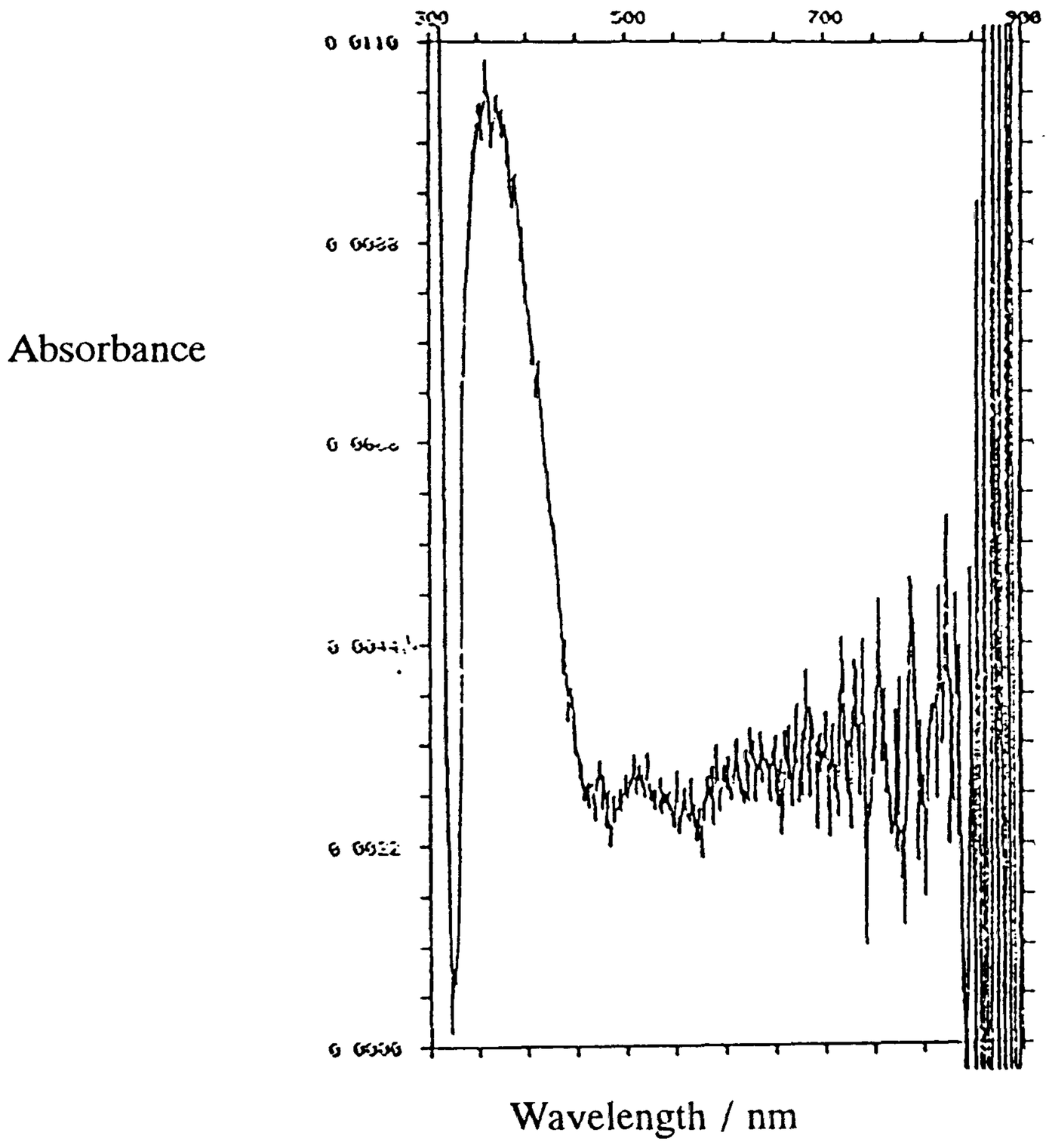

Figure 94. Absorbance spectrum of a monolayer of E-1-methyl-4-{2-(4-octadecyloxyphenyl)ethenyl}pyridinium iodide (B).

3.3.6 Second Harmonic Generation from Monolayers

Several monolayers of (A) were deposited in order to produce some films of equal absorbance. The reproducible monolayers of (B) gave consistent SH responses.

Monolayer	Absorbance	SHG (x quartz) / 10^{-6}
(A)	0.007 ± 0.0005	1.50 ± 0.02
(B)	0.010 ± 0.0005	4.00 ± 0.01

Table 26. LB Film Properties of Monolayers of (A) and (B).

The higher signal of (B) compared to (A) is most probably due to its better deposition properties.

3.3.7 Multilayer LB Films.

It is possible that (A) and (B) will form centrosymmetric multilayers when deposited Y-type. The charge transfer in a monolayer of (A) is aligned in the opposite direction to that in a monolayer of (B). If the two materials were to be deposited as an alternate Y-type multilayer then each layer would have its charge transfer aligned in the same direction. Thus a centrosymmetric multilayer would be formed with additive SH responses.

Initially, bilayers were studied. Therefore (A) was transferred on the upstroke followed by (B) on the downstroke. The transfer ratio of (B) was less than its transfer on the upstroke as a monolayer, but still sufficient to indicate that adequate deposition had occurred, (this slight difference may be evidence of the "1st layer anomaly"). The absorbance of the bilayer was slightly larger than that of the monolayer but the SH response was less. Conversely, a bilayer was studied with (B) as the first layer (upstroke) and (A) as the second layer (downstroke) and similar results were obtained. There are three possible explanations for these observations:

1. the molecules have formed a Z-type bilayer film;
2. a "herringbone" structure has been formed where the angle of the two layers are such that their vertical components are oppositely aligned;

3. the second layer molecules penetrate the first layer to form an interdigitated monolayer;

The first theory is unlikely because Y-type layers are usually more energetically favourable than Z-type. The second system has only been observed for molecules with small hydrophilic heads compared to the hydrophobic tail. The third theory is most likely because of the following observations:

1. there was only a small increase in absorbance for the bilayer despite deposition being indicated by the transfer ratio;

2. since the transfer ratio indicates transfer of a similar amount of material to form the second layer as there was to form the first layer and the absorbance has only increased slightly, ordered Y or Z-type film formation is unlikely;

3. the SH signal dropped, if the second layer does penetrate the first layer the molecules will almost certainly flip so that the hydrophobic tails are adjacent. This results in the direction of the charge transfer in the respective molecules being aligned oppositely, thus cancelling each other. The fact that complete cancellation does not occur may be because a comparatively small number of molecules DO form a second layer. This is supported by the slight increase in absorbance. In addition the respective materials have different SH responses, plus unequal amounts of each material were deposited.

$C_{22}H_{45}PNBr$ was deposited as a bilayer with (B) because it also exhibits charge transfer in the opposite direction to (B) whilst exhibiting a similar SH response from the monolayer. The same results were observed as for bilayers of (A) and (B).

The configuration of the molecules in theory (3) above, is the same as that predicted from the deposition of a mixed solution of (A) and (B). Therefore an equimolar solution of (A) and (B) was prepared and deposited as a Langmuir-Blodgett film. Deposition at 35 mN m^{-1} produced a LB film with the same shaped absorbance spectrum as that of (A) and (B), with a λ_{max} of 0.007 (similar to that of a monolayer of

(A)). This suggests that the molecules have formed a monolayer. The SH response was markedly less than that of (A) which suggests that both sets of molecules have aligned symmetrically in the monolayer. This will have caused substantial cancellation of the individual responses.

Equimolar mixtures of $C_{18}H_{37}PHI$ and (B) also supported this theory. In this case the SH response for the mixture was substantially down on that for pure $C_{18}H_{37}PHI$ but the absorbance indicated that the same amount of $C_{18}H_{37}PHI$ was present. Mixtures of varying molar ratios indicated that there was a linear relationship between the relative amount of (B) with the drop in SH response.

3.3.8 LB Monolayers of Mixtures.

In response to the problems of interdigitation of the monolayer a new strategy was attempted. If the nonlinear material can be mixed with a compatible material and deposited, so that better monolayer films result, then the opportunity for penetration of that layer should be reduced. The material, *sodium octadecylsulphate* ($C_{18}H_{37}OSO_3^-Na^+$), was chosen for three reasons:

1. the hydrophobic tail matches that of (A) and will want to align itself adjacent to the tail of the nonlinear material;
2. as a Langmuir film the Na^+ and I^- should dissolve into the subphase and with the hydrophobic tails adjacent the SO_3^- will be adjacent to the N^+ of the pyridinium ring consequently forming a stable molecule pair;
3. it does not absorb in the visible region.

Therefore an equimolar solution (1×10^{-3} mol dm^{-3}) of (A) and $C_{18}H_{37}OSO_3^-Na^+$ was prepared. Note that (A) was dissolved in chloroform and $C_{18}H_{37}OSO_3^-Na^+$ in distilled methanol. The mixture was transferred to the aqueous subphase and formed a Langmuir film, this film was more stable than films of (A) in similar conditions. The film was compressed and the π - a isotherm compared to that of (A) is shown in figure 95.

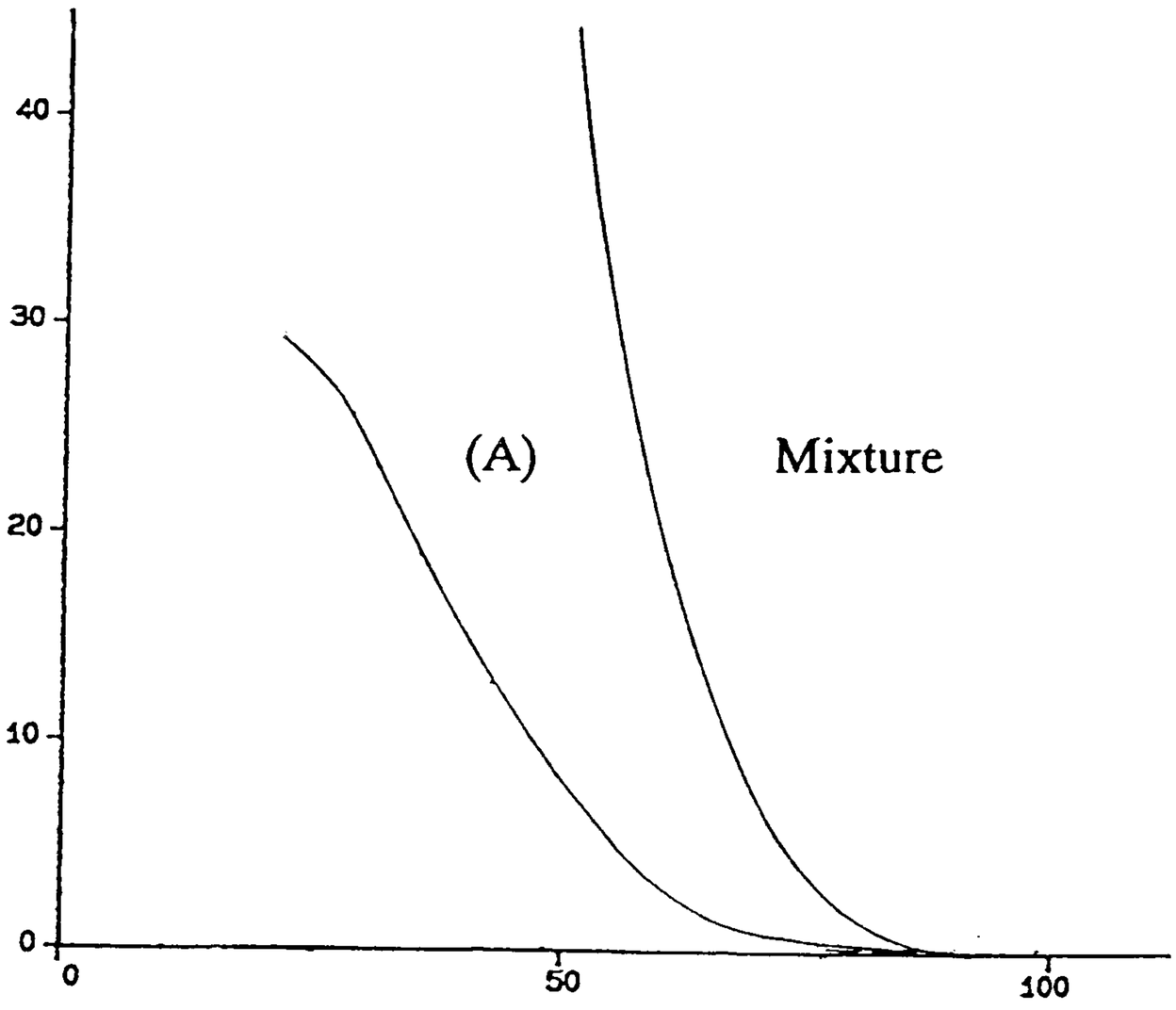

Figure 95. Π - a isotherm of (A):$C_{18}H_{37}OSO_3^-Na^+$ (1:1) compared to pure (A).

It is clear that the slight solubility observed for films of (A) disappears when $C_{18}H_{37}OSO_3^-Na^+$ is added. This is due to the greater hydrophobicity of the complex. The area per molecule at 35 mN m^{-1} is similar to the proposed Van der Waals cross-section of the upright, closely packed complex shown in figure 96. In theory this structure should prevent penetration from molecules transferred onto the monolayer.

A similar mixture of (B) and $C_{18}H_{37}OSO_3^-Na^+$ was prepared but its compression characteristics were very poor. This can be explained if one considers the two molecules. One would expect the SO_3^- group to attach itself to the N^+ part of the pyridinium ring as it does with (A). Therefore the hydrophobic tails of the two molecules are unable to align side by side. A stable Langmuir film is therefore not formed. To overcome this problem, equimolar mixtures of (B) and tetracosanoic acid, sodium salt ($C_{23}H_{47}CO_2Na^+$) were deposited. This was chosen because, in theory, the extra chain length would enable

the hydrophobic and hydrophilic parts to align adjacent to $C_{18}H_{37}$ and N^+ respectively. The compression characteristics were very similar to that of pure (B), and absorbance was also poor.

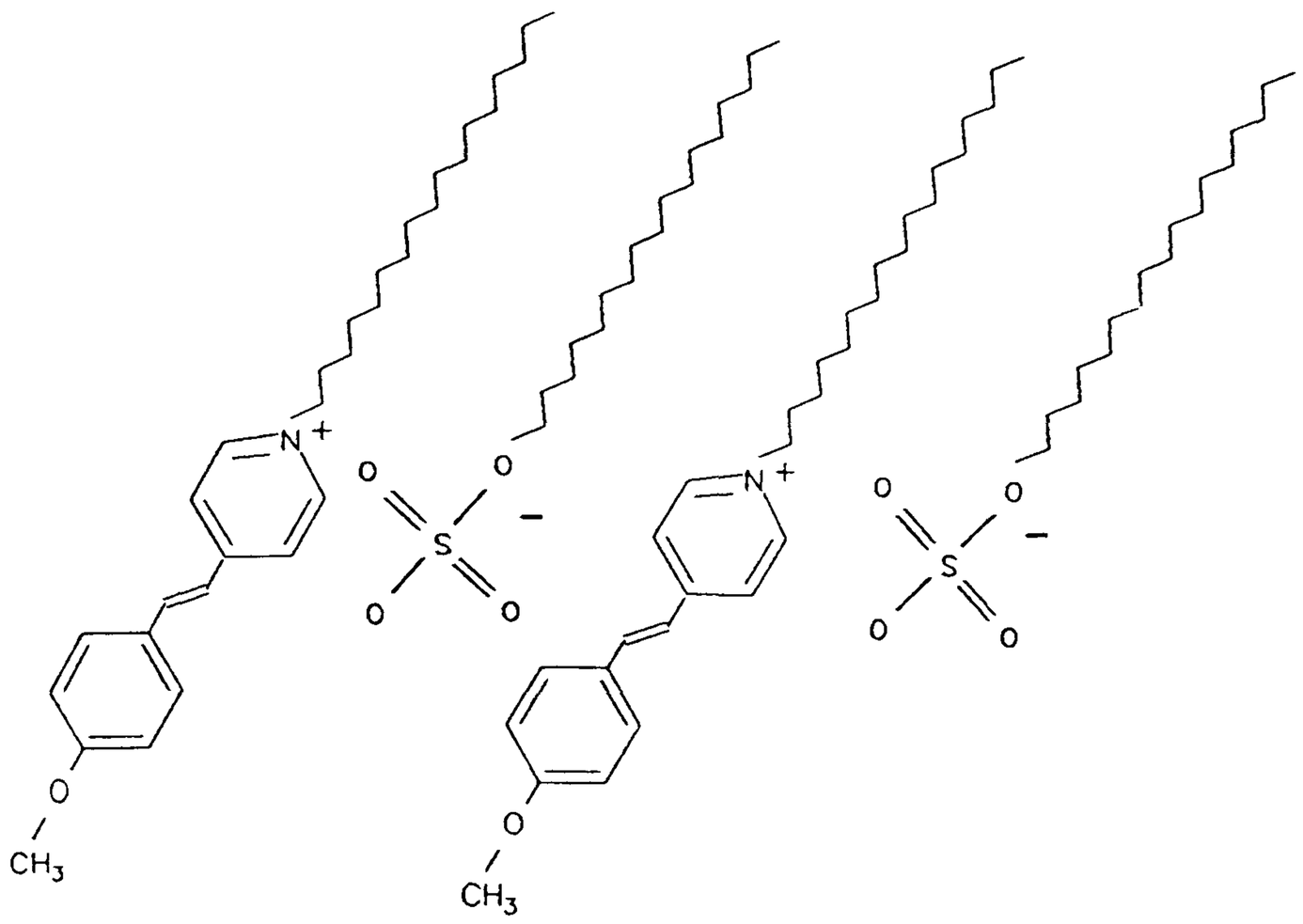

Figure 96. Proposed configuration of (A) and $C_{18}H_{37}OSO_3^-Na^+$ at 35mN m^{-1}.

A monolayer of the (A):$C_{18}H_{37}OSO_3^-Na^+$ mixture, transferred at 35mN m^{-1}, had an absorbance similar in shape to that of pure (A), this is as expected since only (A) absorbs in the visible region. The intensity of absorbance was consistent for a number of monolayers deposited separately in the same conditions. It can be seen that this material does not absorb at the second harmonic wavelength (532 nm).

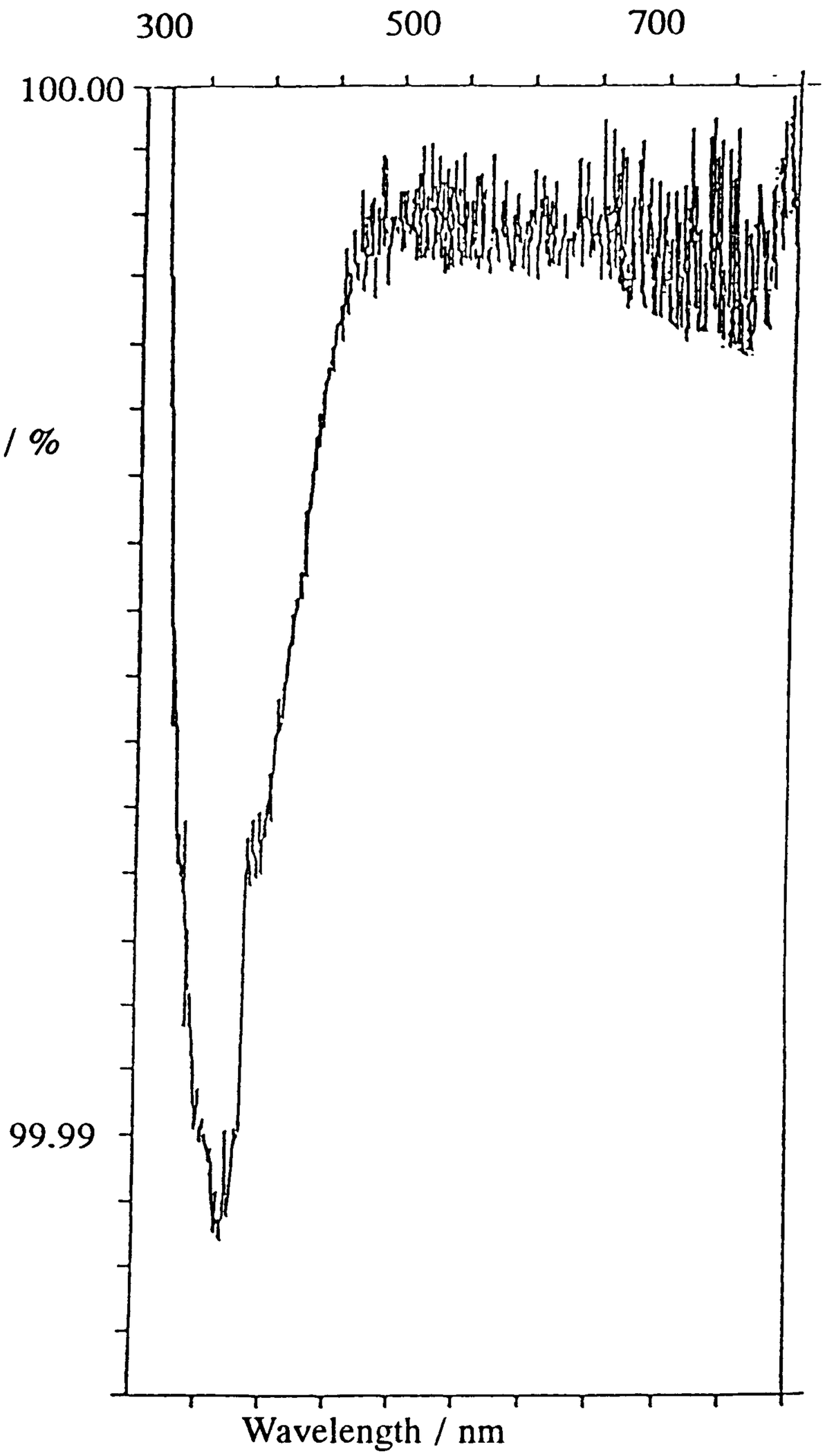

Figure 97. Transmission spectra for a monolayer of (A):$C_{18}H_{37}OSO_3^-Na^+$ showing its transparency in the 450 - 800 nm region.

The SH response from these monolayers was approximately six times that of a monolayer of (A). This response is due purely to charge interactions within the film since no resonant enhancement is possible at 2ω.

Monolayer	Absorbance	SHG (x quartz) / 10^{-6}
(A):$C_{18}H_{37}SO_3^-Na^+$	0.015 ± 0.0005	9.30 ± 0.01

Table 27. Monolayer properties of (A):$C_{18}H_{37}OSO_3^-Na^+$.

Mixtures of different molar ratios were deposited (figure 98). It is evident that the optimum SHG results from the monolayer where the molecules are able to form a complete set of molecule pairs. These molecule pairs produce higher SH signals than that of an individual molecule of (A). This is because the inclination of the molecule pair is different to that of an individual molecule of (A) and inclined in such a way as to give a higher signal per molecule of (A) than for an independent molecule.

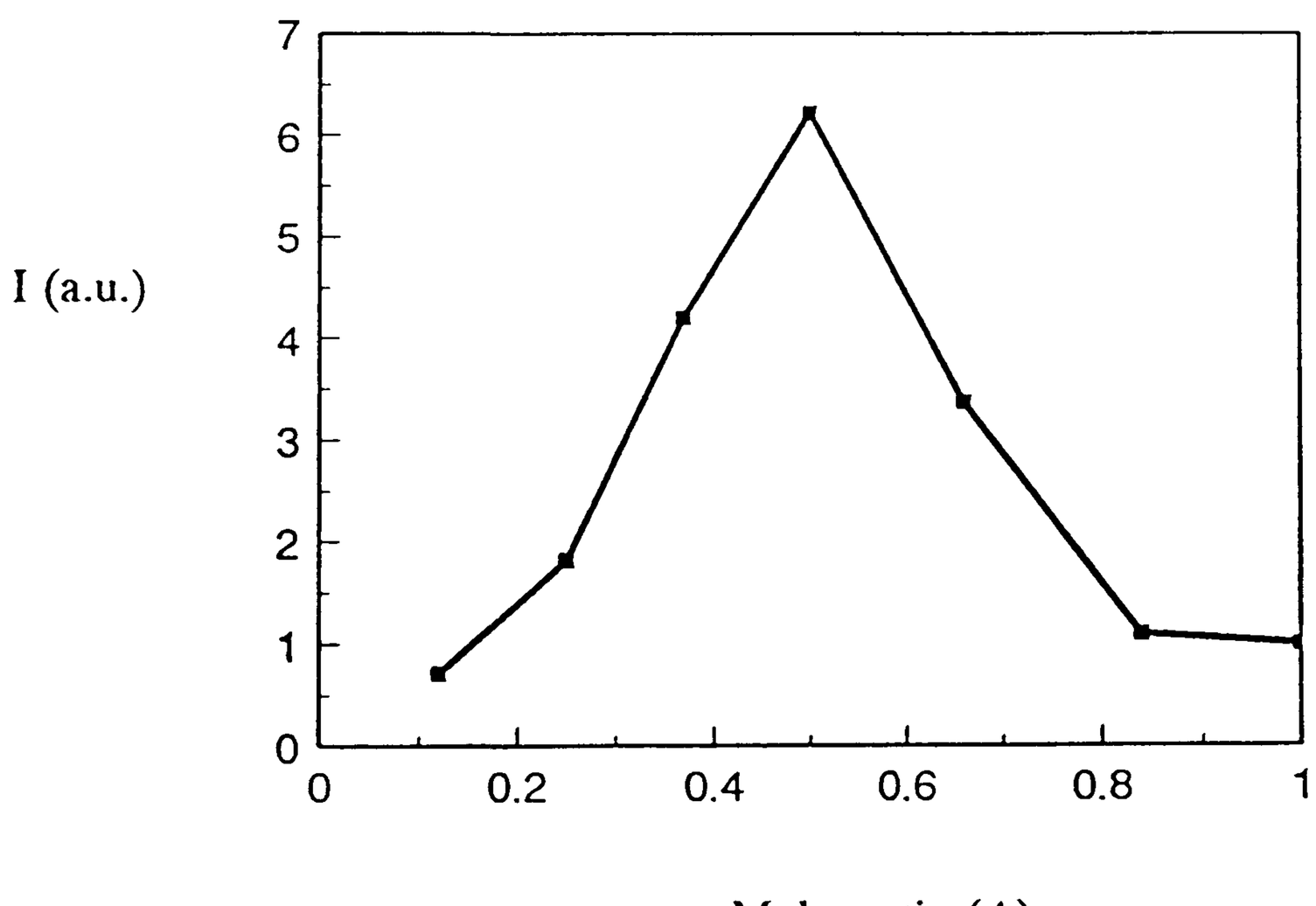

Figure 98. SH response versus molar ratio for monolayers of (A):$C_{18}H_{37}OSO_3^-Na^+$.

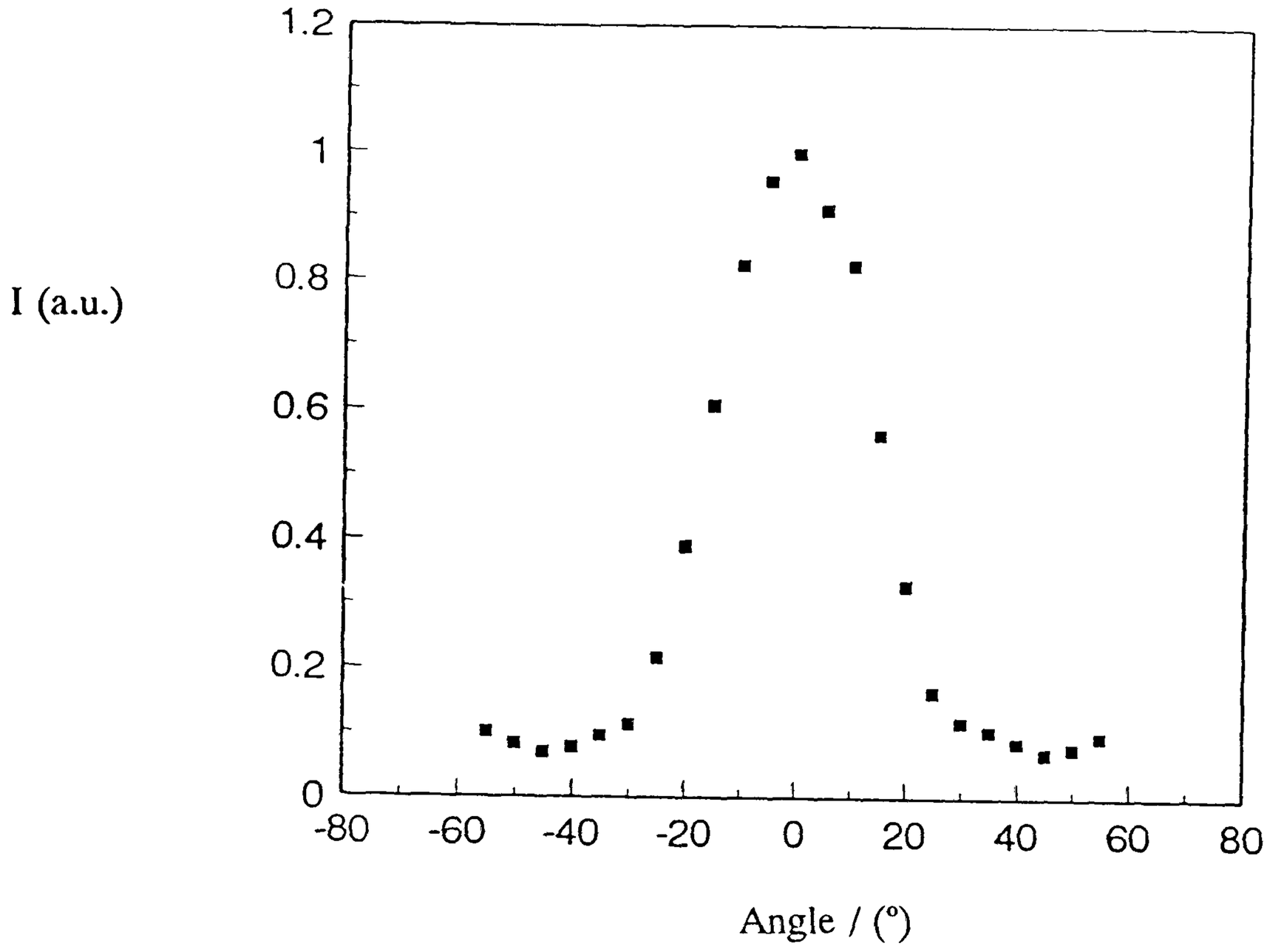

Figure 99. Polarisation dependence of SH response of a monolayer of (A):$C_{18}H_{37}OSO_3^-Na^+$.

The angle of inclination of the molecule pair, calculated from the polarisation dependence of the SH response, is 33.5°. The packing efficiency is at its optimum for the 1:1 mixture where a highly ordered monolayer is produced. At molar ratios greater than 0.5 aggregates of none complexed hemicyanine molecules reduce the SH efficiency. When the molar ratio is less than 0.5 the presence of non-complexed "passive" sulphate molecules reduces the "active" packing ratio.

The effect of spacing in order to enlarge SHG from LB films has been studied previously[134,146,147]. It has been suggested that the increase is due to the prevention of aggregation, but the absorbance spectrum of the pure material (A) shows no indication

of aggregation. The results indicate, however, that $C_{18}H_{37}OSO_3^-Na^+$ prevents phase separation since the spacer is part of the complex.

3.3.9 LB multilayers of mixtures.

A monolayer of the 1:1 mixture, (A):$C_{18}H_{37}OSO_3^-Na^+$ was deposited on the upstroke. The cation $C_{18}H_{37}QBr$ was transferred on the downstroke on to the monolayer and on top of this was deposited another layer of the mixture. A total of five layers of the mixture were deposited. Absorbance spectra indicated that deposition was occurring, however the SH response was not quadratic. This can be explained by incomplete deposition. The results are promising though, since the SH response is increasing, therefore an even better film would be worth studying if a more suitable interleaved layer could be found, for example an analogue of 4,4'-dioctadecyl-3,5,3',5'-tetramethyldipyrrylmethenehydrobromide (DPM).

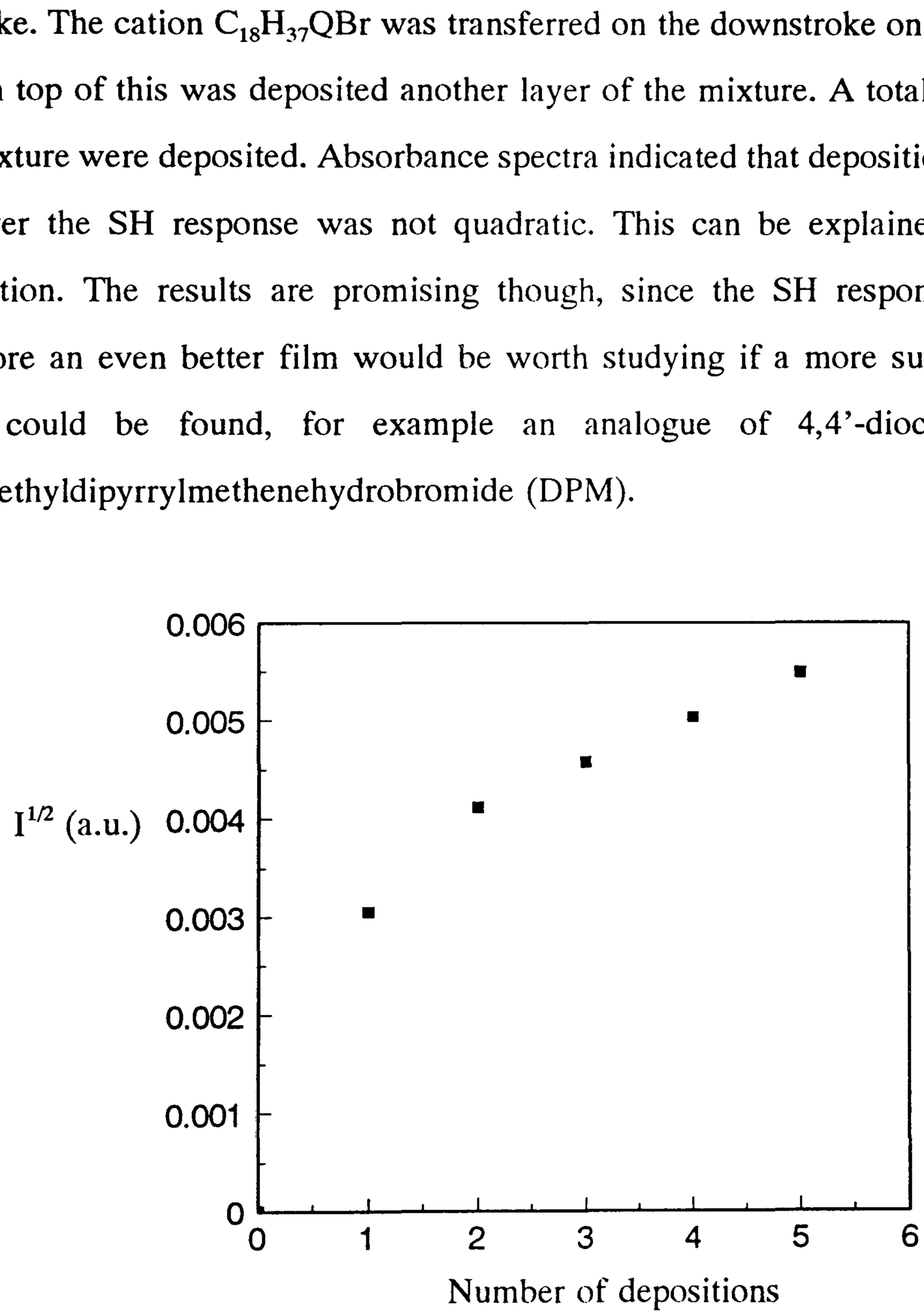

Figure 100. SH response versus number of depositions for an interleaved multilayer of (A):$C_{18}H_{37}SO_3^-Na^+$ / $C_{18}H_{37}QBr$.

Alternating multilayer films of (A):$C_{18}H_{37}OSO_3^-Na^+$, deposited on the upstroke, and (B), deposited on the downstroke, were studied however (B) would not transfer.

3.4 Zwitterionic Adducts

LB films of tetracyanoquinodimethane (TCNQ) based zwitterions have been reported to have a quadratic relationship between SH response and the number of layers in the film[157-159]. The materials shown below offer the prospect of increased SH response because of their conjugation, in addition the C_7H_9 analogues are of interest because they do not contain an aliphatic chain.

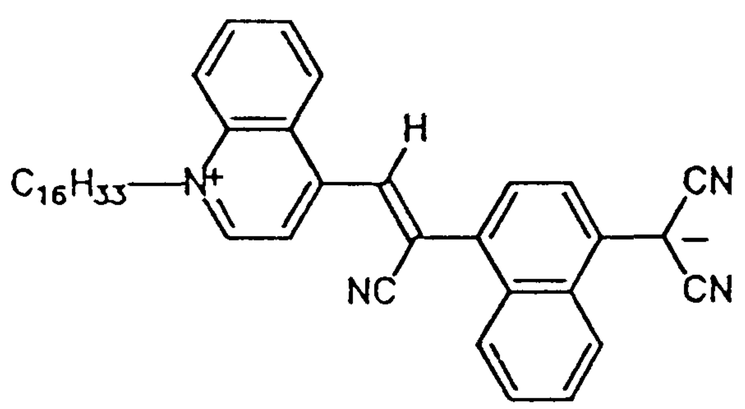

(a)

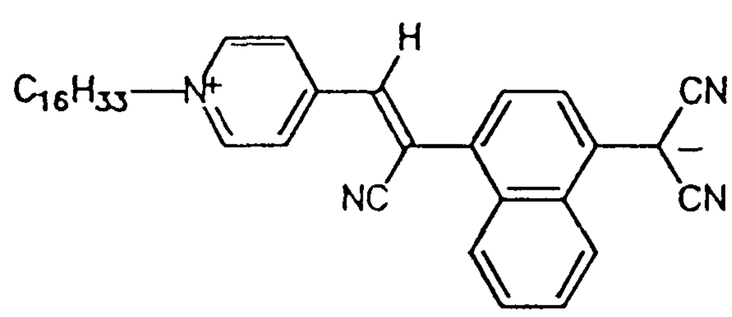

(b)

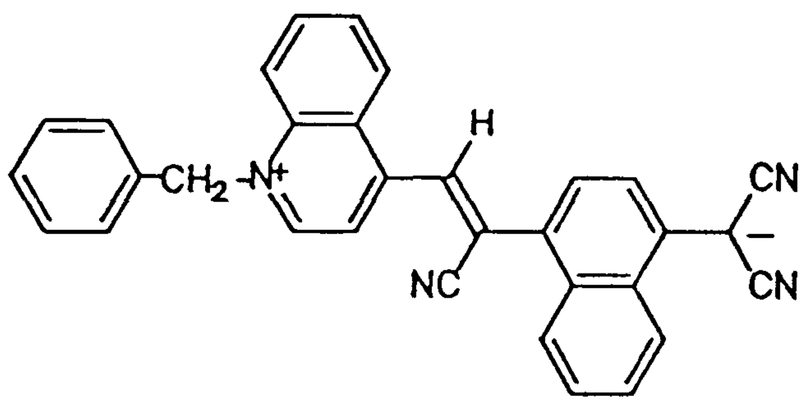

(c)

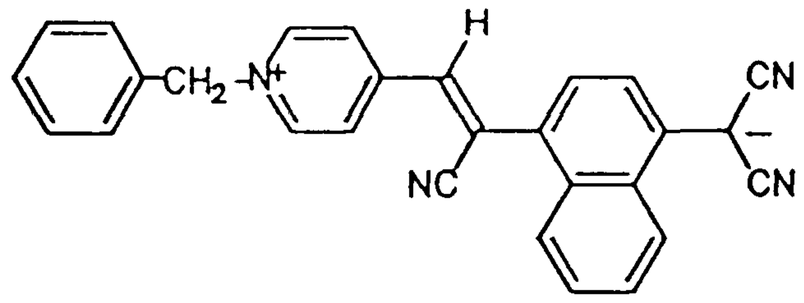

(d)

Figure 101. Zwitterions studied: (a) Z-ß-(N-hexadecyl-4-quinolinium)-α-cyano-4-naphthyldicyanomethanide, $C_{16}H_{33}$QBCNQ; (b) Z-ß-(N-hexadecyl-4-pyridinium)-α-cyano-4-naphthyldicyanomethanide, $C_{16}H_{33}$PBCNQ; (c) Z-ß-(phenylmethyl-4-quinolinium)-α-cyano-4-naphthyldicyanomethanide, C_7H_7QBCNQ; and (d) Z-ß-(phenylmethyl-4-pyridinium)-α-cyano-4-naphthyldicyanomethanide, C_7H_7PBCNQ.

3.4.1 Absorbance spectra of solutions

Spectra from methanol solutions were compared. The quinolinium zwitterions exhibited the same spectrum, as did the pyridinium zwitterions, but the two groups were different due to their different heterocycles. Both groups of solutions produced spectra of high intensity. The absorbance spectra shown in figures 102 and 103 show that the quinolinium analogues have a charge transfer band at a longer wavelength than the pyridinium zwitterions because of the differences in conjugation. The hydrophobic chain had no effect on the absorbance as expected.

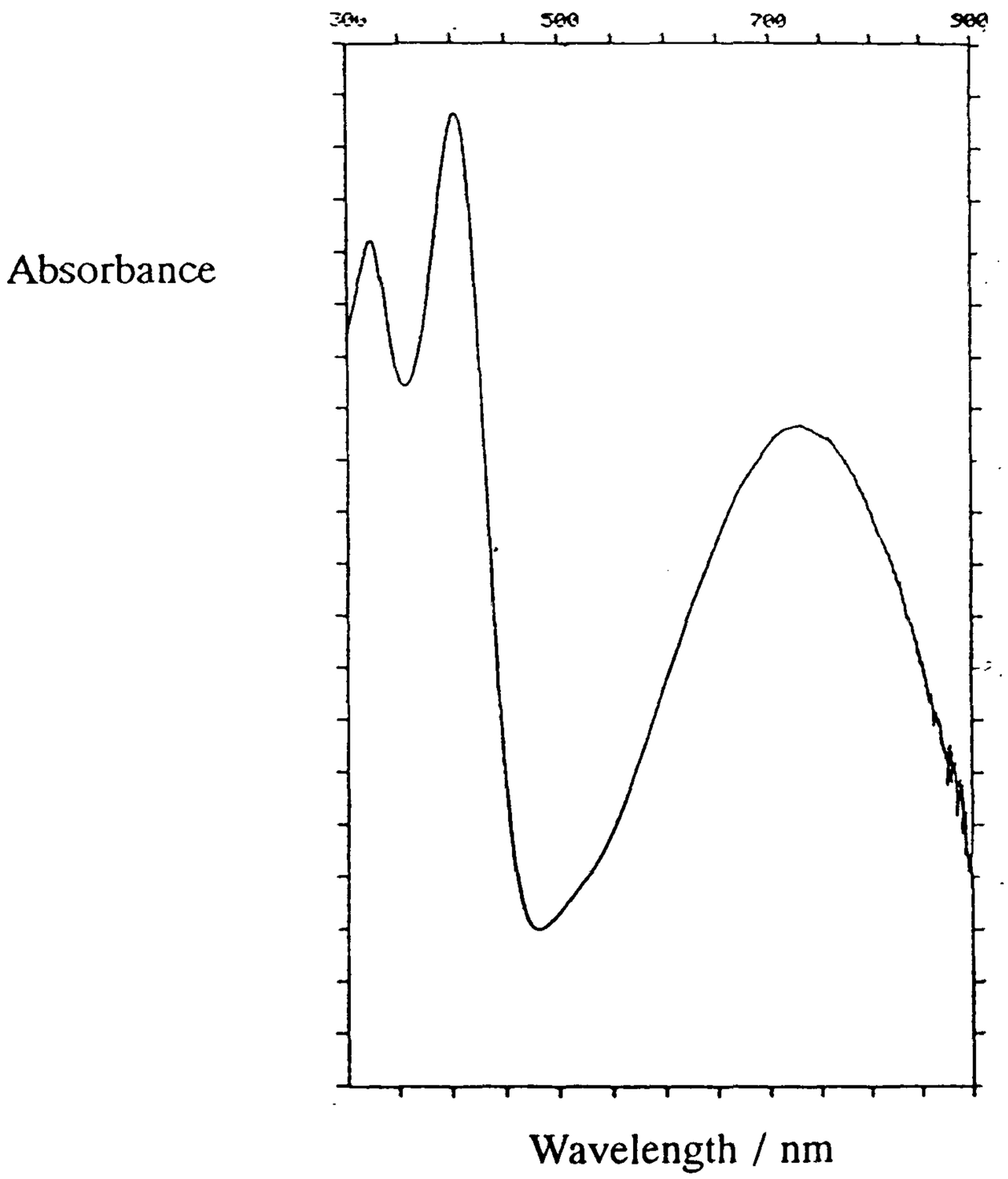

Figure 102. Absorbance spectrum of C_7H_7QBCNQ in methanol.

The effect of solvent on solution spectra illustrates some important points (table 28). One would expect the highly polar nature of the molecules to be effected by the

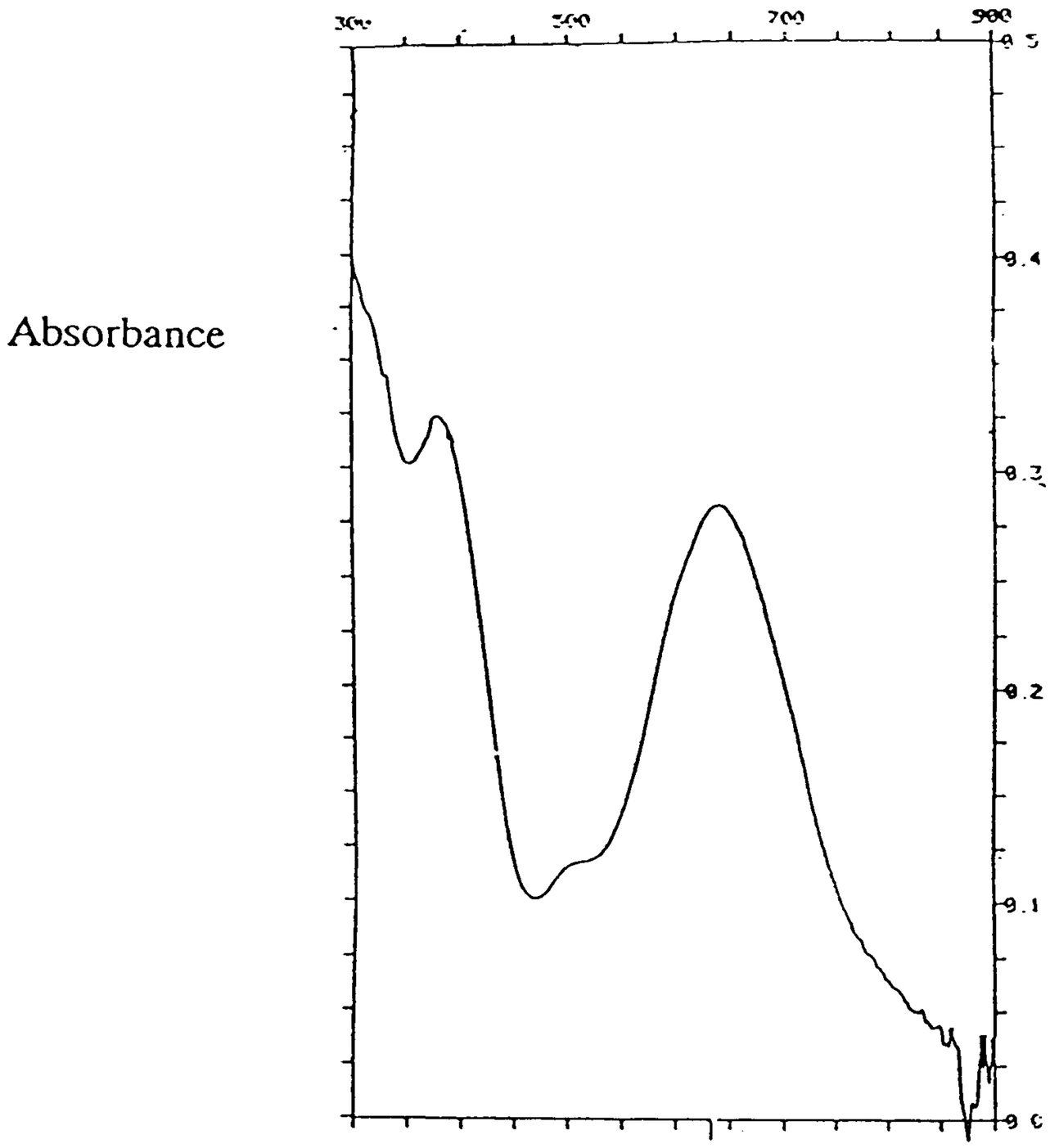

Figure 103. Absorbance spectrum of $C_{16}H_{33}PBCNQ$ in methanol.

Zwitterion	λ_{max}	λ_{max}	λ_{max}	λ_{max}	λ_{max}
	MeOH	C_7H_9	MeCN	$CHCl_3$	CH_2Cl_2
Quinolinium (C_7H_7QBCNQ)	729	765	772	810	827
Pyridinium (C_7H_7PBCNQ)	640	755	657	795	815

Table 28. The effect of solvent on λ_{max} of zwitterions.

polarity of the solvents and this was observed. The aprotic solvents show a hypsochromic shift with increasing polarity. The protic solvent appears to be affected by hydrogen bonding as well as polarity. The absorbance for C_7H_7QBCNQ in acetonitrile (772 nm) is bathochromically shifted compared to an analogous quinolinium zwitterion, Z-ß-(N-hexadecyl-4-quinolinium)-α-cyano-4-styryldicyanomethanide ($C_{16}H_{33}$QBCNQ)[179]. In both materials the intramolecular charge separation and donor ionisation energy are assumed to be constant, therefore the energy of back charge transfer is mainly dependent upon the electron affinities of the anionic end of the molecule. C_7H_7QBCNQ has a charge transfer peak at a longer wavelength than $C_{16}H_{33}$QBCNQ. This is because the former is more conjugated at the acceptor end of the molecule and consequently there is less energy required for the transfer. The charge transfer may be an intermolecular or intramolecular transition. Evidence for the latter comes from concentration studies. C_7H_7QBCNQ has a linear dependence of absorbance on concentration in solution. A nonlinear dependence would indicate intermolecular charge transfer because of the establishment of an equilibrium between the donor and acceptor components.

3.4.2 Molar Absorption Coefficient

In a solution of acetonitrile, $\mathscr{E}(C_7H_7QBCNQ) = 1.14 \times 10^4$ $mol^{-1}m^2$ for λ_{max}. $C_{16}H_{33}$QBCNQ had a similar absorbance for the same concentration and is therefore assumed to have a similar molar absorption coefficient.

3.4.3 Isotherms

The zwitterions were added dropwise to the pure water subphase from dichloromethane solutions. It was found that chloroform solutions were unsuitable for Lanmguir-Blodgett deposition. Π - a isotherms of all four materials are shown in figures 104 and 105.

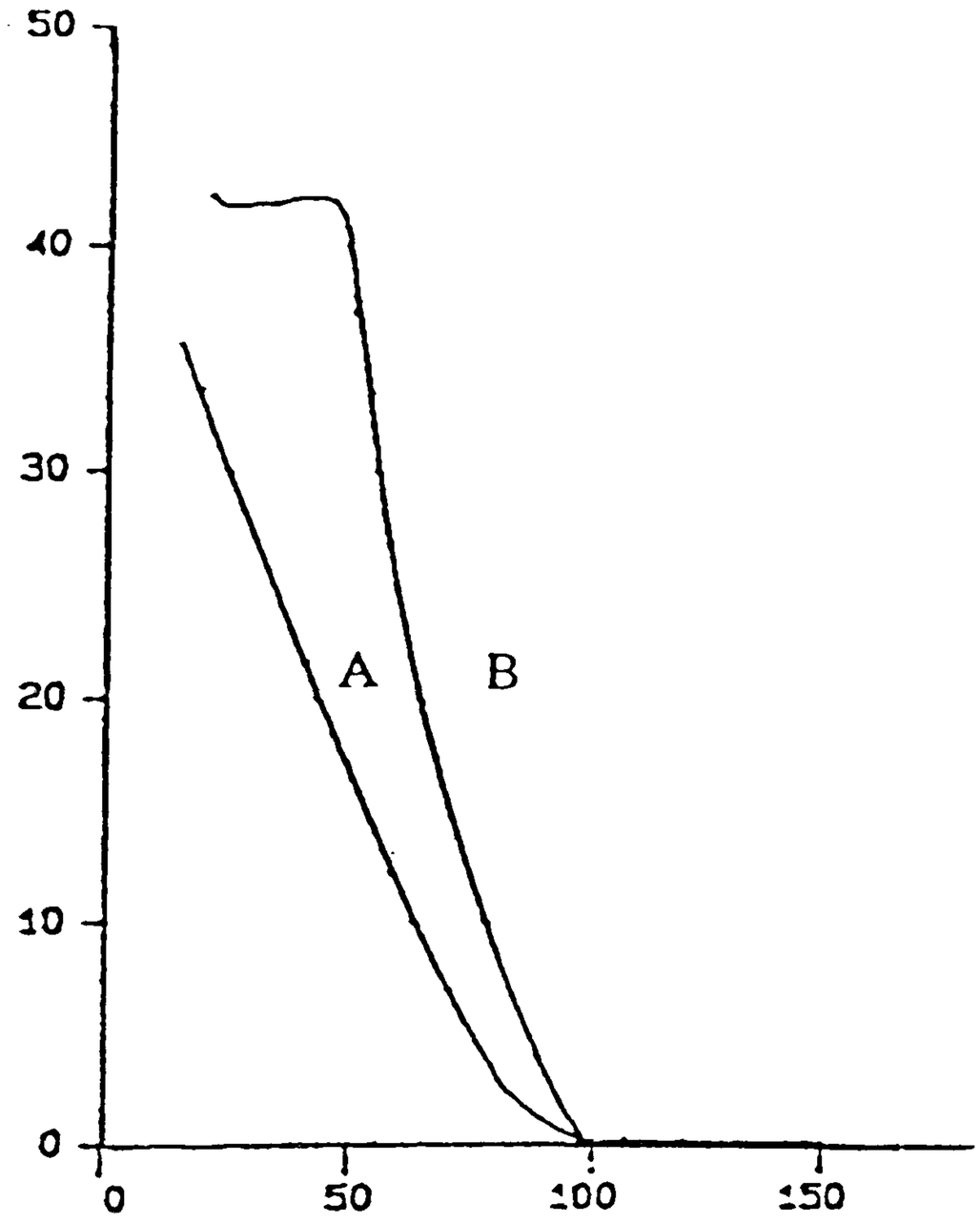

Figure 104. Π - a isotherms of (A), C_7H_7PBCNQ and (B), $C_{16}H_{37}$PBCNQ.

Both pyridinium zwitterions began to increase in pressure at the same area per molecule, ie 100 Å^2, inferring that the hydrophobic chain had no effect on the dispersion of molecules. $C_{16}H_{33}$PBCNQ, however, had a steeper gradient, similar in shape to the π - a isotherm of stearic acid. At a surface pressure of 20 mN m^{-1}, $C_{16}H_{33}$PBCNQ occupied an area of 70 Å^2 per molecule compared to 44Å^2 for C_7H_7PBCNQ. The former also collapsed at a higher pressure than the latter. The lack of a strong hydrophobic chain in C_7H_7PBCNQ may allow slight dissolution as compression occurs and this could be the reason for the differences.

The isotherms of the quinolinium zwitterions show that the difference in heterocycle size affects the close packing, since these materials show similar trends but at higher corresponding areas per molecule.

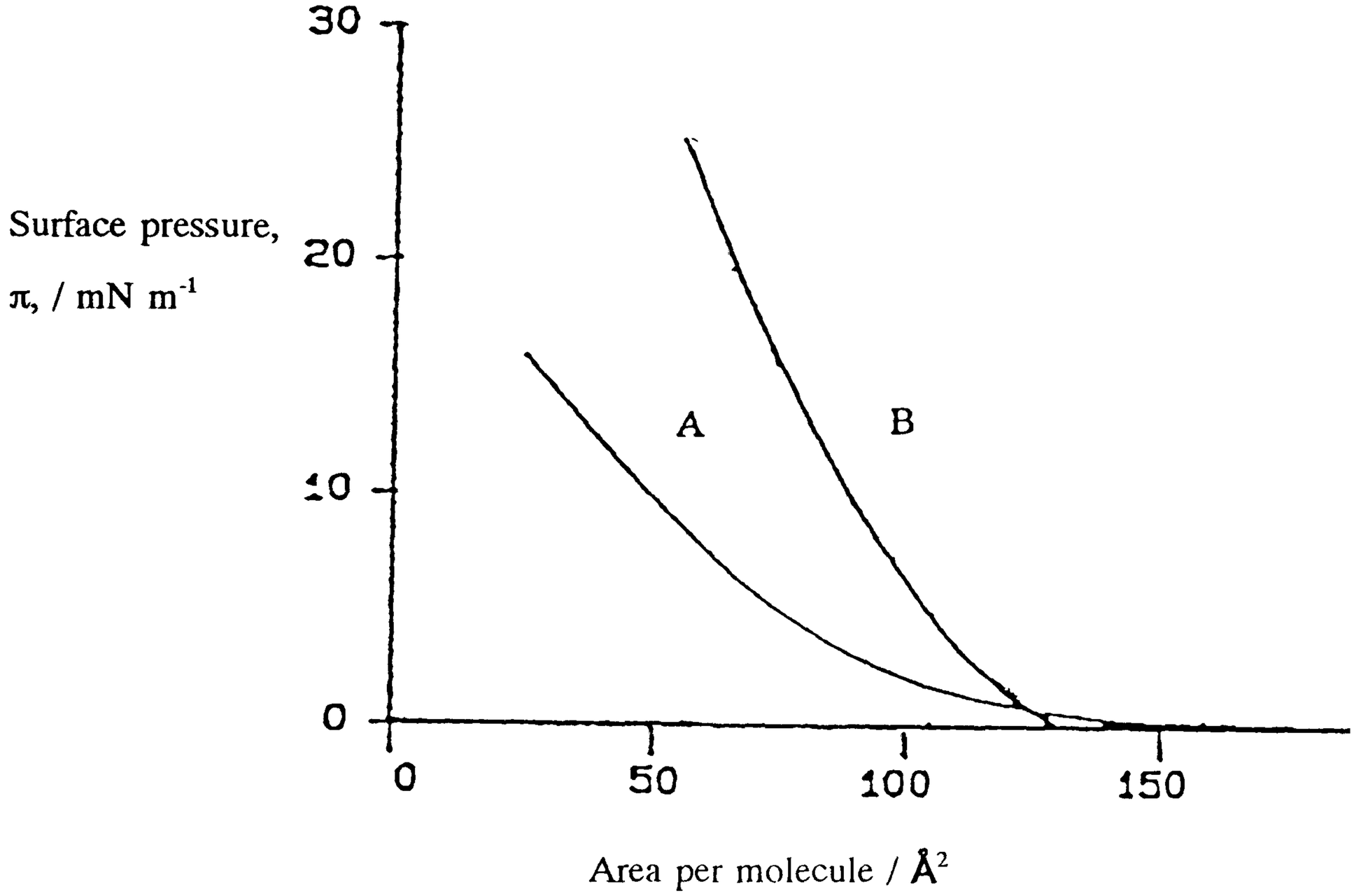

Figure 105. Π - a isotherms of (A) C_7H_7QBCNQ and (B) $C_{16}H_{37}$QBCNQ.

3.4.4 Deposition of Monolayers

The $C_{16}H_{37}$ zwitterions were transferred at a pressure of 35 mN m^{-1}, the benzyl analogues were transferred at their highest stable pressures. No deposition occurred on the downstroke, therefore all monolayers reported are the result of upstroke deposition.

All materials caused the Wilhelmy plate filter paper to drift away from the main area of the trough. This was presumably caused by the columbic effect of the molecules. The benzyl derivatives proved particularly difficult to compress because of their slight solubility. In fact C_7H_7PBCNQ and C_7H_7QBCNQ were deposited by a none standard method. The Langmuir films were compressed slowly until the surface pressure stopped

increasing, the film was then left for a few minutes to stabilise. Further slow compression took the film to a slightly higher pressure whereupon the surface pressure stopped increasing again. This method was repeated until the highest surface pressure possible was attained without collapse occurring. The maximum stable surface pressure achieved was typically 20 mN m^{-1}.

3.4.5 Absorbance Spectra of LB Films.

The absorbance spectrum of a monolayer of C_7H_7PBCNQ clearly indicates a charge transfer peak at 660 nm.

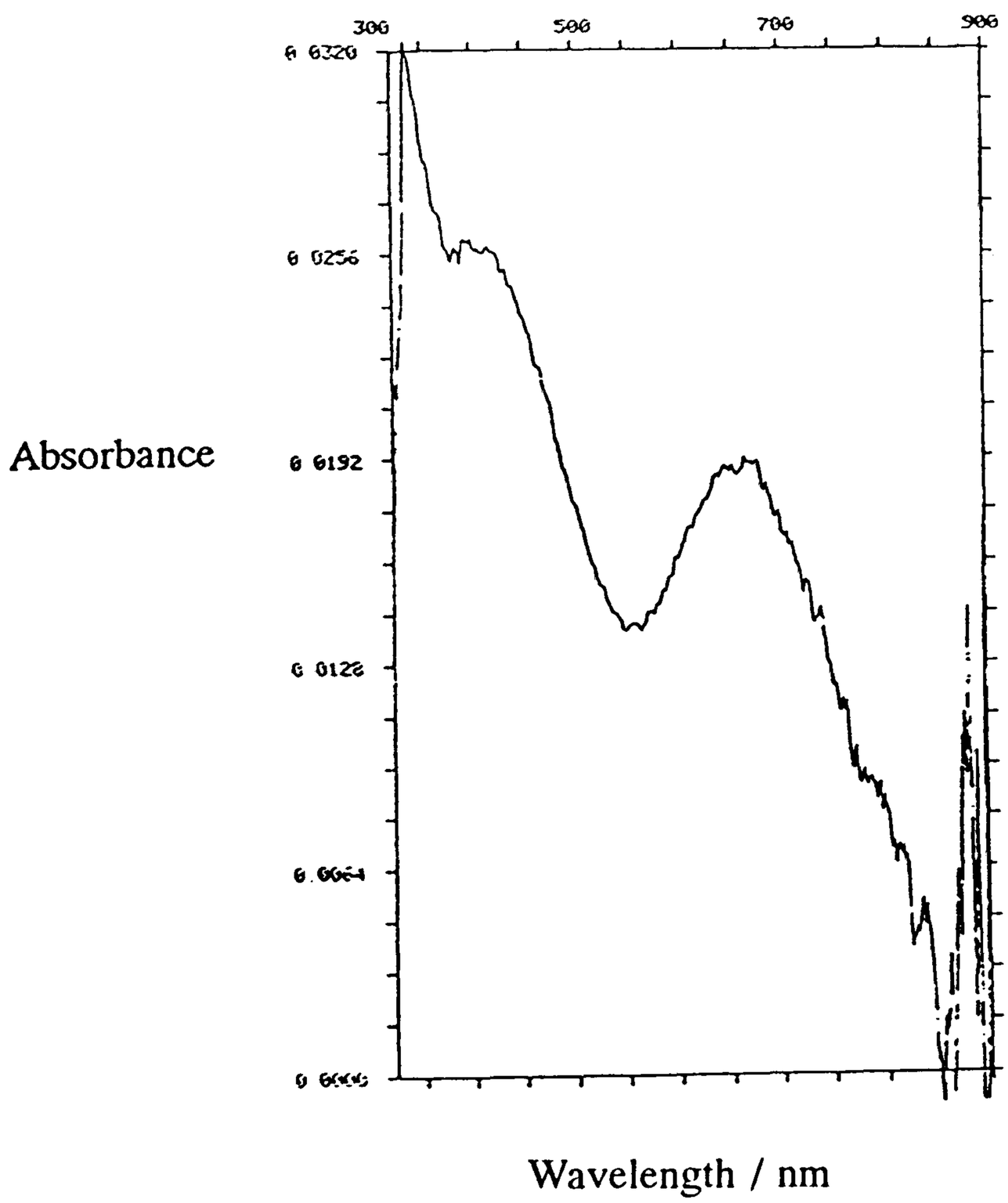

Figure 106. Absorbance spectrum of a monolayer of C_7H_7PBCNQ

Firstly it should be noted that this spectrum is evidence of Langmuir-Blodgett deposition of a material whose molecular structure is not made up of distinct hydrophobic and hydrophilic parts. One would expect the presence of a phenylmethyl group instead of a highly hydrophobic aliphatic chain to inhibit deposition. Whilst the benzyl analogues are not easily transferred to substrates it has been shown that it is possible. If multilayer structures of benzyl and aliphatic analogues could be fabricated, the benzyl films would have a greater layer density in the normal to the substrate because of the smaller size of their hydrophobic part. For optically active materials this is an important factor as this will give the benzyl analogues a greater SHG efficiency.

3.4.6 SHG from Monolayers

The data collected for various films of the benzyl derivatives was inconsistent due to the inconsistent deposition, therefore the signals reported represent the best observed.

Zwitterion	SHG (x quartz) / 10^{-7}
$C_{16}H_{37}$PBCNQ	150.15 ± 0.03
C_7H_7PBCNQ	25.21 ± 0.02
$C_{16}H_{37}$QBCNQ	670.20 ± 0.02
C_7H_7QBCNQ	5.00 ± 0.01

Table 29. SH response from of LB monolayers of zwitterionic materials.

It is evident that the poor monolayer deposition of the benzyl derivatives has resulted in poor films for SHG. Numerous attempts at improving the method of transfer were unsuccessful. The values for the $C_{16}H_{37}$ analogues are very promising. The

absorbance for all four materials was variable but it was noted that a larger SH signal was observed when a relatively larger absorbance was achieved.

3.4.7 Multilayer LB films

Ten layers of $C_{16}H_{37}$PBCNQ were deposited on the upstroke only. Transfer ratios indicated poor deposition, however absorbance data showed an equal increase in absorbance for each layer of approximately 0.02. This shows that deposition occurred on each layer.

A twenty layer film deposited on the downstroke onto a monolayer of $C_{16}H_{37}$PBCNQ had an absorbance spectrum of half the intensity of a corresponding twenty layer film deposited on the upstroke only. Multilayers fabricated on both upstroke and downstroke showed good deposition on the upstroke and poor deposition on the downstroke. This shows that the material prefers Z-type to X-type or Y-type alignment. This method of deposition is possible because of the strong columbic repulsions present in these zwitterions. The anionic ends of the molecules probably repel each other causing one molecule to flip so that its hydrophobic chain is adjacent to the other molecules chromophore.

Multilayer films of varying number of layers were analysed for SHG. All of them were damaged by the intensity of the laser. This was indicated by an initial large signal that quickly reduced to a minimal one. The films may have reorganised after irradiation into a less active form for SHG.

4.0 Conclusion

Tables 30, 31 and 32 (pages 154 - 158) summarise the major achievements of this work. The following conclusions can be made from all of the obtained results.

1. The hemicyanine chromophore gives significant second harmonic generation when incorporated into a Langmuir-Blodgett film.
2. Choice of chain length is important as to the stability of the Langmuir film, transfer properties and subsequent LB film properties. No significant difference in properties is noted between bromide or iodide counterions.
3. In hemicyanine LB monolayers, the SH response is related to the absorbance of the film.
4. In hemicyanine LB multilayers, the SH response increases quadratically in relation to absorbance and in well ordered multilayers, the SH response increases quadratically in relation to the number of nonlinear active layers deposited.
5. Interdigitation has been indicated in a stable Y-type alternating multilayer film.
6. The 1:1 mixing of a spacer material with a nonlinear active material has significantly improved the response of the LB monolayer.
7. Zwitterionic materials containing almost no hydrophobic character have been deposited as LB monolayers and SHG has been detected.

The bulk of this study has been concerned with fundamental research in to fabricating Langmuir-Blodgett films that have a nonlinear response to intense irradiation. These results enable further work in to the development of such systems, and suggestions are listed below.

1. Identify the thermal and mechanical stability of hemicyanine LB films. These results indicate that multilayer films fabricated in an alternate Y-type manner where some interdigitation of the bilayer occurs, offer the best prospects.

2. Improve the multilayer formation of the E-1-octadecyl-4-{2-(4-methyloxyphenyl)ethenyl}pyridinium iodide : sodium octadecylsulphate mixture because this monolayer has a significant SH response from the monolayer, is stable and does not absorb at 532 nm.

3. The spacer material, 4,4'-dioctadecyl-3,5,3',5'-tetramethyldipyrryl-methenehydrobromide (DPM), has a molecular configuration that enables interdigitation of hydrophobic chains from hemicyanine materials in a bilayer. This system should be analysed further.

4. Novel zwitterions containing almost no hydrophobic chain have been deposited, these offer good SH response over a shorter monolayer thickness, if their LB properties can be improved by further study, then stable Z-type multilayers with high SHG efficiency are viable.

Material	Monolayer absorbance	Monolayer SHG / F m^3 V^{-1}	Multilayer film
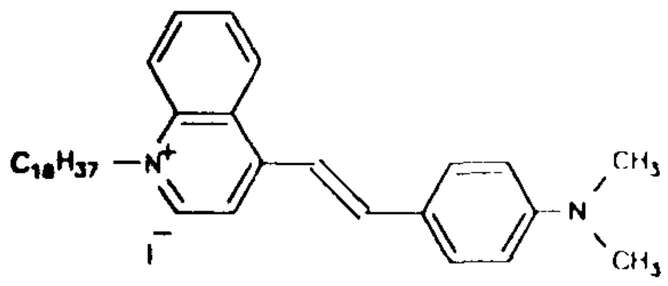 $C_{18}H_{37}QHI$	0.008 (540 nm)	1.22×10^{-47}	Not attempted
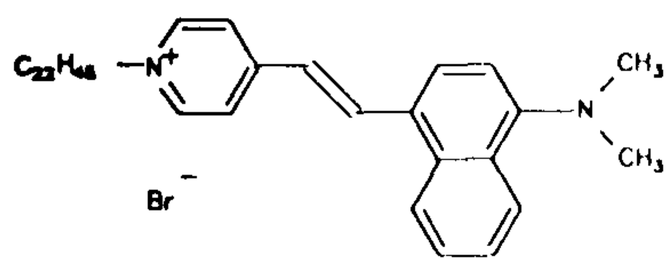 $C_{22}H_{45}QHBr$	0.008 (539 nm)	3.66×10^{-47}	Y-type (alternated) 20 bilayers
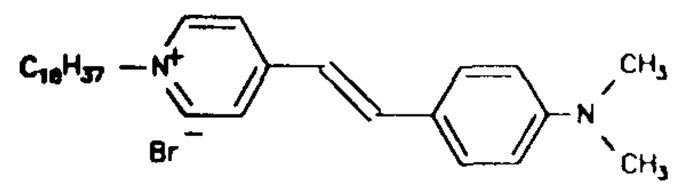 $C_{18}H_{37}PHBr$	0.006 (490 nm)	8.54×10^{-48}	Not attempted
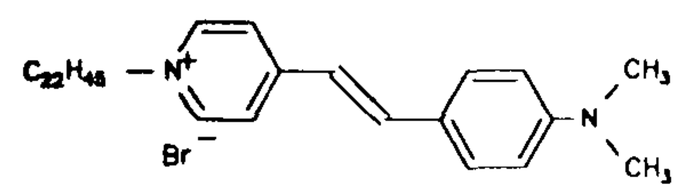 $C_{22}H_{45}PHBr$	0.004 (491 nm)	4.45×10^{-48}	Y-type 37 layers
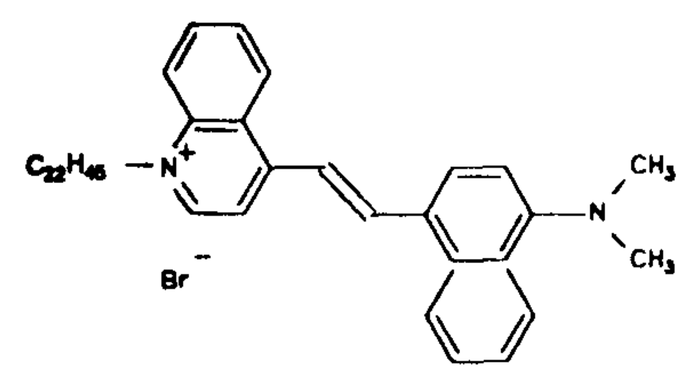 $C_{22}H_{45}QNBr$	0.006 (535 nm)	6.10×10^{-48}	Y-type (alternated) 10 bilayers

Table 30 Summary of Results

Material (continued)	Multilayer absorbance	Multilayer SHG	Quadratic	Notes
$C_{18}H_{37}QHI$	n/a	n/a	n/a	
$C_{22}H_{45}QHBr$	0.07	1.52×10^{-45}	Yes	Resonant enhancement
$C_{18}H_{37}PHBr$	n/a	n/a	n/a	
$C_{22}H_{45}PHBr$	0.023	3.71×10^{-47}	No	Imperfect deposition
$C_{22}H_{45}QNBr$	0.033	3.80×10^{-46}	Yes	Tilt angle = 38° Bilayer thickness = 4.5 nm

Table 30 continued

Material	Monolayer absorbance	Monolayer SHG / F m^3 V^{-1}	Multilayer Film
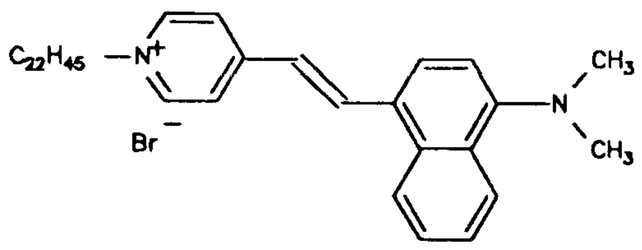 $C_{22}H_{45}PNBr$	0.004 (490 nm)	9.50×10^{-49}	Y-type (alternated) 5 bilayers
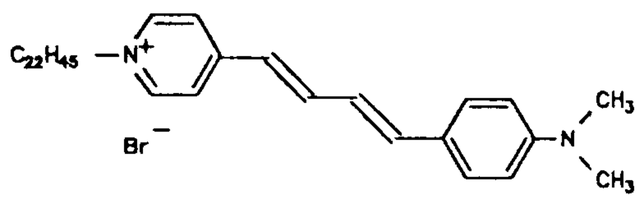 $C_{22}H_{45}PEHBr$	0.003 (490 nm)	4.18×10^{-48}	Y-type (alternated) 5 bilayers
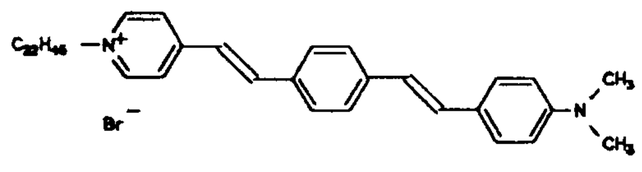 $C_{22}H_{45}PBHBr$	0.001 (470 nm)	1.52×10^{-49}	Y-type (alternated) 10 bilayers
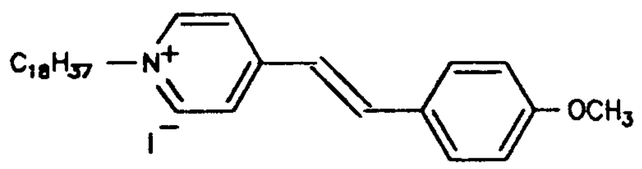 (A)	0.007	5.70×10^{-50}	No, because of interdigitation
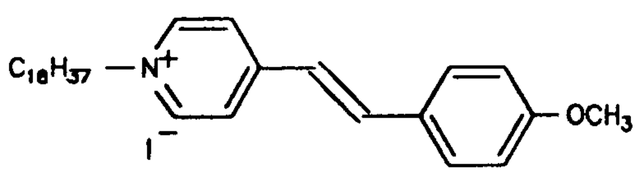 (A) + $C_{18}H_{37}SO_3^-Na^+$	0.015	3.53×10^{-49}	Y-type (alternated) 5 bilayers

Table 31 Summary of results

Material (continued)	Multilayer absorbance	Multilayer SHG / F m^3 V^{-1}	Quadratic	Notes
$C_{22}H_{45}PNBr$	0.015	1.32×10^{-48}	No	Imperfect deposition
$C_{22}H_{45}PEHBr$	0.007	2.19×10^{-47}	No	Quadratic in relation to absorbance
$C_{22}H_{45}PBHBr$	0.010	1.04×10^{-47}	Yes	Highly conjugated material
(A)	n/a	n/a	n/a	SHG increases significantly in mixture.
(A) + $C_{18}H_{37}SO_3^-Na^+$	0.05	1.15×10^{-48}	No	Monolayer tilt angle = 33.5(°)

Table 31 continued

Material	Monolayer absorbance	Monolayer SHG	Multilayer film
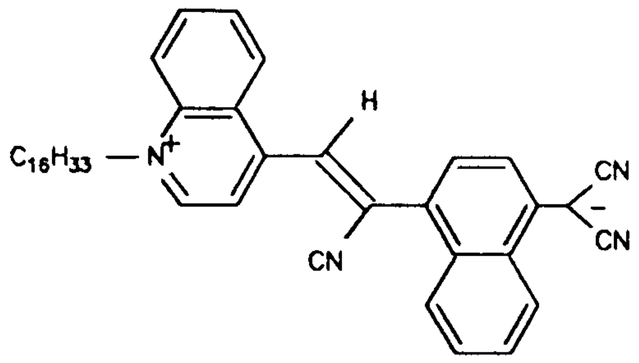 $C_{16}H_{33}QBCNQ$	0.032 (765 nm)	2.55×10^{-48}	No, damaged by laser
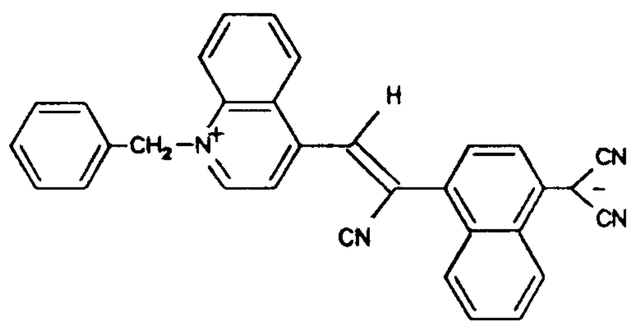 C_7H_7PBCNQ	0.020 (690 nm)	9.50×10^{-50}	No, damaged by laser

Table 32 Summary of Results

5.0 References

1. G.G.Roberts in Langmuir-Blodgett Films ed G.G.Roberts. Plenum Press, New York (1990).
2. A.Barraud, J. Chimie Physique. **85** (1988) No.11/12, 1121-1123.
3. A.Barraud, Synthetic Metals. **28** (1989) 793-800.
4. R.W.Munn, Chemistry in Britain. (1988) 518-524.
5. J.C.McGrath, L.Holt, D.M.Jones and I.M.Ward, Ferroelectrics. **50** (1983) 339-346.
6. H.Warson, Polym-plast. Technol. Eng. **9** (1977) No.1 123-138.
7. G.J.Ashwell in: Spectroscopy of New Materials eds R.J.Clark and R.E.Hester. (1993) John Wiley, New York.
8. A.P.F.Turner, Sensors and Actuators. **17** (1989) 433-450.
9. G.G.Roberts, Advances in Physics. **34** (1985) No.4, 475-512.
10. F.L.Carter, Superlattices and Microstructures, **2** (1986) 113.
11. R.C.Bertelson in Techniques in Chemistry III (Photochromism) ed G.H.Brown. (1971) John Wiley, New York.
12. E.Ando, J.Miyazaki, K.Morimoto, H.Nakahara and K.Fukuda in: Int. Symp. on Future Electron Devices - Bioelectronic and Molecular Electronic Devices. (1985) 47-52.
13. Z.F.Liu, K.Hashimoto and A.Fujishima, Nature. **347** (1990) 658-660.
14. G.J.Ashwell, E.J.Dawnay, A.P.Kuczynski and M.Szablewski in: Mat. Res. Soc. Symp. Proc. **173** (1990) 507-512.
15. M.Emmelius, G.Pawloski and H.W.Vollmann, Angew. Chem. Int. Ed. Engl. **28** (1989) 1445-1473.
16. J.W.Perry in, ACS Symposium Series. **455** (1991) 67-88.
17. D.Bloor in: Organic Materials for Non-linear Optics II ed R.A.Hann and D.Bloor (1989) RCS, Cambridge. 3-21.

18. R.S.Potember, R.C.Hoffman, K.A.Stetyick, R.A.Murphy and K.R.Speck, Johns Hopkins APL Technical Digest. **9** (1988) No.3, 189-199.

19. J.Tsibouklis, J.Cresswell, N.Kalita, C.Pearson, M.C.Petty and W.J.Feast, J. Phys. D: Appl Phys **22** (1989).

20. D.J.Williams, Angew. Chem. Int. Ed. Engl. **23** (1984) 690-703.

21. S.Singh, CRC Handbook of Laser Science and Technology ed M.J.Lever. **3** (1986) 3-11.

22. S.Allen, New Scientist. 1st July (1989) 59-63.

23. K.Tiefenthaler and W.Lutcosj J. Opt. Soc. Am. B. **6** (1989) No.2, 209-220.

24. S.Allen in: ESPRIT '86 Results and Achievements. (1987) 759-773.

25. D.S.Chemla and J.Zyss in: Nonlinear Optical Properties of Organic Molecules and Crystals. (1987) Academic Press, New York.

26. S.Allen in: Molecular Electronics ed G.J.Ashwell (1992) John Wiley, New York.

27. R.T.Bailey, F.R.Cruickshank, P.Pavlides, D.Pugh and J.N.Sherwood, J. Phys. D: Appl. Phys. **24** (1991) 135-145

28. J.Zyss and J.L.Oudar, Phys. Rev. A. **26** (1982) 2028.

29. Y.R.Shen in: The Principles of Nonlinear Optics. (1984) John Wiley, New York.

30. D.Tabor, J. Colloid. Interface. Sci. **75** (1980) 240.

31. B.Franklin, Philos. Trans. R. Soc. London. **64** (1774) 445.

32. Lord Rayleigh, Procs. R. Soc. London **47** (1890) 364.

33. A.Pockels, Nature (London) **43** (1891) 437

34. I.Langmuir, J. Am. Chem. Soc. **39** (1917) 1848.

35. K.B.Blodgett, J. Am. C. Soc. **57** (1935) 1007.

36. H.Kuhn and D.Mobius, Angew. Chem. Int. Ed. **10** (1971) No.9, 620-637.

37. H.Kuhn, J. Chem. Phys. **53** (1970) 101.

38. G.G.Roberts, K.P.Pande and W.A.Barlow, Solid State Electronic Devices. **2** (1978) 169.

39. A.Barraud, C.Rosilio and A.Ruaudel-Teixier, J.Colloid Interface Sci. **62** (1977) 509

40. R.A.Hann in Langmuir-Blodgett Films ed G.G.Roberts. (1990) Plenum Press, New York.

41. P.Martin and M.Szablewski, Nima Technology Users Manual. (1989).

42. M.Goto and E.Asada, Bull Chem Soc Japan. **51** (1978) 2456.

43. I.Langmuir and V.J.Scheafer, J.Am.Chem.Soc. **60** (1938) 1351-1360.

44. A.Ruaudel-Tiexier, M.Vandevyver and A.Barraud, Mol. Cryst. Liq. Cryst. **120** (1985) 319.

45. M.Vandevyver, A.Barraud, P.Lesieur, J.Richard and A.Ruaudel-Teixier, J.Chim.Phys. **83** (1986) 559.

46. A.Barraud, P.Lesieur, A.Ruaudel-Tiexier and M.Vandevyver, Thin Solid Films. **134** (1985) 195-199.

47. P.S.Vincent and G.G.Roberts, Thin Solid Films. **68** (1980) 91.

48. T.Shimidzu, T.Iyoda, M.Ando, A.Otani, T.Keneko and K.Honda, Thin Solid Films. **160** (1988) 67.

49. K.Hong and M.F.Rubner, Thin Solid Films. **160** (1988) 187.

50. P.S.Vincent, W.A.Barlow, F.T.Boyle, J.A.Finney and G.G.Roberts, Thin Solid Films. **60** (1979) 265-277.

51. G.G.Roberts, T.M.McGinnity, W.A.Barlow and P.S.Vincent, Solid State Commun. **32** (1979) 683.

52. G.G.Roberts, T.M.McGinnity, W.A.Barlow and P.S.Vincent, Thin Solid Films. **68** (1980) 223.

53. P.Christie, M.C.Petty, G.G.Roberts, D.H.Richards, D.Service and M.J.Stewart, Thin Solid Films. **134** (1985) 75.

54. M.Suzuki, Chem Lett. (1986) 395.

55. C.Bubeck, B.Tieke and G.Wegner, Ber. Bunsenges. Phys. Chem. **86** (1982) 499.

56. M.Sugi, Thin Solid Films. **152** (1987) 805.

57. T.Fukui, M.Sugi and S.Iizimia, Phys Rev B. **22** (1980) 4898.

58. M.Sugi and S.Iizima, Thin Solid Films. **68** (1980) 199.

59. L.M.Blinov, N.N.Davydova, V.V.Lazarev and S.G.Yudin, Sov. Phys. Solid State. **24** (1982) 1523.

60. G.G.Roberts and D.Holcroft, Thin Solid Films. **180** (1989) 211.

61. M.Petty, Thin Solid Films. **210/211** (1992) 427.

62. J.Tsibouklis, M.Petty, Y.P.Song, R.Richardson, M.C.Petty and W.J.Feast, J. Mater. Sci, **1** (1991) 819.

63. G.G.Roberts, B.Holcroft, T.Richardson and R.Colbrook, J.Chim Phys. **85** (1988) 1093-1097.

64. M.C.Petty, Thin Solid Films. **210/211** (1992) 417-426.

65. Y.L.Hua, M.C.Petty, G.G.Roberts, M.M.Ahmad, M.Hanack and M.Rein, Thin Solid Films. **149** (1987) 163.

66. N.J.Geddes, J.R.Sambles, W.G.Parker, N.R.Crouch and D.J.Jarvis, J. Phys. D: Appl. Phys, **23** (1990) 95.

67. A.Aviram and M.A.Ratner, Chem. Phys. Lett, **29** (1974) 277.

68. R.M.Metzger and C.A.Panetta, Synth Metals. **42** (1991) 1407-1413

69. G.J.Ashwell, J.R.Sambles, A.S.Martin, W.G.Parker and M.Szeblewski, J. Chem. Soc. Chem. Commun. **19** (1990) 1374-1376.

70. T.Moriizumi, Thin Solid Films. **160** (1988) 413-429

71. H.Perez and A.Barruad, Synth Metals. **61** (1993) 23-29.

72. J.B.Lando, H.Y.Wang and W.H.Ko, Polym Prepr (Am Chem Soc Div Polym Chem) **32** (1991) No. 3 378-9

73. S.Baker, G.G.Roberts and M.C.Petty, IEEE Proc part 1, Solid State Electron Devices. **130** 1987 260-3.

74. C.W.Fu, D.A.Batzel, S.E.Rickert, W.H.Ko, M.E.Kenney, Int. Symp. Polym. Adv. Technol 1987. (1988) 269-284.

75. J.W.Grate, S.Rose-Pehrsson and W.R.Barger, Langmuir. **4** (1988) 1293.

76. J.W.Grate, M.Klusty, W.R.Barger and A.W.Snow, Anal. Chem. **62** (1990) 1927.

77. D.G.Zhu, D.F.Cui, M.C.Petty aand M.Harris, Sens Actuators B **12** (1993) 111-114

78. L.Henryjon, G.Derost, A.Ruaudal-Teixier and A.Barraud, Proc. 2nd Int. Conf. Chemical Sensors. (1986)

79. P.J.Travers and L.S.Miller, Thin Solid Films. **208** (1992) 55-61.

80. B.Liedberg, C.Nylander and I.Lundstrom, Sensors and Actuators. **4** (1983) 299-304.

81. C.Nylander, B.Liedberg and T.Lind, Sensors and Actuators, **3** (1982) 79-88.

82. K.Matsubara, S.Kawata and S.Minami, Appl Optics. **27** (1988) No.6, 1160-1163.

83. U.Jonsson, Proc. Bioscience (1992). 260-267.

84. U.Jonsson, BioTechniques. **11** (1991) No.5, 620-627.

85. T.R.Wagner and S.Roth, Synth Met. **54** (1993) 307-314.

86. J.P.Lloyd, C.Pearson and M.C.Petty, Thin Solid Films. **160** (1988) 431.

87. J.Ross and G.G.Roberts, Proc. 2nd Int. Conf. Chemical Sensors. (1986) 704.

88. R.M.Swart in: Langmuir-Blodgett Films ed G.G.Roberts, Plenum Press, New York. (1990) 273-316.

89. T.Miyasaka, K.Koyama and T.Watanabe, Chem. Lett. (1990) 627.

90. T.Miyasaka, Y.Maekawa and K.Koyama, Thin Solid Films. **180** (1989) 73.

91. D.G.Zhu, M.C.Petty, H.Ancelin and J.Yarwood. Thin Solid Films. **176** (1989) 151.

92. Y.Okahata et al, Thin Solid Films. **180** (1989) 65.

93. J.D.Swalen, J. Mol. Electronics. **2** (1986) 155.

94. R.H.Tredgold, M.C.Young, P.Hodge and P.Khoshdel, Thin Solid Films. **151** (1987) 441.

95. C.Bosshard, M.Kupfer, P.Gunter, C.Pasquier, S.Zahir and M.Seifert, SPIE **1273** (1990) 70-76.

96. F.Grunfeld and C.W.Pitt, Thin Solid Films. **99** (1983) 249.

97. T.C.Chen, S.K.Tripathy and G.M.Carter, Mol. Cryst. Liq. Cryst. **106** (1984) 403.

98. J.C.Loelergue, M.Drumont, Y.Levy, P.Robin, J.P.Pocholle and M.Papuchon, Thin Solid Films. **160** (1988) 399-405

99. G.H.Cross, I.R.Peterson and I.R.Girling, Proc SPIE. **824** (1988) 79-85.

100. G.H.Cross, I.R.Girling, I.R.Peterson and N.A.Cade, Electronics Letters. **22** (1986) No.21, 1111-1113.

101. G.H.Cross, Thin Solid Films. **156** (1988) 39-52.

102. J.Tsibouklis, A.R.Werninck, A.J.Shand and G.H.Milburn, Chemtronics **3** (1988).

103. A.J.Heeger, J.Orenstein and D.R.Ulrich, Mat. Res. Soc. Symp. Proc. **107** (1987).

104. F.Kazjar and J.Messier, Thin Solid Films. **132** (1985) 11.

105. F.Kazjar, I.R.Girling and I.R.Peterson, Electronic Letters. **22** (1986) 1231.

106. F.Kazjar, Thin Solid Films. **160** (1988) 209-215.

107. S.Imazeki, Thin Solid Films. **134** (1985) 27.

108. A.N.Broers and M.Pomerantz, Thin Solid Films. **99** (1983) 323.

109. I.R.Peterson and I.R.Girling, Sci. Prog. Oxf. **69** (1985) 533-550.

110. J.D.Magan, P.Lemoine, W.Blau, M.Hogan, D.Lupo, W.Prab, U.Scheunemann, Thin Solid Films. **191** (1990) 349-359.

111. G.K.Drummond, Thin Solid Films. **210** (1992) 69-72.

112. J.Fang, Y.Wei, Z.Sun and P.Stroeve, Phys Lett A. **154** (1991) No.7/8, 396-398.

113. S.Obeng and A.J.Bard, J. Am. Chem. Soc. **113** (1991) 6279-6280.

114. C.Jehoulet, J. Am. Chem. Soc. **114** (1992) 4237-4247.

115. J.Millikan, D.Dominguez, H.Nelson, W.Barger. Chem. Mat. **4** (1992) 252

116. T.Nakamura, Langmuir. **8** (1992) 4-6.

117. O.A.Aksipetrov, N.N.Akhmediev, E.D.Mishina and V.R.Novak, JETP Lett. **37** (1983) No.4, 207-209.

118. O.A.Aktsipetrov, N.N.Akhmediev, I.M.Baranova, E.D.Mishina and V.R.Novak, Sov. Phys. JETP **62** (1985) No.3, 524-530.

119. I.R.Girling, N.A.Cade, P.V.Kolinsky and C.M.Montgomery, Electronic Letters. **21** (1985) No.5, 169-170.

120. I.R.Girling, P.V.Kolinsky, N.A.Cade, J.D.Earls and I.R.Peterson, Optics Commun. **55** (1985) No.4, 289-292.

121. I.R.Girling, N.A.Cade, P.V.Kolinsky, J.D.Earls, G.H.Cross and I.R.Peterson, Thin Solid Films. **132** (1985) 101-112.

122. I.R.Girling, S.R.Jethwa, R.T.Stewart, J.D.Earls, G.H.Cross, N.A.Cade, P.V.Kolinsky, R.J.Jones and I.R.Peterson, Thin Solid Films. **160** (1988) 355-362.

123. D.Lupo, W.Press, U.Scheunemann, A.Laschewsky, H.Ringsdorf and I.Ledoux, J. Opt. Soc. Am. B. **5** (1988) No.2, 300-308.

124. I.R.Peterson in: Organic Materials for Non-linear Optics ed R.A.Hann and D.Bloor (1989) RSC, Cambridge. 317-333.

125. J.Bauer, P.Jeckelen, D.Lupo, W.Prass, U.Scheuenemann, R.Keosian and G.Khanarian in: Organic Materials for Non-linear Optics. Ed R.A.Hann and D.Bloor (1989) RSC, Cambridge. 348-353.

126. C.Bubeck, T.Arndt, T.Sauer, G.Duda and G.Wegner, Adv Mat. **3** (1991) No.1, 54-58.

127. A.Laschewsky, W.Paulus, H.Ringsdorf, D.Lupo, P.Ottenbreit, W.Prab, C.Bubeck, D.Neher and G.Wegner, Makromol. Chem. Macromol. Symp. **46** (1991) 205-210.

128. F.Effenberger, Adv. Mat. **4** (1992) No.6 413-416.

129. L.S.Miller, P.J.Travers, R.S.Sethi, M.J.Goodwin, R.M.Marsden, G.W.Gray and R.M.Scrowston in: Organic Materials for Non-linear Optics. Ed R.A.Hann and D.Bloor (1989) RSC, Cambridge. 361-366.

130. L.M.Hayden, B.L.Anderson, J.Y.S.Lam, B.G.Higgins, P.Stroeve and S.T.Kowel, Thin Solid Films. **160** (1988) 379-388.

131. L.M.Hayden, S.T.Kowel and M.P.Sprinisvan, Optics Commun. **61** (1987) No.5 351-356.

132. D.B.Neal, M.C.Petty, G.G.Roberts, M.M.Ahmad, W.J.Feast, I.R.Girling, N.A.Cade, P.V.Kolinsky and I.R.Peterson, Electronics Letters. **22** (1986) No.9 460-461.

133. M.M.Ahmad, W.J.Feast, D.B.Neal, M.C.Petty and G.G.Roberts, J. Molecular Electronics **2** (1986) 129-133.

134. D.B.Neal, Applic Ferroelectric. (1986) 89-92.

135 J.P.Cresswell in: SPIE **1337** (1990) 358-363.

136. I.Ledoux, D.Josse, P.Vidakovic, J.Zyss, R.A.Hann, P.F.Gordon, D.B.Bothwell, S.K.Gupta, S.Allen, P.Robin, E.Chastaing and J.C.Dubois, Europhysics Letters. **3** (1987) No.7, 803-809.

137. H.Ancelin, G.Briody, J.Yarwood, J.P.Lloyd, M.C.Petty, M.M.Ahmad and W.J.Feast, Langmuir **6** (1990) 172-177.

138. I.Ledoux, D.Josse, P.Fremaux, J.P.Piel, G.Post, J.Zyss, T.McLean, R.A.Hann, P.F.Gordon and S.Allen, Thin Solid Films. **160** (1988) 217-230.

139. I.Ledoux, D.Josse, J.Zyss, T.McLean, P.F.Gordon, R.A.Hann and S.Allen, J. Chimie Physique. **85** (1988) No.11/12, 1085-1090.

140. I.Ledoux and F.Kajzar in: SPIE **1127**. (1989) 137-142.

141. S.Allen, R.A.Hann, S.K.Gupta, P.F.Gordon, B.D.Bothwell, I.Ledoux, P.Vikadovik, J.Zyss, P.Robin, E.Chastaing and J.C.Dubois in: SPIE **682** (1986) 97-102.

142. S.Allen, T.D.McLean, P.F.Gordon, B.D.Bothwell, P.Robin and I.Ledoux in: SPIE **971** (1988) 206-215.

143. M.G.Hutchings, P.F.Gordon and J.O.Morley, Inst. Phys. Conf. Ser. **103** (1989) No.2, 97-106.

144. F.Kazjar and I.Ledoux, Thin Solid Films. **179** (1989) 359-367.

145. I.R.Girling, N.A.Cade, P.V.Kolinsky, R.J.Jones, I.R.Peterson, M.M.Ahmad, D.B.Neal, M.C.Petty, G.g.Roberts and W.J.Feast, J. Opt. Soc. Am. B. **4** (1987) No.6, 950-953.

146. J.S.Schildkraut, T.L.Penner, C.S.Willand and A.Ulman, Optics Letters. **13** (1988) No.2, 134-136.

147. G.Marowsky, A.Gierulski, R.Steinhoff, D.Dorsch, R.Eidenschink and B.Rieger, J. Opt. Am. B **4** (1987) 956.

148. R.Steinhoff, L.F.Chi, G.Marowsky and D.Mobius, J. Opt. Soc. Am. B. **6** (1989) No.4 843-847.

149. G.Marowsky and R.Steinhoff, Optics Letters. **13** (1988) No.9, 707-709.

150. P.Stroeve, D.D.Saperstein and J.F.Rabolt, Thin Solid Films. **179** (1989) 529-534.

151. K.Kajikawa, K.Shirota, H.Takezoe and A.Fukuda, Jap J. Appl. Phys. **29** (1990) No.5, 1050-1062.

152. D.W.Kalina and S.G.Grubb, Thin Solid Films. **160** (1988) 363-371.

153. M.Era, K.Nakamura, T.Tsutsui, S.Saito, H.Niino, K.Takehara, K.Isomura and H.Taniguchi, Jap. J. Appl. Phys. **29** (1990) No.12, 2261-2263.

154. M.Era, H.Kawafuji, T.Tsutsui, S.Saito, K.Takehara, K.Takehara, K.Isomura and H.Taniguchi, Thin Solid Films. **210/211** (1992) 163-165.

155. R.Popovitz-Biro, K.Hill, E.M.Landau, M.Lahav, L.Leiserwitz and J.Sagiv, J. Am. Chem. Soc. **110** (1988) 2672-2674.

156. R.J.Good and R.R.Stromberg, Surface and Colloid Science, Plenum Press, New York. **2** (1979).

157. G.J.Ashwell, E.J.C.Dawnay, A.P.Kuczynski, M.Szablewski, I.M.Sandy, M.R.Bryce, A.Grainger and M.Hasan, J. Chem. Soc. Faraday Trans. **86** (1990) No.7, 1117-1121.

158. G.J.Ashwell, M.Szablewski and A.P.Kuczynski, NATO ASI Ser., Ser B **248** (1990) 647-652.

159. G.J.Ashwell, E.J.Dawnay and A.P.Kuczynski, J. Chem. Soc. Chem. Commun, **19** (1990) 1355-1357.

160. F.Embs, D.Funhoff, A.Laschewsky, U.Licht, H.Ohst, W.Prass, H.Ringsdorf, G.Wegner and R.Wehrmann, Adv Mater. **3** (1991) No.1, 25-31.

161. T.Senoh, K.Sanui and N.Ogata, Chemistry Letters. (1990) 1849-1852.

162 R.Popovitz-Biro, K.Hill, E.Shavit, D.J.Hung, M.Lahav, L.Leiserowitz, J.Sagiv, H.Hsuing, G.R.Meredith and H.Vanherzeele, J. Am Chem Soc. **112** (1990) No. 7 2498-2506.

163. R.C.Hall, G.A.Lindsay, B.Anderson, S.T.Kowel, B.G.Higgins and P.Stroeve, Mat. Res. Soc. Symp. Proc. **108** (1988) 351-356.

164 R.C.Hall, G.A.Lindsay, S.T.Kowel and L.M.Hayden in: SPIE **824** (1987) 121-123.

165. B.L.Anderson, R.C.Hall, B.G.Higgins, G.Lindsay, P.Stroev and S.T.Kowel et al, Synthetic Metals. **28** (1989) 683-688.

166. R.H.Tredgold, M.C.Young, R.Jones, P.Hodge, P.Kolinsky and R.J.Jones, Electronic Letters. **24** (1988) No.6, 308-309.

167. B.L.Anderson, J.M.Hoover, G.A.Lindsay, B.C.Higgins, P.Stroeve and S.T.Kowel, Thin Solid Films. **179** (1989) 413-421.

168. M.C.Young, R.H.Tredgold, P.Hodge, P.Kolinsky and R.J.Jones, Electronic Letters. **26** (1990) No.14, 993.

169. K.Kajikawa, T.Anzai, H.Takerzoe, A.Fukuda, S.Okada, H.Matsuda, H.Nakanishi, T.Abe and H.Ito, Chem. Phys. Letters. **192** (1992) No.1, 113-116.

170. N.Carr, Makromol. Chem. Rapid Commun. **8** (1987) 487.

171. T.L.Penner, N.J.Armstrong, C.S.Willand, J.S.Schildkraut and D.R.Robello in: SPIE **1560** (1991) 377-386.

172. Q.Tang, S.Zahir, C.Bosshard, F.Floersheimer, M.Kuepfer and P.Guenter, Thin Solid Films. **210-211** (1992) 195-197.

173. C.Bosshard, G.Decher, B.Tieke and P.Gunter, SPIE **1017** (1988) 141-147.

174. G.Decher, B.Tieke, C.Bosshard and P.Gunter, Ferrolectrics. (1989) 193-207.

175. C.Bosshard, M.Kupfer, P.Gunter, C.Pasquier, S.Zahir and M.Seifert, Appl. Phys. Lett. **56** (1988) No. 13 1204-1206.

176. G.Decher, F.Klinkhammer, I.R.Peterson and R.Steitz, Thin Solid Films. **178** (1989) 445-451.

177. G.J.Ashwell, Thin Solid Films. **186** (1990) 155-165.

178. M.Szablewski PhD Thesis. "Multi-functional D-π-A materials for molecular electronics." Cranfield Institute of Technology. (1990).

179. Handbook of Chemistry and Physics, 69th edition. CRC Press, (E-59).

180. R.H.Selfridge, S.T.Kowel, P.Stroeve, J.Lam and B.Higgins, Thin Solid Films. **160** (1998) 471-476.

181. G.J.Ashwell, W.A.Crossland, P.J.Martin, P.A.Thompson, A.T.Hewson and S.D.Marsden, Mat. Res. Soc. Symp. Proc. **247** (1992) 787-792.

182. G.J.Ashwell, P.J.Martin, M.Szablewski, P.A.Thompson, A.T.Hewson and S.D.Marsden, Spec.Publ - R.Soc.Chem, **91** (1991) 60-66.

183. G.J.Ashwell, R.C.Hargreaves, C.E.Baldwin, G.S.Bahra and C.R.Brown, Nature. **357** (1992).

6.0 Appendix.

6.1 Abbreviations of Systematic Nomenclature.

$C_{22}H_{45}QBr$: N-docosyl-4-methylquinolinium bromide.

$C_{22}H_{45}PBr$: N-docosyl-4-methylpyridinium bromide.

$C_{16}H_{33}QHBr$: E-1-hexadecyl-4-{2-(4-dimethylaminophenyl)ethenyl} quinolinium bromide.

$C_{18}H_{37}QHBr$: E-1-octadecyl-4-{2-(4-dimethylaminophenyl)ethenyl} quinolinium bromide.

$C_{18}H_{37}QHI$: E-1-octadecyl-4-{2-(4-dimethylaminophenyl)ethenyl} quinolinium iodide.

$C_{20}H_{41}QHBr$: E-1-eicosyl-4-{2-(4-dimethylaminophenyl)ethenyl} quinolinium bromide

$C_{22}H_{45}QHBr$: E-1-docosyl-4-{2-(4-dimethylaminophenyl)ethenyl} quinolinium bromide.

$C_{16}H_{33}PHBr$: E-1-hexadecyl-4-{2-(4-dimethylaminophenyl)ethenyl} pyridinium bromide.

$C_{18}H_{37}PHBr$: E-1-octadecyl-4-{2-(4-dimethylaminophenyl)ethenyl} pyridinium bromide.

$C_{18}H_{37}PHI$: E-1-octadecyl-4-{2-(4-dimethylaminophenyl)ethenyl} pyridinium iodide.

$C_{22}H_{45}PHBr$: E-1-docosyl-4-{2-(4-dimethylaminophenyl)ethenyl} pyridinium bromide.

$C_{18}H_{37}QNBr$: E-1-octadecyl-4-{2-(4-dimethylaminonaphthyl)ethenyl} quinolinium bromide.

$C_{22}H_{45}QNBr$: E-1-docosyl-4-{2-(4-dimethylaminonaphthyl)ethenyl} quinolinium bromide.

$C_{18}H_{37}PNBr$: E-1-octadecyl-4-{2-(4-dimethylaminonaphthyl)ethenyl} pyridinium bromide.

$C_{22}H_{45}PNBr$: E-1-docosyl-4-{2-(4-dimethylaminonaphthyl)ethenyl} pyridinium bromide.

$C_{18}H_{37}PEHBr$: E-1-octadecyl-4-{4-(4-dimethylaminophenyl)-1,3-butadienyl} pyridinium bromide.

$C_{22}H_{45}PEHBr$: E-1-docosyl-4-{4-(4-dimethylaminophenyl)-1,3-butadienyl} pyridinium bromide.

$C_{22}H_{45}PT$: E-1-docosyl-4-{2-(4-methylphenyl)ethenyl}pyridinium bromide.

$C_{22}H_{45}PBHBr$: E-1-docosyl-4-{2-(4-{2-(4-dimethylaminophenyl)ethenyl} benzyl)ethenyl}pyridinium bromide.

(A): E-1-octadecyl-4-{2-(4-methyloxyphenyl)ethenyl} pyridinium iodide.

(B): E-1-methyl-4-{2-(4-octadecyloxyphenyl)ethenyl} pyridinium iodide.

$C_{16}H_{33}QBCNQ$: Z-ß-(n-hexadecyl-4-quinolinium)-α-cyano-4-naphthyl dicyanomethanide.

$C_{7}H_{7}QBCNQ$: Z-ß-(phenylmethyl-4-quinolinium)-α-cyano-4-naphthyl dicyanomethanide.

$C_{16}H_{33}PBCNQ$: Z-ß-(n-hexadecyl-4-pyridinium)-α-cyano-4-naphthyl dicyanomethanide.

$C_{7}H_{7}PBCNQ$: Z-ß-(phenylmethyl-4-pyridinium)-α-cyano-4-naphthyl dicyanomethanide.

Acknowledgements

Thanks to Marek Szablewski, Andrej Kuczynski, Emma Dawnay, Carl Baldwin, and Prof.G.J.Ashwell for their help during my period at Cranfield.

Thanks to Dr.Brian Foulger for the use of facilities in the writing of this thesis.

Special thanks, and love, to my wife Lindsay for her patience, support, understanding and sandwiches.

Bring me fun,

Bring me sunshine,

Bring me love.